# Preparation and Characterization of Low Cost Ceramic Composite Membranes for Microfiltration and Ultrafiltration Applications

**Thesis submitted in partial fulfillment of the requirements for the degree of**

**DOCTOR OF PHILOSOPHY**

by

**Barun Kumar Nandi**


**Department of Chemical Engineering**

**Indian Institute of Technology Guwahati**

**Guwahati - 781039, India**

# PREPARATION AND CHARACTERIZATION OF LOW COST CERAMIC COMPOSITE MEMBRANES FOR MICROFILTRATION AND ULTRAFILTRATION APPLICATIONS




*Barun Kumar Nandi*

# Preparation and Characterization of Low Cost Ceramic Composite Membranes for Microfiltration and Ultrafiltration Applications

*Thesis submitted in partial fulfillment of the requirements for the degree of*

**DOCTOR OF PHILOSOPHY**

*by*

*Barun Kumar Nandi*
*Roll No.: 05610705*


**Department of Chemical Engineering**
**Indian Institute of Technology Guwahati**
**Guwahati - 781039, India**

**August, 2009**

*Dedicated To*

*Shri Shri Thakur Anukulchandra:*

*for whom I have become what I am today.*

**Department of Chemical Engineering**
**Indian Institute of Technology Guwahati**
**Guwahati - 781039, India**

## CERTIFICATE

This is to certify that the thesis entitled **"Preparation and Characterization of Low Cost Ceramic Composite Membranes for Microfiltration and Ultrafiltration Applications"** being submitted by ***Barun Kumar Nandi*** for the award of PhD degree has been carried out under our guidance and supervision. The work documented in this thesis has not been submitted to any other University or Institute for the award of any degree or diploma.

**(Dr. Ramgopal V. S. Uppaluri)**
Associate Professor
Department of Chemical Engineering
Indian Institute of Technology Guwahati
Guwahati - 781039, India.

**(Dr. Mihir Kumar Purkait)**
Associate Professor
Department of Chemical Engineering,
Indian Institute of Technology Guwahati
Guwahati - 781039, India.

# *Acknowledgements*

I would like to express my gratitude to all those who in different ways helped me in completing this research work within the time span of four years directly or indirectly. Foremost, I would like to express my gratitude to my supervisors, **Dr. Ramgopal V. S. Uppaluri** and **Dr. Mihir Kumar Purkait**, for providing me continuous inspiration and guidance throughout the entire course of work. I am indebted to both of them for their useful suggestions and constant encouragement throughout the entire period.

I am grateful to **Dr. Ramgopal V. S. Uppaluri** for his continuous support, interesting discussions and giving me freedom in choosing how to approach different issues. I appreciate very much his expertise in analyzing the experimental data points to model them suitably. His uncompromising approach to complete the experimental, data analysis, writing manuscripts as well as thesis within stipulated time period helped me a lot in completing my research work in this much shorter span of time. The numerous brain storming sessions during the project meetings with him were very useful in enriching my analytical power. It has been an amazing experience working with Dr. Uppaluri, which will help me a lot in my future life to complete work within stipulated time without compromising upon the quality of work.

I would like to express my sincere gratitude to **Dr. Mihir Kumar Purkait** for his meticulous research planning to get an idea on how to perform the research work. I appreciate very much his flexibility and openness in dealing with the specific and general needs of this research work. He taught me how to write and improve the quality of a journal paper and the thesis. I thank him for his patience and amicable nature. It has been a great privilege to work with him.

I must also thank my doctoral committee members **Dr. Pallab Ghosh, Dr. V. S Moholkar**, Department of Chemical Engineering, **Prof. Subhash C. Mishra** and **Prof. Pinakeswar Mahanta,** Department of Mechanical Engineering, for their valuable suggestions and contributions towards my research work.

I must also thank the faculty members of the Department of Chemical Engineering for their kind cooperation during my stay in the department. I am also thankful to all present and ex-

staff members and scientific officers of the Chemical Engineering Department for their genuine help during my entire research period.

I am thankful to the **Central Instruments Facility** of IIT Guwahati for allowing me to carry out **Scanning Electron Microscopy** analysis on my own**,** which has been very important in this research work. In this regard, I should acknowledge the help provided by **Mr. Kula Kamal Senapati**, Scientific Officer, Central Instruments Facility, IIT Guwahati. He taught me how to use the SEM instruments, and take images at various critical conditions of the sample. I am also thankful to the **Central Workshop** of IIT Guwahati for helping me in the fabrication of my experimental setup which was very much essential in my research work.

I was fortunate enough to get excellent batch mates like **Mehabub**, **Pradip**, **Bandana Mam**, **Kabita Mam**, **Ujwala** and **Somen** for their friendly support and timely assistance whenever needed. I am also thankful to my senior research scholar, **Biswanathda**, **Debada**, **Subham** and **Shiba** for their friendly behavior and assistance. Special thanks to **Aparajita** and **Bipul** for their help and co-operation in my research work.

Most of all, I would like to express my deepest sense of gratitude to all my family members, my parents and my wife, **Nita**. Their love, care, sacrifices and encouragement have made it possible for me to come so far. I appreciate the courage, understanding and dedicated support shown by all of them despite many testing times at their end.

*Barun Kumar Nandi*

# *Abstract*

In the past two decades, significant advances in membrane technology research have been reported. Amongst various membrane applications proposed so far, microfiltration (MF) and ultrafiltration (UF) are the most significant in chemical and biochemical processes. Polymeric and ceramic membrane materials are the most relevant materials used for MF and UF membrane processes. While polymeric membranes are inexpensive and are prone to a greater degree of fouling, ceramic membranes are expensive and possess higher corrosion and mechanical resistance. Therefore, the preparation and characterization of low cost ceramic membranes is always encouraging to further the industrial cost effectiveness of membrane technology. This work presents the preparation, characterization and applications of low cost ceramic and polymer - ceramic membranes suitable for MF and UF applications. Among various industrial applications of membranes, treatment of oily wastewater and MF of mosambi juice were chosen as the most important areas of research where low cost ceramic membranes can be used as an alternative to conventional fouling prone polymeric membranes. The entire work carried out in this research work is divided into four major parts:

- Preparation and characterization of comparatively low cost ceramic membranes.
- Application of prepared ceramic membranes for the MF of oil-in-water emulsions.
- Application of prepared ceramic membranes for the MF of mosambi juice.
- Preparation and characterization of polymer-ceramic composite membranes.

In this work we have identified two distinct compositions of inorganic precursors (namely composition A and composition B) using kaolin, quartz, feldspar, sodium carbonate, calcium carbonate, boric acid and sodium metasilicate for the preparation of upper (0.547 - 0.810 μm)

and lower (0.185 - 0.332 μm) submicron pore range ceramic membranes. The identified composition contains 70 - 85 wt % of cheaper precursors and only 15 - 30 wt % of costly precursors. The sintering temperature during membrane fabrication was varied from 800 - 1000 $^{o}$C, which was lower than usual sintering temperature of 1100 $^{o}$C as mentioned in various literatures. The prepared ceramic membranes were characterized by TGA/DTA, XRD, SEM analysis, pore size distribution, porosity, average pore size, gas permeation, liquid permeation and chemical stability to evaluate the membrane structural, permeation and chemical characteristics. Based on materials cost, the membrane cost is estimated to be 130 and 220 \$/m$^2$ for upper and lower submicron range membranes, respectively.

The performance characteristics of the prepared ceramic membranes were studied for the treatment of oil-in-water (o/w) emulsions and MF of mosambi juice in dead end mode of operations. Synthetic o/w emulsions constituting 50 - 250 mg/L oil concentrations were subjected to MF at different trans-membrane pressure differentials ($\Delta P$). Membrane prepared with composition A and sintering temperature of 850 $^{o}$C provided a permeate flux decline from $48.16\times10^{-6}$ - $12.24\times10^{-6}$ m$^3$/m$^2$.s where as oil rejection efficiency of the membrane increased from 97.9 - 98.5 % within 30 minutes of experimental run at a $\Delta P$ of 41.37 kPa for a feed oil concentration of 100 mg/L. The initial permeate flux increased from $48.16\times10^{-6}$ - $100.34\times10^{-6}$ m$^3$/m$^2$.s when $\Delta P$ was increased from 41.37 - 206.84 kPa. However, with an increase in $\Delta P$ from 41.37 to 206.84 kPa, oil rejection efficiency decreased from 98.51 - 97.71 %. Membranes prepared with composition B provided better oil rejection efficiency (97.7 %) and lower permeate flux in comparison with the composition A membrane (97.4 %) for similar experimental conditions. However, all membranes were observed to yield a permeate stream with less than 5 mg/L oil concentration. Various membrane pore blocking

models such as complete pore blocking, standard pore blocking, intermediate pore blocking and cake filtration were used to gain insights into the nature of membrane fouling during permeation.

Four different ceramic composition A membranes with varying pore diameters ($d_l$) and porosities ($\varepsilon_m$) were used for the clarification (MF) of mosambi juice to evaluate the effect of $d_l$ and $\varepsilon_m$ on permeation characteristics (permeate flux and juice quality) of centrifuged mosambi juice (CJ) and enzyme treated centrifuged mosambi juice (ETCJ). Subsequently, a convenient effective permeable area factor ($\varepsilon_m d_l^{\,2}$) was evaluated to provide greater insights in the fouling phenomena. Different physio-chemical properties such as colour, clarity, pH, citric acid content, density, total soluble solid (TSS) and alcohol insoluble solids (AIS) were measured for both feed and permeate juice samples to evaluate the effect of $\varepsilon_m d_l^{\,2}$ on juice quality. Typical permeate fluxes were observed to vary from 5.78 $\times 10^{-6}$ to 13.45 $\times 10^{-6}$ $m^3/m^2.s$ for CJ and 14.07 $\times 10^{-6}$ to 60.64$\times 10^{-6}$ $m^3/m^2.s$ for ETCJ at 82.7 kPa ($\Delta P$) for different membranes whose $\varepsilon_m d_l^{\,2}$ varied from 0.249 to 0.783 $\mu m^2$. Among various membrane pore blocking models, flux decline by cake filtration was found to be the best fitted model. The cake filtration model constant ($k_c$) was found to vary with $\Delta P$ and $\varepsilon_m d_l^{\,2}$ and was empirically correlated. Phenomenological models were proposed to illustrate the dependency of total hydraulic resistance of membrane on $\varepsilon_m d_l^{\,2}$, $\Delta P$ and time ($t$). Based on experimental as well as theoretical investigations, membranes with $\varepsilon_m d_l^{\,2}$ up to 0.443 for CJ and 0.294 for ETCJ and a $\Delta P$ of 82.7 kPa were recommended for MF of mosambi juice. Finally, the long term storage study of the juice revealed that the clarified juice can be stored in refrigerated condition for more than 30 days without significant change in juice quality.

Cellulose acetate (CA) - ceramic composite membranes were prepared using dip coating technique with the prepared low cost ceramic membrane as a support. The dip coating parameters studied experimentally were the concentration of CA solution (varying from 2 - 8 wt %) in acetone and dipping time (varying from 30 - 150 s). The prepared composite membranes were characterized using SEM, gas permeation, pure water flux and UF experiments using bovine serum albumin. It was observed that the membrane prepared with 2 and 4 wt % CA were suitable for MF applications and those with 6 and 8 wt % were for UF applications. Theoretical investigation was conducted to know the macroporus and mesoporous structure of the prepared membranes using Knudsen and viscous permeability analysis of air. A resistances in series model was applied to identify various resistances responsible for flux decline. Phenomenological models were proposed to illustrate the dependency of hydraulic resistance of membrane on the structural parameters such as average pore size, effective porosity as well as dip coating parameters (dipping time and concentration of CA). It was found that, the growth rate of CA film on the ceramic support followed exponential growth law with respect to dipping time. The total hydraulic resistance of the membrane was evaluated to be inversely proportional to the ratio of pore sizes of top layer and ceramic support. The resistance due to the CA film was found to be dependent to the order of 1.73 with respect to concentration of CA. An increase in the concentration of CA was found to be more effective than dipping time to reduce the membrane pore size.

Based on the experimental as well as theoretical findings, it is herewith inferred that the prepared low cost ceramic membrane could be promising for the treatment of o/w emulsions, mosambi juice clarification and for the preparation of polymer-ceramic composite membranes.

# *Contents*

# *List of Tables*

# *List of Figures*

# Abbreviations

| | |
|---|---|
| AIS | alcohol insoluble solids |
| BSA | bovine serum albumin |
| CJ | centrifuged juice |
| CA | cellulose acetate |
| ETCJ | enzyme treated centrifuged juice |
| MF | microfiltration |
| MWCO | molecular weight cut-off |
| NF | nanofiltration |
| o/w | oil-in-water |
| PV | pervaporation |
| PWF | pure water flux |
| RO | reverse osmosis |
| TSS | total soluble solids |
| UF | ultrafiltration |

# Notations

| | |
|---|---|
| $A$ | intercept of Eq. (2.4) (m/s) |
| $B$ | slope of Eq. (2.4) (m/s.kPa) |
| $b, d, e$ | constant in Eq. (6.10) |
| $C$ | concentration of oil/BSA in the feed (mg/L) |
| $C_P$ | concentration of oil/BSA in the permeate (mg/L) |
| $c$ | concentration of CA in acetone (wt %) |
| $d_{cm}$ | hydraulic pore diameter of fouled membrane |
| $d_g$ | pore diameter of the membrane calculated from gas permeation analysis (m) |
| $d_{g,com}$ | pore diameter of composite membrane |
| $d_{g,\sup}$ | pore diameter of support |

| | |
|---|---|
| $d_i$ | pore diameter of $i^{th}$ pore |
| $d_l$ | hydraulic pore radius of the membrane (m) |
| $d_p$ | average particle sizes of juice (CJ and ETCJ) |
| $d_s$ | pore diameter of the membrane calculated from SEM analysis (m) |
| $f_1, f_2, f_3$ | functions |
| $h_{com}$ | total thickness of composite membrane (m) |
| $h_{\sup}$ | total thickness of support (m) |
| $J$ | permeate flux ($m^3/m^2.s$) |
| $J_0$ | initial permeate flux ($m^3/m^2.s$) |
| $J_{cal}$ | calculated permeate flux ($m^3/m^2.s$) |
| $J_{\exp}$ | experimental permeate flux ($m^3/m^2.s$) |
| $J_W$ | pure water flux ($m^3/m^2.s$) |
| $K$ | effective permeability factor (m/s) |
| $k_C^{CJ}$ | cake filtration model constant for CJ ($s/m^2$) |
| $k_C^{ETCJ}$ | cake filtration model constant for ETCJ ($s/m^2$) |
| $K_p$ | constant in Eq. (3.3) (units depend on the parameter $n$) |
| $k_b$ | complete blocking model constant in Eq. (3.4) (1/s) |
| $k_c$ | cake filtration model constant in Eq. (3.7) ($s/m^2$) |
| $k_i$ | intermediate pore blocking model constant in Eq. (3.6) (1/m) |
| $k_s$ | standard pore blocking model constant in Eq. (3.5) ($s^{0.5}/m^{0.5}$) |
| $l_m$ | length of membrane pores (m) |
| $l_{cm}$ | length of fouled membrane pores (m) |
| $M, a$ | constant in Eq. (6.9) |
| $N, f, g$ | constant in Eq. (6.12) |
| $n$ | number of pore |
| $P$ | average pressure (kPa) |

| | |
|---|---|
| $\Delta P$ | trans-membrane pressure (kPa) |
| $P_2$ | membrane pressure at permeate side (kPa) |
| $P_{com}$ | hydraulic permeability of composite membrane, ($m^3/m^2$.s.kPa) |
| $P_m$ | hydraulic permeability of membrane, ($m^3/m^2$.s.kPa) |
| $Q$ | volumetric flow rate of permeate ($m^3$) |
| $q$ | tortuosity of the membrane |
| $R$ | oil/BSA rejection efficiency |
| $R^2$ | square of correlation coefficient |
| $R_{BSA}$ | resistance offered by BSA film ($m^2$.s.kPa/$m^3$) |
| $R_{coat}$ | resistances due to CA coating ($m^2$.s.kPa/$m^3$) |
| $R_{com}$ | hydraulic resistance of composite membrane ($m^2$.s.kPa/$m^3$) |
| $R_f^{\,0}$ | instantaneous fouling resistance of the membrane during MF ($m^2/m^3$) |
| $R_{\text{int}}$ | resistances offered by intermediate layer ($m^2$.s.kPa/$m^3$) |
| $R_m$ | intrinsic membrane resistance ($m^2/m^3$) |
| $R_{\text{sup}}$ | resistance of the support ($m^2$.s.kPa/$m^3$) |
| $R_t$ | total resistance of the membrane during MF ($m^2/m^3$) |
| $R_{top}$ | resistances offered by the top layer ($m^2$.s.kPa/$m^3$) |
| $R_t^{\,0}$ | instantaneous total resistance of the membrane during MF ($m^2/m^3$) |
| $R_{UF}$ | total hydraulic resistance during UF ($m^2$.s.kPa/$m^3$) |
| $r$ | pore radius of the membrane (m) |
| $r_l$ | hydraulic pore radius of the membrane (m) |
| $S$ | effective membrane area ($m^2$) |
| $T$ , $p$ , $u$ | constant in Eq. (4.11) |
| $t$ | time of dipping (s) |
| $\Delta t$ | sampling time (s) |
| $V$ | volume of permeate ($m^3$) |
| $v_g$ | molecular mean velocity of the gas (m/s) |
| $v_{mem}$ | volume of the membrane in wet state ($m^3$) |

| | |
|---|---|
| $w_1$ | weight of membranes in wet condition (kg) |
| $w_2$ | weight of membranes in dry condition (kg) |
| $X$ , $y$ , $z$ | constant in Eq. (4.10) |

## Greek letters

| | |
|---|---|
| $\eta$ | viscosity of gas (kPa.s) |
| $\mu_w$ | viscosity of water (kPa.s) |
| $\rho_{mem}$ | structural density of the membrane (kg/m$^3$) |
| $\rho_{water}$ | density of water (kg/m$^3$) |
| $\varepsilon_{cm}$ | total porosity of the fouled membrane |
| $\varepsilon_{cm} d_{cm}^{\ 2}$ | effective permeable area factor of fouled membrane |
| $\varepsilon_m d_l^{\ 2}$ | effective permeable area factor of fresh membrane |
| $\varepsilon_m$ | total porosity of the membrane (dimensionless) |
| $\varepsilon/q^2$ | effective porosity of the membrane |
| $(\varepsilon/q^2)_{com}$ | effective porosity of the composite membrane |
| $(\varepsilon/q^2)_{\text{sup}}$ | effective porosity of the support |

# Chapter 1:

## Introduction

# *Chapter 1*

# Introduction

*This chapter presents a brief summary of the basic fundamentals, different terminologies and applications involved in membrane technology along with the basis of the problem chosen in this work. State of art on the preparation of ceramic and polymer - ceramic composite membrane and their applications in different applications have been elaborately discussed. Based on the state of art on the membrane preparations and their applications in oil-in-water emulsions and mosambi juice microfiltration, the aims of the present work have been summarized. Finally, the organization of the present work has been presented.*

## 1.1 Background

Membranes are functional semi-permeable active or passive barriers that permit the preferential passage of one or more selected species of components (molecules, particles or polymers) of a gaseous and/or liquid mixtures [1]. In due course of separation, the primary species that are rejected and retained are termed as retentate solutes and the species that pass through the membrane are termed as permeate solutes. In general, the driving force to accomplish desired separation is brought forward by the application of pressure or concentration or voltage difference across the membrane.

Initiated primary by research in the field of reverse osmosis membranes in 1980s, the past three decades have witnessed significant advances in the field of membrane separation technology. Membranes have been found to be advantageous and promising separation technology when compared to other separation technologies such as adsorption, distillation,

extraction and crystallization. In this regard, lower capital cost, higher separation factors, compact design and the elimination of secondary separation units are regarded to be some of the primary advantages of the membrane technology.

The performance of a membrane depends upon various factors such as porosity, pore diameter distributions, particle size distributions amongst the solutes that are processed in addition to the solubility/diffusivity of the permeating molecules. Therefore, membrane technology needs be studied thoroughly in order to ensure its versatility for industrial applications.

### 1.1.1 Classification of membranes

By nature, membrane can be classified into two major types, namely biological and synthetic membrane [2-4]. While biological membranes refer to those that are present in living cells and aid in cellular functional separations, synthetic membranes are those that are prepared using various materials such as solids and liquids. A conventional example for biological membrane is nephrons present in human kidney which facilitate separation of waste compounds (urea and excess sugars) from the blood in living beings.

A broad morphological classification of the synthetic membranes is presented in Fig.1.1 [3]. In general, synthetic membranes are classified into two types, namely solid and liquid membranes. Solid membranes are further classified into dense, porous and electrically charged membranes. Porous membranes possess highly void structures with random distribution of inter-connected pores in a mechanically rigid morphology. The separation occurs in these membranes due to the size difference of the particles and membrane pores. However, dense membranes consist of a dominating non-porous structure and hence separation occurs due to diffusion and activation phenomena. Electrically charged membranes

being porous or dense membranes carry fixed positive or negative charge that aid in the separation of solutions with ions. A further structural classification of various membranes indicates symmetric and asymmetric membranes. Symmetric membranes consist of a single layer with homogenous porous structure. On the other hand, asymmetric membranes possess heterogeneous membrane structure that is accomplished using two or more porous structures or layers. Typically, asymmetric membranes consist of a thin permeable layer with narrow pores on the top of a porous structure with wide pores (support). In an asymmetric membrane, while the thin film provides higher separation and permeation characteristics of the membrane, the support provides higher mechanical strength to the membrane with minimum

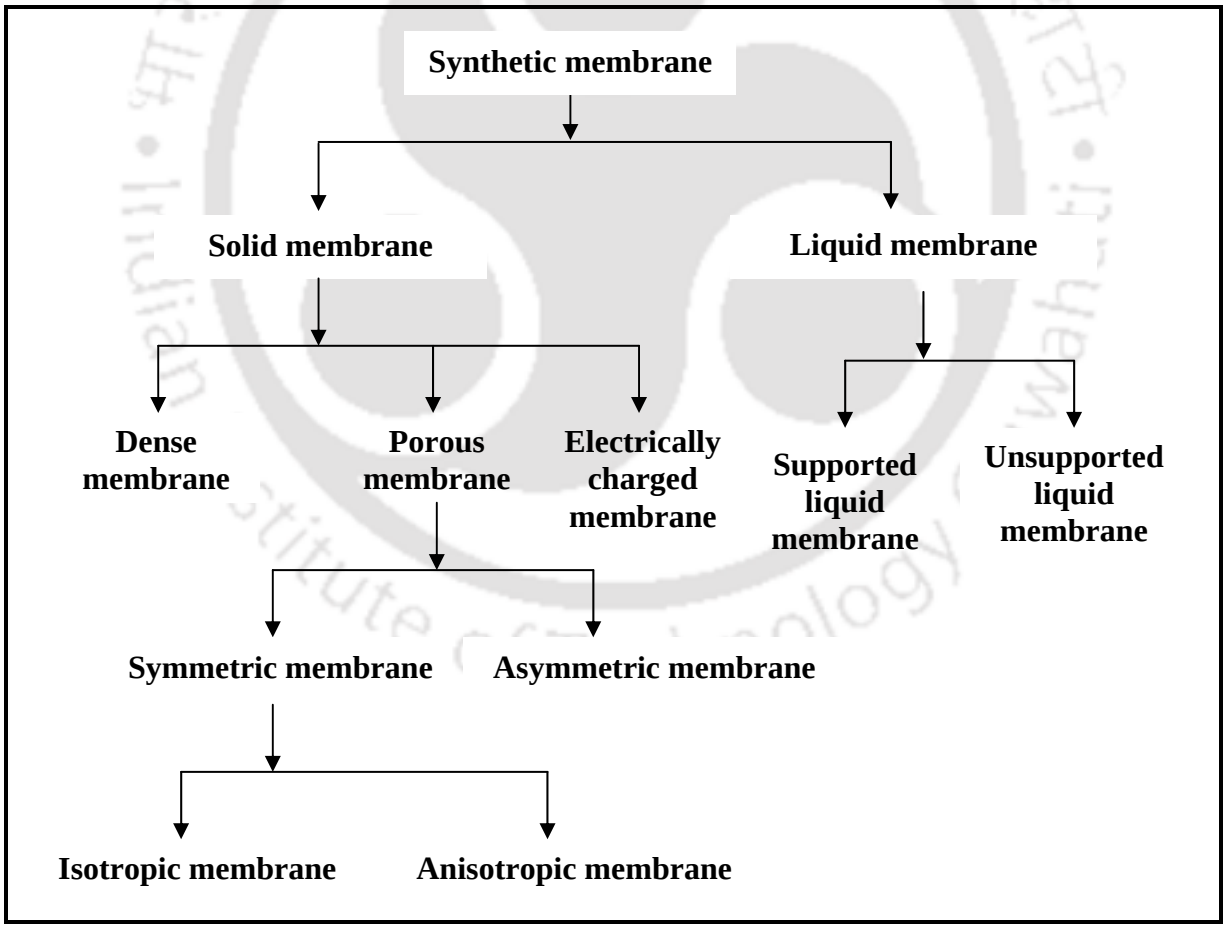


**Figure 1.1: Morphological classification of synthetic membranes [3].**

resistance to permeation. Therefore, asymmetric membranes are always regarded to be advantageous than symmetric membranes. A pore size distribution based classification indicates symmetric membranes to be either isotropic or anisotropic. While uniform membrane pore sizes throughout the membrane structure are present in isotropic membranes, varied pore sizes throughout the membrane structure are present in anisotropic membranes. Solid phase symmetric and asymmetric membranes are primarily used for pressure driven membrane separation processes. Based on the different types of materials with which these membranes are fabricated, the membranes are classified as polymeric and ceramic symmetric membranes and polymer - polymer, polymer - ceramic, ceramic - ceramic asymmetric membranes. While symmetric membranes are typically fabricated using single functional materials, asymmetric multilayered membranes are typically fabricated by depositing a thin film of polymeric, inorganic or any other suitable materials over a porous support.

### 1.1.2 Classification of membrane separation processes

Depending upon the nature of the driving force and transport mechanism of feed materials through the membrane, membrane separation processes can be classified. While some of these processes are well established in the industry, a few of them are still in experimental stages and large scale industrial applications are yet to be realized. Based on the membrane transport mechanism, various membrane separation processes can be classified as [3]

a) **Pressure driven processes:** Microfiltration (MF), ultrafiltration (UF), nanofiltration (NF) and reverse osmosis (RO).
b) **Concentration driven processes:** Gas separation through dense membranes, pervaporation (PV), dialysis, membrane extraction, supported liquid membrane (SLEM) and emulsion liquid membrane (ELM).

c) **Temperature driven processes:** Membrane distillation and thermo-osmosis.

d) **Electrically driven processes:** Electrodialysis, electrofiltration and electrochemical ion exchange.

Table 1.1 presents a summary of the solute separation characteristics of various pressure driven processes such as MF, UF, NF and RO. Typically, MF processes separate suspended particles with the membranes possesses average pore diameters in the range 0.1 – 10 μm. Therefore, particles larger than 0.1 μm are generally considered for separation using these processes. For the separation of these systems, typical pressure differentials applied are below 2.5 bar. The separation of liquid mixtures with finer particle size distributions is achieved using UF, where the pore size of the membranes varies between 0.1 – 0.01 μm (100 – 10 nm) and macromolecules such as viruses, proteins with molecular weight of 1 – 500 kDa are separated. The trans-membrane pressure differential for these processes is below 10 bar. Solutes with even lower particle size distributions are separated using NF membranes that possess pore diameters in the range 1 – 10 nm. These membranes are used for the removal of divalent ions and small molecules from solutions. Reverse omosis membranes possess smallest pore diameters and virtually all suspended and dissolved solids and ionic species are separated with trans-membrane pressure differential of 30 - 100 bar. In this work we primarily address membranes for MF and UF applications.

### 1.1.3 Industrial applications of membranes

Numerous industrial applications of synthetic solid symmetric and asymmetric membranes exist for MF and UF membranes. These are summarized as follows [2, 5]:

**Table 1.1: Pressure driven membrane separation processes and their solute separation characteristics [2].**

| Membrane process | Pore diameter ranges | Pressure (bar) | Retentate | Permeate |
|---|---|---|---|---|
| MF | 0.1 - 10 μm | 0.1 - 2.5 | Suspended particles, bacteria | Dissolved solutes, Water |
| UF | 10 - 100 nm | 2 - 10 | Large molecules, viruses, proteins | Small molecules, Water |
| NF | 1 - 10 nm | 10 - 30 | Small molecules, divalent salts, | Monovalent ions, Water |
| RO | 0.1 - 1 nm | 30 - 100 | All solutes | Water |

a) Treatment of **industrial waste streams** such as oily wastewater, pulp and paper wastewater, leather wastewaters etc., for the removal of various suspended solids in the wastewater streams.

b) Production of **drinking water** from different sources to remove various particles as well as bacteria.

c) Production of **clarified fruit juices** which possess long term storage characteristics and thereby enable the reduction of transportation costs of food products.

d) **Biotechnological applications** such as protein recovery, milk concentration and separation of fat from milk.

The industrial application of other membranes separation processes such as NF, RO, pervaporation, dialysis, electrodialysis and gas separation are presented as follows:

**a) NF and RO:** Desalination of sea water to generate drinking water, treatment of various industrial waste waters, removal of nitrates, fluorides, heavy metals etc.

**b) Pervaporation:** Separation of organic and azeotropic mixtures (such as ethanol-water) those are difficult to separate using conventional methods such as distillation.

**c) Dialysis and electrodialysis:** Removal of different harmful components from human blood during kidney failure.

**d) Gas permeation:** For the production of oxygen enriched air, nitrogen enriched air and hydrogen recovery using porous as well as dense membranes. In addition, dense membranes are used to accomplish carrier facilitated separations.

## 1.2 Major research areas in membrane technology

Membrane technology research involves numerous issues. These are listed as follows [3]:

**a)** Selection of suitable materials for membrane fabrication.

**b)** Parametric optimization of membrane preparation methods using trial and error approach in experimentation.

**c)** Characterization studies of the prepared membrane.

**d)** Identification of suitable application of the developed membrane.

**e)** Evaluation of optimal operating conditions (trans-membrane pressure, feed concentration, temperature etc.,) that enables longer lifespan of the membrane.

**f)** Evaluation of the best membrane module (tubular, disk, hollow fiber and spiral wound modules) and mode of application (dead-end, cross-flow etc.,).

**g)** Modeling and simulation of the membrane technology for design.

**h)** Cost and techno-economic analysis.

In the above list, materials research broadly constitutes (a) – (e). The five major areas of research namely materials research, applications, module development, modeling and

simulation and techno-economic/cost analysis and their evolutionary hierarchy in membrane technology research is presented in Fig. 1.2. As shown, membrane materials research is central theme which facilitates the development of conventional and novel functional materials that ensure applicability, low cost and durable performance. The membrane materials must withstand operating environments such as pH of the feed solution, temperature, pressure etc., In addition, the membranes shall also possess chemical, thermal and mechanical durability. Once these membrane materials are identified, applications that suit the membrane are thoroughly investigated. After this, membrane module development studies including module fabrication and pilot plant studies follow. Module development studies target transformation of lab scale membrane technology to industrial scale systems.

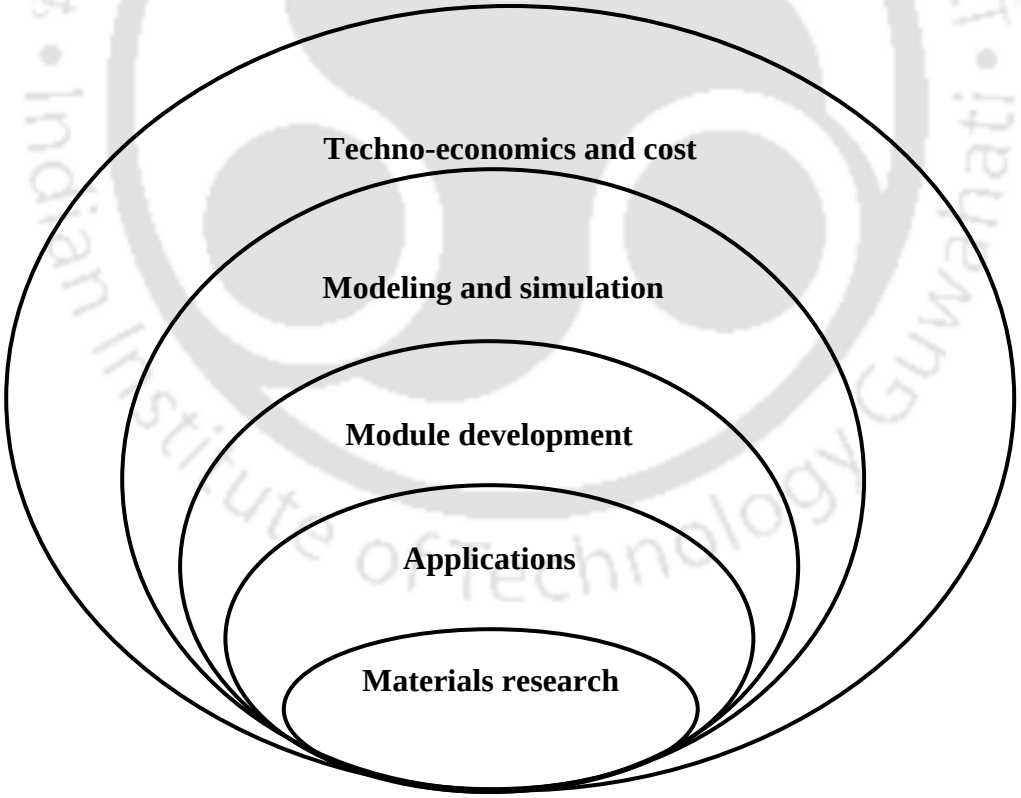


**Figure 1.2: Evolutionary nature of various key research areas in membrane separation technology.**

During this phase, the ease of operation along with the quality of the product and cost of the process are important matters for pursuing the research. Eventually, modeling and simulation of observed module performance is followed up for design purposes which are followed with techno-economic and cost analysis. While modeling and simulation aims to identify suitable models (both time dependent and independent) to correlate the experimental data with minimal error, cost estimation and techno-economic analysis provide insights upon the economics of the membrane process for its industrial and commercial feasibility. In all the above areas, membrane materials research is by far the most important and nearly two thirds of the total research activities are dovetailed towards the development of durable membranes at lower cost for both conventional as well as novel applications. Unless membranes are fabricated with effective functionality using materials research techniques, subsequent areas of research cannot be followed due to the pertinent evolutionary nature and hence industrial scale membrane separation schemes cannot be realized. Therefore, for any industrial application of membrane, emphasis is upon the development of suitable membrane materials. Ideally, the developed membrane shall possess a good combination of permeation and separation characteristics for the chosen application along with good corrosion resistance and mechanical strength.

## 1.3 Membrane materials and trade offs

Polymeric materials and ceramics are the most widely used functional membrane materials to prepare symmetric membranes for industrial scale applications. The asymmetric membranes are usually prepared from symmetric polymeric or ceramic membrane materials or both. In an asymmetric membrane, usually the support layer provides desired mechanical strength and the thin skin layer constituting either polymeric or ceramic materials caters towards the desired

separation characteristics. As inevitable, these materials have various pros and cons and hence tradeoffs. These are further elaborated in this section.

### 1.3.1 Polymeric membranes

Polymeric membranes are thin films of 10 - 100 μm thickness. Different types of polymers such as polysulphone (PSU), cellulose acetate (CA), polyamide (PA), polyethersulphone (PES), polyvinylidene fluoride (PVDF), polyacrylonitrile (PAN), polytetrafluoroethylene (PTFE), polyetherimide (PEI), polypropylene (PP) are used widely to fabricate polymeric membranes. Some of the common **advantages for polymeric membranes** are [3]:

**a)** Wider ranges of pore sizes varying from MF to RO are available.

**b)** Both hydrophobic and hydrophilic membranes are available to minimize fouling during filtration.

**c)** Comparatively low cost than ceramic membrane.

**d)** They are easy to fabricate and use.

**e)** Ease to scale up.

However there exist some basic **disadvantages** of polymeric membranes such as

**a)** Low solvent resistance.

**b)** Lower applicable range of pH and hence low corrosion resistance.

**c)** Low temperature ranges.

**d)** Lower life span (12 – 18 months).

In the recent times, modified polymeric membranes have been developed that can cater towards wider pH ranges. However, their corrosion resistance and resistance to organic solvents have not been resolved to an extent of providing confidence in industrial applications.

### 1.3.2 Ceramic membranes

Typically ceramic membranes are made of various inorganic materials such as α - alumina, γ - alumina, zirconia, silica, titania, kaolin etc. Compared to polymeric membranes, ceramic membranes possess superior chemical, thermal and mechanical stability. The thickness of ceramic membrane is in the range of 2 - 5 mm and some times higher depending on the specific applications. Asymmetric ceramic membranes constitute thin film (10 - 100 μm) of ceramic coating over a thick porous symmetric support.

Some common **advantages for ceramic membranes** are [3];

**a)** Very high corrosion resistance. There exist very few chemicals such as hydrofluoric acid and phosphoric acid for which the ceramic membranes don't have high corrosion resistance. The most useful feature of the ceramic membranes is their ability to tolerate strong doses of chlorine (up to 2000 mg/L in certain cases).

**b)** Applicability to wider pH ranges (0.5 - 14).

**c)** Applicability to wider temperature ranges (350 – 500 $^{o}$C). As a result they are used in industrial scale separations without any feed pre-conditioning steps.

**d)** Longer life span (5 - 10 years). There are many ceramic systems in industry that are operating after 10 - 14 years of installation.

**e)** Less fouling tendency.

**f)** Inertness to common chemicals and solvents.

**g)** Higher mechanical strength.

Since these membranes do not get seriously affected by the frequency and nature of cleaning, they can be subjected to aggressive cleaning agents and regimes, which is very much prevalent in industrial chemical processing units.

However, there exist few **drawbacks of ceramic membranes**. They are presented as follows.

**a)** Most ceramic membranes are available in pore diameters within the MF and UF range (0.010 - 10 μm). In the recent years, few literatures presented the fabrication of NF membranes. Therefore, ceramic membranes are not generally applicable for separation schemes with NF and RO.

**b)** Comparatively higher cost. For instance, 1996 cost indices of polymeric spiral wound modules and ceramic systems were 50 - 100 $/m$^2$ and 500 - 3000 $/m$^2$, respectively. These costs including controls, pumps and fittings were estimated to be 225 - 350 $/m$^2$ and 2200 - 3600 $/m$^2$ for polymeric and ceramic membranes [3], which indicates a ten fold higher cost of ceramic membranes when compared with the polymeric membranes. Though the price of ceramic membranes may have reduced in due course of time, these costs have not been very competitive with polymeric membranes. Therefore, it is expected that the cost of ceramic membranes will be still higher to the extent of 2 - 3 orders of magnitude.

**c)** They are brittle in nature. If dropped or subjected to undue vibrations it may be damaged.

### 1.3.3 Polymeric vs. ceramic membranes

Considering the advantages and disadvantages of both membranes, it can be observed that polymeric membranes are very much useful for laboratory scale use. For laboratory scale use, applicability of the membrane technology towards any particular separation is the main aim but not their life span and cost. However, for industrial scale applications, cost and life span are the most relevant matters along with the separation efficiency. For most of the applications, the life span is evaluated as 12 - 18 months (extendable to 36 months by adopting optimal cleaning schemes) and 10 years for polymeric and ceramic membranes,

respectively [3]. Therefore, though ceramic membranes involve higher initial costs, their ability to provide higher flux and applicability to wide range of temperatures and chemical processing conditions could favor them to be the choice in contrary to the polymeric membranes. Though ceramic membrane possesses separation characteristics similar to polymeric membranes, due to higher cost, they are not yet widely applied in industrial scale applications. Under these circumstances, the development and usages of comparatively low cost ceramic membranes (200 - 400 $\$/m^2$) with longer life span (10 - 15 years) is anticipated to drive the economic competitiveness of ceramic membranes in the industry.

### 1.3.4 Polymer - ceramic composite membranes

Polymer-ceramic asymmetric composite membranes partly overcome some of the disadvantages of ceramic and polymer symmetric membranes. The asymmetric membranes possess wider pore size ranges achieved through the polymeric film layer deposited on the top of a ceramic support possessing higher chemical, mechanical and thermal stability. In addition, the asymmetric membranes use an optimal combination of both polymeric and ceramic membrane layers and hence the cost. Therefore, polymeric ceramic membranes perform widely better than the polymeric symmetric membranes with a marginally higher life span. These features accompanied by marginally higher cost (cost of ceramic support) are beneficial for applications where polymeric membranes are favored than the ceramic membranes. These applications include NF, RO, pervaporation, and gas separation.

## 1.4 General methods for membrane preparation

This section presents an overview of various membrane preparation methods for ceramic symmetric and asymmetric membranes, symmetric polymeric membranes and polymer-

polymer and polymer-ceramic asymmetric membranes. Polymeric membrane preparation methods are not discussed here as the present thesis does not deal with the subject matter.

### 1.4.1 Symmetric ceramic membranes

Symmetric ceramic membranes are fabricated using uni-axial and paste methods [6, 7]. Both these methods involve the preparation of an inorganic mixture using suitable pore forming organic and inorganic materials along with binder materials. The uni-axial method involves casting an inorganic mixture in a suitable disk or tubular shape and kept under very high pressure (30 - 50 MPa). Subsequently, the disk or tubular type mould is sintered to prepare the membrane. The paste method involves the preparation of a paste using the inorganic mixture using suitable solvent which is eventually casted into suitable shape and sintered at high temperature. The properties of the ceramic membrane are largely influenced by the composition of the raw materials, sintering temperature and process including the schedule of heating, sintering and cooling.

### 1.4.2 Asymmetric ceramic membranes

Asymmetric ceramic membranes are prepared by the deposition of thin film of inorganic materials over the porous symmetric ceramic membranes (support). Slip coating followed with casting, sol-gel and dip coating methods are usually deployed for the fabrication of asymmetric ceramic membranes whose properties are dependent upon both support as well as thin skin layer morphology [6, 7]. The slip coating-sintering process involves coating the support surface with a suspension of finer particles in a solution of a cellulosic polymer or poly vinyl alcohol that acts as a binder and viscosity enhancer to hold the particles in the suspension. Subsequently, the membrane is dried and sintered at high temperatures to obtain a

fine microporous surface layer. Usually, several slip-coated layers are applied in series with each layer formed from a suspension of progressively finer particles to yield an isotropic structure. Many commercial ceramic UF membranes are made using slip-coating technique to achieve skin layer pore diameters upto 100 - 200 $^{o}$A. Membranes with even finer pore sizes are fabricated using the sol-gel technique. The sol-gel process involves the transition of the slip coating technique to the colloidal level. The colloidal or polymeric gel solutions of an inorganic hydroxide are initially prepared using controlled hydrolysis of metal salts or metal alkoxides. The particulate-sol method involves the dissolution of alkoxide dissolved in alcohol is followed with the hydrolysis by addition of excess water or acid. The precipitate thus obtained is maintained as a hot solution for extended time periods to yield a stable colloidal solution. The colloidal solution is then cooled and coated onto the microporous membrane support. Later, the membrane is carefully dried to avoid surface defects such as cracks and sintered at 500 - 800 $^{o}$C. During dip coating process, the support is dipped in an inorganic suspension and the inorganic materials penetrate through the pores of the support and as well as deposit over the support surface. Subsequently, the membrane is dried and sintered at high temperature.

### 1.4.3 Polymer - ceramic composite membranes

Polymer-ceramic composite membranes are prepared by deposition of polymeric film over a porous ceramic support. Polymer-ceramic composite membranes characterized with superior combinations of structural integrity, fouling resistance, flux and selectivity have been reported for the UF [8-10] and pervaporation (PV) [11-15] applications. These membranes constitute a polymer skin layer consisting of polysulfone [9], styrene acrylonitrile [10], poly vinyl acetate (PVAc), poly vinyl pyrrolidone (PVP) [11], cellulose acetate (CA) [12], polydimethylsiloxane

(PDMS) [15, 16] and ceramic supports with nominal pore sizes of 0.2 – 2 μm made from kaolin [10], alumina [11] and zirconia [16]. There are several methods available for the preparation of polymer - ceramic composite membrane such as spray coating [10], grafting [11], spin coating [12], self assembly [14], dip coating [16] and vapor deposition [17]. The dip coating technique involves dipping the ceramic membrane support in the polymeric sol for a specified amount of time to yield the polymer-ceramic membrane. Spray coating, spin coating and self assembly are modified versions of dip-coating technique and are applied depending upon various issues such as the physio-chemical properties of the polymeric sol as well as the ceramic support. While spray coating involves spraying the polymeric sol onto the support, spin coating involves rotation of the support in a polymeric sol. Graft polymerization method involves three steps namely pretreatment, surface activation and grafting the polymer over the support. Therefore, though the method is efficient, it is marginally complicated when compared to other fabrication methods. The vapor deposition method involves deposition of the polymeric film by condensation of vapor on the membrane support. Among several fabrication methods outlined, dip coating method is simple, inexpensive and most desirable choice for industrial applications. This is due to the fact that dip coating techniques involves simple fabrication set up which can be used along with an optimal combination of dip coating parameters such as concentration of the polymer, support morphology and time of dip coating to yield the polymer-ceramic composite membrane within a very short span of time.

## 1.5 State of the art

With a brief overview of the contemporary research, this section outlines the research outcome of various literatures so as to identify few promising areas of research that needs to

be addressed in this thesis. The state of the art has been presented for ceramic membranes and polymer-ceramic membranes as these membranes appear to be more promising due to their advantages over the polymeric symmetric and asymmetric membranes.

### 1.5.1 Preparation of ceramic membranes

***Literature survey***

Numerous literatures report the preparation of ceramic membranes using α - alumina, [18 - 20, 21], γ-alumina, zirconia, titania and silica [18, 22 - 24]. The cost of these membranes are significantly high due to the higher costs of the precursors used for the preparation of these membranes. Therefore, these membranes posses higher installation costs that may not be affordable for industrial separation schemes. In addition, most of the literatures indicate that very high sintering temperatures (more than 1100 $^{o}$C) are required for membrane preparation [18 - 24]. The maintenance of high sintering temperature during fabrication process in turn demands higher electrical energy and hence operating costs during fabrication. In addition, higher sintering temperatures may also give rise to enhancement in furnace power specifications and installed cost. Due to these key issues, the economic competitiveness of the inorganic membranes has not been appreciable till date to drive their industrial sustainability.

To circumvent the higher costs of inorganic membranes, existing and ongoing research in the preparation of low cost inorganic membranes are dovetailed towards the usage of low cost inorganic precursors and lower sintering temperatures (below 1000 $^{o}$C). However, these variants in ceramic membrane research need to guarantee cheaper membranes that have the inherent ability to provide consistent performance along with longer life time, in similarity to the existing expensive ceramic membranes. Recently, much work have been reported for the fabrication of inorganic membranes using cheaper raw materials such as apatite powder [25],

**Table 1.2: Summary of literatures on preparation of symmetric MF membranes.**

| Materials | Sintering temperature ($^oC$) | Average pore diameter (μm) | Reference |
|---|---|---|---|
| α -Alumina | 1600 | 1.2 | [20] |
| α -Alumina | 1130 - 1300 | 0.1 - 0.2 | [21] |
| α -Alumina | 1300 - 1500 | 0.17 - 0.15 | [24] |
| Zirconia | 1300 - 1500 | 0.11 - 0.08 | [24] |
| Apatite powder | 1150 - 1200 | 5 - 8 | [25] |
| Cordierite | 1600 | 10 | [20] |
| Cordierite | 1275 | 7 | [26] |
| Fly ash | 1100 - 1130 | 4 - 4.9 | [27] |
| Fly ash | 1380 | 18 | [28] |
| Natural clay | 1100 - 1250 | 9.3 - 10.75 | [29] |
| Natural clay | 1190 | 9.2 | [30] |
| Dolomite and kaolin | 1150 -1 300 | 1.65 - 48.53 | [31] |
| Kaolin and hycast clay | 1100 | 1.3 | [32] |
| Kaolin and Al(OH)3 | 1500 - 1550 | 1.16 - 1.52 | [33] |
| Kaolin, $CaCO_3$, quartz | 850 - 1000 | 0.7 - 1.54 | [34] (Present work) |
| Kaolin, feldspar, quartz | 800 - 950 | 0.185 - 0.332 | [35] (Present work) |

cordierite [20, 26], fly ash [27, 28], natural raw clay [29, 30], dolomite [31] and kaolin [32, 33]. Table 1.2 summarizes the details of raw materials, average pore size and sintering temperature used in these works. From the table it can be observed that for all the cases, the sintering temperature used was more than 1100 $^oC$ and the average pore size of the membranes was more than 1 μm (except for alumina).

It is equally well known that MF membranes with pore size in the submicron range (pore sizes < 1 μm) are preferred for the industrial application to obtain excellent solute separation

efficiency. With regards to the lower ranges of submicron range ceramic membranes (pore sizes ranging from 0.1 – 0.5 μm) available so far, it is also equally important to note that these ceramic membranes consist of an asymmetric membrane structure. These asymmetric membranes typically consist of a submicron skin layer prepared using zeolite [36, 37], zirconia, alumina [26, 29] and titania [38 - 40] on either single or several layers of macroporous structures. Though such an approach favors the reduction of the material cost of the membrane by limiting the thickness of the skin layer, the utilization of expensive precursors such as zeolite and alumina to fabricate the submicron size skin layer contributes to the overall cost of the membrane. In addition, preparation methods for asymmetric membranes in contrast to the symmetric membranes involve additional fabrication complexities that also contribute to the overall cost. Therefore, the preparation of low cost symmetric ceramic membranes with submicron range pore size will be the more economically favorable to the membrane based process industries.

***Possible scope for further research***

A critical review of the above publications and other relevant research findings convey the following conclusions for the fabrication of inorganic membranes. Firstly, there is a need to develop alternate formulations that could provide breakthrough to the development of symmetric inorganic membranes possessing pore size of about 0.5 - 1 μm without using expensive inorganic precursors. Secondly, if a ceramic membrane is prepared by using expensive inorganic precursor formulation, such formulation should contain small quantities of expensive inorganic precursors and larger quantities of inexpensive inorganic precursors. Thirdly, the fabrication of the inorganic membrane with a processing temperature below 1000 $^{o}$C needs to be experimentally tested and verified. The reduction in maximum sintering

temperatures to values below 1000 $^{o}$C would be beneficial for additional cost reduction of membrane fabrication process. Fourthly, the prepared ceramic membrane should provide excellent combination of thermal, mechanical and chemical stability in addition to good separation characteristics for chosen MF and UF applications. In a similar way, the fabrication of a symmetric ceramic MF membrane possessing lower submicron range average pore size (0.1 - 0.5 μm) using low cost inorganic precursors and sintering temperature lower than 1000 $^{o}$ C also needs to be addressed.

## 1.5.2 Preparation of polymer - ceramic composite membranes

***Literature survey***

Experimental research has also been carried out resolve the drawbacks of polymeric membranes and ceramic membranes and to yield polymer - ceramic composite membranes that possess the good characteristics of both polymeric as well as ceramic membranes. Different types of composite membranes such as polymer - polymer, ceramic - ceramic and polymer - ceramic composite membrane have been fabricated. These membranes constitute a polymer skin layer of polymers (eg. polysulfone [8], styreneacrylonitrile [9], polyvinylacetate, polyvinyl pyrrolidone [10], cellulose acetate (CA) [11], polydimethylsiloxane (PDMS) [15, 16]) or inorganic materials (like zeolite, alumina, titania, zirconia etc) over a macroporous polymeric or ceramic support. The primary target for these membranes are to improve corrosive resistance, pH limitation and solvent resistance power for polymeric membranes by modifying the structure of the membrane as well as pore diameters of wider ranges for ceramic membranes. These membranes possess superior combinations of structural integrity, fouling resistance, flux and selectivity when compared to the polymeric or ceramic symmetric membranes.

Numerous articles demonstrated the utility of dip coating technique for the preparation of ceramic - ceramic, polymer - ceramic and polymer - polymer composite membranes. In the field of polymer - ceramic composite membranes, Matsumoto et al., [9] has prepared sulfonated polysulfone - ceramic composite membrane suitable for UF. Song and Hong [12] fabricated cellulose acetate - ceramic membrane using dip coating and rotation drying technique using a ceramic support with an average pore size of 100 nm. The composite membrane was prepared using CA solution concentration of 20 % and was tested for the dehydration of ethanol and isopropanol. Hong and Hong [15] prepared PDMS - ceramic membrane by dip coating method using 20 - 30 wt % polymer concentrations on a ceramic support having average pore size of 370 nm and applied it for the pervaporation (PV) of IPA/water mixture. Similarly, Sachdeva and Kumar [10], Xiangli et al., [16], Aranda et al., [41], Rezac and Koros [42] prepared polymer - ceramic composite membranes using different polymer precursors and commercial ceramic supports to suit UF and PV applications. These works infer that an optimal combination of preparation conditions such as polymer solution concentration, dipping time and cross linking agent concentration (if any) yields composite membrane with superior performance characteristics. Further, membrane permeance or hydraulic resistance was taken as an index to quantify the polymer/ceramic film growth rate and thereby identify optimal combinations of membrane porosity, film thickness and average pore size. Gu and Meng [43], Babaluo et al., [44] and Lev¨anen et al., [45] presented mathematical models supported with experimentation to conclude that the ceramic film growth rate (or membrane hydraulic resistance) on a ceramic support was proportional to the square root of dipping time. Xiangli et al., [29] presented nonlinear models to express the flux (and hence hydraulic resistance) and selectivity of the polymer - ceramic composite

membrane as functions of dip coating parameters such as polymer concentration, cross linking agent concentration and dip coating time using response surface methodology. However, the physical mechanisms that occur during dip coating process have not been analyzed quantitatively to evaluate their contribution towards the properties of the composite membrane such as morphology and transport properties.

***Possible scope for further research***

A critical review of the above publications and other relevant research findings convey the following conclusions for the fabrication of polymeric ceramic composite membranes. Firstly, use of low cost ceramic support rather than using alumina based costly support shall be encouraged to minimize the cost of the composite membrane suitable for industrial competence. Secondly, membrane preparation method needs to be simple and inexpensive with minimal instrumentation without compensating on the desired precision. For this cause, dip coating technique could be a better choice in comparison with other alternative methods such as polymer grafting and spin coating. Dip coating technique also provides opportunities to explore the impact of coating parameters such as polymer concentration in solution and dipping time during the fabrication of composite membrane to obtain membranes with specific pore diameter. Hence, research in this direction should be encouraged. Finally, conceptual phenomenological models have to be developed that enable to quantify the dependency of membrane morphology on the optimality of dip coating parameters as well as ceramic composite membrane performance. These approaches could identify potential pathways for furthering the industrial competitiveness of the polymer-ceramic composite membranes.

### 1.5.3 Applications of membrane technology

To date, both polymeric and ceramic membranes have been found to be suitable in various pressure driven membrane separation applications (MF, UF, NF and RO) such as desalination, food processing, colored effluent treatment, drinking water purification and treatment of industrial wastewater [2, 5]. Among these, while desalination is applicable for NF and RO membranes, all other applications can be regarded to be accomplished by the using MF and UF membranes. Since this work attempts to present research emphasis on low cost ceramic membranes, we consider two major applications such as treatment of industrial oily wastewater streams and juice processing as two most significant applications. This is also due to the fact that these two applications have highly diversified challenging tasks for the membrane technology. While the treatment of wastewater streams requires the production of permeate streams with lower concentration of waste product concentrations, the juice processing application involves careful permeation of all desired components through the membrane filters to achieve a high quality permeate juice that is bereft of pectins and other colloidal suspensions. Therefore, we consider to study the state of the art in the treatment of wastewater and clarifications of fruit juices using membrane technology.

#### 1.5.3.1 Treatment of oil-in-water emulsions

***Literature survey***

Various process industries such as petroleum refineries, petrochemical industries, metallurgical, transportation and food processing industries produce large volumes of oily wastewater. Typical composition ranges of produced oil-in-water (o/w) emulsions vary between 50 - 1000 mg/L of total oil and grease and 50 - 350 mg/L of total suspended solids [46]. Existing tolerance limits of total oil and grease concentrations in wastewater streams is

about 10 - 15 mg/L [46]. To achieve the desired discharge limits, conventional processes such as thermal de-emulsification, biological methods and chemical treatment methods [47-49] are effective for the treatment of o/w waste streams with high feed concentrations (500 - 5000 mg/L). On the other hand, due to the existence of smaller droplet sizes (<1 μm) of the emulsions for lower feed concentrations (50 - 500 mg/L), these methods are ineffective for the removal of oil [50, 51]. Amongst various alternative technologies plausible for such applications, membrane technology is promising due to several advantages such as lower capital cost, higher separation factors, compact design and the elimination of other chemical and mechanical treatment units such as mechanical separation, filtration and chemical de-emulsification [52].

To date, several articles have been published illustrating the excellent potential of polymeric [46, 53 - 55] and ceramic [56 - 59] membranes for the treatment of o/w emulsions. As polymeric membranes are sensitive to both polar and chlorinated solvents, pH and high oil concentrations, they are highly susceptible to fouling and degradation during operation and eventually needs to be replaced frequently. Therefore, the operating cost increases significantly [47]. In addition, each polymeric membrane has its own solvent compatibility and weakness to specific chemicals present in the permeating liquid. For instance, cellulose acetate membranes are severely affected by the presence of chlorine and solvents such as acetone and aniline [2]. Due to this, polymeric membranes possess shorter life span in industrial applications. On the other hand, due to their inherent chemical, thermal and mechanical stability, zirconia [56, 57] and alumina [59] based ceramic membranes are less prone to fouling. Therefore, ceramic membranes offer longer life span and are found to be promising for the treatment of o/w emulsions for industrial scale operation as well [56].

***Possible scope for further research***

Most of the literatures that report the treatment of oily wastewaters address several process technological solutions for feed oil concentrations varying between 500 - 2000 mg/L [47]. These feed systems consist of unstable oil droplets whose sizes are higher than 50 μm and are hence easily removed [53]. However, lower droplet sizes (less than 10 μm) exist for feeds with oil concentrations below 100 mg/L. These oil droplets have been reported to be highly stable and their separation is anticipated to be a challenging one [54]. Therefore, it is very likely that the oil concentrations in discharged process wastewater streams from effluent treatment plants fail to comply with the allowable discharge limits of 10 mg/L [46]. For such complicating scenarios, ceramic membrane technology could provide technological solutions. To the best of our knowledge, the applicability of low cost ceramic membranes to treat wastewaters consisting of oil concentration below 250 mg/L has not been studied till date. This work attempts to address these issues using low cost submicron range ceramic membranes. In addition, the effect of pore size on the performance of submicron range membranes is also one of the subsequent aims of this work.

### 1.5.3.2 Clarification of mosambi juice

***Literature survey***

Fruit and vegetable juices are beverages of high nutritional value. These beverages constitute several key components beneficial for human health such as minerals, vitamins and antioxidants. Traditional methods for juice processing involve filtration using fining agents such as gelatin or diatomaceous earth to remove suspended and colloidal particles and low pressure evaporation [60]. Unfortunately during these processing steps, a major portion of the compounds that contribute towards the quality of the beverage (such as aroma, flavor

compounds, sugar content and acidity) get deteriorated due to thermal and chemical treatment steps [61]. In this regard, the application of membrane technology is found to be beneficial when compared with the conventional methods due to elimination of thermal and chemical processing steps, low energy requirement, lower processing times and ease of scaling up without significant change in juice quality [2]. UF and MF of mosambi [62, 63], orange [64, 65], lemon [66], grape [67], apple [68 - 70], carrot [71], water melon [72, 73], blood orange [74] and pineapple [75] juice have been studied by many investigators. Amongst several beverage processing sectors, citrus fruits constituting orange, lemon, pineapple and mosambi are prominent due to their wider availability, low cost as well as high nutrition value to human health. Citrus fruits primarily constitute both lower molecular weight compounds (such as sugar, acid, salt, flavor, aroma compounds, etc.) as well as higher molecular weight polysaccharides (such as pectic material, cellulose, hemicellulose etc.) in addition to haze causing proteins and microorganisms. The presence of pectic material and protein in fruit juice is responsible for cloudiness and post bottling haze formation as well as their fermentation during long storage [2]. The objective of clarification of fruit juice using membrane filtration is to eliminate the high molecular weight pectic material and its derivatives and retain low molecular weight solutes (valuable for human health) such as sucrose, acid, salt, aroma and flavor compounds in the clarified juice [2].

Rai et al., [76] identified optimal conditions (pectinase concentration: 0.0004 w/v%, heating temperature: 42 $^{o}$C, duration: 100 min,) for enzymatic treatment of mosambi juice. Amongst several treatment methods, the authors indicated that, enzymatic treatment followed by bentonite addition provided the highest permeate flux (23 L/m$^2$.h at 414 kPa and 1200 rpm in a stirred cell) using 50,000 molecular weight cut-off (MWCO) polyamide (polymeric)

membranes. Cassano et al., [74] conducted UF of blood orange juice using commercial tubular polyvinylidenefluoride membranes. They observed that with an increase in operating temperature from 21 - 25 $^{o}$C, 12 % increase in permeate flux occurred. Jesus et al., [64] carried out RO of orange juice using polysulphone/polyethylene composite membrane. They observed that orange juice concentrated by reverse osmosis had a better-preserved characteristic aroma when compared to the juice concentrated by thermal evaporation. Recently, Sarkar et al., [62] studied electric field assisted UF of mosambi juice using polyethersulfone membranes. They observed that the application of electric field reduced membrane fouling and increased permeate flux significantly. Two key factors that influence the permeation characteristics of membranes for beverage processing are the average particle size of the beverage feed and the average pore size of the membrane. The selection of appropriate average pore diameter ($d_l$) for polymeric membranes and ceramic membranes has been investigated by several authors. Rai et al., [63] observed that polymeric membranes with higher $d_l$ did not influence the permeate quality to a large extent during UF of depectinized mosambi juice. However, a ten fold enhancement in membrane flux was observed when $d_l$ of the membrane varied from MWCO of 10 kDa to 0.2 μm. A similar observation has been reported by Youn et al., [68] after conducting UF and MF studies on reconstituted apple juice using two different membranes (MWCO 30 kDa and $d_l$ of 0.01 μm) and different filter-aid pre-treatment steps. Though significant quality variation was not observed, the membrane flux for the MF membrane was observed to be two to three folds higher than the flux obtained with the UF membrane. Jegatheesan et al., [77] reported the performance of zirconia ceramic membranes with $d_l$ of 0.02, 0.05 and 0.10 μm during UF of sugarcane juice. The authors thereby inferred that the juice quality obtained from all three membranes are comparable and

membranes with pore sizes 0.02 - 0.05 μm provided better quality than the membrane with 0.10 μm. Also, the average permeate flux for 0.05 μm membrane was about 1.8 times higher than that obtained for 0.02 μm membrane. Barros et al., [78] reported the performance of polysulfone hollow fiber membrane (100 kDa) and alumina-titania ceramic tubular membrane (0.01 μm) for the clarification of pineapple juice. Similar juice quality was obtained for both the membranes. A higher membrane flux was observed for the ceramic membrane (90 - 150 $kg/m^2.h$) compared to the polymeric membrane (30 - 50 $kg/m^2.h$).

***Possible scope for further research***

A critical insight into the above literatures infers that mainly polymeric membranes have been studied during experimental investigations. This is due to the fact that polymeric membranes are inexpensive in comparison with the ceramic membrane and are very easy to use. However, the major drawback of polymeric membrane is their low corrosion resistance in acidic media and hence they possess lesser life cycle times for juice processing applications. For any industrial application the lifespan of membrane is always a major issue. Many varieties of fruit juices are acidic in nature with pH in the range of 3 - 5. Henceforth, though experimental studies indicate the successful applicability of polymeric membranes for juice processing applications, industrialization of membrane technology for juice processing has not been promising so far. For these circumstances, the usage of ceramic membranes with high corrosion resistance in both acidic as well as basic media shall be more beneficial, especially in the citrus juice sector. Vladisavljevic et al., [70] carried out UF of depectinized apple juice using commercial zirconia ceramic membranes. Jegatheesan et al., [77] reported the performance of commercial zirconia-alumina ceramic membranes with various pore sizes (200, 500 and 1000 nm) for the UF of sugarcane juice. However, the clarification of mosambi

juice using a ceramic membrane, particularly low cost ceramic membrane has not been studied and is the main objective of this study.

## 1.6 Objectives of present study

Based on the state of the art presented in sections 1.5.1, 1.5.2 and 1.5.3, the present PhD thesis incorporates the following major objectives were identified.

1. Preparation and characterization of symmetric low cost submicron range ceramic membrane.
2. Treatment of oily wastewater using prepared ceramic membrane.
3. Microfiltration of mosambi juice using prepared ceramic membrane.
4. Preparation of low cost polymer-ceramic composite membrane.

## 1.7 Organization of the thesis

**Chapter 2** presents a detailed account of the preparation and characterization of low cost symmetric ceramic membranes with upper (0.5 – 1 μm) and lower (0.5 – 0.1 μm) submicron range average pore size. The functional attributes of raw materials, membrane preparation method are outlined first followed with characterizations of the membrane. Subsequently, the effects of sintering temperature on the morphological properties of the membranes such as average pore diameters, porosity and hydraulic permeability have also been addressed.

**Chapter 3** addresses studies upon the application of the fabricated upper range submicron membrane for the MF of synthetic o/w emulsions. Subsequent flux decline phenomena along with the identification of suitable membrane fouling mechanism have been presented.

**Chapter 4** presents results obtained from the MF studies of mosambi juice clarification using prepared upper range submicron membranes. The effects of membrane morphological parameters on the permeate flux and juice quality was investigated. Subsequent flux decline phenomena along with the identification of suitable fouling mechanism have been elaborated. Finally, phenomenological models were proposed to illustrate the dependency of total hydraulic resistance of membrane on membrane morphological parameters, trans-membrane pressure drop and filtration time.

**Chapter 5** addresses the application of fabricated lower range submicron membrane towards the treatment of synthetic o/w emulsions as well as mosambi juice MF. Subsequently, flux decline phenomena along with the identification of suitable membrane fouling mechanism have been presented. Finally, comparative assessment of the performance of upper and lower submicron range membranes has been summarized to identify the suitability of the membranes in both applications.

**Chapter 6** summarizes results obtained from the studies targeted to evaluate the impact of dip coating parameters on the morphology as well as permeation characteristics of low cost polymer-ceramic composite membranes. Phenomenological models targeting the application of hydraulic resistances in series models have also been discussed to identify the impact of support morphology and dip coating parameters on the permeation characteristics of the polymer - ceramic composite membranes.

**Chapter 7** presents various conclusions drawn from the research work. It also provides possible directions for future work.

# Chapter 2:

## Preparation and Characterization of Ceramic Membranes

# Preparation and Characterization of Ceramic Membranes

*This chapter presents studies on the identification of low cost inorganic precursor formulations that can yield inexpensive symmetric ceramic membranes with nominal pore sizes less than 1 μm. Two different inorganic precursor formulations namely composition A and composition B were identified to yield defect free submicron range ceramic membranes. The sintering temperature during membrane preparation was kept below 1000 $^{o}$C. Structural and morphological studies of the prepared membranes were carried out to evaluate the general characteristics of the membranes. Both liquid and gas permeation experiments were carried out to evaluate the membrane performance. Chemical stability study of the membrane was also performed to verify the corrosive resistance. Finally, the cost analysis of the prepared membranes was carried out to compare the membrane cost with the cost of other similar membranes available in literatures.*

## 2.1 Experimental

### 2.1.1 Raw materials

The selection of suitable raw materials and their relative compositions is the most important aspect for the fabrication of ceramic membrane. Different functional properties of the membrane depend upon the raw materials and hence the choice of raw materials and their composition eventually influence membrane morphological parameters. In this work, two types of membranes were prepared by two different compositions of inorganic precursors namely composition A and composition B. Composition A constitutes six common inorganic

**Table 2.1: Raw materials composition (wet and dry basis) of ceramic membranes.**

| Material | Composition A (wt %) | | Composition B (wt %) | |
|---|---|---|---|---|
| | wet basis | dry basis | wet basis | dry basis |
| Kaolin | 29.63 | 40 | 37.04 | 50 |
| Quartz | 11.11 | 15 | 11.11 | 15 |
| Calcium carbonate | 18.52 | 25 | 0 | 0 |
| Feldspar | 0 | 0 | 11.11 | 15 |
| Sodium carbonate | 7.40 | 10 | 7.41 | 10 |
| Boric acid | 3.71 | 5 | 3.7 | 5 |
| Sodium metasilicate | 3.71 | 5 | 3.7 | 5 |
| Water | 25.92 | 0 | 25.93 | 0 |

raw materials such as kaolin, quartz, calcium carbonate, sodium carbonate, boric acid and sodium metasilicate. Composition B was prepared using kaolin, quartz, feldspar, sodium carbonate, boric acid and sodium metasilicate. The formulations for composition A and composition B are summarized in Table 2.1. These formulations were determined from trial and error fabrication procedures through experimentation. It is further interesting to note that to date lower submicron range symmetric membranes prepared from low cost precursors was not addressed and this work uniquely contributed to the same.

Kaolin and sodium metasilicate were obtained from *CDH, India*. Feldspar was obtained from *National Chemicals Ltd, India*, Quartz was collected from *Research Lab Fine Chem Industry, India*. All other inorganic precursors such as calcium carbonate, boric acid, sodium carbonate were obtained from *Merck, India*. All these raw materials used for inorganic membrane preparation were graded at least 99.5 % pure and were used without further purification.

Various raw materials used in this work for the fabrication of inorganic membrane serve for different functional attributes. Kaolin and feldspar provide low plasticity and high refractory

properties to the membrane. Quartz contributes to the mechanical and thermal stability of the membrane. The regulation of porous texture in the ceramic was achieved by calcium carbonate ($CaCO_3$) and sodium carbonate ($Na_2CO_3$). These materials under sintering conditions would dissociate into calcium oxide (CaO) and sodium oxide ($Na_2O$), respectively and release $CO_2$ gas. The path taken by the released carbon dioxide ($CO_2$) gas thereby created the porous texture of the inorganic membrane and contributed to the membrane porosity during the sintering process. On the other hand, sodium carbonate and boric acid act as a colloidal agent and improved dispersion properties of the inorganic precursors thereby addressing homogeneity in the membrane structure. Boric acid also increased membrane mechanical strength by the formation of metallic metaborates at sintering temperatures. In a similar way, sodium metasilicate acts as a binder by creating silicate bonds among the elements to induce higher mechanical strength in the ceramic membrane [79]. The final formulation reported in this work has been deduced from a trial and error based fabrication approach using various ratios of inorganic precursors. The suggested precursor formulations provided crack free membranes with good structural integrity and desired submicron range pore diameters. The main difference between composition A and composition B was in the amount of pore forming materials (sodium carbonate, calcium carbonate) and clay materials (kaolin, quartz and feldspar). Composition A contains about 35 % total pore forming materials and 55 % clay materials. On the other hand, composition B constitutes only 10 % pore forming materials and 80 % clay materials. These alternations in compositions were identified to yield membranes with diverse structural morphologies.

Table 2.2 compared the identified compositions in this work with those presented in the literature. From the table, it can be observed that Potdar et al., [80] have provided optimal

**Table 2.2: Comparison of identified membrane compositions with those presented in literatures.**

| Literature | Materials | Composition (dry basis wt %) | Sintering temperature |
|---|---|---|---|
| Potdar et al., [80] | Kaolin | 12.7 | 900 $^{o}$C |
| | Ball clay | 16.1 | |
| | Quartz | 23.6 | |
| | Feldspar | 5.1 | |
| | Calcium carbonate | 28.1 | |
| | Pyrophallite | 14.3 | |
| Belouatek et al., [32] | Clay | 21 | 1100 $^{o}$C |
| | Kaolin | 35 | |
| | Feldspar | 20 | |
| | Sand | 24 | |
| Nandi et al., [34] Composition A | Kaolin | 40 | 850-1000 $^{o}$C (This work) |
| | Quartz | 15 | |
| | Calcium carbonate | 25 | |
| | Sodium carbonate | 10 | |
| | Boric acid | 5 | |
| | Sodium metasilicate | 5 | |
| Nandi et al., [35] Composition B | Kaolin | 50 | 800-950 $^{o}$C (This work) |
| | Quartz | 15 | |
| | Feldspar | 15 | |
| | Sodium carbonate | 10 | |
| | Boric acid | 5 | |
| | Sodium metasilicate | 5 | |

inorganic formulations (based on dry basis) using kaolin (12.7 wt %), ball clay (16.1 wt %), quartz (23.6 wt %), feldspar (5.1 wt %), $CaCO_3$ (28.1 wt %) and pyrophallite (14.3 wt %) for the fabrication of MF range inorganic membranes. Amongst these precursors, quartz, feldspar

and pyrophallite could be regarded as expensive materials when compared to kaolin, ball clay and calcium carbonate. The total contribution of expensive materials to the composition was 43.3 %. In a similar approach, Belouatek et al., [32] have reported optimal inorganic formulations using clay (21 wt %), kaolin (35 wt %), feldspar (20 wt %) and sand (24 wt %) to prepare inorganic supports applicable for liquid waste treatment. Of these ingredients reported by the authors, only feldspar can be regarded as an expensive raw material when compared to clay, kaolin and sand. In this case, the total contribution of expensive precursors in the formulation was 20 %. Incidentally, the sintering temperature for the membrane preparation was about 1100 $^{o}$C. In this context, costly materials used in this work contributed only 15 % in composition A and 30 % in composition B. Further, the sintering temperature was kept below 1000 $^{o}$C. Therefore, the identified inorganic precursor formulations (composition A and composition B) for membrane fabrication tend to be competent with those of presented in the literature in the context of materials cost. In addition, it can be also inferred that given the challenging task of ceramic membranes in the lower submicron range pore size, the higher contribution of expensive precursors (30 %) was justified.

### 2.1.2 Membrane preparation

The membrane preparation process was initialized by thorough mixing of dry inorganic raw materials as summarized in Table 2.1 followed by addition of distilled water to prepare a paste. Details of the preparation method are shown in Fig. 2.1. Both membranes (composition A and composition B) were prepared using same fabrication procedure. The paste was then cast over gypsum in the shape of a circular compact disk (55 mm diameter and 5 mm thickness) using a stainless steel (SS316) ring of 55 mm inner diameter and 5 mm thickness. Subsequently, the ring was carefully removed and the paste was kept under distributed

pressure of 2 kg for 24 hours to prevent the propagation deformation and drive homogeneity in the inorganic matrix. The paste was then subjected to four different sequential heat treatment steps. The first step involved drying at ambient temperature for 24 hours. During the second heat treatment step, the membrane was dried at 100 $^{o}$C for 12 hours in a hot air oven. The third heat treatment step consists of drying at 250 $^{o}$C for 24 hours. During the transition from 100 - 250 $^{o}$C, low heating rate was maintained in order to eliminate the induction of thermal stresses generated due to loss of moisture. The final heat treatment step

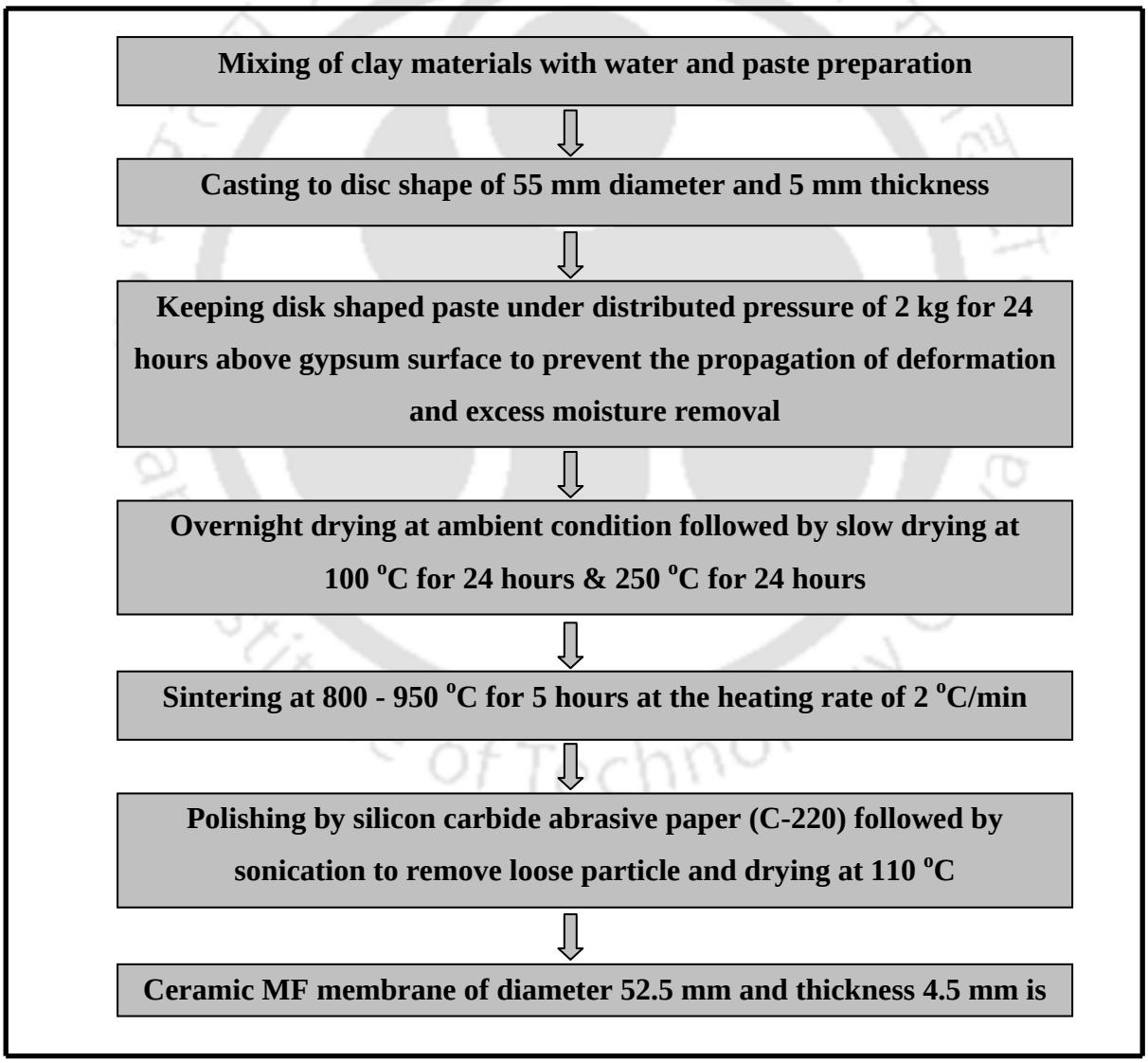


**Figure 2.1: An outline of membrane preparation procedures.**

**Table 2.3: Nomenclature of various prepared ceramic membranes.**

| Composition type | Sintering temperatures ($^{o}$C) | | | | |
|---|---|---|---|---|---|
| | **800** | **850** | **900** | **950** | **1000** |
| A | - | A1 | A2 | A3 | A4 |
| B | B1 | B2 | B3 | B4 | - |

involved heating of the membrane from 250 $^{o}$C to desired sintering temperature at a heating rate of 2 $^{o}$C per minute. Eventually, the membrane was kept for 5 hours for sintering. The membranes were sintered at different temperatures (850, 900, 950 and 1000 $^{o}$C for composition A and 800, 850, 900 and 950 $^{o}$C for composition B) to study the effect of sintering temperature on membrane morphological properties. The selection of minimum sintering temperatures was based on TGA and XRD analysis. Subsequent cooling of the membrane was carried out by atmospheric cooling procedure adopted by switching off the muffle furnace that was previously maintained at the desired sintering temperature. After sintering, membrane achieved hard, rigid and porous texture. Finally, the prepared membrane was polished with silicon carbide abrasive paper (C-220) to obtain a smooth, flat membrane of diameter 52.5 mm and thickness 4.5 mm. Nomenclature of different membranes prepared using various sintering temperatures is summarized in Table 2.3.

## 2.1.3 Characterization techniques

### 2.1.3.1 Structural characterizations

The structural characterization of membranes involves thermogravimetric analysis (TGA), differential thermal analysis (DTA), X ray diffraction analysis (XRD), morphological study using scanning electron microscope (SEM), total porosity determination, structural density measurement and evaluation of pore size distributions from SEM images.

***Thermogravimetric analysis***

TGA and DTA (*Make: Mettler Toledo, USA; Model: TGA/SDTA 851$^e$*) of the sample mixtures were conducted to identify the temperature regimes where predominant weight losses (and hence transformations) occur in the membrane. Thereby, an insight could be gained to analyze the effect of various temperature regimes on the porous structure, pore diameter and mechanical strength of the membrane. TGA and DTA were carried out by heating the dry inorganic powder mixture in a $\alpha$ - alumina crucible from room temperature to 1000 $^{o}$C at a heating rate of 10 $^{o}$C per minute.

***XRD analysis***

XRD analysis was conducted to evaluate the extent of different phase transformations that occurred during sintering.

***Surface morphology***

Membrane morphological studies were carried out using SEM (*Make: Oxford, UK; Model: LEO 1430VP*) to analyze the presence of possible defects and estimate the membrane pore size. The estimation of average membrane pore size ($d_s$) and pore size distribution from SEM micrographs was carried out using ImageJ software (Version 1.40). Individual pore diameters were measured for about 500 pores using ImgeJ software for different pores visible in the SEM [81]. Since pore size distribution and average pore size distribution values are critically dependent on the sampling procedure, five SEM pictures were evaluated using the software. These micrographs were taken randomly from the selected sections of the membranes in order to obtain pore size distributions representing the existing porous texture of the membrane. The area average pore diameter ($d_s$) from SEM analysis of the membrane was evaluated by assuming cylindrical porous texture of the membrane as;

$$d_s = \left[ \frac{\sum_{i=1}^{n} n_i d_i^{\,2}}{\sum_{i=1}^{n} n_i} \right]^{0.5} \qquad (2.1)$$

Where, $n$ is the number of pore, $d_i$ is the pore diameter (μm) of $i^{th}$ pore.

***Porosity and structural density***

The total porosity of the membrane was estimated using Archimedes principle. The experimental procedure involved the measurement of the volume of the wetting liquid that displaced air in a dry membrane after equilibrating the membrane with water for 12 hours. Total porosity ($\varepsilon_m$) and structural density ($\rho_{mem}$) of the membrane were estimated using the following equations [3]:

$$\varepsilon_m(\%) = \left[ \frac{w_1 - w_2}{\rho_{water}} \right] \times \frac{100}{v_{mem}} \qquad (2.2)$$

$$\rho_{mem} = \frac{w_2}{v_{mem}} \qquad (2.3)$$

### 2.1.3.2 Permeation characterizations

***Experimental set up***

A schematic of experimental set up used for both air and water permeation experiment is presented in Fig. 2.2. The set up constitutes a Teflon tubular cell (125 ml capacity) with a flat circular teflon base plate that houses the ceramic membrane. The membrane was kept in the teflon casing and sealed with epoxy resin (*Mseal, Pidilite Industries Ltd, Mumbai, India*). During air permeation experiments, the outlet of the setup was connected to a gas flow meter using a silicon tube for measuring the gas flow rate at various trans-membrane pressure differentials. During liquid permeation experiments, the feed (de-ionized water) was filled in

the tubular section from the top. The cell was pressurized with compressed air. The outlet of the setup was disconnected from the gas flow meter and liquid permeate was collected in a beaker. Liquid permeate flux was measured using a digital scale weight machine.

***Gas transport characteristics***

Air permeation experiments were conducted to quantify membrane morphological parameters such as average pore size ($d_g$) and effective porosity that contribute to the transport. Therefore, gas permeation experimentation was adopted to observe the distribution of

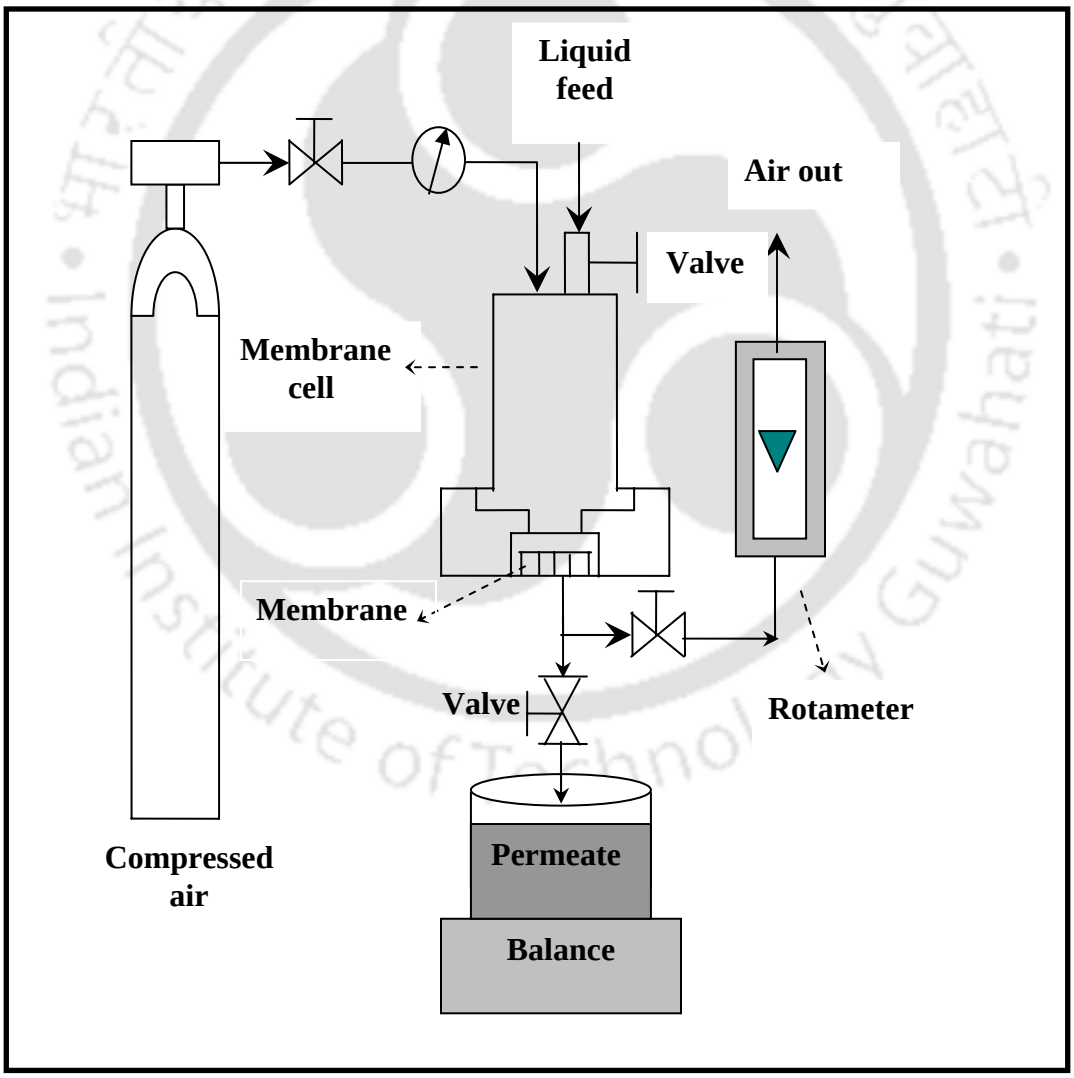


**Figure 2.2: Experimental setup for permeation experiments.**

percentage pores in the macropores (pore dia >50 nm) and mesopores (pore dia <50 nm) [3] in the membrane matrix and contribution of macropores and mesopores to the overall membrane flux. The average pore diameter ($d_g$) and effective porosity ($\varepsilon/q^2$) of the membrane were determined from the plot of effective permeability factor ($K$) of the membrane and average pressure on the membrane ($P$) using following expressions [82]:

$$K = 2.133 \times \frac{r \times v_g}{l_m} \times \frac{\varepsilon}{q^2} + 1.6 \times \frac{r^2}{l_m \times \eta} \times \frac{\varepsilon}{q^2} \times P \tag{2.4}$$

$$d_g = 2 \times r = 2.666 \times \frac{B}{A} \times v_g \times \eta \tag{2.5}$$

where, $A = 2.133 \times \frac{r \times v_g}{l_m} \times \frac{\varepsilon}{q^2}$ (2.6)

$$B = 1.6 \frac{r^2}{l_m \times \eta} \times \frac{\varepsilon}{q^2} \tag{2.7}$$

and $K = \frac{Q \times P_2}{S \times \Delta P}$ (2.8)

The average pore diameter ($d_g$) was calculated using Eq. (2.5) for known values of $\eta$, $v$, $A$ and $B$. $A$ and $B$ were obtained as the slope ($B$) and intercept ($A$) of the linear plot of $K$ vs. $P$. After calculating the values of $d_g$, the effective porosity ($\varepsilon/q^2$) of the membrane was calculated using Eq. (2.4) for known values of $A$. In Eq. (2.4), the first term (intercept) corresponds to Knudsen permeance and the second term (slope) corresponds to the viscous permeance. Henceforth the values of the slope and intercept obtained from the graph can be used to evaluate the percentage contribution of pores (and pore sizes) towards viscous and Knudsen flow transport mechanisms. In other words, gaseous flux characterization of the

ceramic membrane can yield qualitative information with respect to the pore sizes contributing to Knudsen or viscous flow regimes.

***Liquid permeation characteristics***

Permeation experiments using pure water (deionised water) were carried out for the determination of the hydraulic permeability ($P_m$) and hydraulic pore diameter ($d_l$) of the membrane. The permeation tests involve the measurement of permeate liquid volume as a function of time at specific values of trans-membrane pressure drop ($\Delta P$). The liquid flux was measured at an interval of 10 seconds to verify the variation of flux with time. These experiments were performed until the total liquid permeate collected was 80 ml at a specific pressure differential. Physical observations during liquid permeation tests confirmed that the flow rate did not vary during the 10 second intervals. All permeation experiments were conducted at a temperature of 25 $^{o}$C. Before conducting liquid permeation experiments, the membranes were compacted at $\Delta P$ of 310 kPa for composition A and 414 kPa for composition B membranes. These pressures were higher than the maximum operating pressure during experiments (250 and 345 kPa for composition A and composition B membranes, respectively). Membrane compaction was carried out to obtain steady pure water flux through the membrane. The hydraulic permeability ($P_m$) and hydraulic pore radius ($d_l$) of the membranes were evaluated by assuming presence of cylindrical pores in the membrane matrix using the following expressions [2, 3]:

$$J_W = \frac{Q}{S.\Delta t} = \frac{\Delta P}{\mu_w}\frac{\varepsilon_m d_l^{\,2}}{32 l_m} = P_m \times \Delta P \qquad (2.9)$$

$$P_m = \frac{\varepsilon_m d_l^{\,2}}{32 \times l_m \times \mu_w} \qquad (2.10)$$

$$d_l = \left[ \frac{32 \times \mu_W \times l_m \times P_m}{\varepsilon_m} \right]^{0.5} \quad (2.11)$$

In Eq. (2.9), $\varepsilon_m d_l^{\,2}$ corresponds to effective permeable area factor that determines the actual permeable area available during filtration. It can also be analyzed that higher values of $\varepsilon_m d_l^{\,2}$ enable higher permeate fluxes and hence higher permeability of the membrane. A further account of $\varepsilon_m d_l^{\,2}$ has been presented in chapter 4 (section 4.2.1).

#### 2.1.3.3 Chemical stability

All membranes were tested for their corrosion resistance using NaOH solution (pH 13) and HCl (pH 1.5). The chemical resistance of the membrane was measured by measuring its weight after leaving the membrane in contact with the above solutions for seven consecutive days at atmospheric conditions and evaluating the net weight loss after drying the membrane. Further, porosity measurements before and after acid or alkali treatment were conducted in order to verify any change in the porosity when the membrane was exposed to corrosive environment. Energy Dispersive X- ray (EDX) analysis of the membranes before and after corrosion test was carried out to verify any change in elemental composition.

## 2.2 Results and discussion

### 2.2.1 Characterization of clay materials

Major constituents of kaolin are alumina silicates with the following chemical composition (by wt %) $SiO_2$: 46.5 %, $Al_2O_3$: 39.5 % and $H_2O$: 14 %. Spectrum obtained from XRD analysis (*Make: Bruker Axs, USA; Model: D8 ADVANCE*) of kaolin is illustrated in Fig. 2.3a. The XRD spectrum was matched with the JCPDS [83] data base file (PDF-01-089-6538)

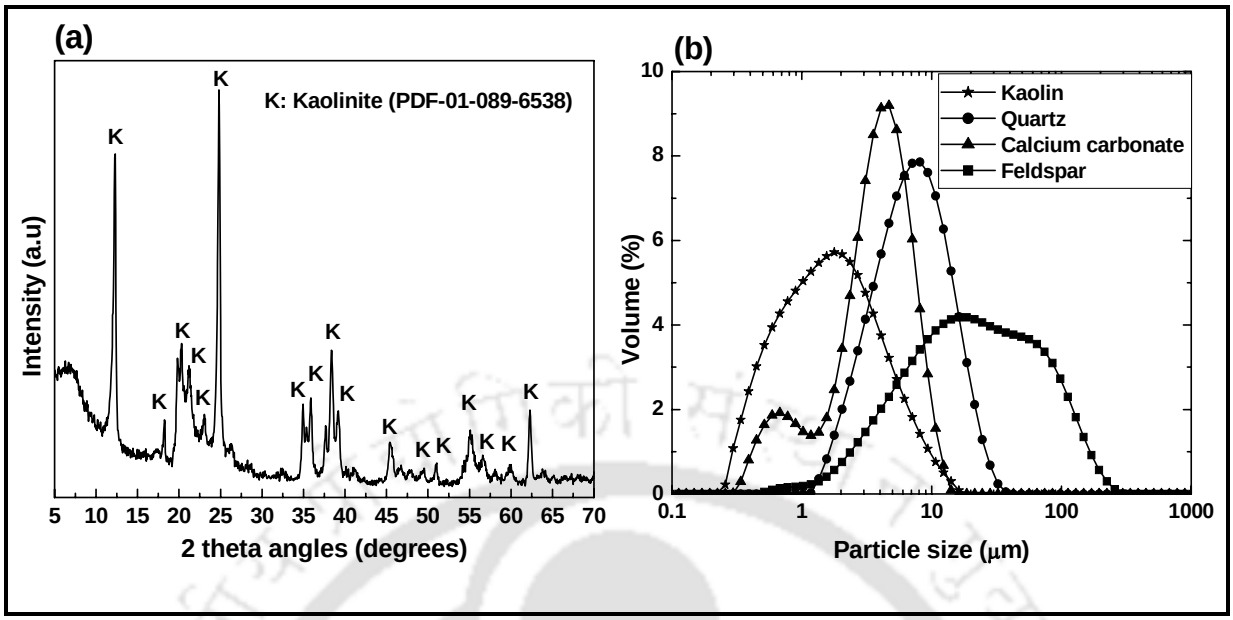


**Figure 2.3: Characterization results for various raw materials. (a) XRD diagram of kaolin powder (b) particle size distribution for kaolin, quartz, $CaCO_3$ and feldspar.**

which conveyed that the kaolin used in our work is ideal kaolinite ($Al_2Si_2O_5(OH)_4$ ). Particle size distribution (*Make: Malvern, USA: Model: Mastersizer 2000*) of major inorganic materials such as kaolin, feldspar, calcium carbonate and quartz used for the membrane fabrication process are shown in Fig. 2.3b. From the figure, it can be observed that particle size varied from 18.67 - 0.224 μm for kaolin, 240 - 0.479 μm for feldspar, 16.257 - 0.296 μm for calcium carbonate and 37.24 - 1.18 μm for quartz. The average particle size of kaolin, feldspar, calcium carbonate and quartz were 2.37, 36.32, 4.108 and 8.4 μm, respectively.

## 2.2.2 Structural characterization of membranes

### 2.2.2.1 Thermogravimetric analysis

Results obtained from TGA and DTA analysis are presented in Figs. 2.4a and 2.4b, for composition A and composition B, respectively. The figures convey that a highly non-linear variation exists in weight loss due to the presence of complex phase transformations and

interactions. For composition A, the total weight loss of the sample was observed to be about 28.5 %. About 2.5 % weight loss was observed below 105 $^{o}$C due to the removal of weakly bonded water molecules in the sample mixture. This specific water loss was characterized by an endothermic peak at 105 $^{o}$C in the DTA curve. Similar observations were also observed for composition B. The total weight loss for the composition B sample was observed to 19.5 %. About 5 % weight loss was observed below 106 $^{o}$C. The weight loss of the sample between 105 - 400 $^{o}$C was around 4 % for composition A and around 4.5 % for composition B, which can be correlated with the pre-dehydration of kaolin and crystal water of boric acid. The pre-dehydration process of kaolin takes place due to the reorganization of the octahedral layer and it first occurred at the OH of the surface [84]. The second endothermic peak in the DTA curve corresponds to the loss of structural hydroxyl groups at 513 $^{o}$C for composition A and at 529 $^{o}$C for composition B. This was due to the transformation of kaolinite to metakaolinite according to the following reaction [85]:

$$Al_2O_3.2SiO_2.2H_2O\,(\text{kaolinite}) \rightarrow Al_2O_3.2SiO_2\,(\text{metakaolinite}) + 2H_2O \qquad (2.12)$$

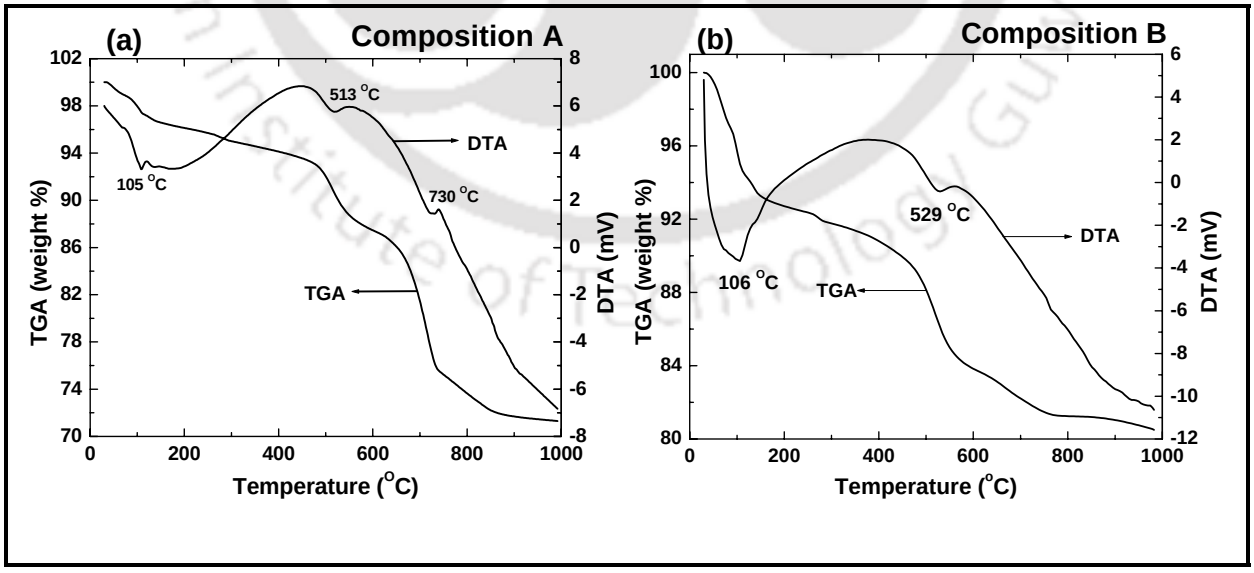


**Figure 2.4: TGA-DTA curves for (a) composition A and (b) composition B membranes.**

For composition A, the formation of $CO_2$ (and hence enhancement of the porous structure of the membrane) occurred at 730 $^oC$ with a corresponding weight loss of 10 % in the temperature regime of 663 $^oC$ to 745 $^oC$. This was due the calcination of $CaCO_3$ in this temperature regime. Calcinations of $Na_2CO_3$ started at temperature 800 $^oC$ and ended in temperature 843 $^oC$ which corresponds to very minute loss of mass in the TGA curve. The sample corresponded to very insignificant weight loss above 843 $^oC$ as conveyed by the TGA curve. This result infers that minimum sintering temperature for the membrane fabrication shall be above 843 $^oC$. On the other hand, for composition B, the formation of $CO_2$ started at 730 $^oC$ with a corresponding weight loss of 2 % in the temperature regime of 663 to 764 $^oC$. This was due to calcination of $Na_2CO_3$ in this temperature regime. It was observed in the TGA curve that the sample corresponded to very insignificant weight loss above 764 $^oC$. This result infers that minimum sintering temperature for the membrane fabrication using composition B shall be above 764 $^oC$. A little variation in the temperature of calcinations as well as pre-dehydration process of kaolin was due to the mixed properties (presence of other raw materials which acts as catalyst or anti-catalyst responsible for early or delay in phase change) of the raw materials. These observations further justified that all phase transformations were complete well below the chosen sintering temperature ranges (850 - 1000 $^oC$ for composition A and 800 - 950 $^oC$ for composition B). Henceforth, high sintering temperatures (more than 1100 $^oC$) as presented in various works [25 - 33] were not required for the preparation of membranes using the chosen inorganic precursor formulations.

#### 2.2.2.2 Phase characterization by XRD analysis

From the TGA - DTA analysis it was observed that above sintering temperature of 843 $^oC$ (composition A) and 764 $^oC$ (composition B), almost no significant weight loss occurred. To

verify this hypothesis, XRD analysis of membrane structure at temperatures higher than 843 $^{o}$C (composition A) and 764 $^{o}$C (composition B) was carried out. Figs. 2.5a and 2.5b summarize XRD graphs for four different samples calcined at 25, 850, 900 and 1000 $^{o}$C (composition A) and 25, 800, 900 and 950 $^{o}$C (composition B) for five hours in muffle furnace. The observation of peaks and trends in the XRD graphs of Fig. 2.5a conveyed that the inorganic mixture originally consisted of kaolinite, quartz and inyoite as main components. The XRD graph obtained for the sample calcined at 850 $^{o}$C depicted that peaks corresponding to kaolinite disappeared due to conversion of kaolinite to metakaolinite. In this regard, it could be pointed out that the formation of metakaolinite was illustrated by TGA-DTA curve trends at a temperature of 513 $^{o}$C. The other phases that appear are nephiline and

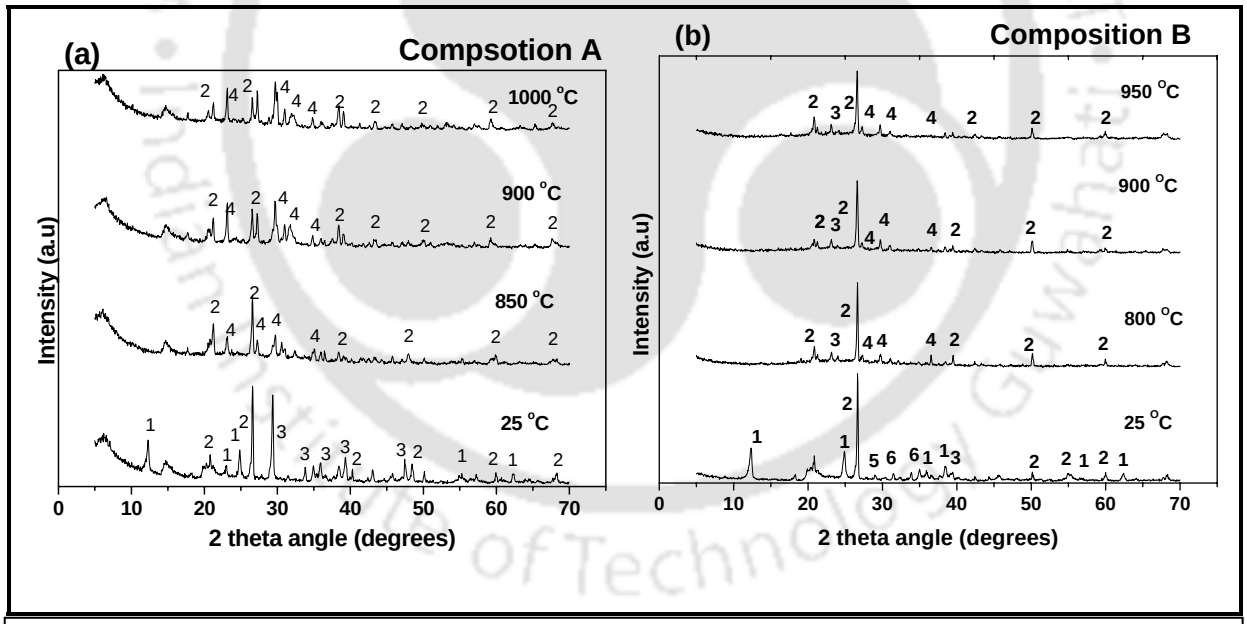


**1**: Kaolinite (PDF- 01-089-6538) **2**: Quartz (PDF-01-075-0443)

**3**: Inyoite (PDF-00-006-0361) **4**: Nephiline (PDF-00-019-1176)

**5**: Hydrogen Borate (PDF-00-022-1109) **6**: Sodium Calcium Silicate (PDF-00-002-0951)

**Figure 2.5: XRD patterns at various sintering temperatures for (a) composition A and (b) composition B membranes.**

quartz. Nephiline ($Na_2O$, $Al_2O_3$, $2SiO_2$) was produced by the reaction of sodium oxide ($Na_2O$) and metakaolinite at temperature of 800 $^oC$ [86]. A critical observation of the peaks at higher temperature revealed that no other significant phase transformation occurred above 850 $^oC$ to 1000 $^oC$. This inferred that the membrane skeletal structure constitutes mainly metakaolinite, quartz and nephiline. From the XRD analysis, it was concluded that a sintering temperature of 850 $^oC$ was sufficient for composition A membranes. All XRD diffractogram graphs indicate no change in the peak trends corresponding to quartz, thereby inferring that quartz phase was not at all affected by sintering of inorganic materials within the temperature considered in this work. Therefore, the sintering temperature above 850 $^oC$ considered in this work was justified. Similar observations were also observed from Fig. 2.5b for composition B, where above sintering temperature of 800 $^oC$, no other significant phase transformation was observed. Hence sintering temperatures above 800 $^oC$ were justified for composition B.

**2.2.2.3 Surface morphology**

Results obtained from SEM analysis for membranes sintered at four different temperatures are shown in Fig. 2.6 (for composition A membranes) and Fig. 2.7 (for composition B membranes). All membranes showed a surface with rough morphological structure. For composition A membranes, as observed in Fig. 2.6, the ceramic substrates sintered at lower temperature (850 and 900 $^oC$) possessed highly porous structure. The membranes sintered at 950 and 1000 $^oC$ were more consolidated due to the fact that sintering temperatures over 900 $^oC$ enabled greater agglomeration of particles to yield more dense structure. Due to this reason, the porosity of the membrane reduced with an increase in sintering temperature. An overall observation of the images shows that, for all the membranes maximum number of pores were within the range of 0.3 - 0.6 μm for composition A membranes. A superficial

observation of the SEM indicated that the membrane did not have any pinholes cracks and the maximum observable pore size of the surface is about 5 μm. These attributes of the membrane make it suitable for MF applications. Similar observations were also found in Fig. 2.7. As less amount of pore forming materials were used composition B membranes ($Na_2CO_3$ of 10 wt % in composition B membranes as compared to $CaCO_3$ + $Na_2CO_3$ of 35 wt % in composition A membranes), both numbers of pores and pore sizes were comparatively less for composition B

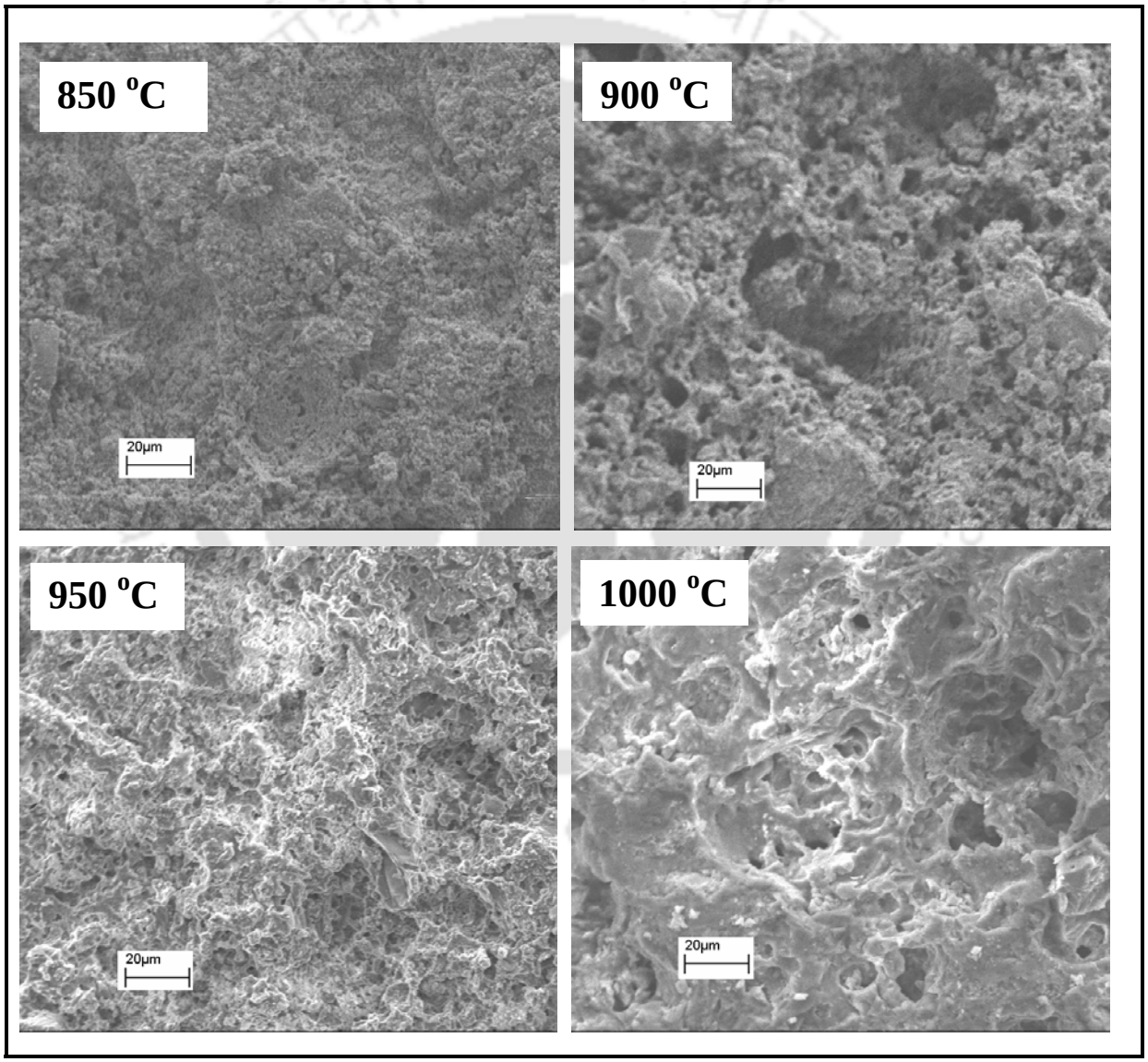


**Figure 2.6: Top surface SEM images of prepared membranes using composition A at various sintering temperatures (a) 850 °C (b) 900 °C (c) 950 °C (d) 1000 °C.**

membranes. As a result higher magnification (Magnification of 6000X for composition B and 500X for composition A) SEM images were taken for comparative assessment. Membranes sintered at lower temperature (800 and 850 $^{o}$C) possessed highly porous structure in comparison to the membrane sintered at 900 and 950 $^{o}$C for composition B membranes. Maximum numbers of pores were below 0.3 μm, which was substantial lower than the pore sizes obtained with composition A. Also the membrane did not have any pinholes cracks and the maximum observable pore size of the surface was about 2 μm.

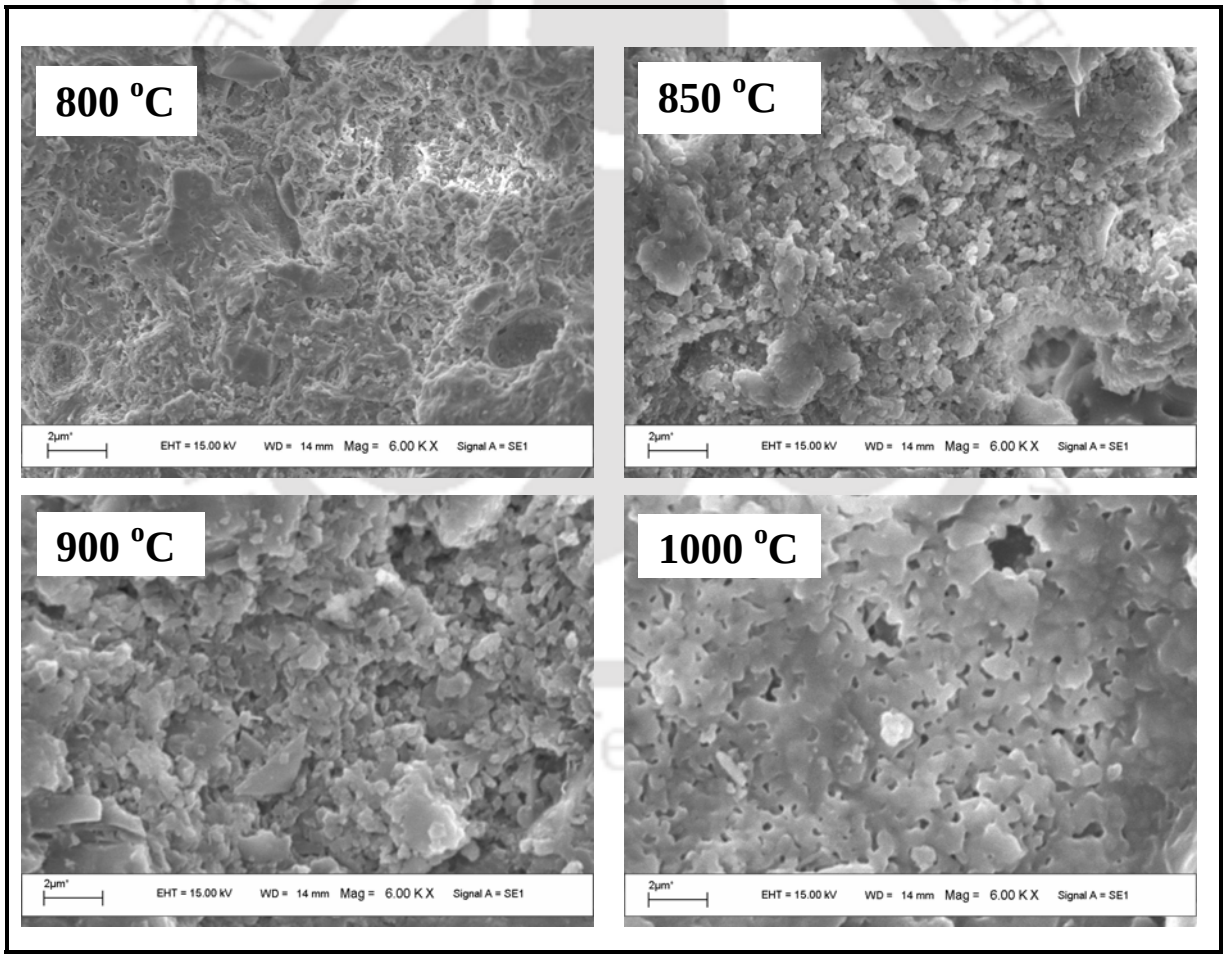


**Figure 2.7: Top surface SEM images of prepared membranes using composition B at various sintering temperatures (a) 850 $^{o}$C (b) 900 $^{o}$C (c) 950 $^{o}$C (d) 1000 $^{o}$C.**

### 2.2.2.4 Pore size analysis based on SEM

Pore size distribution of the membranes obtained form SEM image analysis are shown in Fig. 2.8a and Fig. 2.8b for composition A and composition B membranes, respectively. The average pore diameters of membranes were evaluated using Eq. (2.1) and are summarized in Table 2.4. It can be observed from the Fig. 2.8a, Fig. 2.8b and Table 2.4 that the pore size distribution was closely related to the sintering temperature. The mean pore size of the membrane increased with an increase in the sintering temperature, and the pore size distribution broadens at the same time. As observed from Fig 2.8a, for all sintering temperatures maximum numbers of pores (65 - 75 %) were in the range of 0.3 - 0.6 μm. The average pore diameters for composition A membranes were evaluated to be 0.55, 0.70, 0.78 and 0.81 μm for membranes sintered at 850, 900, 950 and 1000 $^{o}$C, respectively. Similar observations were also evident for composition B membranes where maximum numbers of pores (75 - 90 %) were in the range of 0.1 - 0.3 μm for all sintering temperatures. The mean

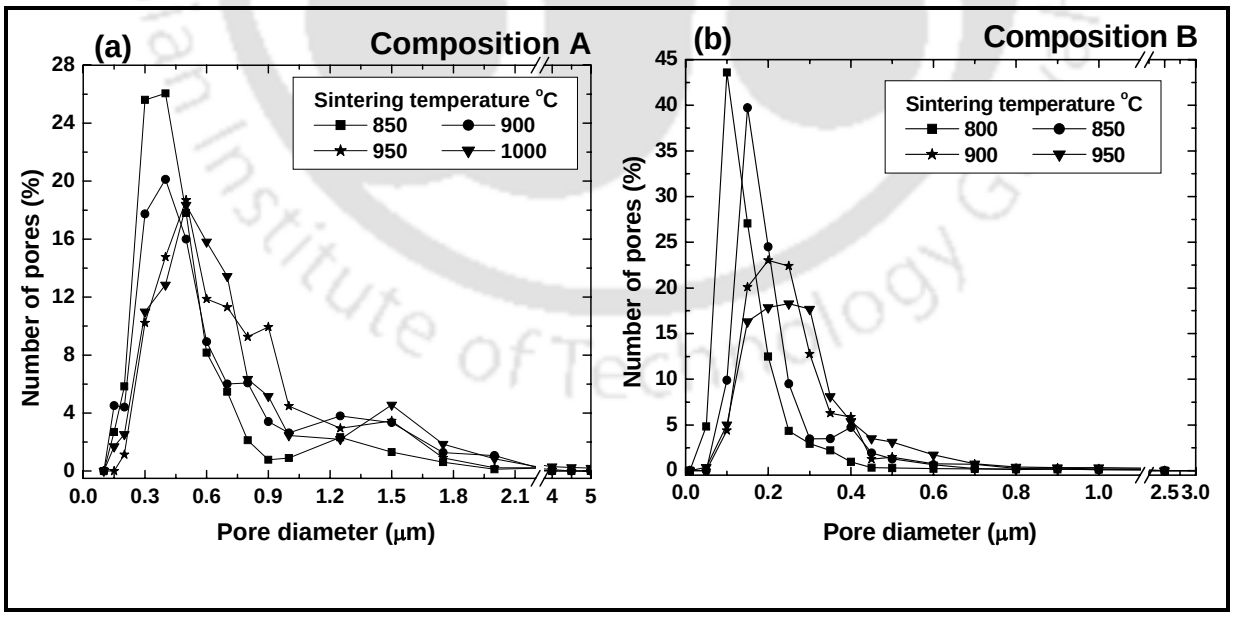


**Figure 2.8: Pore size distributions (based on SEM) of prepared ceramic membranes at various sintering temperatures for (a) composition A and (b) composition B membranes.**

**Table 2.4: Average membrane pore diameters ($d_s$) obtained from SEM analysis.**

| Sintering temperature ($^oC$) | Pore diameter ($d_s$, μm) | |
|---|---|---|
| | **Composition A** | **Composition B** |
| 800 | - | 0.185 |
| 850 | 0.547 | 0.239 |
| 900 | 0.702 | 0.285 |
| 950 | 0.780 | 0.332 |
| 1000 | 0.810 | - |

pore sizes of the composition B membranes were evaluated to be 0.185, 0.239, 0.285 and 0.332 μm for membranes sintered at 800, 850, 900 and 950 $^oC$, respectively. An increase in average pore size with sintering temperature was partly due to the growth of grains that lead to the formation of large pores and elimination of small pores at higher sintering temperatures.

**2.2.2.5 Porosity and structural density**

The variation of membrane porosity and structural density of membrane with varying sintering temperature are shown in Figs. 2.9a and 2.9b for composition A and composition B, respectively. From the figures it can be observed that structural density of the membrane increased with an increase in sintering temperature. However, the total porosity reduced with increasing sintering temperature. For composition A membranes, porosity decreased from 42 - 33 % where as structural density increases from 1260 - 1360 kg/m$^3$ with an increase in sintering temperature from 850 - 1000 $^oC$. Similarly, for composition B membranes, porosity and structural density of the membrane sintered at 800 $^oC$ were 34.4 % and 1280 kg/m$^3$, respectively. When the sintering temperature was increased to 950 $^oC$, porosity of the membrane decreased to 19.5 % where as structural density increased to1540 kg/m$^3$. This was due to the reason that higher sintering temperatures enable densification of the porous

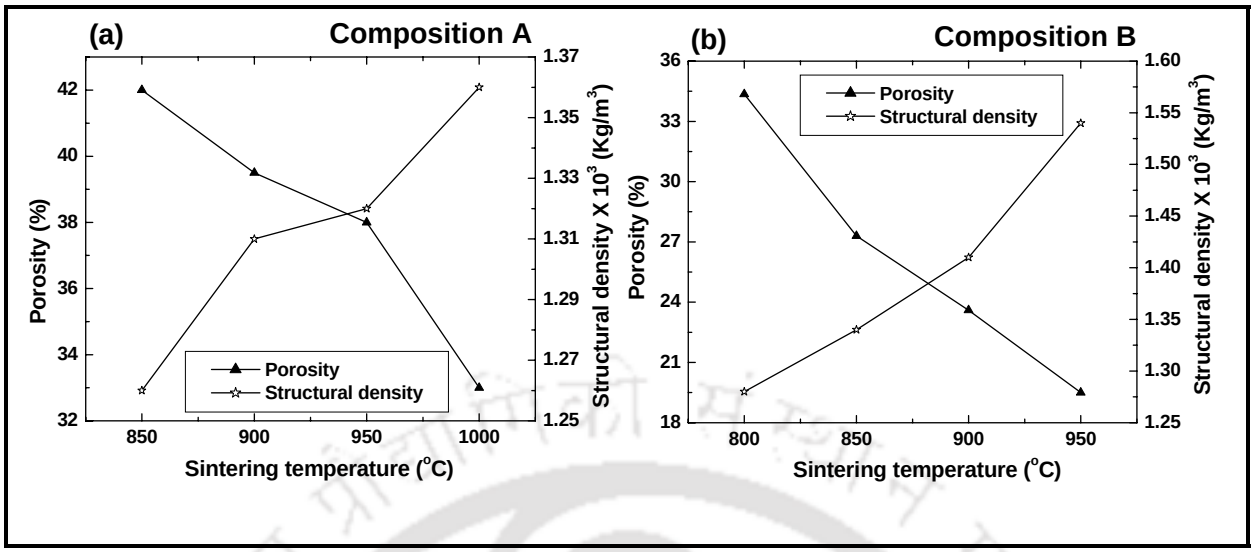


**Figure 2.9: Variation of membrane porosity and structural density with sintering temperatures for (a) composition A and (b) composition B membranes.**

structure to enhance structural density and reduce membrane porosity. This was also reasoned with the fact that with increasing sintering temperature, the number of pores representing small pore sizes reduced and hence the overall pore volume and porosity decreased.

## 2.2.3 Permeation characterization of membranes

### 2.2.3.1 Membrane compaction

The compaction profiles for different membranes prepared in this work are shown in Fig. 2.10. From the figure, it can be observed that the PWF was initially high and declined gradually to reach a steady state value after 60 - 90 minutes for all fabricated membranes. The reduction in PWF was due to the fact that the walls of the pores become closer, denser and uniform during compaction [3]. For the A3 membrane, the observed pure water flux at the beginning of compaction was $6.4\times10^{-4}$ $m^3/m^2.s$ which subsequently reached to a steady state value of $5.0\times10^{-4}$ $m^3/m^2.s$.

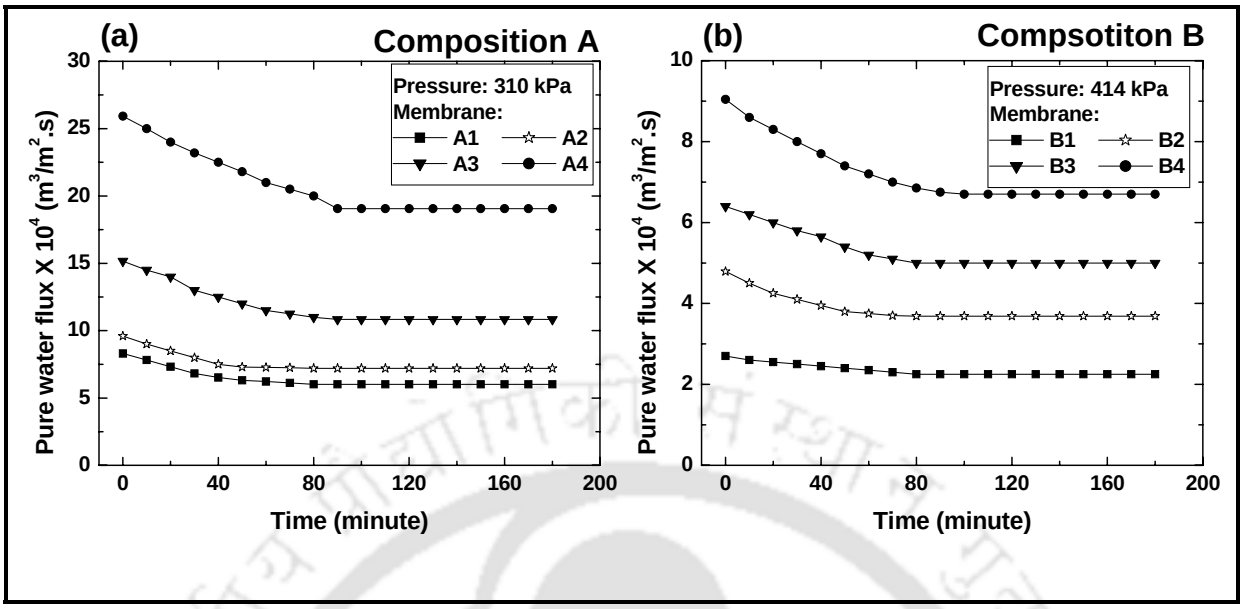


**Figure 2.10: Variation of pure water flux with time during compaction study for (a) composition A and (b) composition B membranes.**

### 2.2.3.2 Hydraulic pore diameter, permeability and effective permeable area factor

The variation of hydraulic pore diameter and hydraulic permeability of the membranes with sintering temperatures are summarized in Table 2.5. As shown, for composition A membranes, the hydraulic pore diameter increased from 0.77 - 1.54 μm with an increase in the sintering temperature from 850 - 1000 $^{o}$C. Therefore, $\varepsilon_m d_l^{\,2}$ (from $249.02\times10^{-3}$ - $783.63\times10^{-3}$ μm$^2$) as well as $P_m$ ($19.44\times10^{-10}$ - $61.36\times10^{-10}$ m$^3$/m$^2$.s.Pa) also increased. Similarly for composition B membranes, the hydraulic pore diameter increased from 0.237 - 0.645 μm with an increase in the sintering temperature from 800 - 950 $^{o}$C and hence $\varepsilon_m d_l^{\,2}$ (from $19.32\times10^{-3}$ - $81.12\times10^{-3}$ μm$^2$) as well as $P_m$ ($1.51\times10^{-10}$ - $6.33\times10^{-10}$ m$^3$/m$^2$.s.Pa) also increased. The enhancement in hydraulic pore diameter with increasing sintering temperature was due to the growth of grains at higher sintering temperatures that lead to the formation of larger pores and elimination of smaller pores from the porous structure (as discussed in section 2.2.2.3).

**Table 2.5: Characteristic parameters obtained from water permeation experiments for membranes prepared at various sintering temperatures.**

| Composition type | Membrane | $\varepsilon_m$ | $d_l$ (μm) | $\varepsilon_m d_l^2 \times 10^3$ (μm$^2$) | $P_m \times 10^{10}$ (m$^3$/m$^2$.s.Pa) |
|---|---|---|---|---|---|
| A | A1 | 0.42 | 0.77 | 249.02 | 19.44 |
| | A2 | 0.395 | 0.863 | 294.19 | 22.93 |
| | A3 | 0.38 | 1.08 | 443.23 | 34.75 |
| | A4 | 0.33 | 1.54 | 783.63 | 61.36 |
| B | B1 | 0.344 | 0.237 | 19.32 | 1.51 |
| | B2 | 0.273 | 0.359 | 35.18 | 2.75 |
| | B3 | 0.236 | 0.511 | 61.62 | 4.83 |
| | B4 | 0.195 | 0.645 | 81.12 | 6.33 |

Similar trends were reported in literature for other types of clay based inorganic membranes [29, 31].

### 2.2.3.3 Gas transport

Figures 2.11a and 2.11b presents the variation of effective permeability factor ($K$) with average pressure ($P$) for composition A and composition B membranes, respectively. For composition A membranes, the measured gas permeance for the membranes were $2.08\times10^3$, $3.34\times10^3$, $3.59\times10^3$ and $4.53\times10^3$ $m^3m^{-2}h^{-1}MPa^{-1}$ at a $\Delta P$ of 0.206 MPa for A1, A2, A3 and A4 membranes, respectively. Similarly for composition B, the measured gas permeance for the membranes were $1.26\times10^{-4}$, $1.544\times10^{-4}$, $1.63\times10^{-4}$ and $1.93\times10^{-4}$ $m^3/m^2$.s.kPa at a $\Delta P$ of 206.84 kPa for B1, B2, B3 and B4 membranes, respectively. Table 2.6 summarizes parameters evaluated from graphical analysis of trans-membrane flux data. As shown in the table, the average pore diameter obtained from theoretical analysis of permeation data for composition A membranes (A1, A2, A3 and A4) varied from 0.31 - 0.56 μm. In this regard,

measured pore radius from SEM analysis could be observed to vary from 0.55 - 0.81 μm which was close to the values evaluated from liquid permeation data. Similarly, for composition B membranes, the average pore diameter obtained from theoretical analysis of permeation data varied from 0.162 - 285 μm. This was also close to the evaluated pore diameter from SEM analysis (from 0.185 - 0.332 μm). The table also summarized effective porosity factor values ranging from 0.477 - 0.368 for membrane prepared using composition A and 0.315 - 0.198 for membrane prepared using composition B, which truly represent and contribute to the membrane transport. In this regard, it can be observed that the constant average porosity of the membrane was about 0.42 - 0.33 for membrane prepared using composition A and 0.344 - 0.195 for composition B membranes, which were close to the predicted value of the effective porosity. Henceforth, the assumption of cylindrical pores in the calculation procedure was justified with the fact that tortuosity is close to one.

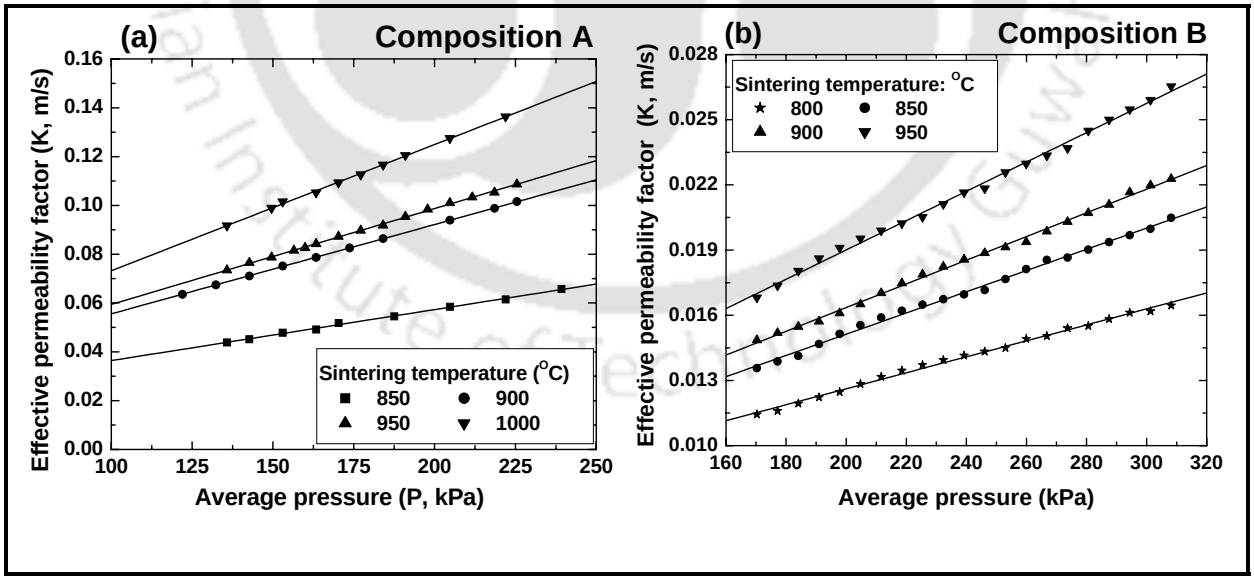


**Figure 2.11: Variation of effective permeability factor with mean pressure for the membranes prepared using (a) composition A and (b) composition B.**

**Table 2.6: Various membrane parameters evaluated from graphical analysis of gas permeation data.**

| Composition type | Membrane | A $\times 10^2$ (m/s) | B $\times 10^7$ (m/s.Pa) | $d_s$ (nm) | $\frac{\varepsilon}{q^2}$ | Viscous flux (%) | Knudsen flux (%) |
|---|---|---|---|---|---|---|---|
| A | A1 | 1.55 | 2.09 | 313 | 0.477 | 65-76 | 35-24 |
| | A2 | 1.89 | 3.66 | 449 | 0.405 | 70 – 81 | 30-19 |
| | A3 | 2.02 | 3.93 | 452 | 0.428 | 73-82 | 27-18 |
| | A4 | 2.14 | 5.17 | 560 | 0.368 | 77-84 | 23-16 |
| B | B1 | 5.26 | 3.68 | 162 | 0.315 | 54-68 | 46-32 |
| | B2 | 5.35 | 4.89 | 211 | 0.259 | 61-74 | 39-26 |
| | B3 | 5.45 | 5.45 | 223 | 0.241 | 63-76 | 37-24 |
| | B4 | 5.51 | 6.75 | 285 | 0.198 | 67-79 | 33-21 |

However, the most important relevance of gas permeation data was the ability to judge upon the percentage contribution of Knudsen and viscous diffusion to the trans-membrane flux. As presented in Table 2.6, for A2 membrane, the viscous flux contributed to 70 to 81 percent to the total flux and 19 to 30 percent was contributed by Knudsen flux. This conveys that, about 70 to 81 percent of the pores in the membrane have pore sizes well above the regime where Knudsen diffusion dominates (1 - 20 nm). The reduction in the percent contribution of Knudsen flux to the total flux with increasing sintering temperatures is due to enhancement in pore sizes as well as the distributions at higher sintering temperatures (Figs. 2.6 and 2.7).

### 2.2.3.4 Comparative study of pore diameters from different methods

With respect to the trends in average pore diameters calculated from SEM ($d_s$ presented in Table 2.4), air permeation ($d_g$ presented in Table 2.6) and pure water permeation ($d_l$ presented in Table 2.5), it was observed that average pore diameter calculated from air permeation ($d_g$) provided the minimum pore diameter and pure water permeation ($d_l$)

provided the highest pore diameter. The average pore diameters calculated from SEM analysis were in between $d_g$ and $d_l$. As gas molecules are more likely to pass through small voids or interstices than water molecules, gas permeation experiments provided the smallest pore diameters. On the other hand, liquid permeation experiments not only detected actual pores but also other non-interconnected voids of the porous matrix. Hence, $d_l$ was higher than $d_g$. For the calculation of $d_s$ using SEM images, only pores greater than 50 nm were considered on the membrane surface. Therefore, there was a possibility that this method may overestimate the mean pore size by considering the wider pores on the surface and ignoring the smaller pores. As a result, $d_s$ was higher than $d_g$ and may be higher or lower than $d_l$ (lower than $d_l$ in the present study). However, since hydraulic permeability involves the transport of liquid through pores accountable for MF process, the most appropriate average pore size of the membrane could be inferred from liquid flux data but not gaseous flux data or SEM images. Gaseous flux characterization enables one to evaluate the percentage distribution of micro-pores of varying sizes and their contribution to the overall transport behavior of the membrane. Pore diameters using SEM image provides an approximate estimate upon the possible pore diameters and their distributions. These trends are in agreement with the experimental data reported in the literature [81].

### 2.2.4 Chemical stability

It was observed that the weight loss of membranes during chemical stability tests was not significant and was less than 4 % for all membranes (both composition A and composition B membranes). However, a maximum increase of 8 % in membrane porosity was observed for all membranes after both HCl and NaOH tests. Results obtained from EDX analysis of the A2

**Table 2.7: EDX analysis of the A2 membrane before and after corrosion test.**

| Elements | Membrane (wt %) | Membrane after acid corrosion test (wt %) | Membrane after base corrosion test (wt %) |
|---|---|---|---|
| Oxygen | 49.24 | 48.55 | 50.26 |
| Sodium | 7.96 | 7.21 | 8.43 |
| Aluminum | 11.84 | 12.60 | 11.32 |
| Silicon | 14.82 | 16.45 | 14.43 |
| Calcium | 16.14 | 15.19 | 15.56 |

membrane before and after corrosion test is shown in Table 2.7. It can be inferred from the table that the elemental composition of the membrane remains unchanged after acid and basic treatment. Similar results were obtained for the other membranes as well. The observed trends in weight loss and EDX analysis during corrosion tests convey that the membranes possessed excellent corrosion resistance and are suitable for MF applications involving acidic and basic media. Similar chemical resistance are reported for kaolin [86] and apatite [26] based membranes.

### 2.2.5 Cost of the membranes

Industrially competitive aspect of membrane technology lies in its cost. Table 2.8 summarized the retail prices of various inorganic precursors that were used for the fabrication of the membranes. Based on the inorganic precursor formulation, the overall cost of the membranes using retail cost indices have also been presented in the table. The retail prices of the precursors have been obtained from the catalog of companies summarized in section 2.1.1. The materials cost of the membranes has been estimated to be 130 and 220 $\$/m^2$ for composition A and composition B membranes, respectively. The reported cost of the membrane based on raw materials costs is anticipated to be useful to provide economic

**Table 2.8: Cost analysis of prepared membranes using the retail cost of raw materials.**

| **Material** | **Retail price ($/kg)** | **Composition (A)** | | **Composition B** | |
|---|---|---|---|---|---|
| | | **wt %** | **Cost contribution ($/kg mixture)** | **wt %** | **Cost contribution ($/kg mixture)** |
| Kaolin | 5 | 40 | 2 | 50 | 2.5 |
| Quartz | 64 | 15 | 9.6 | 15 | 9.6 |
| Calcium carbonate | 2.4 | 25 | 1.05 | 0 | 0 |
| Feldspar | 70 | 0 | 0 | 15 | 10.5 |
| Sodium carbonate | 4.6 | 10 | 0.46 | 10 | 0.46 |
| Boric acid | 4.6 | 5 | 0.28 | 5 | 0.28 |
| Sodium metasilicate | 8.4 | 5 | 0.42 | 5 | 0.42 |
| Water | 0 | 0 | 0 | 0 | |
| Total numbers of membranes prepared per kg dry mixture = 50<br>(0.02 kg dry mixture/membrane of 4.5 mm thickness and 52.5 mm diameter)<br>Total surface area obtained = $50 \times 3.14 \times (0.0525)^2 / 4 =$ **0.108 $m^2$**<br>Cost of the membranes = **130 $/m^2$** (composition A) **220 $/m^2$**(composition B) | | | | | |

benchmarks for different small scale applications such as research and pilot scale utilization of inorganic membranes. Higher cost of composition B membranes was due to usage of higher quantities of expensive materials (total quartz and feldspar content of 30 % for composition B). However, for large scale production the cost of raw materials will be much lower than the reported cost data. Including shipment, fabrication and other costs, the average cost of inorganic membranes using large scale production methods may vary between 200 - 400 $/m$^2$ for composition A and 400 - 600 $/m$^2$ for composition B membranes. Contemporary elemental costs of various polymeric membranes and α-alumina ceramic symmetric membrane vary form 50 - 200 $/m$^2$ [2] and 2000 - 4000 $/m$^2$, respectively [87]. Therefore, it can be inferred from cost analysis that cost of the inorganic membranes based on

kaolin would be closer to the cost of the polymeric membranes deployed for industrial configurations and could be slightly expensive than the modules prepared with polymeric membranes owing to the costs involved in manufacturing and bare module costs. The reported value of the membrane cost is conceptual in nature and may vary significantly depending on the fouling characteristics, on time performance, membrane durability, long term stability and life cycle of the ceramic membrane in process applications. However, corrosion resistance data presented in this work instill confidence in the long term performance and hence the projected membrane cost is anticipated to be close to the reported value.

# Chapter 3:

## Treatment of Oily Wastewater using Ceramic Membrane

# Treatment of Oily Wastewater using Ceramic Membrane

*This chapter addresses studies upon the application of prepared submicron range membrane (A1) for the treatment of oily wastewater. Synthetic oil-in-water emulsions were subjected to MF in batch mode of operation. The aim of these experiments were to observe the effect of oil concentration as well as trans-membrane pressure differential on the permeate flux and oil rejection efficiency of the membrane. Subsequently flux decline was analyzed using different pore blocking models such as complete pore blocking, standard pore blocking, intermediate pore blocking and cake filtration to gain insights into the nature of membrane fouling during permeation.*

## 3.1 Experimental

### 3.1.1 Membrane

Microfiltration (MF) of oil-in-water (o/w) emulsions was carried out using A1 membrane. Chapter 2 presented a detailed account upon the properties the membrane. A summary of the various properties of A1 membrane is presented in Table 3.1.

### 3.1.2 Preparation of oil-in-water emulsions

Crude oil collected from *Guwahati Refinery, Indian Oil Corporation Limited (IOCL), India*, was used without any treatment to prepare synthetic o/w emulsions. The crude oil was obtained from *Assam crude oil reservoirs*. Assam crude is typically characterized to possess high degree of aromatic and wax content [88]. Emulsions were prepared using distilled water and crude oil by placing the o/w mixture in a sonicator tank (*Make: Elmasonic; Model: S30H*)

**Table 3.1: A summary of ceramic membrane (A1) properties.**

| **Properties** | **Value** |
|---|---|
| Membrane permeable area, $S$ ($m^2$) | $1.66 \times 10^{-3}$ |
| Thickness, $l_m$ (m) | $4.5 \times 10^{-3}$ |
| Hydraulic pore diameter, $d_l$ (μm) | 0.77 |
| Intrinsic membrane resistance, $R_m$ ($m^2/m^3$) | $5.78 \times 10^{11}$ |
| Total porosity, $\varepsilon_m$ | 42 % |
| Material cost ($/$m^2$) | 130 |

for 15 hours at a temperature of 25 $^{o}$C. The disappearance of oily layer on the water surface confirmed the achievement of emulsification process during sonication. No surfactant was added externally to stabilize the emulsion as the natural surfactants present in the crude oil were sufficient to yield a highly stable emulsion. The onset of the stable emulsion was further tested by measuring the droplet size distribution, absorbance at 235 nm wavelength, pH and viscosity of the emulsions regularly. After two weeks time period, coalescence of the oil droplets was observed that lead to the formation of a thin oil film on the water surface. Similar observations were also found by Huotari et al., [89]. Therefore, all MF experiments were carried out with emulsions prepared within 10 days.

### 3.1.3 Microfiltration of oil-in-water emulsions

Dead-end MF experiments of synthetic o/w emulsions were carried out in the experimental setup shown in Fig.2.2 (chapter 2). Four different concentrations of oil (50, 75, 100 and 150 mg/L) and five trans-membrane pressure differentials ($\Delta P$) (41.37, 82.74, 124.11, 165.47 and 206.84 kPa) were used to observe the effect of oil concentration as well as $\Delta P$ on the permeate flux and oil rejection efficiency of the membrane. Permeate from the bottom of the

cell was collected and its cumulative weight was measured with the help of an electronic balance. Permeate was collected at 5 minutes interval for the measurement of its oil concentration where as flux data was taken in the interval of 1 minute during experiments. All experiments were conducted at room temperature (~25 $^{o}$C). The permeate flux ( $J$ ) and the percent oil rejection ( $R$ ) was calculated using the following equations:

$$J = \frac{V}{S \times \Delta t} \tag{3.1}$$

$$\mathrm{R}\,(\%) = \left(1 - \frac{C_P}{C}\right) \times 100 \tag{3.2}$$

The oil concentrations in permeate and feed were determined using UV-Vis spectrophotometer (*Make: Perkin Elmer Precisel, USA; Model: Lambda 35*) by measuring absorbance at a wave length of 235 nm where maximum absorbance was observed [46, 89].

### 3.1.4 Membrane cleaning

After each experimental run, the membrane was cleaned with '*Surfexcel*', a laboratory detergent solution. The pure water flux (PWF) of each membrane was verified before and after cleaning the membrane. The difference between the PWF of cleaned membrane and fresh membrane was found to be negligible. The membrane cleaning between each two runs was carried out using the following steps:

Step 1: Tap water washing for 5 minutes.

Step 2: Soaking the used membrane in detergent water solution for 30 minutes.

Step 3: Tap water washing for 5 minutes.

Step 4: Backflushing using tapwater.

Step 5: Soaking the clean membrane in de-ionized water for 15 minutes.

Step 6: Rinsing the membrane thoroughly with de-ionized water for the removal of residual detergent from the membrane for 5 minutes.

## 3.2 Related theory of membrane fouling mechanism

Hermia (1982) [90] proposed four empirical models to present membrane fouling mechanisms in dead-end filtration based on constant pressure: complete pore blocking, standard pore blocking, intermediate pore blocking and cake filtration. Parameters associated to these models subsequently have a physical relevance. The models were developed using constant pressure filtration law as:

$$\frac{d^2t}{dV^2} = K_p\left(\frac{dt}{dV}\right)^n \tag{3.3}$$

where the selection of values for parameter $n$ = 2, 1.5, 1 and 0 corresponds to complete pore blocking, standard pore blocking, intermediate pore blocking and cake filtration, respectively. Figure 3.1 shows the schematics of different membrane fouling mechanisms. Complete pore blocking occurs when the sizes of the solute particles are greater than the size of the membrane pores. As a result, pore blocking occurs over the membrane surface and not inside the membrane pores (Fig. 3.1a). Standard pore blocking hypothesizes that the molecules enter the membrane pores and deposit over the pore walls due to the irregularity of pore passages, thereby reducing the membrane pore volume. This type of fouling is caused by particles smaller than the membrane pore size and pore blocking occurs inside the membrane pores. Thereby, the volumes of membrane pores decrease proportionally to the filtered permeate volume (Fig. 3.1b). Intermediate blocking occurs when the solute particle size is similar to the membrane pore size. In this model, it is assume that a membrane pore is not necessarily blocked by the solute molecules and some particles may settle over others. Therefore, the

non-blocked membrane surface area diminished with time and some molecules are expected to obstruct the membrane pore entrance without blocking the pore completely (Fig. 3.1c). Cake filtration corresponds to a scenario where particles larger than the average pore size accumulate on the membrane surface thus forming a "cake" (Fig. 3.1d). Thereby, the cake grows with time and provides an additional porous barrier (and hence hydraulic resistance) to the permeating liquid. Substituting $n$ = 2, 1.5, 1 and 0 in Eq (3.3), various pore blocking models can be represented using the following linearized expressions [91]:

a) $n = 2$ : Complete pore blocking: $\ln\left(J^{-1}\right) = \ln\left(J_0^{-1}\right) + k_b t$ (3.4)

b) $n = 1.5$ : Standard pore blocking: $J^{-0.5} = J_0^{-0.5} + k_s t$ (3.5)

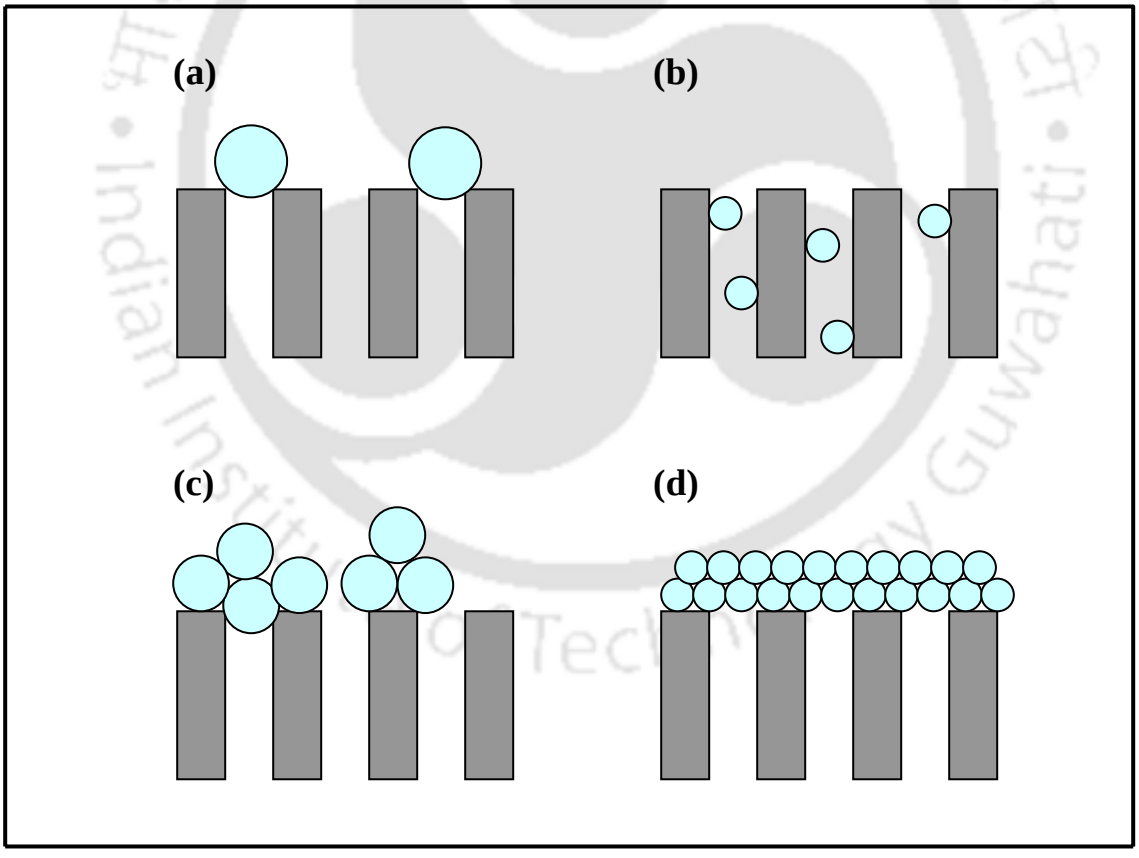


**Figure 3.1: Schematic representation of various pore blocking mechanisms (a) complete pore blocking, (b) standard pore blocking, (c) intermediate pore blocking and (d) cake filtration.**

c) $n = 1$: Intermediate pore blocking: $J^{-1} = J_0^{-1} + k_i t$ (3.6)

d) $n = 0$: Cake filtration: $J^{-2} = J_0^{-2} + k_c t$ (3.7)

Therefore, a plot of $\ln(J^{-1})$ vs. $t$, $J^{-0.5}$ vs. $t$, $J^{-1}$ vs. $t$ and $J^{-2}$ vs. $t$ shall be a straight line with slope of $k_b$, $k_s$, $k_i$ and $k_c$ and with y-intercept of $\ln(J_0^{-1})$, $J_0^{-0.5}$, $J_0^{-1}$ and $J_0^{-2}$ for complete pore blocking, standard pore blocking, intermediate pore blocking and cake filtration model, respectively. The appropriate fitness and competence of various fouling models can be confirmed by comparing the values of coefficient of correlation ($R^2$) obtained from the linear regression analysis.

## 3.3 Results and discussion

### 3.3.1 Emulsion droplet size distribution

Droplet sizes and their distributions in the prepared o/w emulsions were measured using a laser particle size analyzer (*Make: Malvern, USA; Model: Mastersizer 2000*). Figure 3.2 shows the droplet size distribution of emulsion at various oil concentrations in conjunction with the pore size distributions of A1 membrane. As indicated by the profile, a bimodal distribution of the oil droplet curve was apparent for all four emulsions studied in this work. The droplet size of the emulsion varied between 0.04 - 100 μm, with more than 96 % of the oil droplets possessing sizes between 0.04 - 10 μm. Further, it can also be observed that the volume percent of emulsions with smaller droplet sizes (0.1 μm) increased with an increase in the oil concentration. However, with an increase in oil concentration, the volume percent of the bigger oil droplets (10 - 100 μm) increased, which eventually contributed to the overall increase in the average droplet size. However, the droplet volume distribution for these

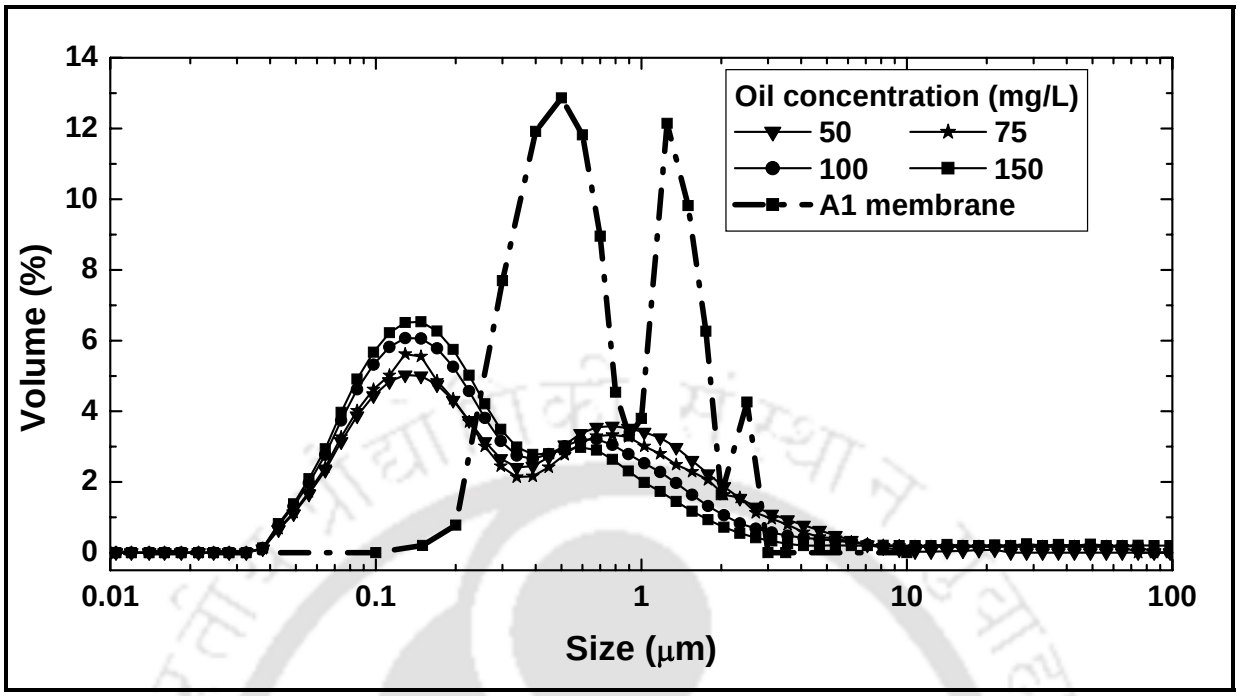


**Figure 3.2: Droplet size distribution of oil-in-water emulsion at various oil concentrations in conjunction with the pore size distributions of A1 membrane.**

droplets is insignificant to visualize in the Fig. 3.2. A similar observation was found for the enhancement of average oil droplet size with increasing concentration in the literature [92] for oily wastewater systems. The average droplet sizes of the emulsions were 0.56, 0.75, 0.78 and 0.85 μm for emulsions prepared with 50, 75, 100 and 150 mg/L oil concentration, respectively. Details comparison of membrane pore size distribution and emulsion particle size distribution has been discussed in section 3.3.4.

### 3.3.2 Effect of trans-membrane pressure and oil concentration on flux

Variations in permeate flux with permeation time for five different trans-membrane pressure differentials (41.37, 82.74, 124.11, 165.47 and 206.84 kPa) are shown in Figs. 3.3a, 3.3b, 3.3c and 3.3d for 50, 75, 100 and 150 mg/L initial feed oil concentrations, respectively. From the figures, it can be observed that the permeate flux declined sharply within the initial 5 - 10

minutes of operation and becomes gradual thereafter for all four oil concentrations. For the feed oil concentration of 100 mg/L, permeate flux reduced from $48.16\times10^{-6}$ - $12.24\times10^{-6}$ $m^3/m^2.s$ within 30 minutes of experimental run at a $\Delta P$ of 41.37 kPa (Fig. 3.3c). This decline in flux with time was due to pore blocking of ceramic porous structure and formation of a thin oily film layer over the membrane surface. It was also observed that permeate flux increased with an increase in $\Delta P$. The initial permeate flux was observed to increased from $48.16\times10^{-6}$

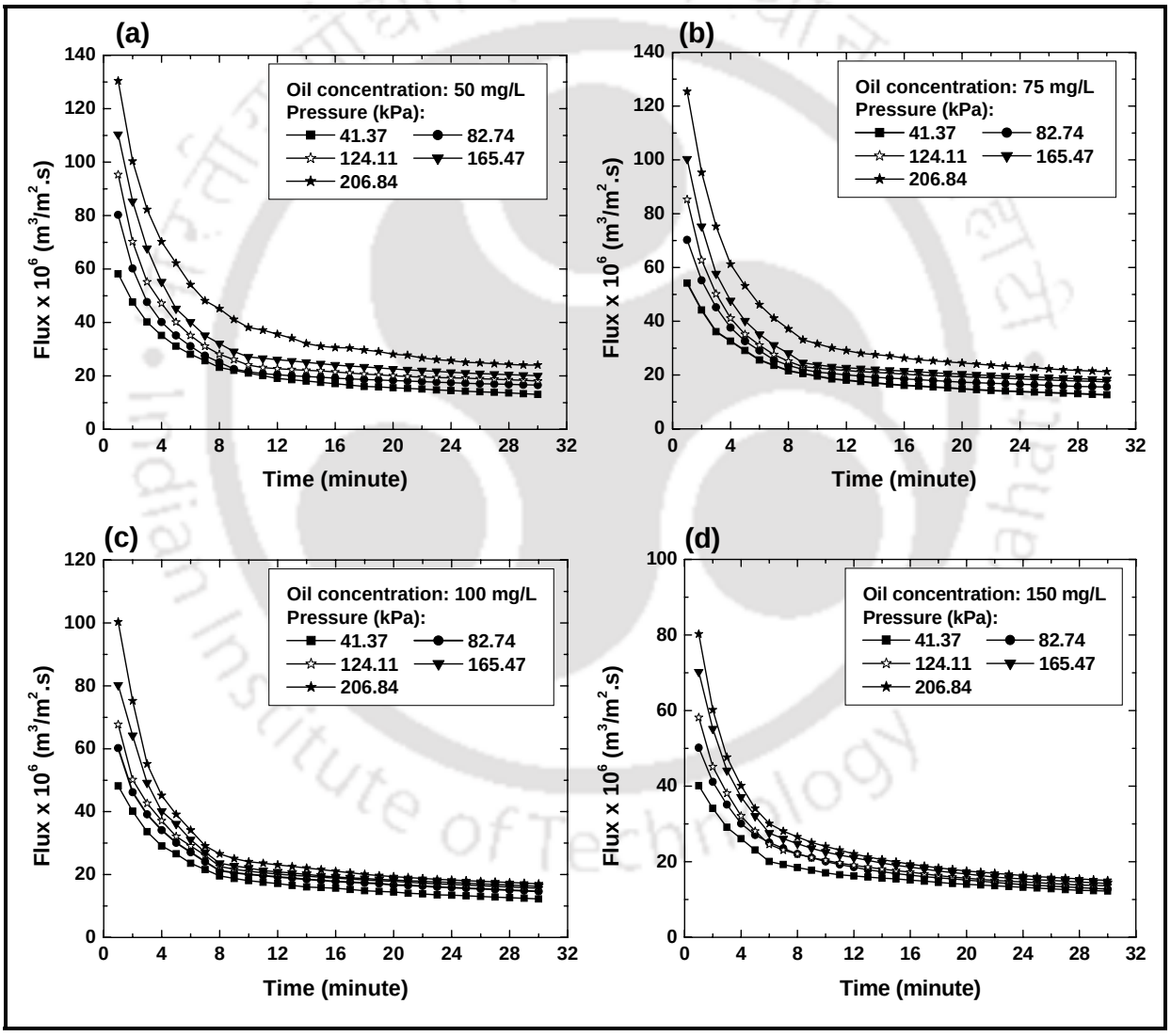


**Figure 3.3: Variation of permeate flux with time and trans-membrane pressure differentials for feed emulsions prepared with (a) 50 mg/L, (b) 75 mg/L, (c) 100 mg/L and (d) 150 mg/L oil concentration.**

- 100.34 $\times 10^{-6}$ $m^3/m^2.s$ when $\Delta P$ was increased from 41.37 kPa - 206.84 kPa for an oil concentration of 100 mg/L. The enhancement in permeate flux with an increase in $\Delta P$ was due to higher driving force. Similar trends were observed at other three $\Delta P$ shown in the figure and also for the other three concentrations (50, 75, 150 mg/L) studied in this work. An overall observation of these figures inferred that the permeate flux decreased with an increase in oil concentration. At a $\Delta P$ of 206.84 kPa, the initial permeate flux decreased from 130.44 $\times 10^{-6}$ - 80.27 $\times 10^{-6}$ $m^3/m^2.s$ with an increase in oil concentration from 50 - 150 mg/L. This was due to the fact that with an increase in feed concentration, droplet sizes of the emulsions increased and thereby enhanced membrane fouling.

### 3.3.3 Effect of trans-membrane pressure and oil concentration on rejection

Percent rejection of crude oil with time at five different trans-membrane pressure drops are shown in Figs. 3.4a, 3.4b, 3.4c and 3.4d for 50, 75, 100 and 150 mg/L initial feed oil concentrations, respectively. It can be observed from the figures that the rejection efficiency of the membrane slightly increased with time. For 100 mg/L oil concentration, oil rejection efficiency of the membrane increased from 97.9 (5 minute) - 98.5 % (30 minute) at a $\Delta P$ of 41.37 kPa (Fig. 3.4c). An increase in oil rejection efficiency with time was due to the reduction of pore diameter of the membranes by adsorption of oil droplets in the membrane pores. Also, the rejection efficiency was observed to decrease with an increase in pressure. With an increase in $\Delta P$ from 41.37 - 206.84 kPa, oil rejection efficiency decreased from 97.29 - 96.74 % for 50 mg/L oil concentration. Similar trends were also observed for the other three concentrations (50, 75 and 150 mg/L) studied in this work. The observed rejection efficiency trends agree with the data reported in the literature [59] using $ZrO_2$ membranes. A reduction in oil rejection efficiency with an increase in $\Delta P$ is in accordance with the

hypothesis that higher pressures facilitate the enhancement of wetting and coalescence of oil droplets, thereby imposing some oil droplets to pass through the membrane pores and reach the permeate stream. Also the oil rejection efficiency of the membrane was found to decrease with reduction in oil concentration. The maximum rejection is found to be 98.62 % for 150 mg/L feed concentration at $\Delta P$ of 41.37 kPa. This was due to lower droplet size of the oil at lower concentration.

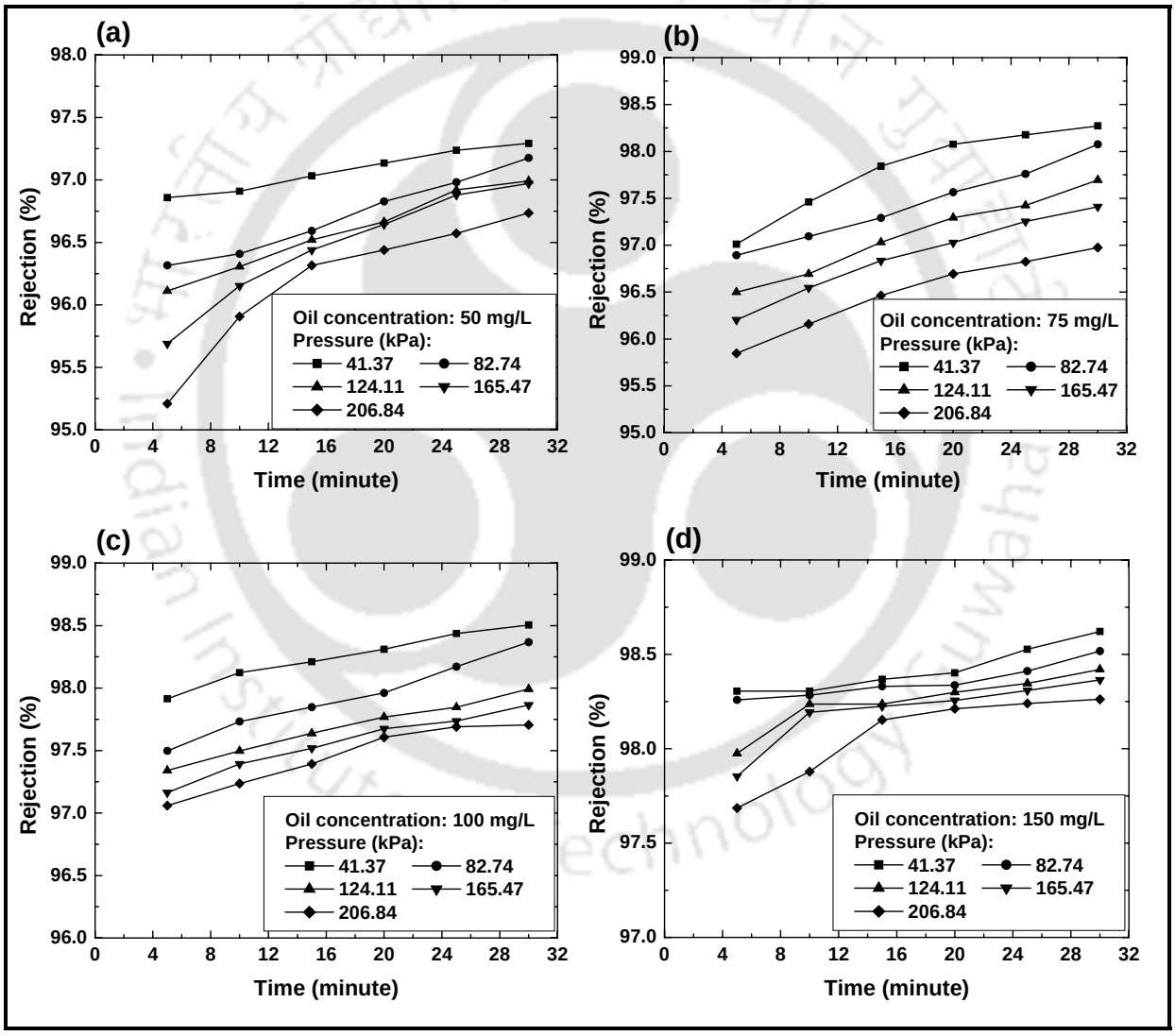


**Figure 3.4: Variation of oil rejection with time and trans-membrane pressure differentials for feed emulsions prepared with (a) 50 mg/L, (b) 75 mg/L, (c) 100 mg/L and (d) 150 mg/L oil concentration.**

### 3.3.4 Identification of competent flux decline mechanism

The identification of competent flux decline mechanism is very important for any MF processes. The decline in permeate flux during dead end MF of o/w emulsions was analyzed using different membrane pore blocking models as discussed in section 3.2. To find the most prominent fouling mechanism among the pore blocking models, linear plots corresponding to Eqs. (4) - (7) were prepared. Figures 3.5 - 3.8 illustrate the fitness of complete pore blocking, standard pore blocking, intermediate pore blocking and cake filtration model, respectively for all oil concentrations. From all figures, it was observed that the experimental data sets followed two linear trends corresponding to initial phase of 5 - 10 minutes and the rest upto 30 minutes. It can also be observed in these figures that initial phases were 10, 8, 7 and 5 minutes for initial oil concentrations of 50, 75, 100 and 150 mg/L, respectively. A reduction in initial time regime with oil concentration was due to the presence of higher amount of oil droplets at higher oil concentrations which facilitated pore blocking within lesser time frames. Overall, the flux decline with time occurred due to two different pore blocking mechanisms. Similar trends results were also observed during treatment of oily wastewater with a polymeric membrane [91]. Henceforth, the experimental flux data was further analyzed separately in two time regimes, namely the initial regime (during the first 5 - 10 minutes of MF) and the later regime to identify the most competent combinations of models in both the regimes. In order to visualize the most competent fouling phenomena during the initial phases, linear regression analysis was carried out to obtain slope, intercept as well as correlation coefficients ($R^2$) of all flux data. To find the most prominent fouling mechanism, values of $R^2$ were considered. Table 3.2 summarized the calculated values of all the models for both regimes namely initial and later regime. For the initial regime, it can be critically

observed from Fig. 3.8 that there exists negative intercept for cake filtration model. As negative intercept values infer to negative initial permeate flux, this model could not be justified physically and henceforth was ignored in the subsequent analysis of flux decline for initial regime. Further, it can be also observed in Table 3.2 for the same regime that $R^2$ values for all other models (standard pore blocking, complete pore blocking and intermediate pore

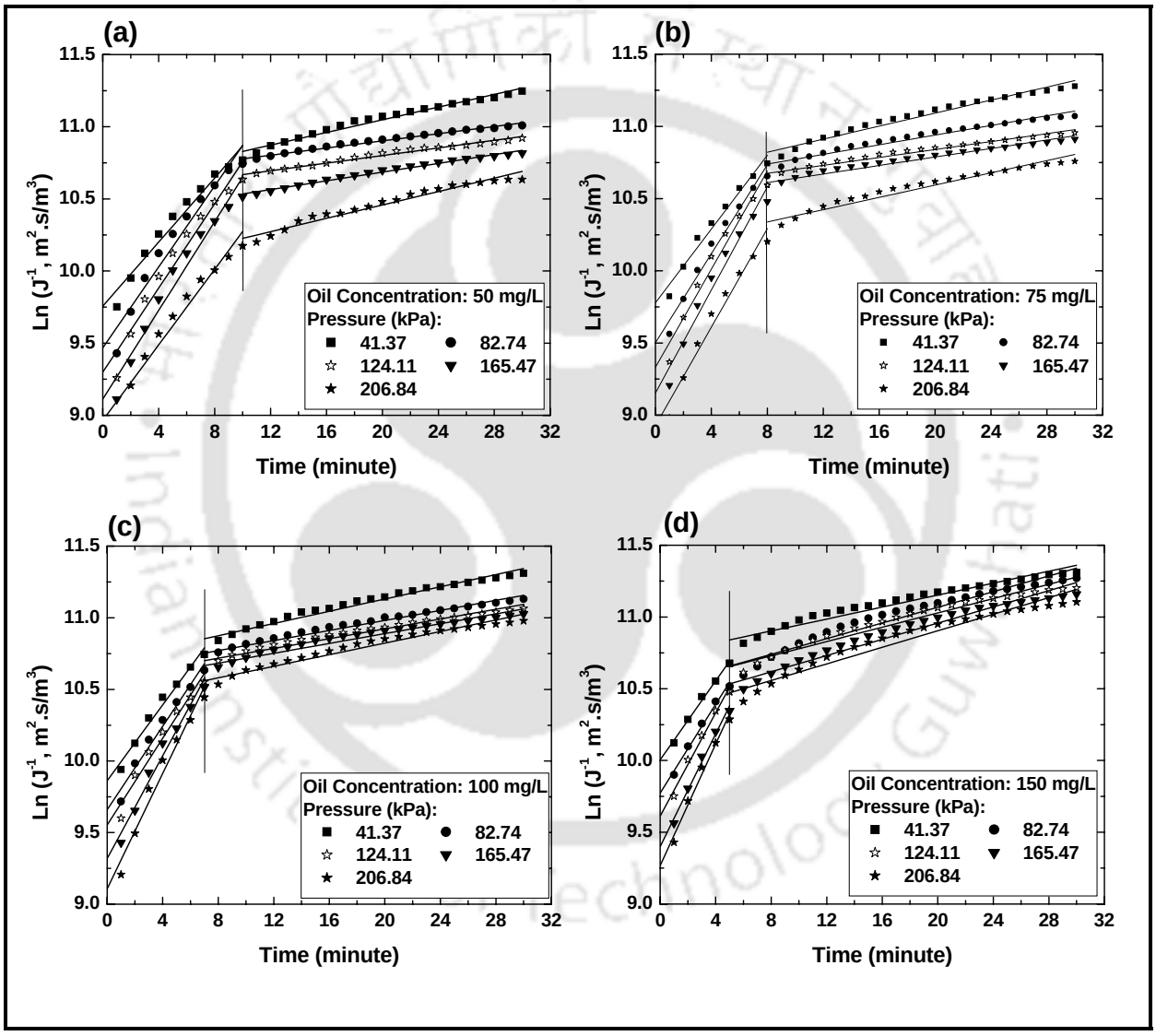


**Figure 3.5: Linear plot of permeate flux variation with time for complete pore blocking model. Initial oil concentration: (a) 50 mg/L, (b) 75 mg/L, (c) 100 mg/L and (d) 150 mg/L.**

blocking) were in appreciable range (0.954 - 0.999). To further analyze the applicability of various models, percent error of experimental flux and predicted permeate flux using slope and intercept values for the models were evaluated and analyzed. Percent error of permeate flux was calculated using the expression:

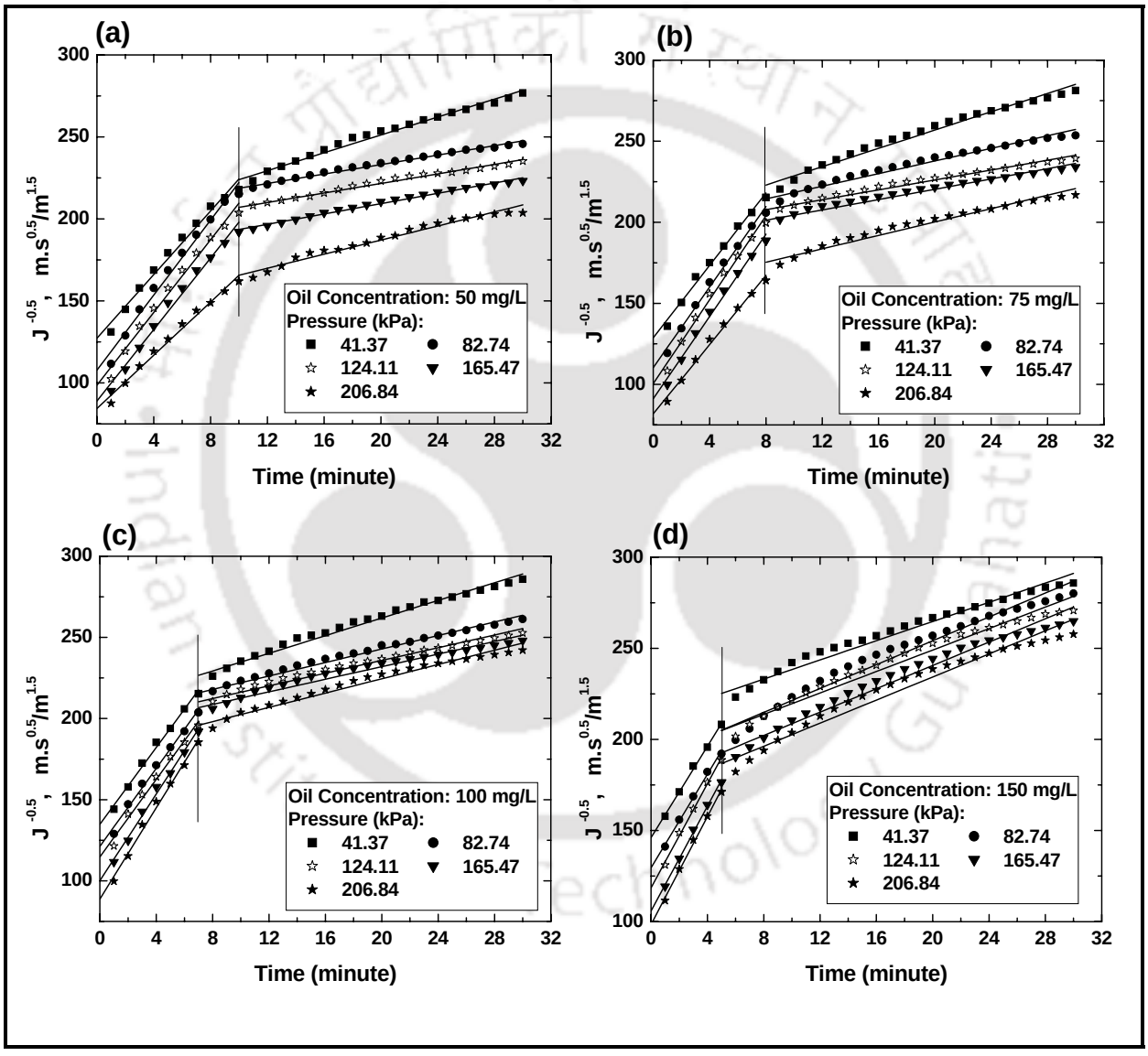


**Figure 3.6: Linear plot of permeate flux variation with time for standard pore blocking model. Initial oil concentration: (a) 50 mg/L, (b) 75 mg/L, (c) 100 mg/L and (d) 150 mg/L.**

$$Error(\%) = \left( \frac{J_{\exp} - J_{cal}}{J_{\exp}} \right) \times 100 \qquad (3.8)$$

Figure 3.9a shows results obtained from error analysis for experimental condition of 150 mg/L initial oil concentration and 41.37 kPa trans-membrane pressure drop. Based on the observations from Fig. 3.9a, it can be inferred that intermediate pore blocking model is the

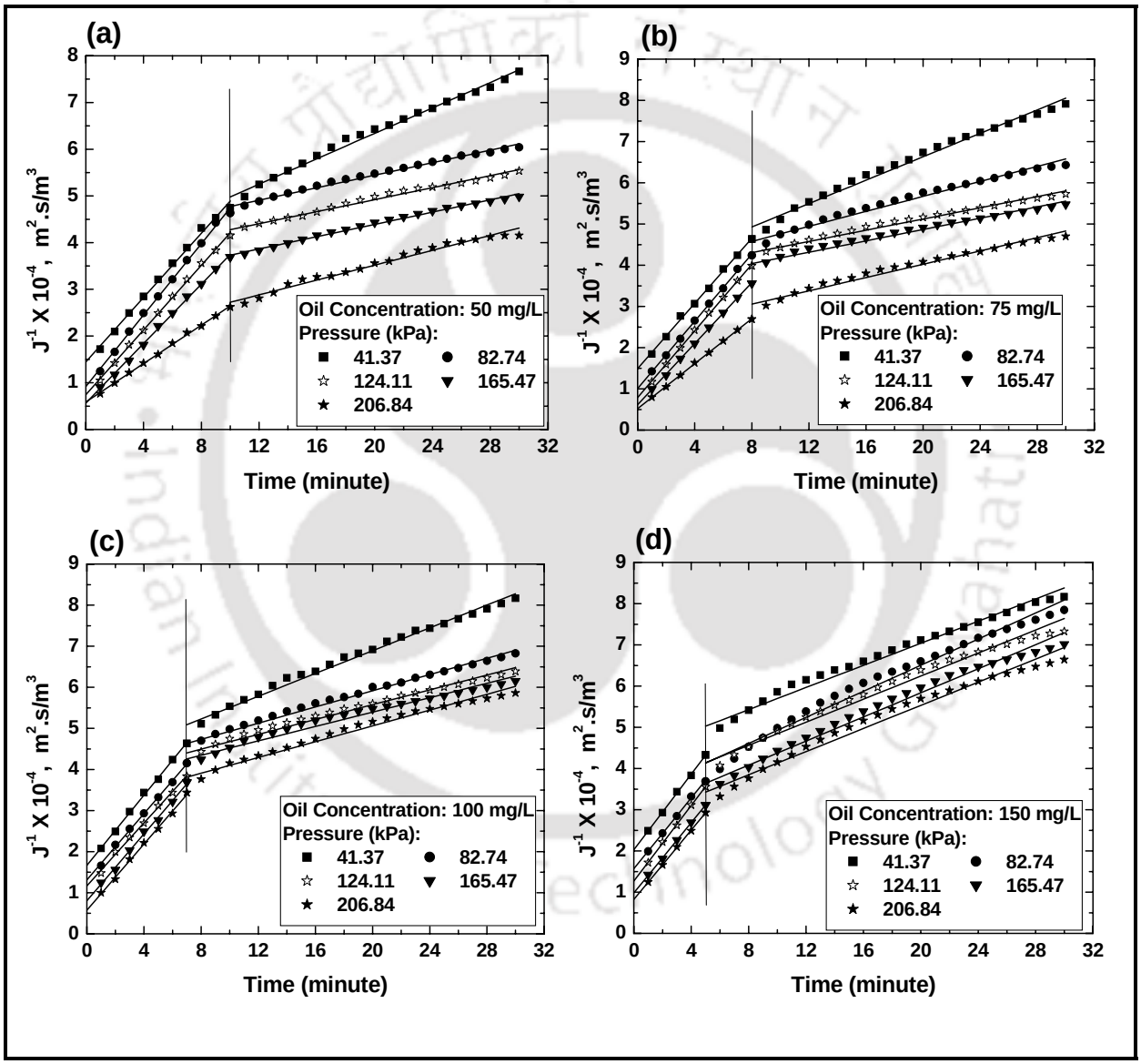


**Figure 3.7: Linear plot of permeate flux variation with time for intermediate pore blocking model at various initial oil concentrations: (a) 50 mg/L, (b) 75 mg/L, (c) 100 mg/L and (d) 150 mg/L.**

most appropriate model to account for the flux decline mechanism during the initial regime with the lowest errors. Similar observations were also observed for other experimental conditions (different initial oil concentrations and different $\Delta P$) as well. On the other hand, for the later regime error analysis was carried out for all the models. Figure 3.9b shows results obtained from error analysis using Eq. (3.8) for 75 mg/L initial oil concentration and $\Delta P$ of 124.11 kPa. Based on the observations from Fig. 3.9b, it can be inferred errors were minimum

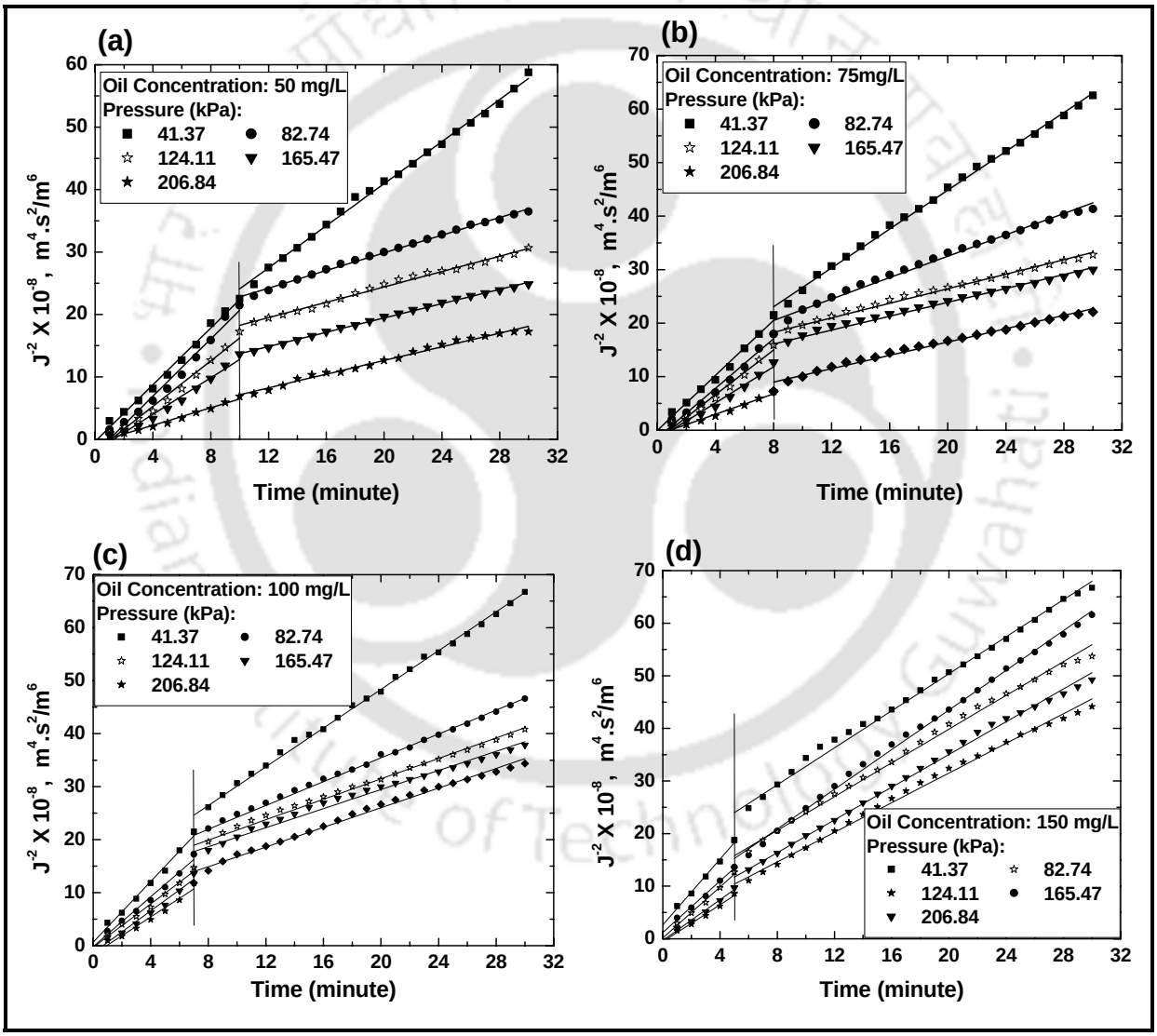


**Figure 3.8: Linear plot of permeate flux variation with time for cake filtration model. Initial oil concentration: (a) 50 mg/L, (b) 75 mg/L, (c) 100 mg/L and (d) 150 mg/L.**

**Table 3.2: Correlation coefficients obtained from linear regression analysis of permeate flux data for various membrane pore blocking models.**

| C (mg/L) | Pressure (kPa) | Complete pore blocking | | Standard pore blocking | | Intermediate pore blocking | | Cake filtration | |
|---|---|---|---|---|---|---|---|---|---|
| | | Initial regime | Final regime | Initial regime | Final regime | Initial regime | Final regime | Initial regime | Final regime |
| 50 | 41.37 | 0.963 | 0.972 | 0.984 | 0.982 | 0.995 | 0.989 | 0.992 | 0.997 |
| | 82.74 | 0.955 | 0.978 | 0.985 | 0.983 | 0.998 | 0.987 | 0.981 | 0.994 |
| | 124.11 | 0.954 | 0.977 | 0.986 | 0.982 | 0.999 | 0.986 | 0.981 | 0.991 |
| | 165.47 | 0.960 | 0.987 | 0.988 | 0.991 | 0.998 | 0.994 | 0.977 | 0.998 |
| | 206.84 | 0.962 | 0.962 | 0.988 | 0.972 | 0.999 | 0.989 | 0.983 | 0.989 |
| 75 | 41.37 | 0.974 | 0.964 | 0.991 | 0.976 | 0.998 | 0.986 | 0.988 | 0.997 |
| | 82.74 | 0.975 | 0.950 | 0.993 | 0.962 | 0.999 | 0.973 | 0.981 | 0.994 |
| | 124.11 | 0.964 | 0.982 | 0.989 | 0.987 | 0.999 | 0.991 | 0.982 | 0.996 |
| | 165.47 | 0.967 | 0.982 | 0.991 | 0.987 | 1.000 | 0.991 | 0.978 | 0.996 |
| | 206.84 | 0.970 | 0.962 | 0.992 | 0.973 | 1.000 | 0.982 | 0.978 | 0.994 |
| 100 | 41.37 | 0.981 | 0.959 | 0.993 | 0.973 | 0.998 | 0.984 | 0.990 | 0.996 |
| | 82.74 | 0.974 | 0.946 | 0.991 | 0.961 | 0.998 | 0.973 | 0.986 | 0.999 |
| | 124.11 | 0.966 | 0.914 | 0.987 | 0.935 | 0.997 | 0.993 | 0.989 | 0.998 |
| | 165.47 | 0.978 | 0.963 | 0.993 | 0.972 | 0.997 | 0.980 | 0.971 | 0.991 |
| | 206.84 | 0.970 | 0.967 | 0.992 | 0.976 | 0.998 | 0.984 | 0.967 | 0.994 |
| 150 | 41.37 | 0.993 | 0.968 | 0.997 | 0.979 | 0.999 | 0.988 | 0.992 | 0.997 |
| | 82.74 | 0.989 | 0.950 | 0.996 | 0.968 | 0.999 | 0.982 | 0.994 | 0.998 |
| | 124.11 | 0.986 | 0.958 | 0.996 | 0.972 | 0.999 | 0.983 | 0.989 | 0.996 |
| | 165.47 | 0.989 | 0.959 | 0.997 | 0.974 | 1.000 | 0.985 | 0.987 | 0.997 |
| | 206.84 | 0.984 | 0.944 | 0.996 | 0.963 | 1.000 | 0.978 | 0.985 | 0.996 |

for cake filtration model. Hence cake filtration model was selected as the most appropriate pore blocking model to represent the flux decline during the later regime with lowest error. Therefore, based on the physical observation as well as the fitness of the cake filtration model,

it was inferred that a thin layer of oil droplets formed during the membrane process justifies the fitness of a cake layer model. Therefore, it was herewith inferred that intermediate pore blocking followed with cake filtration represent the most competent combination of fouling mechanisms for the observed membrane flux decline. Table 3.3 summarized the final values of slope and intercept for both regimes. Based on these values predicted values of flux were calculated. Table 3.4 summarized the values of maximum and average errors for all data sets. Figure 3.10 presents a parity plot between experimental and calculated flux based on the combinations of the two most appropriate models in the initial and later regimes. As shown, a good fitness between experimental and evaluated values was observed and henceforth, the suggested model combination was inferred to be applicable for the analysis, design, planning and scheduling of time dependent MF processes for oil-water emulsion separation in the process industries.

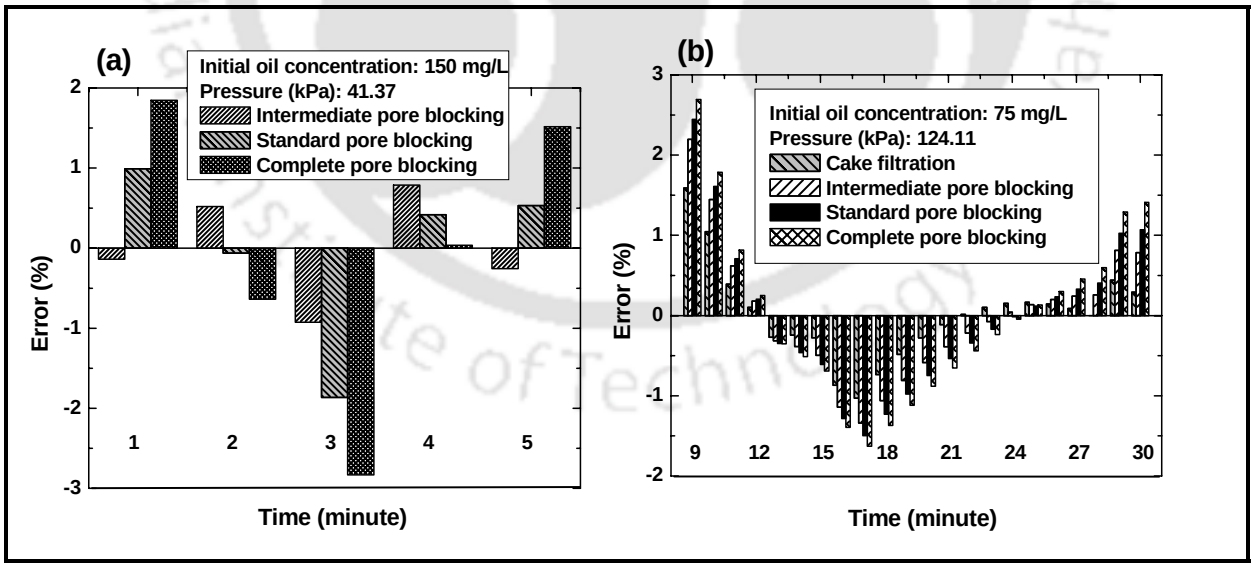


**Figure 3.9: Variation of error (%) with time for the initial and final flux decline regimes (a) initial oil concentration: 150 mg/L and trans-membrane pressure: 41.37 kPa and (b) initial oil concentration: 75 mg/L and trans-membrane pressure: 124.11 kPa.**

**Table 3.3: Slope and intercept values obtained from linear regression analysis for initial (intermediate pore blocking) and final (cake filtration) flux decline regimes.**

| C (mg/L) | Pressure (kPa) | Initial regime (Intermediate pore blocking) | | Final regime (Cake filtration) | |
|---|---|---|---|---|---|
| | | $(J_0^{-1})$ | $(k_i)$ | $(J_0^{-2})\times 10^{-7}$ | $(k_C)\times 10^{-7}$ |
| 50 | 41.37 | 14458 | 3446.5 | 72.39 | 16.85 |
| | 82.74 | 9204 | 3824 | 157.27 | 7.07 |
| | 124.11 | 7447 | 3465 | 121.15 | 6.15 |
| | 165.47 | 5667 | 3181 | 79.95 | 5.72 |
| | 206.84 | 5888 | 2057 | 16.65 | 5.48 |
| 75 | 41.37 | 1492 | 3952 | 89.87 | 17.95 |
| | 82.74 | 1009 | 4081 | 132.78 | 9.66 |
| | 124.11 | 7905 | 4039 | 135.56 | 6.48 |
| | 165.47 | 6174 | 3703 | 119.44 | 6.04 |
| | 206.84 | 5185 | 2731 | 45.44 | 5.99 |
| 100 | 41.37 | 16650 | 4272 | 126.53 | 17.90 |
| | 82.74 | 13128 | 4032 | 139.41 | 10.80 |
| | 124.11 | 11666 | 3831 | 133.27 | 9.14 |
| | 165.47 | 8024 | 4067 | 125.60 | 8.52 |
| | 206.84 | 5725 | 4024 | 80.59 | 9.02 |
| 150 | 41.37 | 20296 | 4585 | 163.22 | 17.08 |
| | 82.74 | 15708 | 4287 | 61.59 | 18.69 |
| | 124.11 | 12714 | 4582 | 84.46 | 15.74 |
| | 165.47 | 9829 | 4263 | 43.50 | 15.36 |
| | 206.84 | 8251 | 4202 | 37.27 | 13.91 |

A critical analysis of the membrane permeation characteristics based on pore size distribution also yields conclusive insights upon pertinent flux decline phenomena. Based on SEM based pore size distributions summarized in chapter 2, it can be observed that the membrane pores varied from 0.15 - 2.5 μm. On the other hand, droplet size distribution for all oil

**Table 3.4: A summary of errors evaluated using best fit flux decline models (intermediate pore blocking followed with cake filtration).**

| C (mg/L) | Pressure (kPa) | Maximum error | Average error |
|---|---|---|---|
| 50 | 41.37 | 4.03 | 0.90 |
| | 82.74 | 4.38 | 0.74 |
| | 124.11 | 3.86 | 0.79 |
| | 165.47 | 2.93 | 0.78 |
| | 206.84 | 3.50 | 1.23 |
| 75 | 41.37 | 3.39 | 0.77 |
| | 82.74 | 2.33 | 0.71 |
| | 124.11 | 1.83 | 0.49 |
| | 165.47 | 2.42 | 0.47 |
| | 206.84 | 2.64 | 0.92 |
| 100 | 41.37 | 1.86 | 0.61 |
| | 82.74 | 3.20 | 0.71 |
| | 124.11 | 4.72 | 0.95 |
| | 165.47 | 3.62 | 1.30 |
| | 206.84 | 3.52 | 1.10 |
| 150 | 41.37 | 2.78 | 0.74 |
| | 82.74 | 3.64 | 0.80 |
| | 124.11 | 2.45 | 0.79 |
| | 165.47 | 1.48 | 0.60 |
| | 206.84 | 3.24 | 0.97 |

concentrations varied from 0.04 - 100 μm (Fig. 3.2). Therefore, amongst these droplets it can be expected that droplets with size distributions 0.04 - 0.15 μm would not get rejected by the membrane and droplets with sizes above 2.5 μm (6 - 7.62 %) would be rejected fully by the membrane. Also droplets in the range 0.15 - 2.5 μm either enter the pores or rejected by the membrane and contribute to intermediate pore blocking and cake filtration. Therefore,

droplets with sizes above 2.5 μm contribute towards the formation of a thin oily layer over the membrane that is realized as cake filtration phenomena during filtration studies. Henceforth, it is apparent that the pertinent flux decline shall constitute an initial phase of intermediate pore blocking followed with cake filtration. These insights are in accordance with fouling phenomena trends evaluated previously in this section.

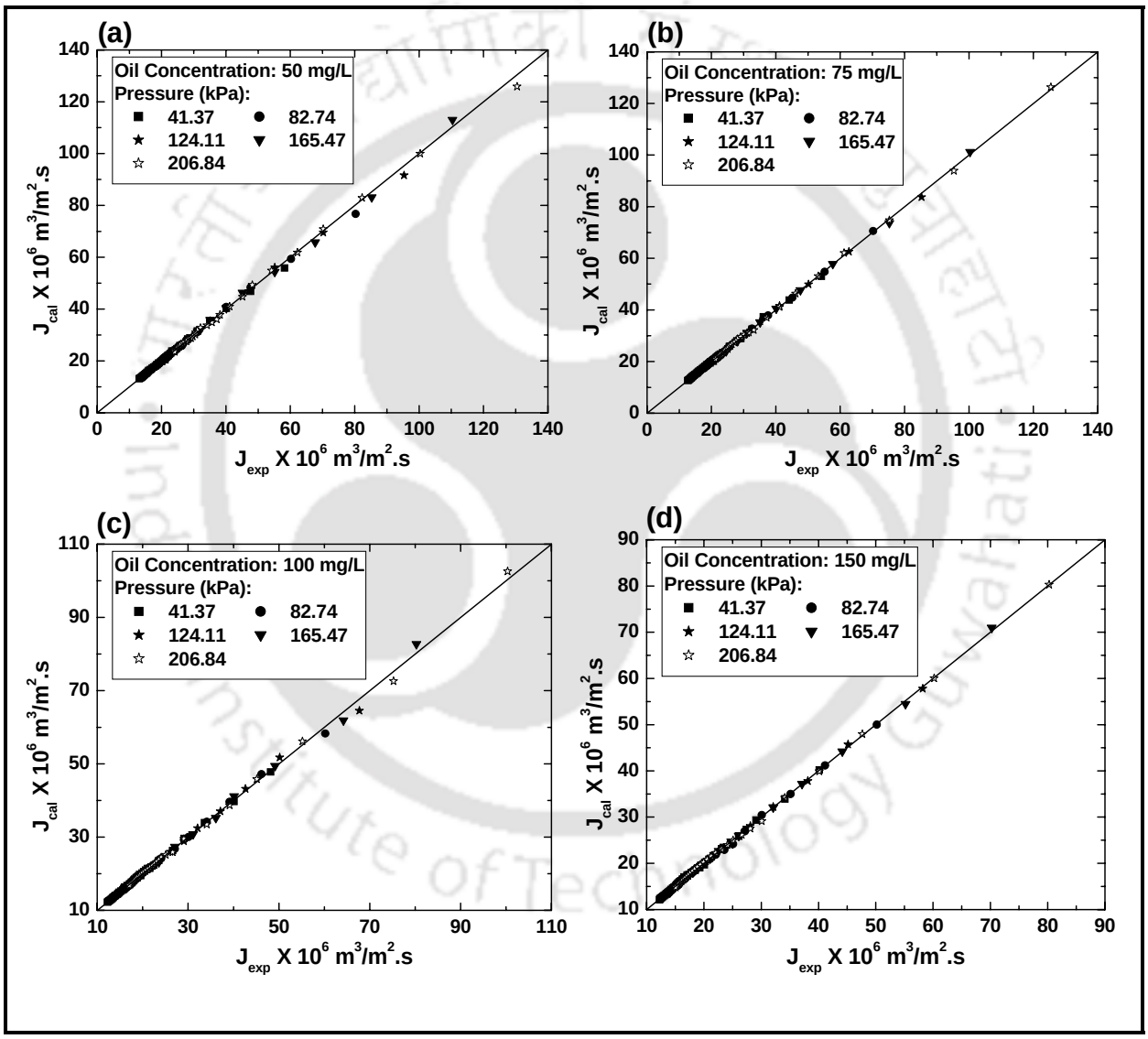


**Figure 3.10: Parity plot of experimental and evaluated permeate flux using a combination of intermediate pore blocking and cake filtration model.**

# Chapter 4:

## Microfiltration of Mosambi Juice using Ceramic Membranes

# *Chapter 4*

# Microfiltration of Mosambi Juice using Ceramic Membranes

*This chapter addresses the influence of membrane pore size and porosity on the permeation characteristics of centrifuged mosambi juice as well as enzyme treated centrifuged mosambi juice using the prepared membranes (A1, A2, A3 and A4). Different physio-chemical properties of the mosambi juice such as colour, clarity, pH, citric acid content, total soluble solid, alcohol insoluble solid were measured before and after the MF to evaluate the effect of effective permeability factor on juice quality. Various membrane pore blocking models were used to identify the most prominent flux decline mechanism. Based on observed MF flux decline data, phenomenological models were proposed to illustrate the dependency of total hydraulic resistance of membrane on effective permeability factor, trans-membrane pressure differential and filtration time. Finally, the stability of the clarified juice for long term storage was also studied by keeping the clarified juices up to 30 days in refrigerated condition.*

## 4.1 Experimental

### 4.1.1 Membrane

Four different membranes namely A1, A2, A3 and A4 fabricated using composition A were used for MF of mosambi juice. Various morphological properties of these membranes are summarized in Table 4.1.

**Table 4.1: Morphological properties for various membranes (A1, A2, A3 and A4).**

| Membrane name | $d_l$, μm | $\varepsilon_m$ | $\varepsilon_m d_l^2$, μm$^2$ | $R_m \times 10^{-11}$, m$^2$/m$^3$ |
|---|---|---|---|---|
| A1 | 0.77 | 0.420 | 0.249 | 5.78 |
| A2 | 0.86 | 0.395 | 0.294 | 4.90 |
| A3 | 1.08 | 0.38 | 0.443 | 3.23 |
| A4 | 1.54 | 0.33 | 0.783 | 1.83 |

### 4.1.2 Juice preparation and pre-treatment

Mosambi fruits (sweet orange, *Citrus sinensis (L.) Osbeck*) of proper maturity and ripeness were purchased from the local market and used for juice extraction. The juice was extracted from depulped fruits in a manually operated screw type juice extractor. Pectinase (*SRL, India*) with activity 3.5 units/mg (proteins Lowry) was used for enzymatic treatment of mosambi juice. The extracted juice was centrifuged (*Make: Eltek India; Model: TC 8100 D*) at 4000 rpm for 20 minutes to prepare the centrifuged juice (CJ). The enzyme treated centrifuged juice (ETCJ) was prepared by pre-treatment of mosambi juice with pectinase followed by centrifugation at 4000 rpm for 20 minutes. The centrifugation speed and duration was determined from a trial and error method to remove maximum amount of suspended solids from the juice and achieve juice with highest clarity and minimum colour. The enzymatic pretreatment of the juice was carried out by heating the juice at 42 $^{o}$C temperature for 100 minutes with enzyme an concentration of 0.0004 w/v%. Subsequently, the suspension was heated to 90 $^{o}$C for 5 minutes in a water bath to inactivate the remaining enzyme in the juice. Finally, the juice was cooled to ambient temperature (25 $^{o}$C) and centrifuged at 4000 rpm for 20 minutes.

### 4.1.3 Microfiltration studies

Dead-end MF experiments were carried out in a membrane permeation cell of capacity 300 ml. A schematic of the experimental setup has been shown in Fig. 2.2 in chapter 2. MF experiments were carried out with both CJ and ETCJ for all the membranes (A1, A2, A3 and A4) at a trans-membrane pressure drop ( $\Delta P$ ) of 82.74 kPa to evaluate the effect of pore sizes on permeation characteristics. Four different $\Delta P$ of 41.37, 82.74, 124.11 and 165.47 kPa were used to study the pressure effect on the permeation characteristics. The permeate flux was measured using methods similar to those mentioned in chapter 3 (Eq. 3.1).

### 4.1.4 Membrane cleaning

After MF experiment, a thick gel layer was observed over the membrane surface. To regain membrane permeability membrane cleaning was carried out. For this purpose, the SS casing containing the membrane was first removed from the set up. Then the membrane surface was cleaned with soft nylon brush and washed with tap water. Subsequently, the membrane was kept in a sonicator bath for 15 minutes to remove loose particles inside the membrane pores. Finally, the membrane was fixed in the experimental set up and 50 ml alkaline solution (0.02 N NaOH) was passed through the membrane at 41.37 kPa. After this cleaning procedure, it was observed that the membrane regained more than 98 % of pure water flux of the fresh membrane.

### 4.1.5 Analytical methods

Particle size distributions of CJ and ETCJ samples were measured using a laser particle size analyzer (*Make: Malvern, USA; Model: Mastersizer 2000*). All juice samples (FJ, CJ, ETCJ and permeate of CJ, ETCJ) were analyzed for colour, clarity, soluble solids, pH, acidity,

viscosity, density and alcohol insoluble solids (AIS). Colour and clarity of the juice were evaluated by measuring the absorbance at 420 nm and transmittance at 660 nm, respectively using a UV/Vis spectrophotometer (*Make: Perkin Elmer Precisel, USA; Model: Lambda 35)* [63]. TSS was determined (in $^{o}$Brix) using a digital refractometer (*Make: Atago, India; Model: DR-A1*). The pH of the samples was measured using a water and soil analysis kit (*Make: VSI Electronics, India; Model: VSI-06D1*,). Acidity measurements were carried out by titrating 10 mL of the juice sample with 0.1 N NaOH until the solution pH reaches to 8.2 and was expressed as wt % anhydrous citric acid equivalent. Viscosity of the juice samples was measured using a glass Oswald capillary viscometer (*Make: Pisco, India; Model: D 30797*). The density was measured using 25 mL pycnometer. AIS were used as a measure of pectic material in the juice. AIS were measured by mixing 20 g juice with 300 mL of 80 % methanol solution and simmering for 30 minutes. Subsequently, the solution was filtered and the residue was again washed with 80 % alcohol solution followed by drying at 100 $^{o}$C for 2 hours. After drying, the final residue was weighed and expressed as AIS in wt % [93].

## 4.2 Applicable theory

Theoretically the effects of membrane morphology on flux decline characteristics can be studied from the analysis of pure water flux and permeate flux through the membrane. Pure water flux ($J_W$) through a membrane can be expressed conveniently as a function of membrane porosity ($\varepsilon_m$), pore diameter ($d_l$) and pore length ($l_m$) as [2]:

$$J_W = \frac{\Delta P}{\mu_w}\frac{1}{R_m} = \frac{\Delta P}{\mu_w}\frac{\varepsilon_m d_l^{\,2}}{32 l_m} \tag{4.1}$$

During a MF run, the membrane is fouled by the suspended solids causing variations in the morphological properties of the membrane ($\varepsilon_m$, $d_l$, $l_m$). Theoretically, the fouled membrane can be assumed as a composite membrane with porosity ($\varepsilon_{cm}$), pore diameter ($d_{cm}$) and pore length ($l_{cm}$) which vary as functions of time due to continuous fouling of the membrane. Thereby, the permeate flux of the composite membrane can be expressed similar to Eq. (4.1):

$$J_J(t) = \frac{\Delta P}{\mu_J}\frac{1}{R_t} = \frac{\Delta P}{\mu_J}\frac{\varepsilon_{cm} d_{cm}^{\ 2}}{32 l_{cm}} \tag{4.2}$$

A ratio of the Eq. (4.1) and (4.2) can relate the original morphological parameters to the time variant morphological parameters as:

$$\frac{J_J(t)}{J_W} = \frac{\mu_w}{\mu_J}\frac{\varepsilon_{cm} d_{cm}^{\ 2}}{\varepsilon_m d_l^{\ 2}}\frac{l_m}{l_{cm}} \tag{4.3}$$

For composite membrane as the thickness of the cake/gel layer varies negligibly with respect to the pore length ($l_{cm} \approx l_m$), Eq. (4.3) is further modified as:

$$\varepsilon_{cm} d_{cm}^{\ 2} = \varepsilon_m d_l^{\ 2}\frac{J_J(t)}{J_W}\frac{\mu_J}{\mu_w} \tag{4.4}$$

In expressions (4.1) - (4.4), $\varepsilon_m d_l^{\ 2}$ and $\varepsilon_{cm} d_{cm}^{\ 2}$ correspond to effective permeable area factors that determine the actual permeable area available during filtration for the fresh and fouled membrane, respectively. It can also be analyzed that higher values of $\varepsilon_{cm} d_{cm}^{\ 2}$ enable higher permeate fluxes. Further, the rate of decrease of $\varepsilon_{cm} d_{cm}^{\ 2}$ with time indicates the fouling rate of the membrane. In other words, a slower variation of $\varepsilon_{cm} d_{cm}^{\ 2}$ with time indicates lower fouling rate of the membrane. The reduction in the value of $\varepsilon_{cm} d_{cm}^{\ 2}$ can be brought forward by a reduction in either effective membrane porosity ($\varepsilon_{cm}$) or pore diameter ($d_{cm}$) or both. A

reduction in $d_{cm}$ enables enhancement in permeate quality due to increased rejection capability of the membrane. Therefore, the morphological parameter based analysis in conjunction with permeate quality data is anticipated to identify suitable membrane property parameters for juice processing. Additionally, the effect of $\Delta P$ on morphological parameters can be also investigated to identify suitable range of $\Delta P$ causing lower fouling rates.

## 4.3 Results and discussion

### 4.3.1 Effect of pretreatment on juice quality

Table 4.2 summarizes various physio-chemical properties such as colour, clarity, TSS, acidity (as citric acid), pH, density, viscosity and AIS for FJ, CJ and ETCJ. From the table it can be inferred that the pretreatment of juice primarily affects the colour, clarity, viscosity, AIS values. On the other hand, valuable parameters of the juice such as TSS (a measure of sugar content), acidity, pH and density do not get altered significantly. Substantial improvement in the colour, clarity and viscosity were observed for CJ and ETCJ when compared to those corresponding to FJ. This was due to the removal of coloured suspended particles from the juice. Therefore, colour of the juice decreased (from 4.5 of FJ to 0.69 for CJ and 0.48 for ETCJ) and clarity increased (from 0.18 % (FJ) to 53.73 % (CJ) and 67.87 % (ETCJ)). Due to the same reason, the viscosity also decreased (from 3.56 (FJ) to 1.61 mPa.s (CJ) and 1.56 mPa.s (ETCJ)). The removal of pectic materials by enzyme treatment is further supported by the AIS values (0.34 (CJ) and 0.2 wt % (ETCJ)). A minute reduction in the juice density was observed after pre-treatment, which is attributed to the elimination of bigger suspended particles during centrifugation and enzyme treatment. The reduction in juice viscosity and AIS during pretreatment is advantageous for subsequent clarification by MF as they enhance

**Table 4.2: Physico-chemical properties of fresh and pre-treated mosambi juice.**

| Juice type | Colour ($A_{420}$) | Clarity ( $\%T_{660}$) | TSS ($^{o}$Brix) | Citric acid (wt %) | pH | Density (g/cm$^3$) | Viscosity (mPa.S) | AIS (wt %) |
|---|---|---|---|---|---|---|---|---|
| FJ | 4.50 | 0.18 | 9.2 | 0.84 | 3.79 | 1.04 | 3.56 | 0.92 |
| CJ | 0.69 | 53.73 | 9.1 | 0.84 | 3.80 | 1.038 | 1.61 | 0.34 |
| ETCJ | 0.48 | 67.87 | 9.1 | 0.84 | 3.80 | 1.037 | 1.56 | 0.2 |

the permeate flux. These variations in parameters also contribute towards longer life cycle of the membrane due to reduced fouling at lower concentrations of pectic material in the juice.

### 4.3.2 Effect of pore size on permeate flux

Permeate flux decline profiles for CJ and ETCJ at a $\Delta P$ of 82.74 kPa for different membranes (A1, A2, A3 and A4) are shown in Figs. 4.1a and 4.1b, respectively. From both the figures it can be observed that, permeate flux declined sharply within the initial phase of 10 - 15 minutes and becomes gradual thereafter. The decline in flux with time was due to pore blocking of ceramic porous structure as well as gel/cake layer formation over the membrane surface due to deposition of rejected pectic materials present in the juice. For CJ, the permeate flux decreased from $33.17\times10^{-6}$ to $5.79\times10^{-6}$ m$^3$/m$^2$.s for A1, $45.12\times10^{-6}$ to $7.69\times10^{-6}$ m$^3$/m$^2$.s for A2, $72.45\times10^{-6}$ to $10.12\times10^{-6}$ m$^3$/m$^2$.s for A3 and $92.37\times10^{-6}$ to $13.46\times10^{-6}$ m$^3$/m$^2$.s for A4 membrane during 40 minutes of experimental run (Fig. 4.1a). Increasing trends in permeate flux for A1 to A4 membranes were due to enhancement in effective permeable area factor ($\varepsilon_m d_m^{\,2}$). Similar flux decline trends were also observed for ETCJ (Fig. 4.1b). For ETCJ, initial permeate flux varied from $59.71\times10^{-6}$ m$^3$/m$^2$.s (A1) to $185.78\times10^{-6}$ m$^3$/m$^2$.s (A4). Also, permeate flux was higher for ETCJ compared to the CJ. This was due to

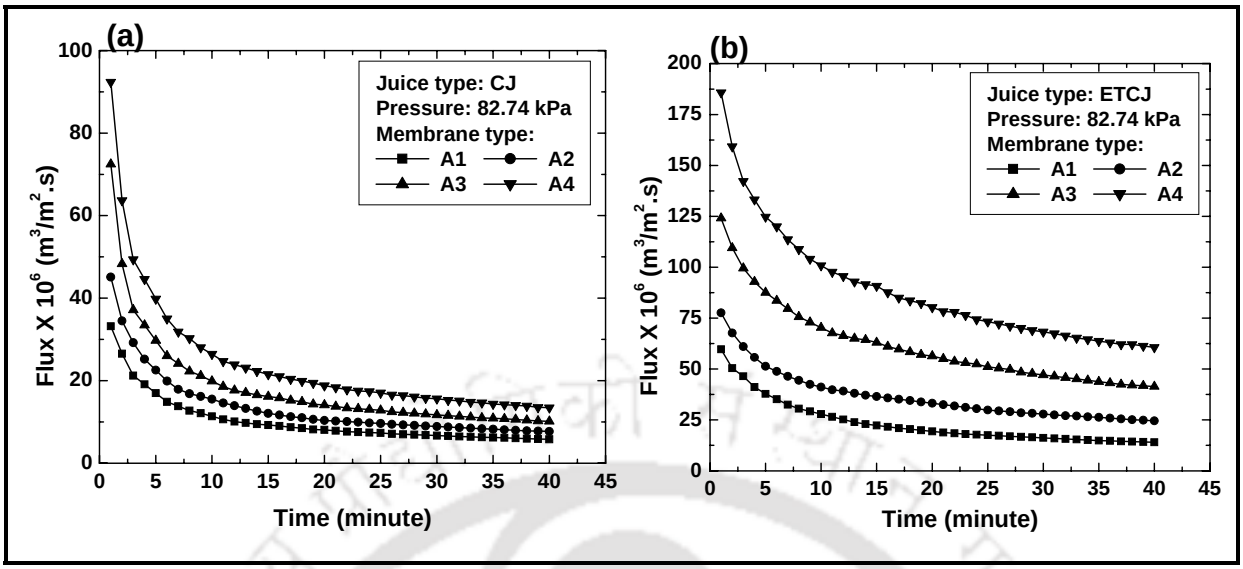


**Figure 4.1: Variation of permeate flux with time for various membranes at a trans-membrane pressure drop of 82.74 kPa for (a) CJ and (b) ETCJ.**

the presence of higher amounts of pectic material in the CJ (causing higher amount of gel layer formation) as well as higher viscosity of the centrifuged juice. However, a critical observation of the flux decline profile for CJ and ETCJ reveals that the flux decline profiles for CJ were placed more adjacent to one another when compared to the ETCJ flux decline profiles. This was due to the high quantity of pectic materials in CJ that causes severe fouling irrespective of pore diameters. However, for ETCJ the flux decline profiles have been observed to vary significantly with an increase in effective permeable area factor ($\varepsilon_m d_l^{\,2}$). Therefore, the membrane morphology was found to have predominant influence for the MF of ETCJ and smaller effect for the MF of CJ.

### 4.3.3 Effect of operating pressure on permeate flux

Permeate flux decline profiles of A2 membrane for CJ and ETCJ at various $\Delta P$ (41.37, 82.74, 124.11 and 165.47 kPa) are shown in Fig. 4.2a and 4.2b, respectively. From both the

figures, it can be observed that permeate flux declined sharply within the initial phase of 10 - 15 minutes and becomes gradual thereafter. Decline in flux with time was due to pore blocking and gel/cake layer formation as discussed earlier. From both the figures, it was observed that permeate flux increased with an increase in $\Delta P$. The initial permeate flux increased from $29.13\times10^{-6}$ to $69\times10^{-6}$ $m^3/m^2.s$ for CJ and $42.46\times10^{-6}$ to $138\times10^{-6}$ $m^3/m^2.s$ for ETCJ when $\Delta P$ was increased from 41.37 to 165.47 kPa. An increase in permeate flux with $\Delta P$ was due to the higher driving force across the membrane. Higher permeate flux for ETCJ compared to the CJ was due to the presence of higher amounts of pectin materials in the CJ as discussed earlier.

### 4.3.4 Effect of membrane pore size on permeate juice quality

The pore size distributions of A1 and A4 membranes and particle size distributions of CJ and ETCJ are shown in Fig. 4.3. Pore size distributions of other membranes (A2 and A3) were in between A1 and A4 membranes. It can be observed from the pore size distribution of the

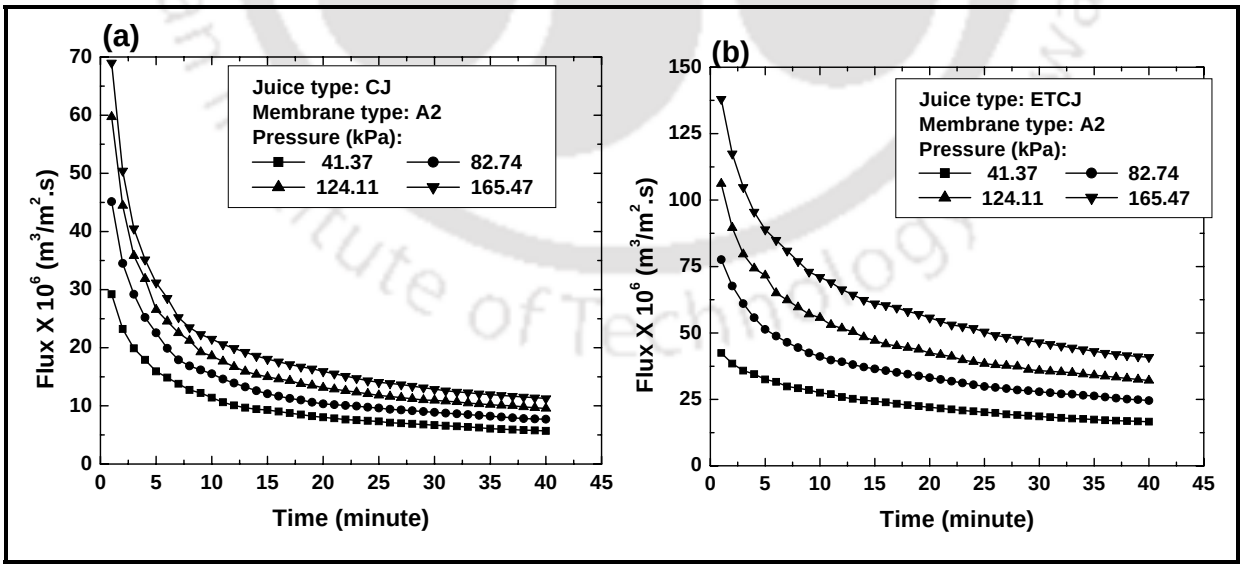


**Figure 4.2: Variation of permeate flux with time for A2 membrane at various trans-membrane pressure drops for (a) CJ and (b) ETCJ.**

membranes that maximum pore diameter was 2.5 μm and 3 μm for A1 and A4 membranes, respectively with more than 60 % of the pores having pore diameter below 1 μm. The obtained hydraulic pore diameters of the membranes were 0.77, 0.86, 1.08 and 1.54 μm for A1, A2, A3 and A4 membranes, respectively (Table 4.1). On the other hand, the particle size distributions of CJ and ETCJ indicate that the particle sizes in the juice samples varied from 0.038 - 8.15 μm. For CJ, 84.74 % of the particles were within the range of 0.038 - 2.5 μm and 15.26 % of the particles were within the range 2.5 - 8.15 μm. The average particle size for CJ was evaluated as 0.818 μm. For ETCJ, 96.2 % of the particles were within the range 0.038 - 2.5 μm and 3.8 % of the particles were within 2.5 - 8.15 μm. The average particle size of ETCJ was 0.365 μm.

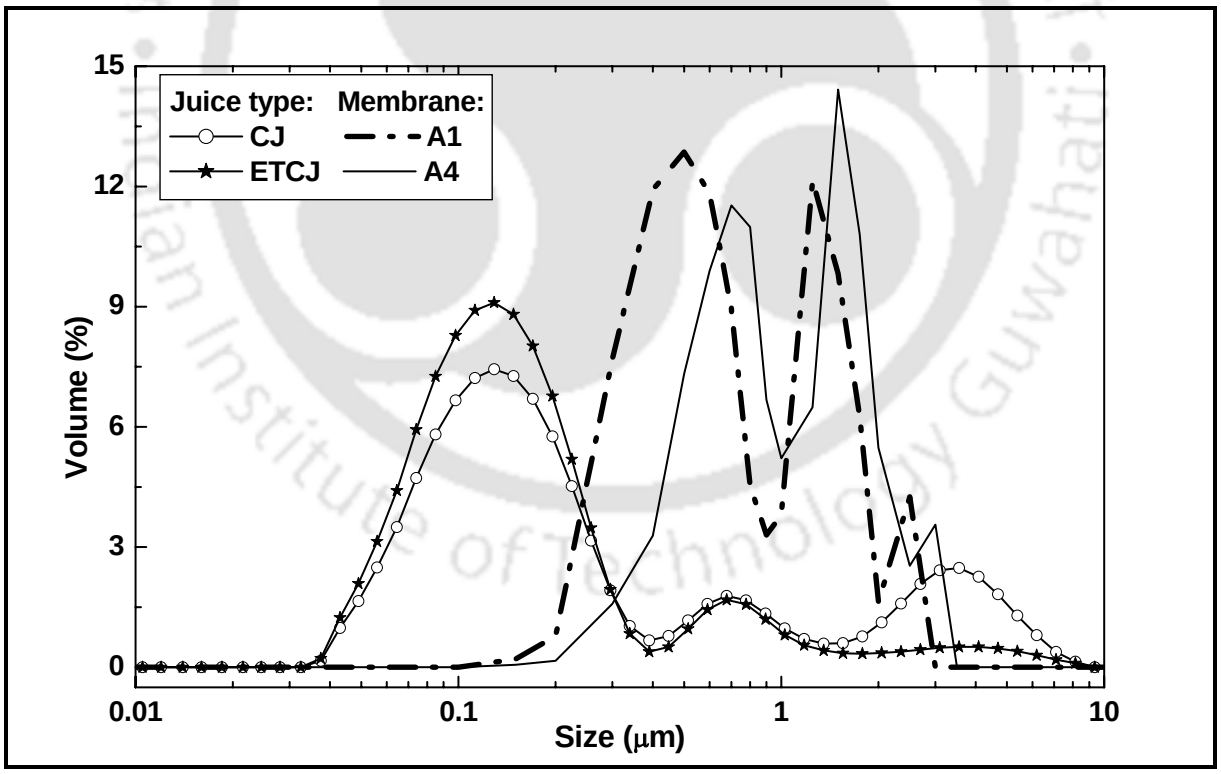


**Figure 4.3: Particle size distributions of CJ and ETCJ in conjunction with the pore size distributions of A1 and A4 membranes.**

Table 4.3 presents various physio-chemical properties of clarified CJ and ETCJ for different membranes (A1, A2, A3 and A4) at a $\Delta P$ of 82.74 kPa. From the table, it can be observed that there was significant improvement in the colour and clarity of the mosambi juice after filtration. For CJ using A1 membrane, colour decreased from 0.69 - 0.076, clarity increased from 53.73 - 94.39% and AIS decreased from 0.34 - 0.03%. With an increase in pore size of the membranes (A1 to A4), the quality of juice reduced marginally. For A4 membrane, measured colour, clarity, and AIS were 0.33, 84.61% and 0.10, respectively. A reduction in the permeate juice quality for A4 membrane was due to higher pore diameter of the membrane. With an increase in pore diameter, suspended particles with bigger size pass through the membrane and reduce the juice quality. For ETCJ, similar trends were also observed. However, permeate quality of ETCJ was observed to be better than that obtained from CJ. This was due to the lower amount of suspended materials in the corresponding feed juice. However, valuable properties of the juices such as pH, soluble solids, acidity and density did not vary significantly for both CJ and ETCJ for all the membranes. Similar observations were reported for UF of mosambi juice using polymeric membranes [63]. Therefore, these observations infer that the prepared ceramic membranes can be promising for juice processing.

An important observation in this study was that the average particle sizes ($d_p$) of CJ (0.815 μm) and ETCJ (0.365 μm) were not in comparable range with the hydraulic pore diameter of the membranes (0.77 – 1.54 μm). Despite such large variation, appreciable juice quality was obtained. This was due to the reason that around 15.26 % and 3.8 % suspended particles were present in the CJ and ETCJ, respectively and they were above the maximum pore diameter of the membrane (3 μm). These particles were directly rejected by the membranes and form a gel

**Table 4.3: Physico-chemical properties of membrane clarified mosambi juice for CJ and ETCJ at a trans-membrane pressure drop of 82.74 kPa.**

| Juice type | Membrane | Colour ($A_{420}$) | Clarity ( $\%T_{660}$) | TSS ($^oBrix$) | Citric acid (wt %) | pH | Density ($g/cm^3$) | Viscosity (mPa.S) | AIS (wt %) |
|---|---|---|---|---|---|---|---|---|---|
| CJ | A1 | 0.076 | 94.39 | 9.1 | 0.81 | 3.84 | 1.03 | 1.44 | 0.03 |
| | A2 | 0.143 | 90.54 | 9.1 | 0.81 | 3.84 | 1.03 | 1.45 | 0.06 |
| | A3 | 0.266 | 87.26 | 9.1 | 0.81 | 3.84 | 1.03 | 1.49 | 0.09 |
| | A4 | 0.330 | 84.61 | 9.1 | 0.81 | 3.84 | 1.03 | 1.51 | 0.10 |
| ETCJ | A1 | 0.068 | 96.44 | 9.1 | 0.81 | 3.85 | 1.03 | 1.42 | 0.01 |
| | A2 | 0.081 | 94.19 | 9.1 | 0.81 | 3.85 | 1.03 | 1.42 | 0.02 |
| | A3 | 0.131 | 91.21 | 9.1 | 0.81 | 3.85 | 1.03 | 1.45 | 0.04 |
| | A4 | 0.312 | 87.20 | 9.1 | 0.81 | 3.85 | 1.03 | 1.45 | 0.05 |

layer on the membrane. Similar results were also found by Obermeyer et al., [94] during RO and UF of whey solutions for the separation of milk proteins where better rejection was observed by the deposition of the gel layer during the membrane transport process. The morphology of the gel layer was influenced by other parameters such as pressure, membrane pore size, porosity and juice type (CJ and ETCJ). This layer acts as a thin film over the membrane with lower pore diameter than the actual membrane and substantially controlled the separation characteristics of the membrane. As a result, although average pore diameters of the membrane were higher than the average particle size of the membrane, appreciable separation of suspended particles was observed. Hence, the permeate characteristics are strongly influenced by the size distributions of suspended particles of the juice and membrane pores, but not the $d_p$ and $d_l$. Further, it can be also observed that the comparative variations in these distribution parameters play a critical role in the formation of a gel layer with appropriate morphology (porosity, pore size and thickness) and hence permeate flux and quality.

### 4.3.5 Effect of operating pressure on permeate juice quality

Variations in physio-chemical properties of clarified CJ and ETCJ for A2 membrane with varying $\Delta P$ (41.37, 82.74, 124.11 and 165.47 kPa) are presented in Table 4.4. From the table, it can be observed that colour, clarity, viscosity and AIS of the permeate juice varied marginally with $\Delta P$ for both CJ and ETCJ. The colour increased from 0.112 to 0.154 for CJ and from 0.072 to 0.134 for ETCJ, respectively when $\Delta P$ was increased from 41.37 to 165.47 kPa. Similarly, the clarity of juice decreased and viscosity and AIS increased with $\Delta P$. The reduction in the quality of the permeate juice with $\Delta P$ was due to higher driving force across the membrane. With an increase in driving force, some of the suspended particles passed through the membrane pores and reached the permeate stream due to which overall quality of the juice decreased. However, quality of the ETCJ permeate was higher than that obtained with CJ. This was due to the lower quantity of pectin materials in ETCJ when compared to the CJ as elaborated in section 4.3.1.

**Table 4.4: Physico-chemical properties of A2 membrane clarified mosambi juice for CJ and ETCJ at various values of trans-membrane pressure differentials.**

| Juice type | $\Delta P$ (kPa) | Colour ($A_{420}$) | Clarity ($\%T_{660}$) | TSS ($^{o}$Brix) | Citric acid (wt %) | pH | Density (g/cm$^3$) | Viscosity (mPa.S) | AIS (wt %) |
|---|---|---|---|---|---|---|---|---|---|
| CJ | 41.37 | 0.112 | 92.26 | 9.1 | 0.80 | 3.87 | 1.03 | 1.45 | 0.04 |
| | 82.74 | 0.143 | 90.54 | 9.1 | 0.81 | 3.84 | 1.03 | 1.45 | 0.06 |
| | 124.11 | 0.148 | 89.83 | 9.1 | 0.81 | 3.84 | 1.03 | 1.46 | 0.07 |
| | 165.47 | 0.154 | 87.67 | 9.1 | 0.81 | 3.84 | 1.03 | 1.46 | 0.08 |
| ETCJ | 41.37 | 0.072 | 95.85 | 9.1 | 0.78 | 3.9 | 1.03 | 1.42 | 0.02 |
| | 82.74 | 0.081 | 94.19 | 9.1 | 0.81 | 3.85 | 1.03 | 1.42 | 0.02 |
| | 124.11 | 0.091 | 92.59 | 9.1 | 0.81 | 3.85 | 1.03 | 1.42 | 0.03 |
| | 165.47 | 0.134 | 90.93 | 9.1 | 0.81 | 3.85 | 1.03 | 1.42 | 0.03 |

### 4.3.6 Analysis of membrane fouling mechanism

As outlined in section 3.2, the decline in permeate flux during dead end MF of o/w emulsions has been analyzed using different membrane pore blocking models. Figures 4.4 and 4.5 illustrate the fitness of different pore blocking models (complete pore blocking, standard pore

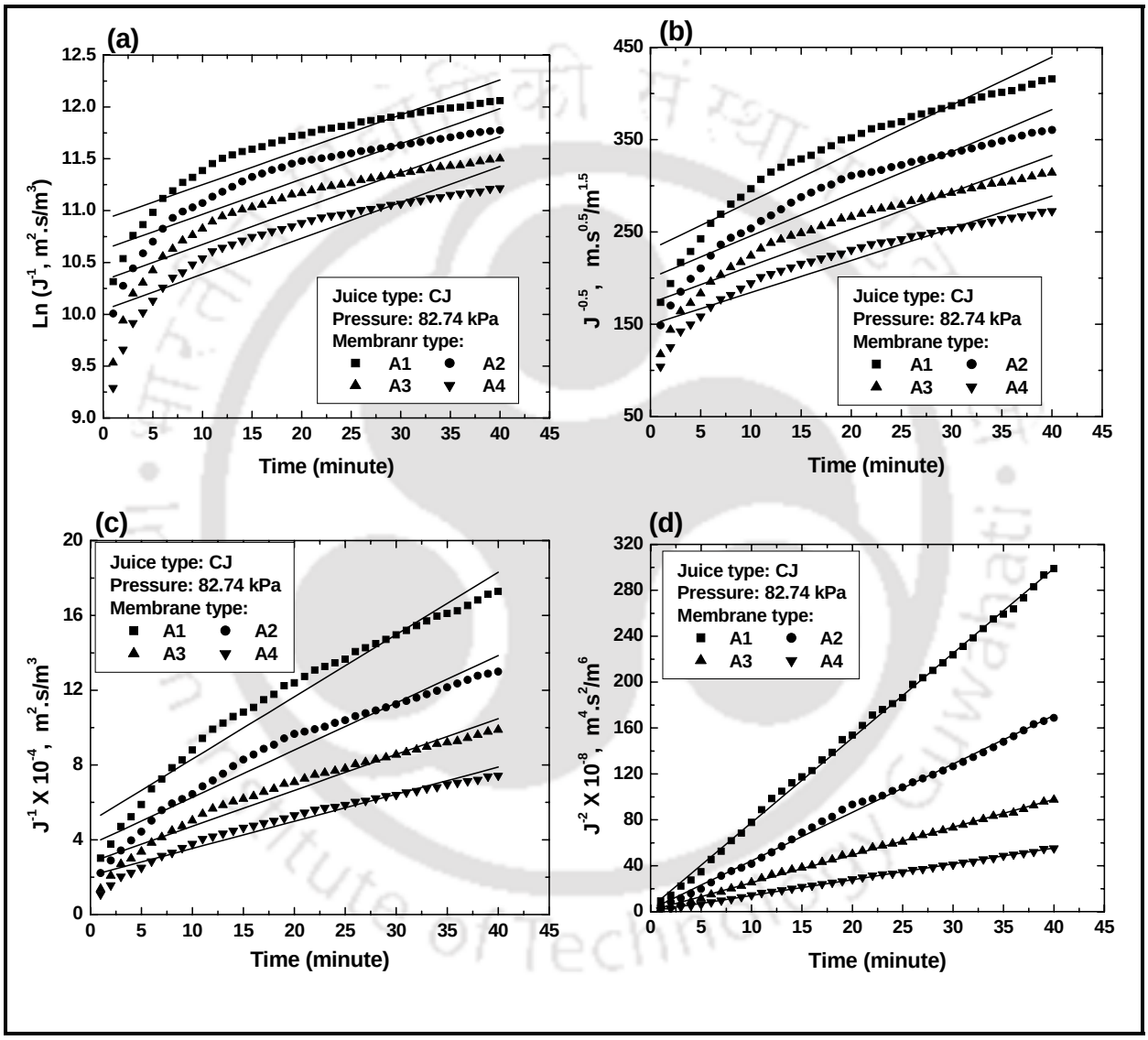


**Figure 4.4: Linearized plots of CJ permeate flux variation with time at constant pressure differential (82.74 kPa) for various membranes (a) complete pore blocking model, (b) standard pore blocking model, (c) intermediate pore blocking model and (d) cake filtration model.**

blocking, intermediate pore blocking and cake filtration model) for different membranes (A1, A2, A3 and A4) at $\Delta P$ of 82.74 kPa for CJ and ETCJ, respectively. Figures 4.6 and 4.7 illustrate the fitness of different pore blocking models (complete pore blocking, standard pore blocking, intermediate pore blocking and cake filtration model) for A2 membrane with

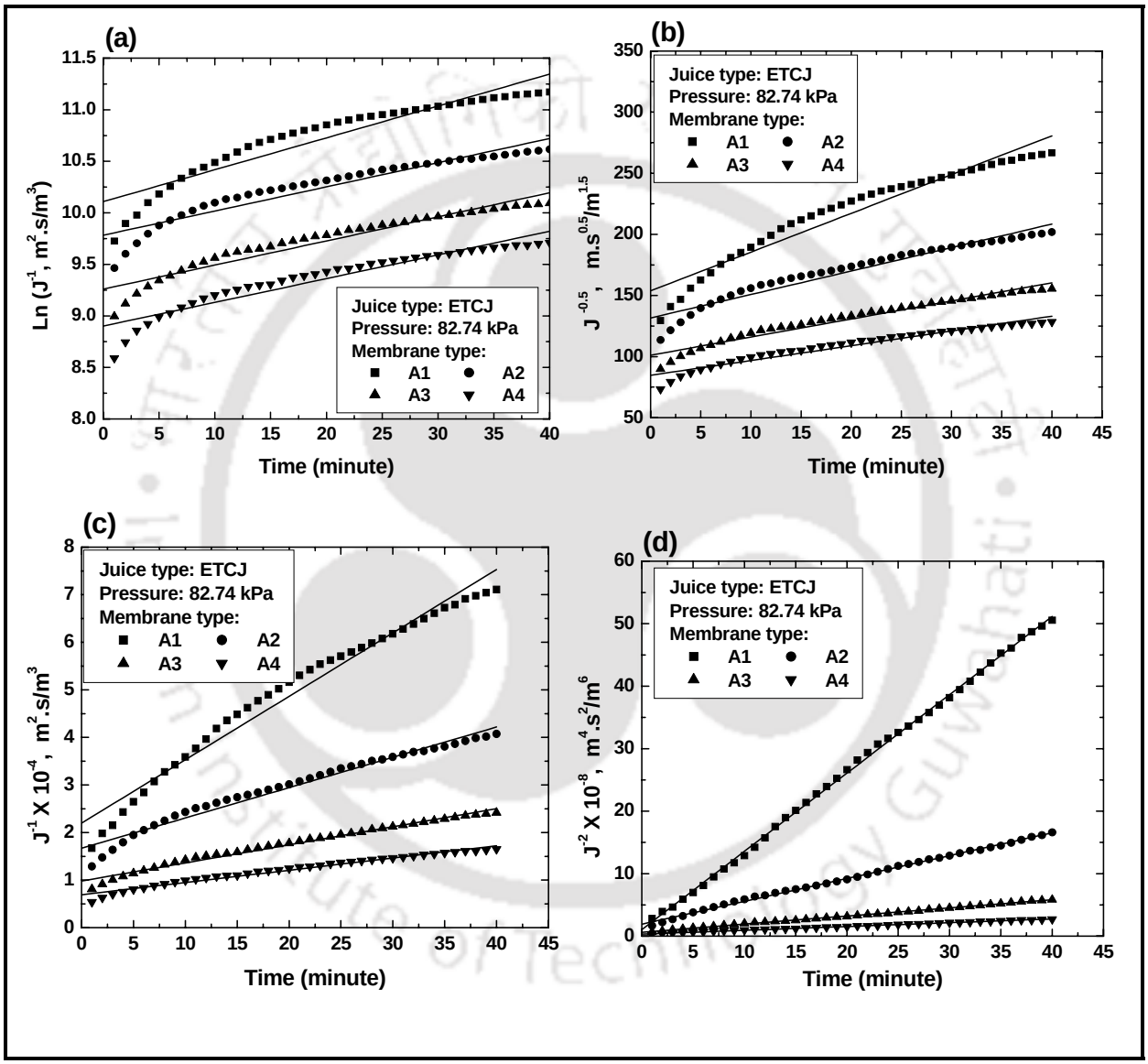


**Figure 4.5: Linearized plots of ETCJ permeate flux variation with time at constant pressure differential (82.74 kPa) for various membranes (a) complete pore blocking model, (b) standard pore blocking model, (c) intermediate pore blocking model and (d) cake filtration model.**

varying $\Delta P$ (41.37, 82.74, 124.11 and 165.47 kPa) for CJ and ETCJ, respectively. A critical observation of scatter trends in all the figures indicate that two linear trends are adopted during the duration of the MF experimental runs. Therefore, these trends indicate that there exist two different paradigms of fouling phenomena that correspond to the initial 4 to 5

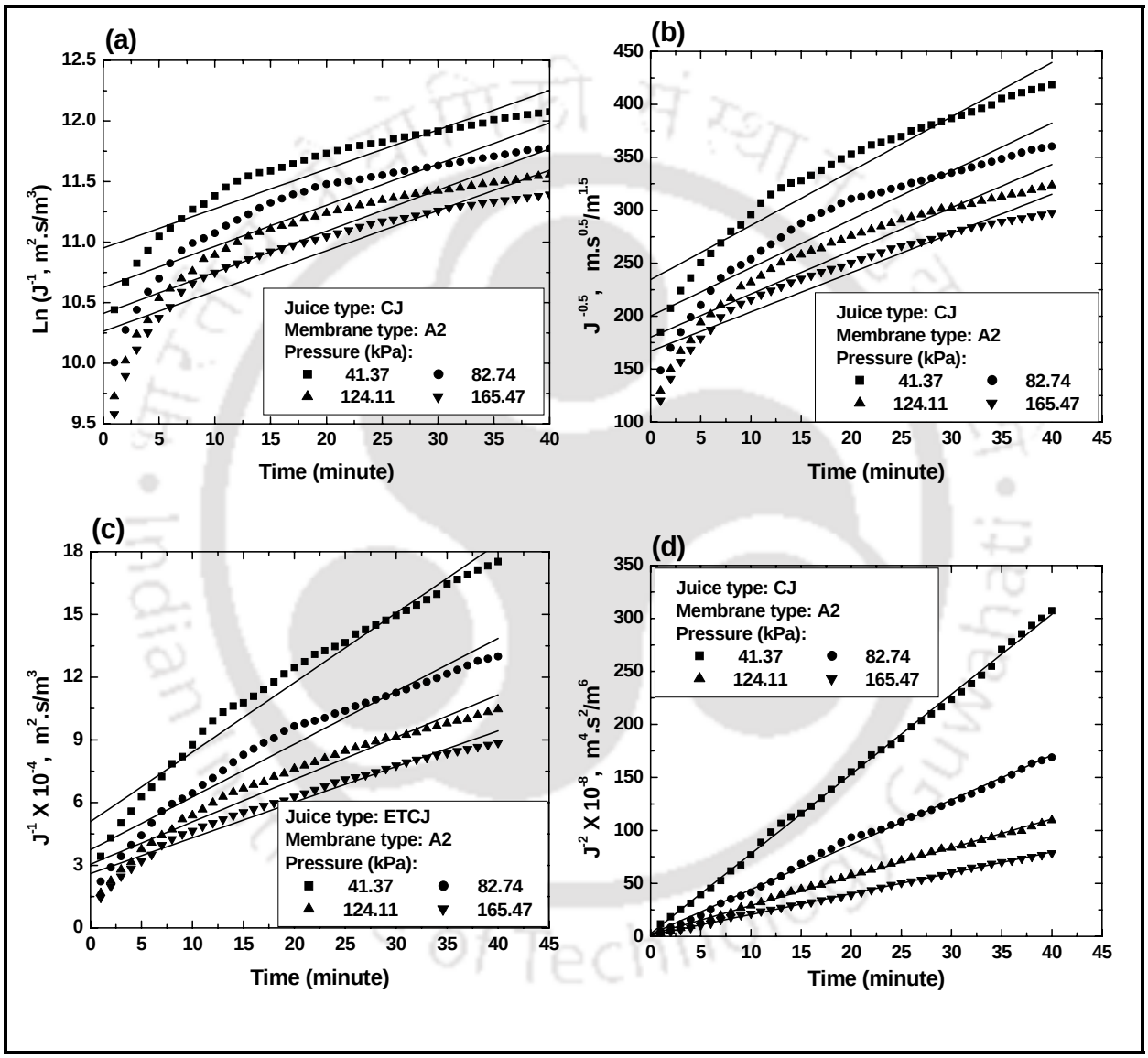


**Figure 4.6: Linearized plots of CJ permeate flux variation with time for A2 membrane at various trans-membrane pressure differentials (a) complete pore blocking model, (b) standard pore blocking model, (c) intermediate pore blocking model and (d) cake filtration model.**

minutes of the MF run and the rest for all experimental investigations. In order to visualize the most competent fouling phenomena during the initial phase of membrane performance (about 5 minutes), the correlation coefficients ($R^2$) have been evaluated by considering all models. Amongst these models, it was found that the fitness of intermediate pore blocking

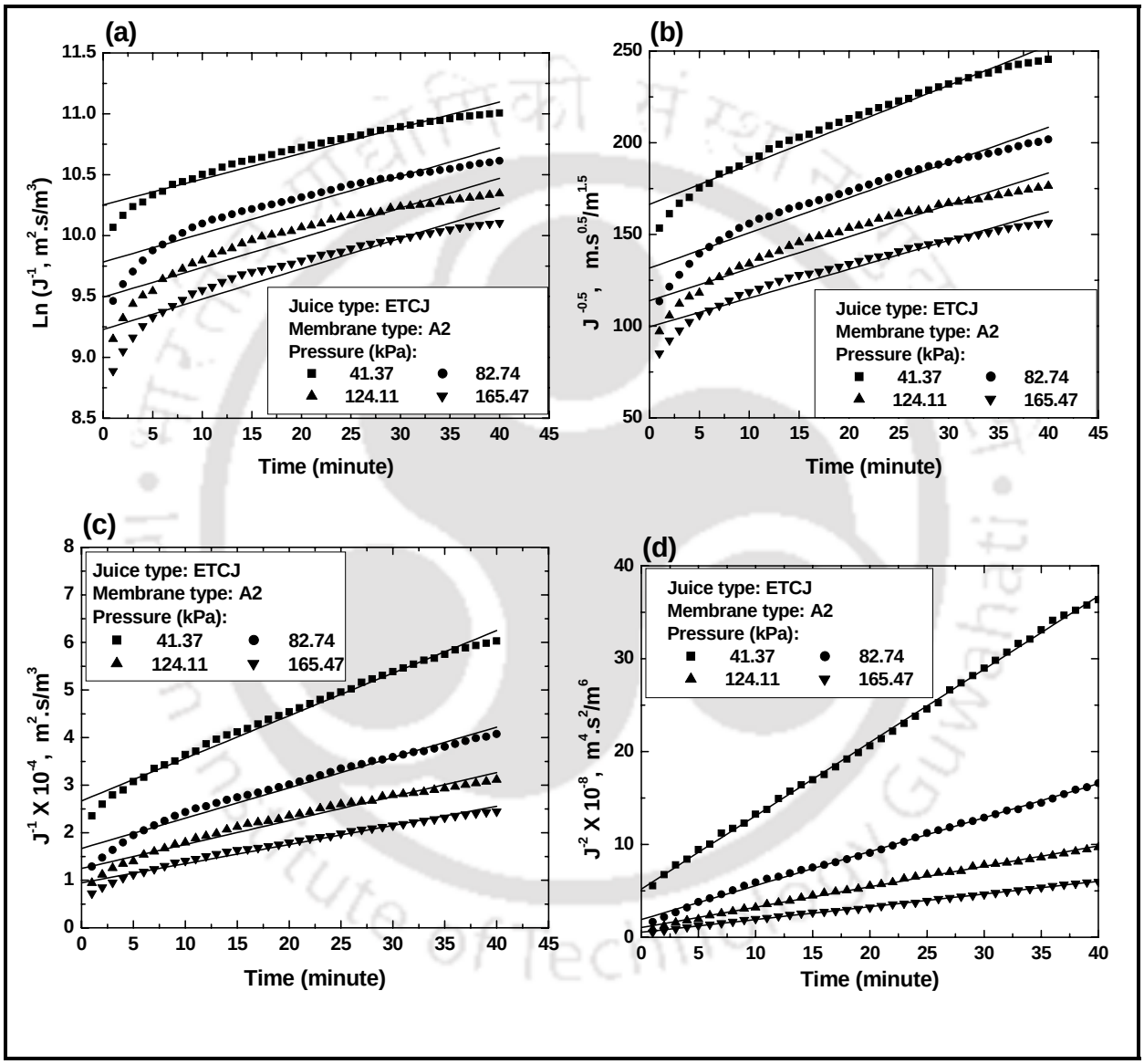


**Figure 4.7: Linearized plots of ETCJ permeate flux variation with time for A2 membrane at various trans-membrane pressure differentials (a) complete pore blocking model, (b) standard pore blocking model, (c) intermediate pore blocking model and (d) cake filtration model.**

**Table 4.5: Summary of parameters associated to various pore blocking models for CJ and ETCJ for all membranes (A1, A2, A3 and A4) at a trans-membrane pressure differential of 82.74 kPa.**

| Juice type | Membrane | Complete pore blocking | | | Standard pore blocking | | | Intermediate pore blocking | | | Cake filtration | | |
|---|---|---|---|---|---|---|---|---|---|---|---|---|---|
| | | $k_b \times 10^2$ | $\ln(J_0^{-1})$ | $R^2$ | $k_S$ | $J_0^{-0.5}$ | $R^2$ | $k_i$ | $J_0^{-1} \times 10^{-4}$ | $R^2$ | $k_C \times 10^{-7}$ | $J_0^{-2} \times 10^{-7}$ | $R^2$ |
| CJ | A1 | 3.37 | 10.91 | 0.828 | 5.21 | 231.0 | 0.905 | 3333 | 4.98 | 0.958 | 73.92 | 34.93 | 0.999 |
| | A2 | 3.40 | 10.63 | 0.826 | 4.56 | 200.1 | 0.902 | 2529 | 3.74 | 0.954 | 42.24 | 19.79 | 0.997 |
| | A3 | 3.46 | 10.33 | 0.799 | 4.00 | 173.0 | 0.892 | 1920 | 2.81 | 0.953 | 24.19 | 10.01 | 0.999 |
| | A4 | 3.47 | 10.04 | 0.810 | 3.48 | 149.6 | 0.899 | 1451 | 2.09 | 0.957 | 13.78 | 2.95 | 0.999 |
| ETCJ | A1 | 3.09 | 10.11 | 0.886 | 3.17 | 1538 | 0.938 | 1333 | 2.20 | 0.973 | 12.53 | 10.51 | 0.999 |
| | A2 | 2.35 | 9.78 | 0.897 | 1.92 | 131.6 | 0.940 | 637 | 1.67 | 0.971 | 3.66 | 19.13 | 0.998 |
| | A3 | 2.34 | 9.26 | 0.923 | 1.48 | 101.1 | 0.957 | 380 | 0.98 | 0.982 | 1.30 | 6.42 | 0.999 |
| | A4 | 2.30 | 8.90 | 0.905 | 1.21 | 84.73 | 0.945 | 257 | 0.69 | 0.974 | 0.61 | 3.35 | 0.998 |

**Table 4.6: Summary of parameters associated to various pore blocking models for CJ and ETCJ using A2 membrane at various trans-membrane pressure differentials.**

| Juice type | Pressure (kPa) | Complete pore blocking | | | Standard pore blocking | | | Intermediate pore blocking | | | Cake filtration | | |
|---|---|---|---|---|---|---|---|---|---|---|---|---|---|
| | | $k_b \times 10^2$ | $\ln(J_0^{-1})$ | $R^2$ | $k_S$ | $J_0^{-0.5}$ | $R^2$ | $k_i$ | $J_0^{-1} \times 10^{-4}$ | $R^2$ | $k_C \times 10^{-7}$ | $J_0^{-2} \times 10^{-7}$ | $R^2$ |
| CJ | 41.37 | 3.25 | 10.95 | 0.862 | 5.13 | 234.4 | 0.927 | 3328 | 5.09 | 0.970 | 75.34 | 25.58 | 0.999 |
| | 82.74 | 3.40 | 10.63 | 0.826 | 4.56 | 200.1 | 0.902 | 2529 | 3.74 | 0.954 | 42.24 | 19.79 | 0.997 |
| | 124.11 | 3.40 | 10.41 | 0.810 | 4.08 | 180.2 | 0.894 | 2026 | 3.05 | 0.951 | 27.24 | 17.97 | 0.998 |
| | 165.47 | 3.33 | 102.6 | 0.822 | 3.70 | 167.1 | 0.906 | 1705 | 2.61 | 0.961 | 19.64 | 10.28 | 0.999 |
| ETCJ | 41.37 | 2.11 | 10.25 | 0.946 | 2.16 | 166.4 | 0.971 | 895 | 2.67 | 0.988 | 7.89 | 54.97 | 0.999 |
| | 82.74 | 2.35 | 9.78 | 0.897 | 1.92 | 131.6 | 0.940 | 637 | 1.67 | 0.971 | 3.66 | 19.13 | 0.998 |
| | 124.11 | 2.44 | 9.49 | 0.890 | 1.74 | 113.9 | 0.934 | 504 | 1.25 | 0.966 | 2.20 | 10.41 | 0.997 |
| | 165.47 | 2.49 | 9.23 | 0.901 | 1.57 | 99.6 | 0.946 | 402 | 0.948 | 0.976 | 1.37 | 5.41 | 0.999 |

and cake filtration models varied from 0.989 to 0.999 with variation in membrane type (A1, A2, A3 and A4) and $\Delta P$ (41.37, 82.74, 124.11 and 165.47 kPa). On the other hand, for the second regime (from 5 to 40 minutes of experimental run), cake filtration model $R^2$ values have always been found to be highest (0.998). Therefore, it was herewith inferred that intermediate pore blocking followed with cake filtration represent the most competent combination of fouling mechanisms for the observed membrane flux decline. Since it will be also convenient to identify a single most competent model to represent the entire flux decline regime, the $R^2$ values of all four models have been as well compared. Table 4.5 summarizes different model parameters (slope, intercept and correlation coefficient) for all pore blocking models for various membranes (A1, A2, A3 and A4) and at a $\Delta P$ of 82.74 kPa for CJ and ETCJ. Table 4.6 summarizes fitness of different pore blocking model parameters (slope, intercept and correlation coefficient) for A2 membrane for varying $\Delta P$ (41.37, 82.74, 124.11 and 165.47 kPa) for CJ and ETCJ. An overall observation of the Figures 4.4 inferred that Fig. 4.4d represents the observed flux decline trends better than all other models. To confirm the fitness of the models, correlation coefficients ($R^2$) of different models summarized in tables 4.5 and 4.6 were used as a basis. As presented in these tables, $R^2$ values varied from 0.799 to 0.946 for complete pore blocking, 0.892 to 0.971 for standard pore blocking, 0.951 to 0.988 for intermediate pore blocking and 0.997 to 0.999 for cake filtration model. As cake filtration model provided the highest values of $R^2$, this model was identified as the best fitted model to represent the flux decline mechanism for CJ. Similar trends were also observed for ETCJ at constant $\Delta P$ of 82.74 kPa for all membranes and for both CJ and ETCJ. Therefore, cake filtration was chosen as the best fitted model to represent the fouling mechanism associated to the MF for all the cases studied here.

The pertinent flux decline phenomena were also analyzed by a comparative assessment of membrane pore size distributions and particle size distributions of CJ and ETCJ. From SEM based pore size distributions summarized in Chapter 2, it can be observed that the membrane pore size distributions varied from 0.15 - 5 μm with negligible number of pores existing above 2.5 μm. On the other hand, particle size distribution of both CJ and ETCJ varied from 0.04 - 10 μm. Amongst these, particles with size distributions varying from 0.04 - 0.15 μm will pass through the membrane and particles with sizes above 2.5 μm (13.67 % for CJ and 3.41 % for ETCJ) will be rejected by the membrane and contribute towards the formation of a gel layer. Also particles in the range 0.15 – 2.5 μm either enter the pores or rejected by the membrane and contribute to intermediate pore blocking and cake filtration. Since 3.41 - 13.67 % of particles were above maximum pore diameter of the membrane, the realization of cake filtration is anticipated as the pertinent flux decline phenomena. Therefore, as good numbers of particles were available with particle sizes above 2.5 μm, it is apparent that cake filtration dominates after the initial phase of 4-5 minutes of intermediate pore blocking. These insights are in accordance with the flux decline modeling analysis presented earlier in this section.

According to the definitions and physical significance of Hermia's [90] model parameters expressed in Eqs. 3.4 – 3.7 (chapter 3), magnitude of $k_b$, $k_s$, $k_i$ and $k_c$ values refers to severity of fouling. Tables 4.5 and 4.6 indicate that for both CJ and ETCJ, $k_c$ decreases with an increase in ΔP as well as $\varepsilon_m d_l^{\,2}$, thereby inferring that the rate of increase in membrane fouling reduces with an increase in ΔP and $\varepsilon_m d_l^{\,2}$. This was due to several reasons. Firstly, higher ΔP enables lower adsorption of non-permeating particles on the walls of the membrane pores due to the higher liquid velocity through the membrane pores. Secondly, due to higher

driving force (ΔP), some of the blocked pores get cleaned by permeating liquid. This was further confirmed by the reduction in the overall quality of permeate juice (color, clarity, viscosity and AIS in Table 4.3 and 4.4) due to the passage of higher amount of suspended solids and pectic materials at higher ΔP. The comparison of $k_c$ values obtained for CJ and ETCJ further indicates that lower $k_c$ values exist for ETCJ. This is due to lower concentration of pectic material in ETCJ when compared to CJ. Figures 4.8a and 4.8b present the variation of $k_c$ with $\varepsilon_m d_l^{\,2}$ and $\Delta P$, respectively that can be suitably correlated using nonlinear expressions as follows:

a) At constant $\Delta P$ of 82.74 kPa with varying $\varepsilon_m d_l^{\,2}$

$$k_c^{\,CJ} = 4.921\times10^{7}\times\exp\left(0.666/\varepsilon_m d_l^{\,2}\right) \qquad R^2 = 0.980 \qquad (4.5)$$

$$k_c^{\,ETCJ} = 7.446\times10^{4}\times\exp\left(1.848/\varepsilon_m d_l^{\,2}\right) \qquad R^2 = 0.988 \qquad (4.6)$$

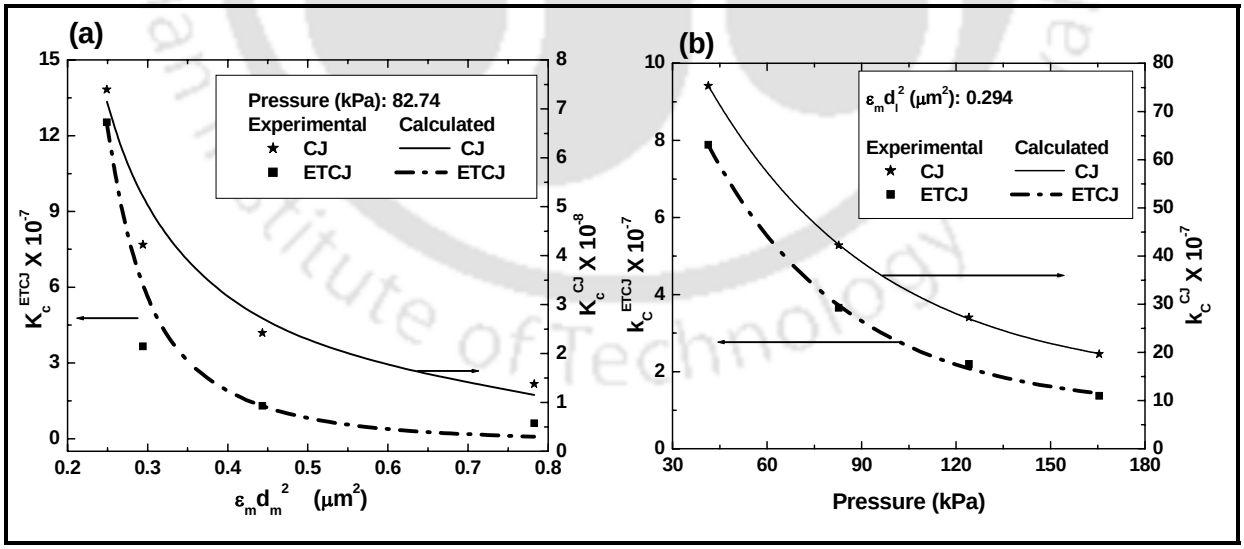


**Figure 4.8: Variation of cake filtration constant ($k_c$) with (a) membrane morphological parameters at constant trans-membrane pressure differential (82.74 kPa) and (b) trans-membrane pressure differentials at constant membrane (A2) morphological parameter.**

b) For constant $\varepsilon_m d_l^{\,2}$ of 0.294 with varying $\Delta P$

$$k_c^{\,CJ} = 2.825\times10^{7}\times\Delta P^{-0.97} \qquad R^2 = 0.994 \qquad (4.7)$$

$$k_c^{\,ETCJ} = 8.289\times10^{9}\times\Delta P^{-1.24} \qquad R^2 = 0.994 \qquad (4.8)$$

The above expressions are valid within the $\varepsilon_m d_l^{\,2}$ range of $0.249 \le \varepsilon_m d_l^{\,2} \le 0.783$ μm$^2$ and pressure range $41.37 \le \Delta P \le 165.47$ kPa.

## 4.3.7 Phenomenological modeling

### 4.3.7.1 Effect of membrane morphology on total resistance

During MF of mosambi juice, the total hydraulic resistance ($R_t$) increases with time due to continuous membrane fouling. The variation of $R_t$ with time is also dependent on $\Delta P$ and $\varepsilon_m d_l^{\,2}$. Therefore, phenomenological expression for $R_t(t)$ as a function of other dependent variables such as time ($t$), $\Delta P$ and $\varepsilon_m d_l^{\,2}$ can be presented as:

$$R_t(t) = \frac{\Delta P}{\mu_J J_J(t)} = f\left(t, \Delta p, \varepsilon_m d_l^{\,2}\right) \qquad (4.9)$$

In the above expression, the fitness of the most appropriate non-linear functions for time ($t$), $\Delta P$ and $\varepsilon_m d_l^{\,2}$ was determined from the non-linear regression analysis of the experimental data using genetic algorithm. From the analysis, $R_t(t)$ was found to adopt the following empirical correlation at constant $\Delta P$

$$R_t = X\times\exp\left[\frac{y}{\varepsilon_m d_l^{\,2}}\right]\times\left(\frac{t}{60}\right)^{z} \qquad (4.10)$$

Table 4.7 presents a summary of values of regression parameters $X$, $y$ and $z$ obtained from the non-linear regression analysis. Figs. 4.9a and 4.9b illustrate the variation of calculated and

**Table 4.7: Non-linear regression parameters ( $X$ , $y$ and $z$ ) corresponding to Eq. (4.10).**

| Juice type | $X \times 10^{-10}$ | $y$ | $z$ | Average error (%) | Maximum error (%) |
|---|---|---|---|---|---|
| CJ | 45.20 | 0.298 | 0.508 | 4.25 | 14.69 |
| ETCJ | 12.74 | 0.492 | 0.352 | 8.98 | 22.21 |

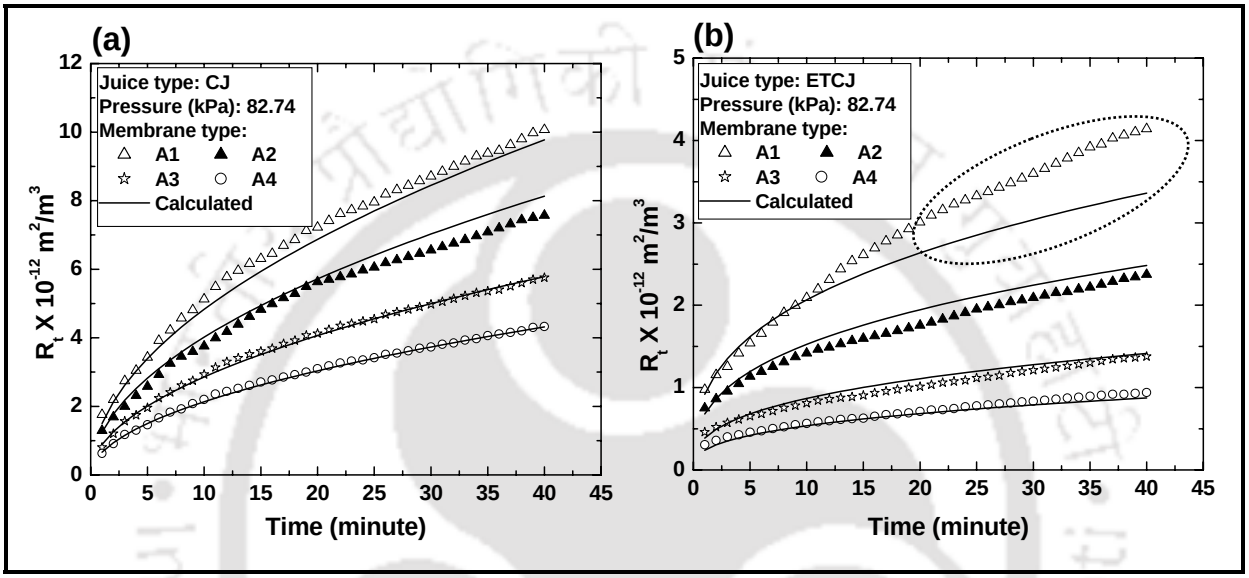


**Figure 4.9: Variation of experimental and calculated total membrane resistance with time for various membranes at a trans-membrane pressure drop of 82.74 kPa; (a) CJ and (b) ETCJ.**

experimentally obtained $R_t$ values for CJ and ETCJ, respectively. From the figure it can be observed that the calculated values of $R_t$ matches with the experimental data. The average error for predicted hydraulic resistance $R_t$ was evaluated to be 4.25 % for CJ and 8.98 % for ETCJ. Also, significant deviations were observed for lower values of $\varepsilon_m d_l^{\,2}$ (A1 membrane) and at higher time for ETCJ. This was possibly due to the fact that A1 membrane having lowest pore size was more prone to adsorb smaller particles in the membrane pores to contribute to a drastic reduction in membrane flux. Therefore, $R_t$ of the membrane was

comparably higher for the membrane and phenomenological model outlined in Eq. (4.10) could not closely describe the pertinent permeation characteristics of the membrane and other suitable parameters such as average particle size may have to be included to model the pertinent flux decline for better fitness. However, since for all other cases (including A1 membrane for CJ) the chosen model was in good agreement with the experimentally evaluated values of $R_t$, a further complication of the phenomenological model was not considered in this work. In conclusion, it is affirmed that A1 membrane is more prone to fouling during MF of ETCJ.

#### 4.3.7.2 Effect of operating pressure on total resistance

Based on non-linear regression analysis, $R_t(t)$ was found to adopt the following empirical correlation for a chosen value of $\varepsilon_m d_l^{\,2}$:

$$R_t = T \times (\Delta P)^p \times (t/60)^u \qquad (4.11)$$

A summary of regression parameters $T$, $p$ and $u$ have been shown in table 4.8. Figures 4.10a and 4.10b present the variation of calculated and experimentally obtained $R_t$ values for CJ and ETCJ, respectively. From the figure it can be observed that the fitness of the calculated values of $R_t$ with the experimental observed $R_t$ was in acceptable range for all values of $\Delta P$. The average error for CJ and ETCJ was calculated as 3.35 and 4.77 %, respectively. This indicated that the fouling of the membrane follows a power law trend with an increase in $\Delta P$. An increase in $R_t$ with an increase in $\Delta P$ was due to the removal of higher quantities of suspended solids at higher $\Delta P$. From the figure it also can be observed that the difference between the trend lines decreases with an increase in $\Delta P$ (rate of increase $R_t$ with $\Delta P$). This indicates that fouling severity decreased with an increase in $\Delta P$.

**Table 4.8: Regression parameters $T$, $p$ and $u$ obtained from the non-linear regression analysis of Eq. (4.11) for CJ and ETCJ.**

| Juice type | $T \times 10^{-10}$ | $p$ | $u$ | Average error (%) | Maximum error (%) |
|---|---|---|---|---|---|
| CJ | 12.83 | 0.507 | 0.492 | 3.35 | 15.30 |
| ETCJ | 15.10 | 0.331 | 0.331 | 4.77 | 24.52 |

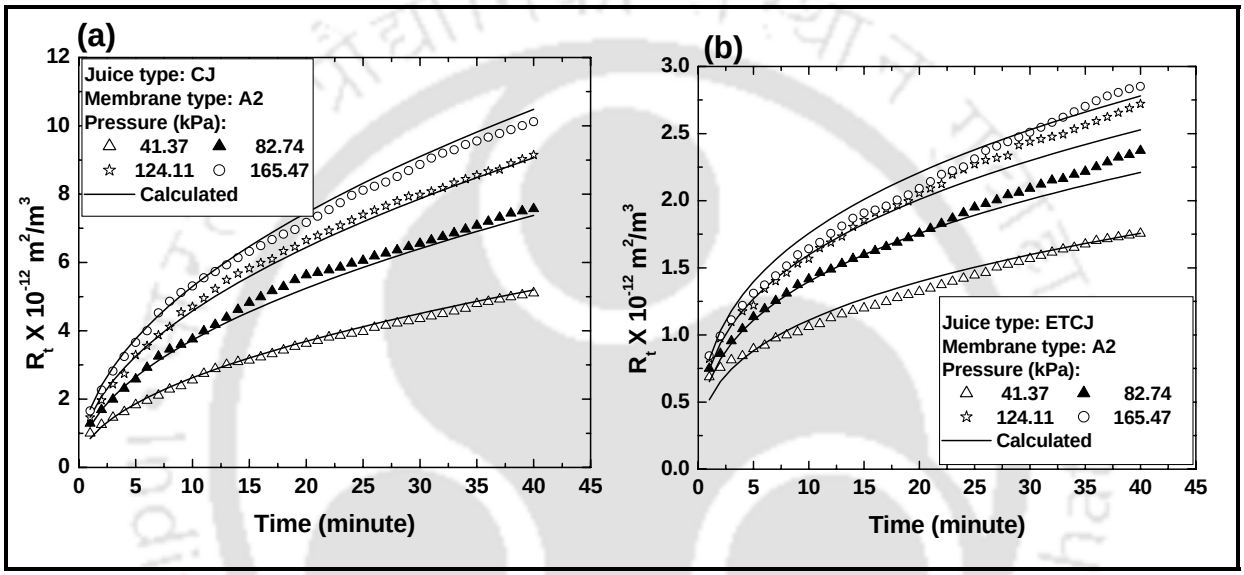


**Figure 4.10: Variation of experimental and calculated total membrane resistance with time for A2 membrane at various trans-membrane pressure differentials; (a) CJ and (b) ETCJ.**

This observation is also in agreement with the observed trends of $k_c$ values discussed in section 4.3.6 (Fig. 4.5).

#### 4.3.7.3 Effect of membrane morphology on membrane fouling characteristics

The variation of effective permeable area factor ($\varepsilon_{cm} d_{cm}^{\ 2}$) of the composite membrane (fouled membrane) with time for different membranes are shown in Fig. 4.11a and 4.11b for CJ and ETCJ, respectively. From these figures, it can be observed that $\varepsilon_{cm} d_{cm}^{\ 2}$ reduced sharply

within the initial phase of 10 to 15 minutes and becomes gradual thereafter with time. The reduction in $\varepsilon_{cm} d_{cm}^{\ 2}$ with time was due to membrane pore blocking as well as deposition of suspended particles over the membrane. Calculated values of $\varepsilon_{cm} d_{cm}^{\ 2}$ were found to vary between 0.241 - 0.015 μm$^2$ and 0.466 - 0.035 μm$^2$ for CJ and ETCJ, respectively. Generally, it was observed that with an increase in $\varepsilon_m d_l^{\ 2}$ of membranes (A1 - A4), $\varepsilon_{cm} d_{cm}^{\ 2}$ increased. This conveys that a membrane with higher $\varepsilon_m d_l^{\ 2}$ was less prone to fouling. Observed higher values of $\varepsilon_{cm} d_{cm}^{\ 2}$ for ETCJ (Fig. 4.8b) when compared to those for CJ (Fig. 4.8a) was due to the lower pectin concentrations (expressed as AIS) in ETCJ. Thereby, the pectin concentration in the juice was observed to play a dominating role in influencing the morphology of the fouled membrane. From the figures, it can also be observed that the $\varepsilon_{cm} d_{cm}^{\ 2}$ profiles of ETCJ were distinctly spaced for all membranes. This conveyed that the fouling of membranes with ETCJ was lower than that with CJ. Since higher pore sizes of the

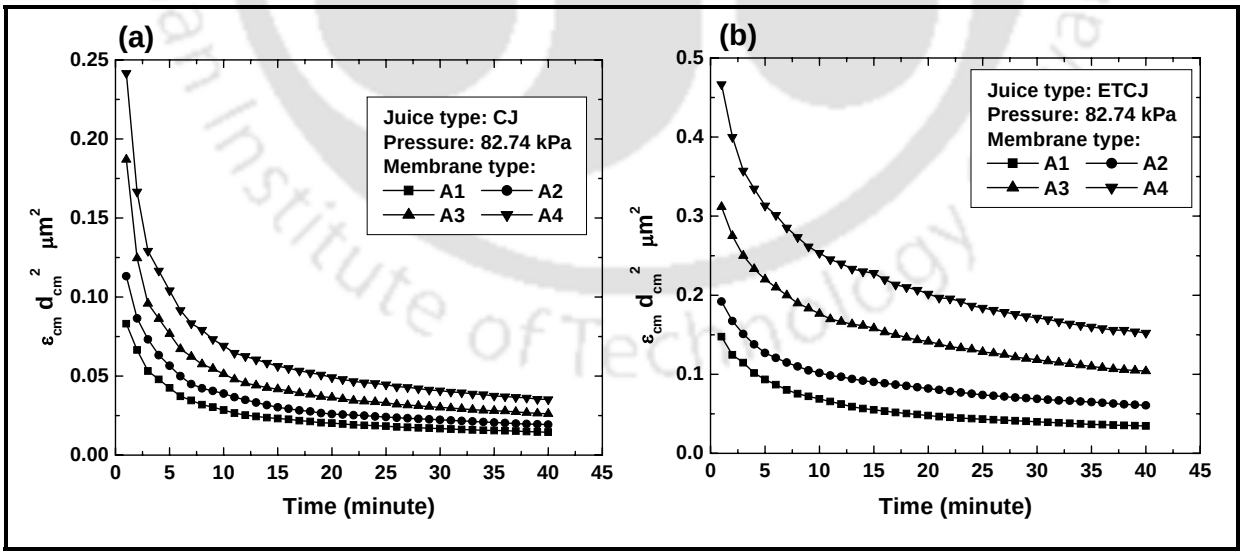


**Figure 4.11: Variation of effective permeable area factor with time for various membranes at a trans-membrane pressure drop of 82.74 kPa; (a) CJ and (b) ETCJ.**

membrane favored lower fouling and also lower juice quality (Table 4.3), the selection of membranes competent for juice processing needs to be further analyzed from the perspective of the permeate juice quality. For ETCJ, it can be observed from table 3.3 that the juice quality was lowest for A4 and hence, A4 is not suitable for juice processing though it has the lowest fouling tendency (highest $\varepsilon_{cm} d_{cm}^{\ 2}$) amongst all studied membranes. Subsequently while considering A1, A2 and A3, permeate juice quality for these membranes were almost similar (clarity > 90%, minimum AIS). However, as A3 provides lowest fouling tendency (highest $\varepsilon_{cm} d_{cm}^{\ 2}$), it was concluded to be the most suitable membranes for ETCJ processing. A similar analysis can be also conducted using the $\varepsilon_{cm} d_{cm}^{\ 2}$ values obtained for CJ along with permeate juice quality for these membranes. In contrary to the profiles obtained for ETCJ, $\varepsilon_{cm} d_{cm}^{\ 2}$ profiles for CJ have been observed to be closely placed. This conveys that all the membranes were highly prone to fouling due to the dominating influence of higher pectin concentration in the MF of CJ. Observing the permeate juice quality for all the membranes; it has been found that only A1 and A2 provide juice with clarity greater than 90 %. Since A2 membrane provided higher $\varepsilon_{cm} d_{cm}^{\ 2}$, it was inferred as the most suitable membrane for CJ processing.

#### 4.3.7.4 Effect of pressure on membrane fouling characteristics

The variation of effective permeable area factors $\varepsilon_{cm} d_{cm}^{\ 2}$ with time at different values of $\Delta P$ are shown in Fig. 4.12a and 4.12b for CJ and ETCJ, respectively. From these figures, it can be observed that $\varepsilon_{cm} d_{cm}^{\ 2}$ decreased with time due to fouling phenomena for both CJ and ETCJ. Calculated values of $\varepsilon_{cm} d_{cm}^{\ 2}$ varied from 0.147 - 0.0143 $\mu m^2$ and 0.21 - 0.05 $\mu m^2$ for CJ and

ETCJ, respectively. From the figures, it can be observed that $\varepsilon_{cm} d_{cm}^{\ 2}$ decreased with an increase in $\Delta P$. This was due to the higher amount of pore blocking brought forward by the filtration of larger volumes of the juice at higher pressure differentials (driving force). The observation of higher values of $\varepsilon_{cm} d_{cm}^{\ 2}$ for ETCJ compared to CJ indicated that the membrane was less prone to fouling for ETCJ. For both CJ and ETCJ, the $\varepsilon_{cm} d_{cm}^{\ 2}$ profile corresponding to 41.37 kPa was placed distinctly from those existing at higher values of $\Delta P$. Also $\Delta P$ value of 41.37 kPa provided minimum fouling for the membranes. In addition, it can be also noted that, an increase in $\Delta P$ from 41.37 kPa to 82.74 kPa enabled a proportionate reduction in the $\varepsilon_{cm} d_{cm}^{\ 2}$ profiles for both CJ and ETCJ. However, such proportional reduction was not observed at higher values of $\Delta P$ for both the cases. Theoretically, an optimum value of $\Delta P$ should provide higher membrane flux, appreciable levels of juice quality and enable the operability of the process far from the saturation state of membrane fouling. Therefore, from Figures 4.9 and from Table 4.4, the optimum $\Delta P$ was

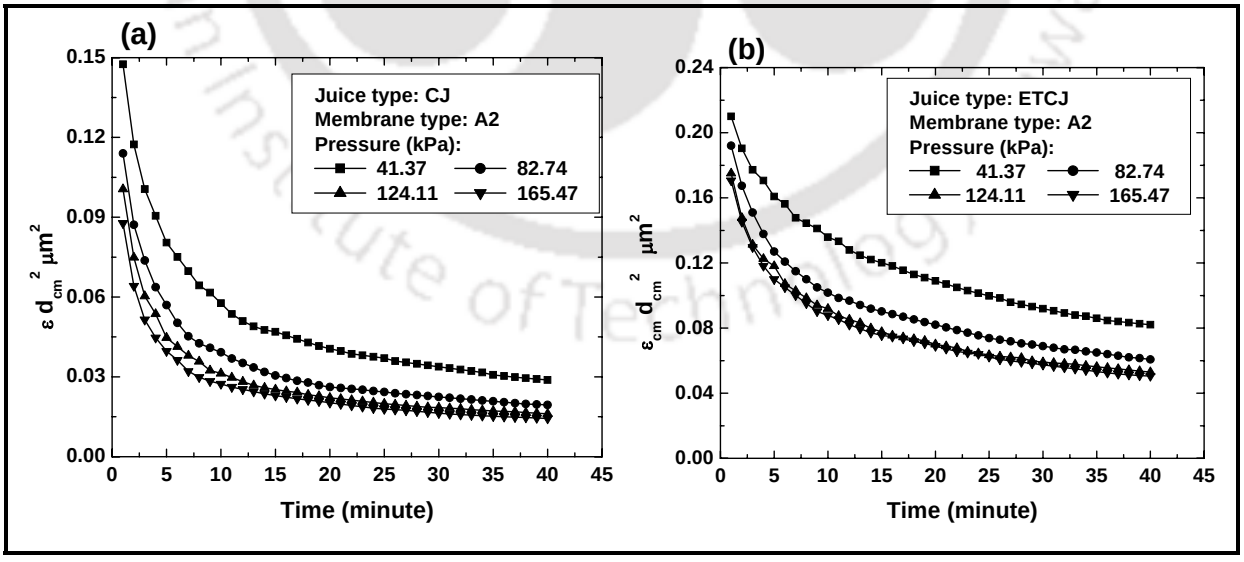


**Figure 4.12: Variation of effective permeable area factor for A2 membrane with time at various trans-membrane pressure differentials; (a) CJ and (b) ETCJ.**

identified to be 82.74 kPa, as $\Delta P$ values lower than this value reduce the flux and $\Delta P$ values greater than this value drive the membrane process towards the state of saturation in membrane fouling.

### 4.3.8 Long term storage studies

The stability of juice without substantial variation in its physio-chemical properties during storage is always a significant factor to consider for the characterization of processes involved in juice processing. To observe the stability of the valuable parameters of clarified juices for long term storage, 500 ml of CJ and ETCJ permeate (A1 membrane, $\Delta P$ of 41.37 kPa) were kept in refrigerated condition for 30 days. During storage, important parameters of the juice such as colour, clarity, TSS, pH, citric acid and density were measured. Table 4.9 shows the obtained results for the juices. From the table it can be observed that overall quality of the CJ and ETCJ degrade with time, with higher degradation rate for CJ. For example, TSS decreased from 9.1 - 7.3 for CJ and 8.4 for ETCJ during 30 days of storage. This was due to the presence of pectic materials in the juice that undergo fermentation even in refrigerated storage conditions. The fermentation reactions enable a significant reduction in the sugar content ($^{o}$Brix) of the juice along with the alteration in colour, clarity, and pH. Higher reduction rate was observed for CJ due to the higher amount of pectic materials (AIS) in the juice. After membrane clarification, both permeate samples of CJ and ETCJ have been found to be more stable than CJ and ETCJ samples. For CJ, TSS decreased from 9.1 to 8.7, clarity decreased from 94.39 to 84.26 % during 30 days of storage. However, for ETCJ permeate stability was significantly higher than CJ permeate. Higher stability of ETCJ was due to the fact that almost all pectic materials were removed during enzymatic treatment and subsequent MF. These pre-processing steps enable lesser production of unwanted products by

fermentation reactions during storage. In general, all observations justified enzymatic treatment and centrifugation of the mosambi juice as an important pre-processing step before MF based clarification to substantially enhance the juice quality and stability.

**Table 4.9: Summary of results obtained during the long term storage study. Permeate juice samples were obtained using A1 membrane at a trans-membrane pressure drop of 41.37 kPa.**

| Juice type | Day | Colour ($A_{420}$) | Clarity ( $\%T_{660}$) | TSS ($^{o}$Brix) | Citric acid (wt %) | pH | Density ($g/cm^3$) |
|---|---|---|---|---|---|---|---|
| CJ | 1st | 0.69 | 53.73 | 9.1 | 0.84 | 3.80 | 1.038 |
| | 7th | 0.59 | 53.54 | 8.6 | 0.87 | 3.75 | 1.035 |
| | 15th | 1.231 | 46.85 | 8.2 | 0.90 | 3.65 | 1.033 |
| | 21st | 1.865 | 30.28 | 7.6 | 0.96 | 3.5 | 1.032 |
| | 30th | 2.464 | 21.56 | 7.3 | 1.01 | 3.4 | 1.031 |
| CJ permeate (A1/ 41.37 kPa.) | 1st | 0.076 | 94.39 | 9.1 | 0.81 | 3.84 | 1.03 |
| | 7th | 0.101 | 92.92 | 9 | 0.81 | 3.82 | 1.03 |
| | 15th | 0.132 | 88.92 | 8.9 | 0.82 | 3.79 | 1.03 |
| | 21st | 0.164 | 86.65 | 8.8 | 0.87 | 3.75 | 1.03 |
| | 30th | 0.204 | 84.26 | 8.7 | 0.88 | 3.70 | 1.03 |
| ETCJ | 1st | 0.48 | 67.87 | 9.1 | 0.84 | 3.80 | 1.037 |
| | 7th | 0.59 | 63.54 | 9 | 0.85 | 3.78 | 1.036 |
| | 15th | 0.89 | 60.85 | 8.8 | 0.87 | 3.75 | 1.036 |
| | 21st | 0.99 | 58.54 | 8.6 | 0.88 | 3.72 | 1.035 |
| | 30th | 1.231 | 56.85 | 8.4 | 0.89 | 3.67 | 1.034 |
| ETCJ permeate (A1/ 41.37 kPa.) | 1st | 0.068 | 96.44 | 9.1 | 0.81 | 3.85 | 1.03 |
| | 7th | 0.075 | 95.18 | 9.1 | 0.81 | 3.84 | 1.03 |
| | 15th | 0.091 | 94.36 | 9.0 | 0.81 | 3.84 | 1.03 |
| | 21st | 0.109 | 93.27 | 9.0 | 0.8 | 3.83 | 1.03 |
| | 30th | 0.118 | 90.61 | 9.0 | 0.80 | 3.82 | 1.03 |

# Chapter 5:

# Microfiltration of Oily Wastewater and Mosambi Juice using B3 Membrane

# *Chapter 5*

# Microfiltration of Oily Wastewater and Mosambi Juice using B3 Membrane

*This chapter addresses the separation characteristics of membranes prepared using composition B. Amongst membranes B1-B4, B3 membrane was chosen for real time application. Similar to the procedures outlined in chapter 3 and 4, MF studies were conducted using B3 membrane for the separation of o/w emulsions and clarification of mosambi juice. Both permeate flux and quality of permeate have been measured along with the analysis of fouling mechanisms. Finally a comparasion of performance of the composition A membranes and B3 membrane is reported in this chapter.*

## 5.1 Experimental

Dead-end MF experiments with synthetic o/w emulsions were conducted with two different oil concentrations (125 and 250 mg/L) at four different trans-membrane pressure differentials ($\Delta P$) (68.95, 137.90, 206.84 and 275.79 kPa). On the other hand, dead-end MF of mosambi juice was carried out with varying trans-membrane pressure differentials (137.90, 206.84, 275.79 and 344.74 kPa) for both CJ and ETCJ. Details with respect to the preparation of o/w emulsions and mosambi juice, experimental set up etc., have been discussed in chapter 3 and chapter 4 for o/w emulsions and mosambi juice, respectively. Amongst B1, B2, B3 and B4 membranes, B3 membrane was taken to verify the general performance of composition B membranes in real time applications. Since B3 possessed lower pore size in comparison with composition A membranes, comparatively higher $\Delta P$ were used to obtain adequate permeate flux during experiments. The actual separation characteristics for individual membrane might

**Table 5.1: A summary of various characteristics of B3 membrane.**

| Properties | Value |
|---|---|
| Membrane permeable area, $S$ ($m^2$) | $1.66 \times 10^{-3}$ |
| Thickness, $l$ (m) | $4.5 \times 10^{-3}$ |
| Average pore diameter from SEM analysis $d_s$ (μm) | 0.285 |
| Hydraulic pore diameter, $d_l$ (μm) | 0.51 |
| Intrinsic membrane resistance, $R_m$ ($m^2/m^3$) | $9.26 \times 10^{11}$ |
| Total porosity, $\varepsilon_m$ | 23.6 % |

vary from membrane to membrane due to their differences in pore diameter and porosity. A detailed account of the B3 membrane properties has been discussed in chapter 2. A summary of various properties are presented in Table 5.1.

## 5.2 Results and discussion

### 5.2.1 Microfiltration of oil-in-water emulsions

Permeate flux profiles with time at various values $\Delta P$ (68.95, 137.90, 206.84 and 275.79 kPa) and crude oil feed concentrations (125 and 250 mg/L) are shown in Figs. 5.1a and 5.1b. From these figures it was observed that the permeate flux declined sharply within the initial 5 - 10 minutes of operation and becomes gradual thereafter. The permeate flux decreased from $32.6\times10^{-6}$ - $7.4\times10^{-6}$ $m^3/m^2.s$ at the end of 30 minutes of experimental run at a trans-membrane pressure drop of 68.95 kPa (Fig. 5.1a). This decline in flux with time was due to pore blocking of ceramic porous structure and concentration polarization over the membrane surface. It was also observed that the permeate flux increased with an increase in $\Delta P$. From Fig. 5.1a, it may be observed that the permeate flux increased from $32.6\times10^{-6}$ - $62.2 \times10^{-6}$ $m^3/m^2.s$ when $\Delta P$ was increased from 68.95 - 275.79 kPa. An increase in permeate flux with

$\Delta P$ was due to the higher driving force across the membrane. Similar flux decline trends with trans-membrane pressure and operating time were also observed for 250 mg/L oil concentrations as shown in Fig. 5.1b. An overall observation of both figures conveys that the permeate flux reduced with increasing oil concentration. This was due to the fact that with an increase in feed concentration, droplet sizes of the emulsions increase and thereby enhance membrane fouling. The percent rejection of crude oil with time for different $\Delta P$ (68.95, 137.90, 206.84 and 275.79 kPa) and crude oil feed concentration (125 and 250 mg/L) are shown in Figs. 5.2a and 5.2b. From the figure, it can be observed that the percent oil rejection decreased with increase in $\Delta P$. However, it can be observed that the percent rejection increases with oil concentration. For example, at an initial oil concentration of 125 mg/L, the percent oil rejection decreased from 98.4 - 97.3 % with an increase in $\Delta P$ from 68.95 to 275.79 kPa. The reduction in percent oil rejection with an increase in $\Delta P$ was due to the reason that, higher pressures facilitate the enhancement of wetting and coalescence of oil

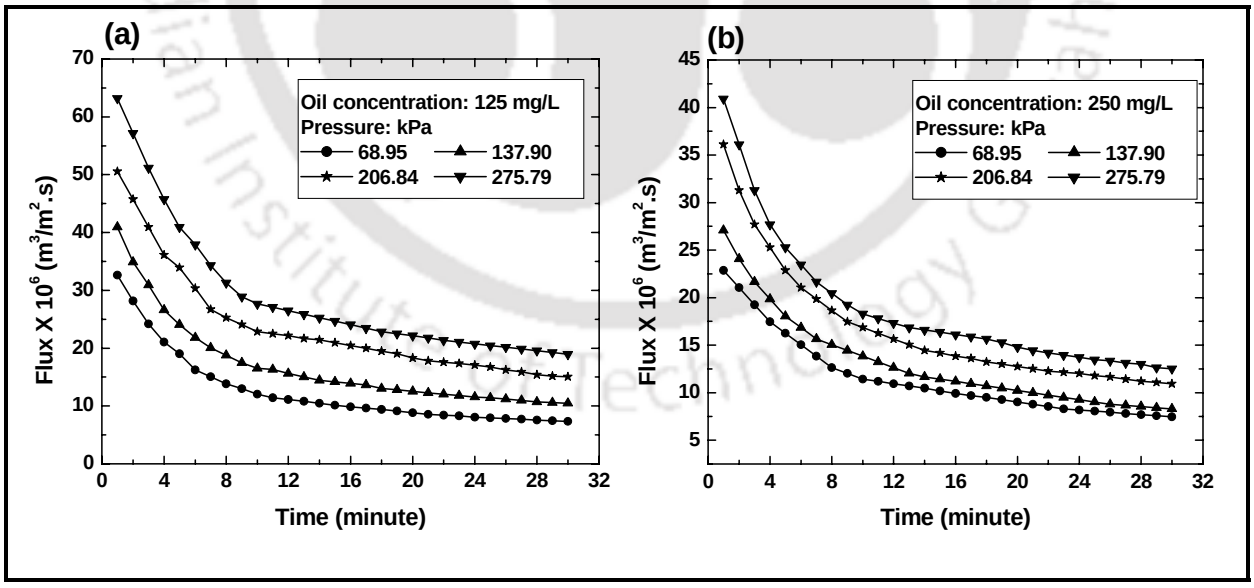


**Figure 5.1: Variation of permeate flux with time at various trans-membrane pressure differentials for an initial oil concentration of (a) 125 mg/L and (b) 250 mg/L.**

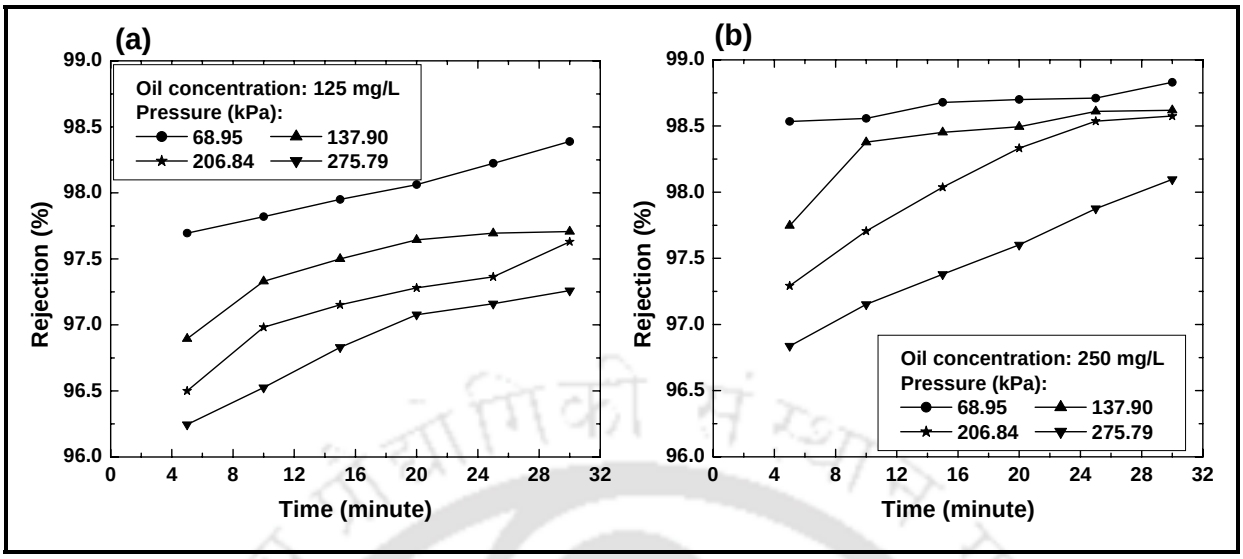


**Figure 5.2: Variation of oil rejection (%) with time at various trans-membrane pressure differentials for an initial oil concentration of (a) 125 mg/L and (b) 250 mg/L.**

droplets. Due to this reason, some oil droplets pass through the membrane pores and reach the permeate stream. It may also be observed from the figure that percent oil rejection increased from 97.3 - 98.1 % with an increase in initial oil concentration from 125 - 250 mg/L at 275.79 kPa. The oil rejection efficiency of the membrane was observed to increase marginally (less than 1 %) with time. These observations and trends are similar to those reported for A1 membrane as outlined in chapter 3.

### 5.2.2 Identification of flux decline mechanism for oil-in-water emulsions

The identification of flux decline mechanism for MF of o/w emulsions was carried out using different pore blocking models as summarized in section 3.2. Figures 5.3 and 5.4 illustrate linear plots corresponding to the various pore blocking models at two different initial oil concentrations of 125 and 250 mg/L, respectively. From these figures, it can be observed that the decline in permeate flux can be explained by either cake filtration model or a combination of two different pore blocking models. To identify the most relevant option among these, $R^2$

values were taken into consideration. It was observed that $R^2$ values of cake filtration model for the entire time duration varied in the range of 0.996 - 0.999. However, among several combinations of different pore blocking models, the representation of initial regime (4 - 5 minutes) flux decline using intermediate pore blocking model and latter regime using cake

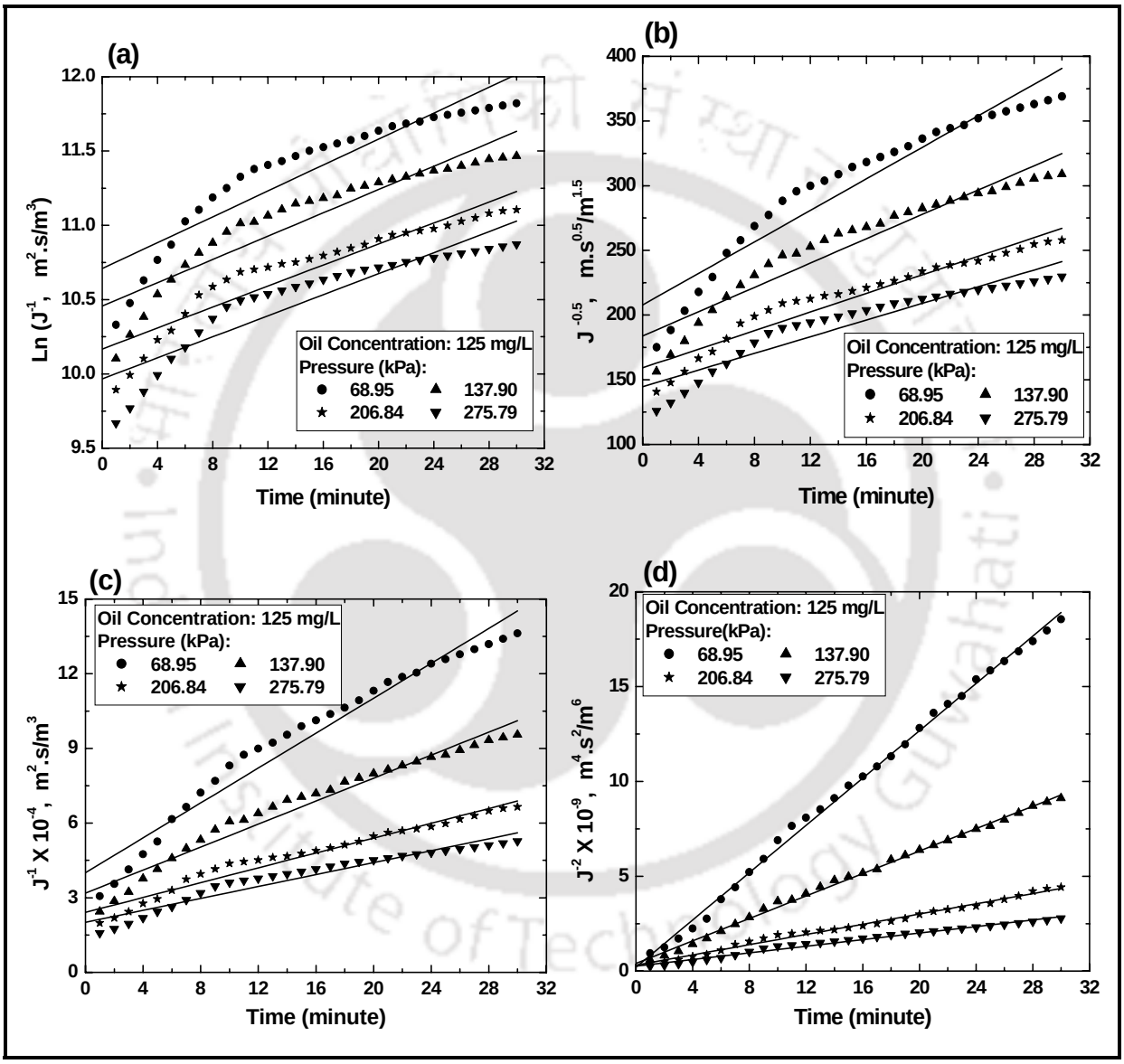


**Figure 5.3: Linear plots of permeate flux variation with time for various pore blocking models at an initial oil concentration of 125 mg/L; (a) complete pore blocking model, (b) standard pore blocking model, (c) intermediate pore blocking model and (d) cake filtration model.**

filtration model gave the highest $R^2$ values (in the range of 0.998 - 0.999). As these $R^2$ values were higher than those obtained for cake filtration model, it is herewith inferred that intermediate pore blocking followed with cake filtration represent the most competent combination of fouling mechanisms for the observed membrane flux decline. However, since $R^2$ values of cake filtration model and combination of models (intermediate pore blocking

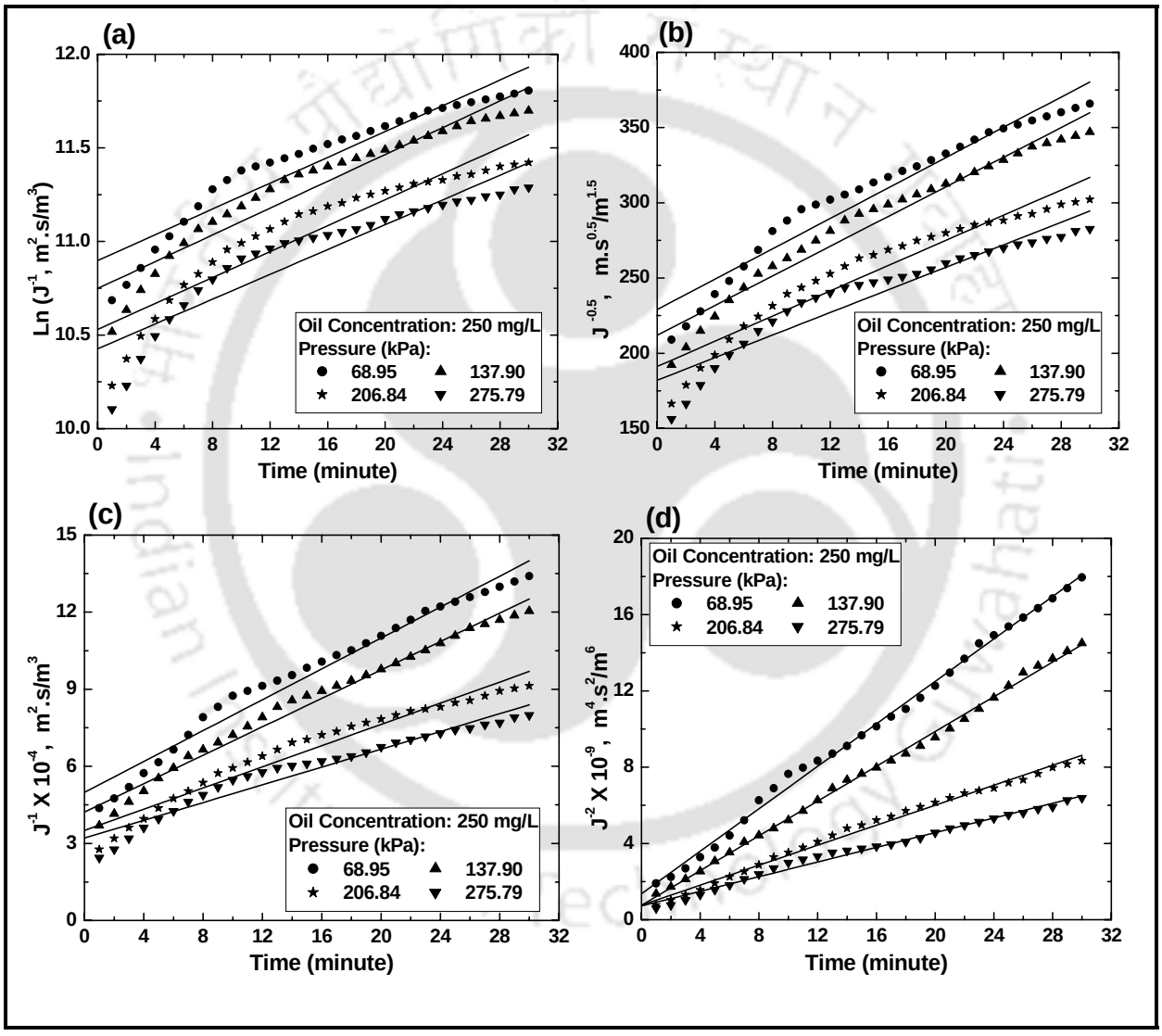


**Figure 5.4: Linear plots of permeate flux variation with time for various pore blocking models at an initial oil concentration of 250 mg/L; (a) complete pore blocking model, (b) standard pore blocking model, (c) intermediate pore blocking model and (d) cake filtration model.**

followed by cake filtration) were marginally different, for the convenience of identification of a single most competent model to represent the entire flux decline regime, it was finally inferred that cake filtration could also represent the pertinent flux decline phenomena in the entire range of operation. Koltuniewicz et al., [95] also reported that the flux decline during dead-end MF of o/w emulsion using both polymeric and ceramic membrane followed cake filtration model. Therefore, the hypothesis that flux decline of the membrane was due to the cake filtration appears to be consistent during the dead end MF of o/w emulsions.

Table 5.2 summarizes the calculated values of slope ($k_c$) and intercept ($J_0^{-2}$) for the cake filtration models. From the Table 5.2, it was observed that $k_c$ decreased with an increase in $\Delta P$. According to the definitions and physical significance of Hermia's [90] model parameters discussed in section 4.3.6, this indicates that the membrane fouling decreases with an increase in $\Delta P$. This was due to several reasons. Firstly, higher $\Delta P$ enables lower adsorption of oil on the walls of membrane pores. Secondly, due to higher driving force ($\Delta P$), some of the blocked pores get cleaned by the permeating liquid. This was further confirmed by the reduction in the oil rejection efficiency at higher $\Delta P$ (Fig. 5.2). For design purposes, the variation of $k_c$ and $J_0^{-2}$ with $\Delta P$ can be suitably correlated using linear expressions:

For oil concentration of 125 mg/L

$$k_c = 102.96 \times 10^7 \times \exp(-0.0094 \times \Delta P) \qquad R^2 = 0.987 \qquad (5.1)$$

$$\left(J_0^{-2}\right) = 71.81 \times 10^9 \times (\Delta P)^{-0.9769} \qquad R^2 = 0.971 \qquad (5.2)$$

For oil concentration of 250 mg/L

**Table 5.2: Cake filtration model parameters (slope, intercept and $R^2$) evaluated from all experimental data.**

| C (mg/L) | Pressure (kPa) | Slope $\times 10^{-7}$ ($k_c$) | Intercept $\times 10^{-7}$ ($J_0^{-2}$) | $R^2$ |
|---|---|---|---|---|
| 125 | 68.95 | 5520 | 123.11 | 0.996 |
| | 137.90 | 29.07 | 50.19 | 0.999 |
| | 206.84 | 12.80 | 40.39 | 0.998 |
| | 275.79 | 83.58 | 31.26 | 0.998 |
| 250 | 68.95 | 57.18 | 119.08 | 0.999 |
| | 137.90 | 45.07 | 84.27 | 0.999 |
| | 206.84 | 26.53 | 63.81 | 0.996 |
| | 275.79 | 19.77 | 60.09 | 0.997 |

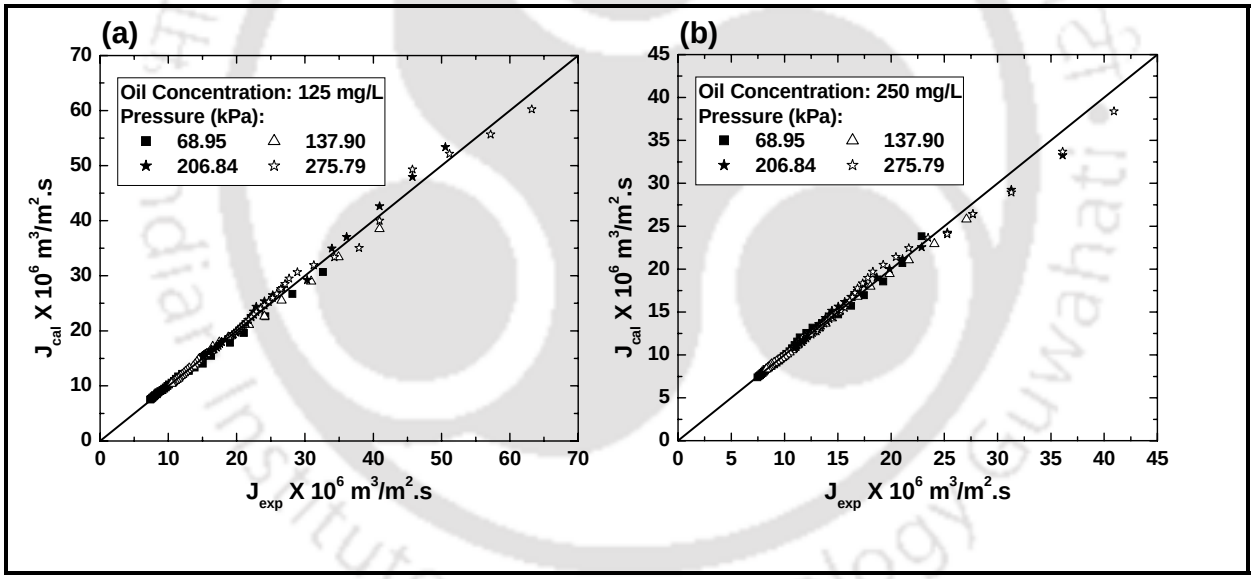


**Figure 5.5: Parity plot of experimental and calculated permeate flux using cake filtration model.**

$$k_c = 86.337 \times 10^7 \times \exp(-0.0054 \times \Delta P) \qquad R^2 = 0.979 \qquad (5.3)$$

$$\left(J_0^{-2}\right) = 10.54 \times 10^9 \times (\Delta P)^{-0.516} \qquad R^2 = 0.985 \qquad (5.4)$$

within the pressure range $68.95 \le \Delta P \le 275.79$.

A parity plot between experimental and calculated flux based on the cake filtration model has been shown in Fig. 5.5. From the figure, a good fitness between experimental and evaluated values was observed and henceforth, the cake filtration model was inferred to be the best fitted pore blocking model.

### 5.2.3 Microfiltration of mosambi juice

Permeate flux decline profiles at different values of $\Delta P$ (137.90, 206.84, 275.79 and 344.74 kPa) for CJ and ETCJ are shown in Figs. 5.6a and 5.6b, respectively. From both the figures, it can be observed that permeate flux declined sharply within the initial phase of 5 - 10 minutes and becomes gradual thereafter. The decline in flux with time was due to pore blocking of ceramic porous structure and gel layer formation over the membrane surface by pectic materials present in the juice. The permeate flux decreased from $12.67\times10^{-6}$ - $5.94\times10^{-6}$ $m^3/m^2.s$ for CJ (Fig. 5.5a) and from $58.49\times10^{-6}$ - $22.62\times10^{-6}$ $m^3/m^2.s$ for ETCJ (Fig. 5.5b) at the end of 40 minutes of experimental run at $\Delta P$ of 137.90 kPa. From the figures, it may

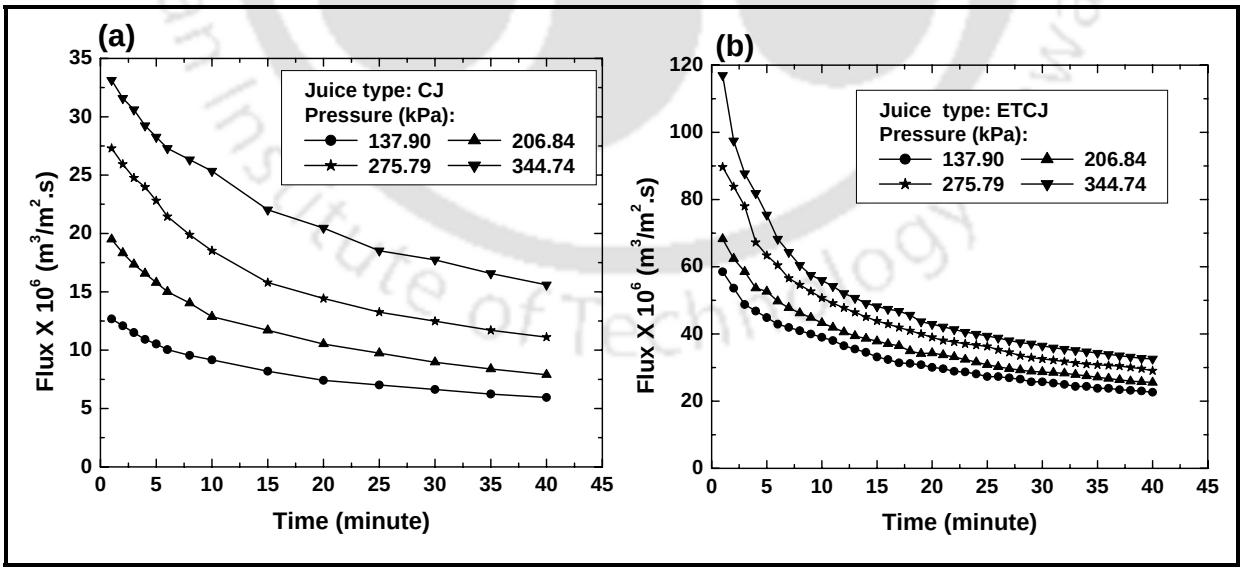


**Figure 5.6: Variation of permeate flux with time at various trans-membrane pressure differentials for (a) CJ and (b) ETCJ.**

also be observed that permeate flux increased with an increase in $\Delta P$. The initial permeate flux increased from $12.67\times10^{-6}$ - $33.15\times10^{-6}$ $m^3/m^2.s$ for CJ and $58.49\times10^{-6}$ - $117\times10^{-6}$ $m^3/m^2.s$ for ETCJ when $\Delta P$ was increased from 137.90 - 344.74 kPa. An increase in permeate flux with $\Delta P$ was due to the higher driving force across the membrane. Also, the permeate flux was higher for ETCJ compared to the CJ. This was due to the presence of higher amounts of pectic materials in the CJ (causing greater gel layer formation) as well as higher viscosity of the CJ. The observed flux data using the ceramic membrane have been found to be better than those obtained using polymeric membranes. The ceramic membrane provided a flux decline of $138.6\times10^{-6}$ - $20\times10^{-6}$ $m^3/m^2.s$ within 40 minutes of experimental run for a trans-membrane pressure differential of 137.90 - 44.7 kPa which is comparable to the flux reported by Rai et al., 2006 [63] using polymeric membranes ($250\times10^{-6}$ - $1.94\times10^{-6}$ $m^3/m^2.s$ at 138 kPa within 27 minutes of experimental run). Further, the polymeric membranes provided 98 % reduction in the flux due to fouling phenomena which is quite high in comparison to the ceramic membrane (84 %). In other words, the ceramic membrane performed better than the polymeric membrane.

### 5.2.4 Identification of flux decline mechanism for mosambi juice

Similar to the procedures outlined in chapter 3 and chapter 4, pore blocking models were used to identify the decline in permeate flux. Figures 5.7 and 5.8 illustrate the fitness of different pore blocking models corresponding to flux data for CJ and ETCJ, respectively. Similar to the trends presented in chapter 4, trends in Fig. 5.7 and 5.8 indicate that there exist two different paradigms of fouling phenomena that can be represented using two linear trends. These correspond to the initial 4 to 5 minutes of the MF run and the rest for all experimental investigations. An analysis of $R^2$ values for all models revealed that for the first regime,

fitness of intermediate pore blocking was highest (varied between 0.989 - 0.999 and 0.98 - 0.989 for CJ and ETCJ, respectively). On the other hand, for the second regime (from 5 - 40 minutes of experimental run), cake filtration model $R^2$ values have been found to be highest (0.998). Therefore, flux decline due to intermediate pore blocking followed by cake filtration was inferred to be the most competent combination of fouling mechanisms. However, when a single most competent model was considered to represent the entire flux decline regime, it has

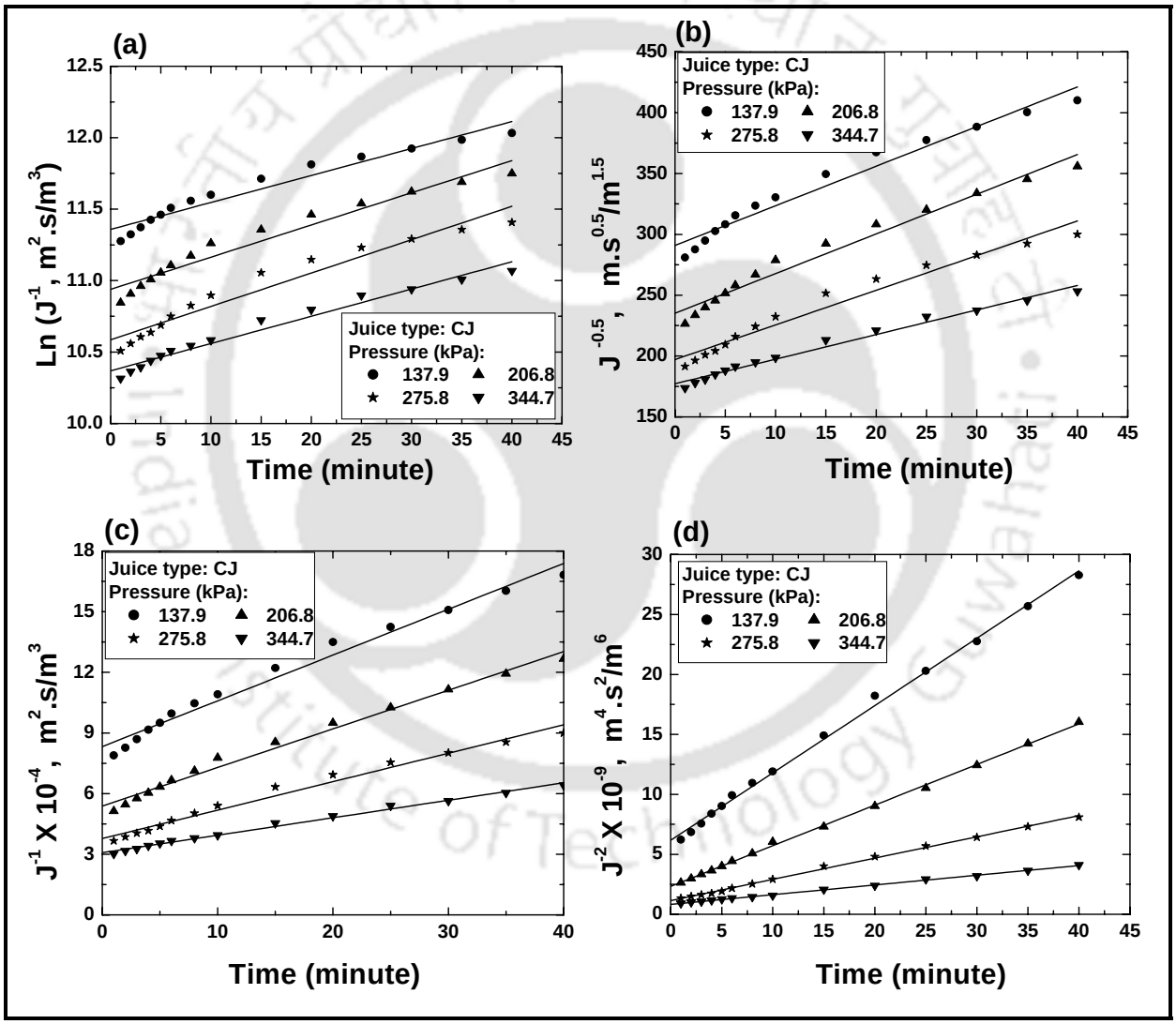


**Figure 5.7: Linearized plots of variation in permeate flux with time at various trans-membrane pressure differentials for CJ; (a) complete pore blocking model, (b) standard pore blocking model, (c) intermediate pore blocking model and (d) cake filtration model.**

been observed that the cake filtration model provided the best values of $R^2$ = 0.998 (Table 5.2). Since the variation in $R^2$ for single model (cake filtration) and combination model (intermediate pore blocking followed with cake filtration) have been found to be insignificant, it has been finally inferred that cake filtration could also represent the pertinent flux decline phenomena. Critical observation of Fig. 5.7d and 5.8d also inferred that the fitness cake

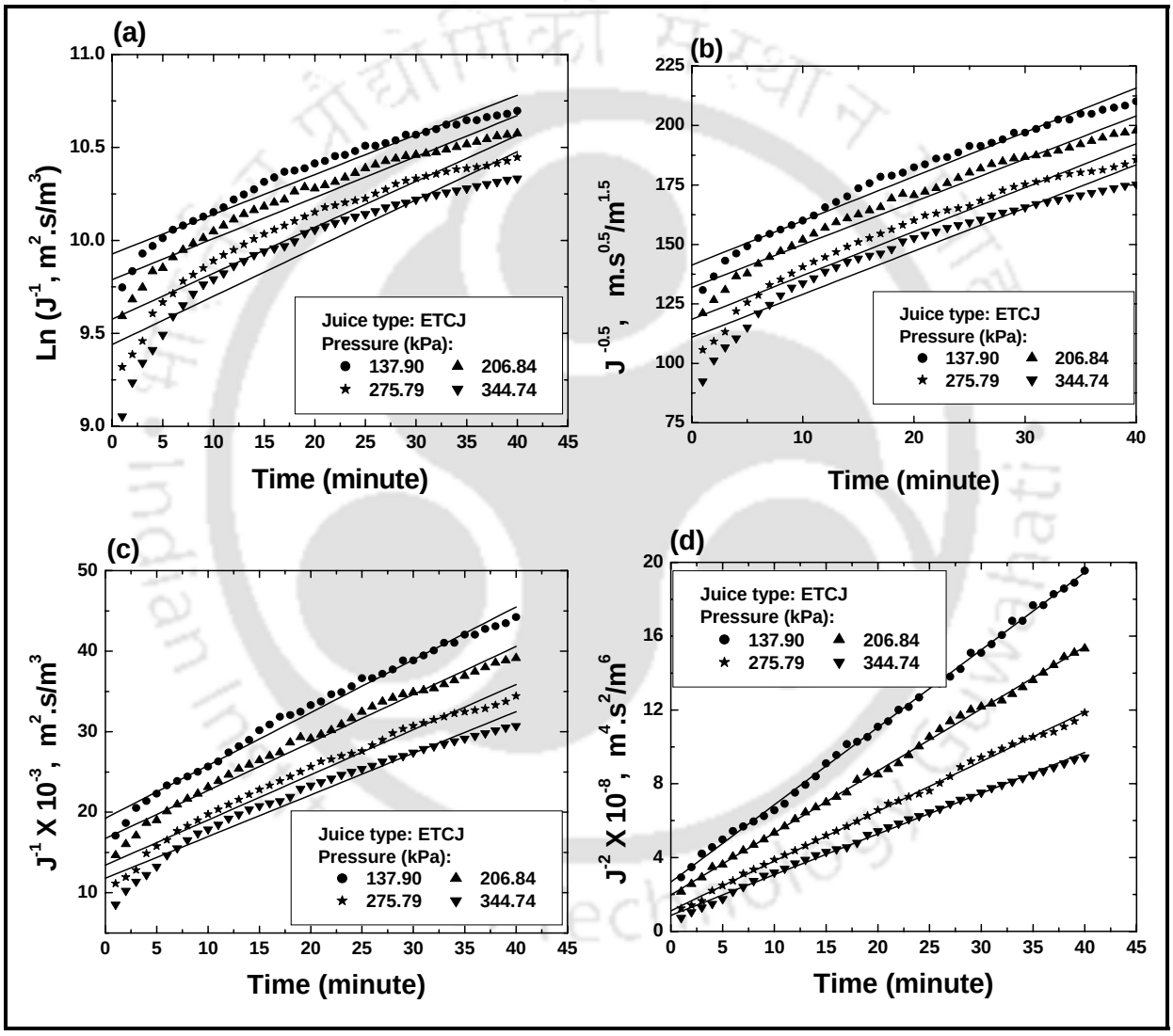


**Figure 5.8: Linearized plots of variation in permeate flux with time at various trans-membrane pressure differentials for ETCJ; (a) complete pore blocking model, (b) standard pore blocking model, (c) intermediate pore blocking model and (d) cake filtration model.**

**Table 5.3: Summary of parameters associated to various pore blocking models.**

| Juice type | Pressure (kPa) | Complete pore blocking | | | Standard pore blocking | | | Intermediate pore blocking | | | Cake filtration | | |
|---|---|---|---|---|---|---|---|---|---|---|---|---|---|
| | | $k_b \times 10^2 \ln(J_0^{-1})$ | | $R^2$ | $k_S$ | $J_0^{-0.5}$ | $R^2$ | $k_i$ | $J_0^{-1} \times 10^{-4}$ | $R^2$ | $k_C \times 10^{-7}$ | $J_0^{-2} \times 10^{-8}$ | $R^2$ |
| CJ | 137.90 | 1.77 | 11.37 | 0.947 | 3.10 | 292.33 | 0.967 | 2190 | 8.39 | 0.983 | 56.01 | 61.87 | 0.998 |
| | 206.84 | 2.11 | 10.95 | 0.950 | 3.11 | 236.57 | 0.973 | 1851 | 5.44 | 0.988 | 34.04 | 23.12 | 0.999 |
| | 275.79 | 2.17 | 10.60 | 0.942 | 2.69 | 198.51 | 0.965 | 1351 | 3.83 | 0.982 | 17.65 | 11.44 | 0.999 |
| | 344.74 | 1.80 | 10.38 | 0.967 | 1.93 | 178.04 | 0.982 | 836 | 3.10 | 0.992 | 8.06 | 8.27 | 0.999 |
| ETCJ | 137.90 | 1.98 | 9.95 | 0.944 | 1.76 | 142.78 | 0.970 | 634 | 1.96 | 0.987 | 4.23 | 2.62 | 0.999 |
| | 206.84 | 2.03 | 9.81 | 0.931 | 1.69 | 133.54 | 0.961 | 570 | 1.71 | 0.982 | 3.35 | 2.00 | 0.999 |
| | 275.79 | 2.26 | 9.61 | 0.904 | 1.73 | 120.26 | 0.946 | 536 | 1.38 | 0.975 | 2.70 | 1.12 | 0.998 |
| | 344.74 | 2.34 | 9.48 | 0.866 | 1.67 | 113.03 | 0.920 | 486 | 1.23 | 0.959 | 2.16 | 0.93 | 0.997 |

filtration model was far better than all other models (Figs. 5.7 a- c and 5.8a - c). Hence, cake filtration model was identified as the best fitted model to represent the flux decline mechanism for both CJ and ETCJ.

Different values of $k_c$ summarized in Table 5.3 indicates that for both CJ and ETCJ, $k_c$ reduced with an increase in ΔP, thereby inferring that the fouling of membrane reduced with an increase in ΔP. This is similar to the observations reported previously in section 4.3.6 (chapter 4). The variation of $k_c$ with $\Delta P$ are presented in Fig. 5.9 and were suitably correlated using linear expressions as

$$k_c{}^{CJ} = 8.948\times10^{8} - 2.562\times10^{6}\,\Delta P \qquad R^2 = 0.989 \qquad (5.5)$$

$$k_c{}^{ETCJ} = 5.686\times10^{7} - 1.090\times10^{5}\,\Delta P \qquad R^2 = 0.996 \qquad (5.6)$$

within the pressure range $137.90 \le \Delta P \le 344.74$

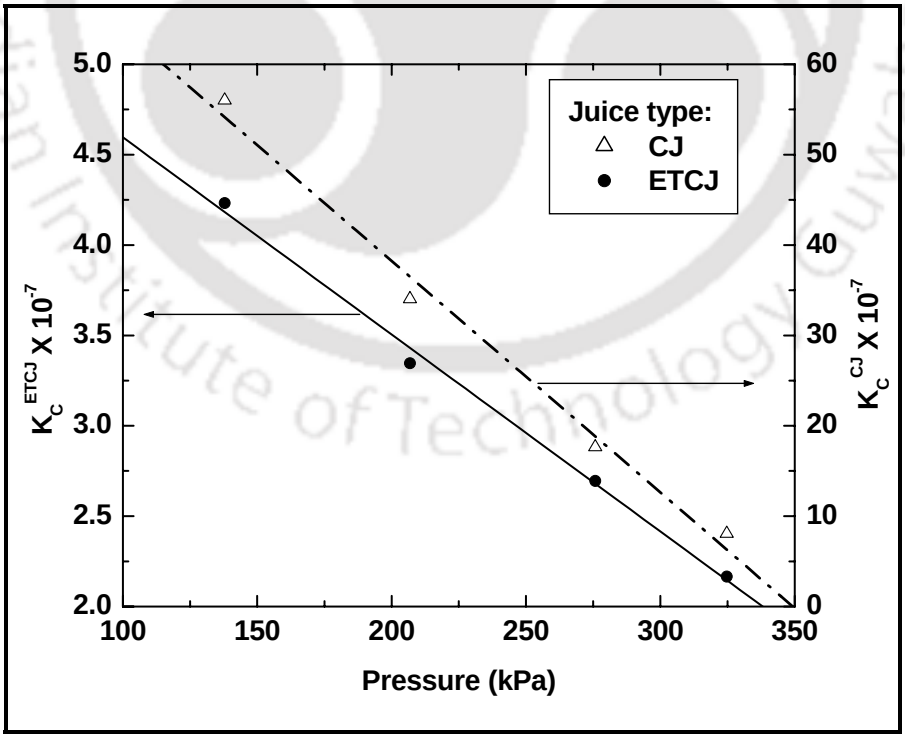


**Figure 5.9: Variation of $k_c$ with trans-membrane pressure differentials.**

Using the values of $J_0^{-2}$ summarized in Table 5.3, the initial instantaneous fouling resistance of the membrane ($R_f^0$) during MF was calculated as:

$$J_0 = \frac{\Delta P}{\mu_p \left(R_t^0\right)} = \frac{\Delta P}{\mu_p \left(R_m + R_f^0\right)} \tag{5.7}$$

In the above expression, $R_f^0$ corresponds to the fouling membrane resistance due to the membrane fouling at zero time. This hydraulic resistance was due to the presence of both soluble and insoluble solids in the feed juice and henceforth relates to the magnitude of the instantaneous initial fouling of the membrane. Subsequently, $R_t^0$ and $R_f^0$ were evaluated from Eq. (5.7) using $R_m$ values summarized in Table 5.1. Table 5.4 presents the variation of $R_f^0$ with ΔP and its percentage contribution to the $R_t^0$. As shown, percent contribution $R_f^0$ varies from 85.6 to 87.6 % for CJ and 41 to 60 % for ETCJ. Higher values of $R_f^0$ for CJ

**Table 5.4: Variation of total and initial instantaneous fouling resistance with trans-membrane pressure differential for CJ and ETCJ.**

| Juice type | Pressure (kPa) | $R_t^0 \times 10^{-11}$ ($m^2/m^3$) | $R_f^0 \times 10^{-11}$ ($m^2/m^3$) | % $R_m$ | % $R_f^0$ |
|---|---|---|---|---|---|
| CJ | 137.90 | 74.81 | 65.55 | 12.38 | 87.62 |
| | 206.84 | 68.59 | 59.33 | 13.50 | 86.50 |
| | 275.79 | 64.32 | 55.06 | 14.40 | 85.60 |
| | 344.74 | 64.40 | 55.14 | 14.38 | 85.62 |
| ETCJ | 137.90 | 15.71 | 6.45 | 58.94 | 41.06 |
| | 206.84 | 20.60 | 11.34 | 44.95 | 55.05 |
| | 275.79 | 20.54 | 11.28 | 45.09 | 54.91 |
| | 344.74 | 23.39 | 14.13 | 39.58 | 60.42 |

were due to the presence of higher amounts of pectic material compounds in CJ when compared to that in ETCJ. In other words, enzyme treatment can be regarded to be of paramount significance to induce lower fouling even instantaneously.

### 5.2.5 Permeate quality after filtration

Table 5.5 presents various physio-chemical properties of clarified CJ and ETCJ. It can be observed from the table that there was significant improvement in the colour and clarity of the mosambi juice after filtration. The colour decreased from 0.69 of FJ to 0.0953 for CJ and from 0.48 to 0.0232 for ETCJ. Also, clarity increased from 53.73 to 93.39 % for CJ and 67.87 to 98.98 % for ETCJ. This was due to the removal of pectic materials present in the juice. 100 % removal of AIS content was observed for ETCJ. However, negligible amount of AIS was found in permeate of CJ. The viscosity decreased from 1.61 to 1.45 mPa.s and 1.56 to 1.42 mPa.s for CJ and ETCJ, respectively. However, valuable properties of the juices such as pH, soluble solids, acidity and density did not vary significantly for both CJ and ETCJ.

**Table 5.5: Physico-chemical properties of clarified mosambi juice.**

| Juice type | Pressure (kPa) | Colour ($A_{420}$) | Clarity ( $\%T_{660}$) | TSS ($^{o}$Brix) | Citric acid (wt %) | pH | Density ($g/cm^3$) | Viscosity (mPa.S) | AIS (wt %) |
|---|---|---|---|---|---|---|---|---|---|
| CJ | 137.90 | 0.0953 | 93.39 | 9.1 | 0.80 | 3.87 | 1.03 | 1.45 | 0.04 |
| | 206.84 | 0.1016 | 93.16 | 9.1 | 0.81 | 3.84 | 1.03 | 1.45 | 0.04 |
| | 275.79 | 0.1049 | 92.97 | 9.1 | 0.81 | 3.84 | 1.03 | 1.46 | 0.05 |
| | 344.74 | 0.1162 | 92.56 | 9.1 | 0.81 | 3.84 | 1.03 | 1.46 | 0.05 |
| ETCJ | 137.90 | 0.0232 | 98.98 | 9.1 | 0.78 | 3.9 | 1.03 | 1.42 | Nil |
| | 206.84 | 0.0342 | 98.61 | 9.1 | 0.81 | 3.85 | 1.03 | 1.43 | Nil |
| | 275.79 | 0.0512 | 98.01 | 9.1 | 0.81 | 3.85 | 1.03 | 1.43 | Nil |
| | 344.74 | 0.0586 | 97.08 | 9.1 | 0.81 | 3.85 | 1.03 | 1.43 | Nil |

### 5.2.6 Long term storage studies

Similar to chapter 4, long stability studies of clarified juices were carried out by keeping 500 ml of CJ and ETCJ permeate obtained at $\Delta P$ of 137.90 kPa in refrigerated condition for 30 days. During storage, important parameters of the juice such as colour, clarity, TSS, pH, citric acid and density were measured. Table 5.6 shows the obtained results for the juice samples. From the table it was inferred that, during 30 days of storage variation of juice properties was found to be negligible for ETCJ permeate, where as small variation for CJ permeate was observed. Since all pectic materials were removed during MF, significant contribution of fermentation reactions to alter the juice quality has not been observed for ETCJ permeate. However for CJ permeate samples, negligible amount of AIS were present in the permeate juice (0.04 %) and some contributions from fermentation reactions to alter the juice quality slightly were observed. These observations further justify deploying enzymatic treatment of the mosambi juice before MF based clarification to substantially enhance the juice quality and stability.

## 5.3 Comparison between A1 and B3 membranes performance

### 5.3.1 Microfiltration of oil-in-water emulsions

Comparing the overall permeate flux and rejection behavior of B3 membrane and A1 membrane (presented in chapter 3) for o/w emulsions, it can be observed that membrane A1 offers higher permeate flux than B3 membrane. For example, at a constant $\Delta P$ of 206.84 kPa, permeate flux reduced from 100.34 $\times 10^{-6}$ - 17.05 $\times 10^{-6}$ $m^3/m^2.s$ and from 80.27$\times 10^{-6}$ -15.05 $\times 10^{-6}$ $m^3/m^2.s$, within 30 minutes of experimental run for oil concentration of 100 and 150 mg/L, respectively for A1 membrane (Figs. 3.3c and 3.3d). On the other hand, for the B3

**Table 5.6: Summary of results obtained during the long term storage study. Permeate juice samples were obtained at a trans-membrane pressure drop of 41.37 kPa.**

| Juice type | Day | Colour ($A_{420}$) | Clarity ( $\%T_{660}$) | TSS ($^{o}$Brix) | Citric acid (wt %) | pH | Density (g/cm$^3$) |
|---|---|---|---|---|---|---|---|
| CJ | 1st | 0.076 | 94.39 | 9.1 | 0.81 | 3.84 | 1.03 |
| | 7th | 0.101 | 92.92 | 9 | 0.81 | 3.82 | 1.03 |
| | 15th | 0.132 | 88.92 | 8.9 | 0.82 | 3.79 | 1.03 |
| | 21st | 0.164 | 86.65 | 8.8 | 0.87 | 3.75 | 1.03 |
| | 30th | 0.204 | 84.26 | 8.7 | 0.88 | 3.70 | 1.03 |
| ETCJ | 1st | 0.068 | 96.44 | 9.1 | 0.81 | 3.85 | 1.03 |
| | 7th | 0.075 | 95.18 | 9.1 | 0.81 | 3.84 | 1.03 |
| | 15th | 0.091 | 94.36 | 9.0 | 0.81 | 3.84 | 1.03 |
| | 21st | 0.109 | 93.27 | 9.0 | 0.8 | 3.83 | 1.03 |
| | 30th | 0.118 | 90.61 | 9.0 | 0.80 | 3.82 | 1.03 |

membrane for the same $\Delta P$, permeate flux varied from 50.55 $\times 10^{-6}$ -15.05 $\times 10^{-6}$ within 30 minutes of experimental run for oil concentration of 125mg/L (Fig. 5.1a). This was due to the fact that porosity and average pore size of membrane and hence effective permeability factor ($\varepsilon_m d_l^{\,2}$) of A1 is higher than B3 membrane. However, due to its lower pore size oil rejection efficiency of B3 membrane (97.7 % after 30 minutes for 125 mg/l) was better than A1 (97.4% (100 mg/L) and 97.5 % (150 mg/L) after 30 minutes) membrane.

On the other hand, comparing the fouling mechanism of membrane A1 (as discussed in chapter 3) with that of B3 membrane, it can be observed for A1 membrane flux decline was initially was due to intermediate pore blocking and latter due to cake filtration. However, for B3 membrane flux decline was due to cake filtration. These variations can be explained by the average pore diameter of membrane and droplet size of emulsion in both the cases. For A1

membrane, the droplet sizes of oil were very much similar to the membrane average pore diameter. Due to this reason, initially smaller droplets entered through the pores and pore blocking occurred. After certain period of operation depending upon the oil concentration, pore blocking reaches saturation and bigger oil droplets rejected by the membrane eventually get deposited over the membrane surface to yield a thin oily film. This leads to cake filtration in the latter regime. However, for B3 membrane the average pore size of the membrane was lower than the oil droplet sizes. Due to this reason, maximum numbers of oil droplets were rejected by the membrane and lead to the formation of a thin film. Even though very less numbers of smaller oil droplets block the pores initially, the overall flux decline was predominantly due to the thin film. Therefore, the oil rejection efficiency of B3 membrane was comparatively higher (less than 1 %) than that of A1 membrane. It was also evident that membrane A1 provided higher flux and similar product quality when compared to B3. Therefore, using A1 membrane would be beneficial for industrial processing. Membrane B3 can be recommended for processing even lower feed concentration (eg., < 100 mg/L) due to its lower pore size in comparison to A1 membrane.

### 5.3.2 Microfiltration of mosambi juice

Comparing the overall permeate flux and permeate juice quality of B3 membrane and A1 to A4 membranes as discussed in chapter 4, it can be observed that A1 - A4 membranes offered higher permeate flux than B3 membrane. This was due to the reason that porosity and average pore size of membrane and hence effective permeability factor of composition A membranes were higher than that of the B3 membrane. However, due to its lower pore size permeate juice quality was better for B3 membrane than composition A membranes (Tables 4.3, 4.4 and 5.5). Therefore, it can be seen that both permeate flux and quality need to be considered to choose

either A1-A4 or B3 membrane for industrial application. As permeate quality of A1, A2 and A3 membranes are comparable with B3 membrane (clarity more than 90 % and only 2-3 % less than B3 membrane) with significantly higher flux, A1, A2 and A3 membranes are recommended for industrial applications. B3 membrane can be used when very high quality permeate is required irrespective of permeate flux.

# Chapter 6:

## Preparation of Cellulose Acetate - Ceramic Composite Membranes

# Preparation of Cellulose Acetate - Ceramic Composite Membranes

*This chapter presents the preparation of cellulose acetate (CA) - ceramic composite membranes using dip coating technique. The fabricated composite membranes were characterized to evaluate the effect of dip coating parameters (CA concentration in solution and dipping time) using scanning electron microscope, gas permeation, pure water flux and UF of bovine serum albumin. Theoretical investigations were conducted to know the macroporus and mesoporous structure of the prepared membranes using Knudsen and viscous permeability analysis of air. Phenomenological models were proposed to illustrate the dependency of hydraulic resistance of membrane on the structural parameters such as average pore size, effective porosity as well as dip coating parameters such as dipping time and concentration of CA.*

## 6.1 Experimental

### 6.1.1 Raw materials

Cellulose acetate (molecular weight 30 kDa and acetyl content 39.8 wt %) was procured from *Loba chemicals Ltd., India*. Acetone, solvent used for dissolving cellulose acetate was purchased from *Merck, India*. Bovine serum albumin (BSA) with molecular weight of 69 kDa was purchased from *SRL Chemicals Ltd., India*. The raw materials were graded at least 99.5 % pure and used without any further purification. Ceramic MF membrane A4 ( $d_{g,\mathrm{sup}}$ = 560 nm and $\left(\varepsilon/q^2\right)_{\mathrm{sup}}$ = 0.33) prepared using composition A with a sintering temperature of 1000 $^{o}$C

was used as a support for preparation of composite membrane. A detailed account of the preparation and characterization techniques has been presented in chapter 2.

### 6.1.2 Preparation of composite membranes

CA solution was prepared by dissolving CA flakes of 2, 4, 6 and 8 g in 100 ml acetone separately in a stopper conical flask of 250 ml capacity. The mixtures were stirred using a magnetic stirrer for 24 hrs to ensure uniform and complete dissolution of cellulose acetate in acetone. Prior to the dip coating process, the ceramic supports were kept in acetone for 3 hrs to displace air bubbles present in the membrane porous structure and restrict the penetration of CA solution into the membrane pores during dip coating. Surfaces other than the top surface of the support were covered using Teflon tape to prevent CA deposition. Coating of CA over the support was carried out by dipping the support in the CA solution with dipping time varied from 30 - 150 s. After coating process, the composite membranes were kept on a flat glass surface at ambient temperature for 24 hrs to yield a thin coating of CA on the ceramic support. During this time, acetone of the top layer evaporates and thereby contributes to the pore formation and hence membrane morphology and separation capabilities [10]. The composite membrane thus prepared constituted a ceramic support that was dominated with macroporous structure and a CA top layer that was dominated with mesoporous and microporous structure. Finally, the composite membrane was dried at 45 $^{o}$C for 3 hrs in a hot air oven to accomplish complete removal of acetone from the membrane structure. The nomenclature of various composite membranes fabricated with varying CA concentration in acetone (2 - 8 wt %) and dipping time (30 - 150 s) are presented in Table 6.1.

**Table 6.1: Nomenclature of various prepared composite membranes.**

| Time (s) | CA concentration (wt %) | | | |
|---|---|---|---|---|
| | **2** | **4** | **6** | **8** |
| 30 | M-2-30 | M-4-30 | M-6-30 | M-8-30 |
| 60 | M-2-60 | M-4-60 | M-6-60 | M-8-60 |
| 90 | M-2-90 | M-4-90 | M-6-90 | M-8-90 |
| 120 | M-2-120 | M-4-120 | M-6-120 | M-8-120 |
| 150 | M-2-150 | M-4-150 | M-6-150 | M-8-150 |

### 6.1.3 Characterization methods

Characterization techniques involves the structural characterization of the support and composite membranes by SEM, flux characterization using gas (air) and liquid (water) permeation, compaction study and solute rejection experiments using BSA. SEM analysis were carried out for the evaluation of membrane morphology, presence of surface/cross-sectional defects such as pinholes and cracks (if any) and estimation of membrane thickness for those cases where substantial film thickness were present (more than 500 nm). Air flux characterization aims to quantify membrane morphological parameters such as average pore size and porosity that contribute to the transport. Pure water flux (PWF) characterization was anticipated to provide insights into the physical effects of dip coating parameters on liquid transport properties as well as solute rejection properties during UF experiments. The membrane compaction study conducted for all membranes was aimed to achieve rigid porous structure and size in the membranes to accomplish consistency in hydraulic characterization tests. During compaction, the cell was initially filled with 110 ml deionised water and pressurized at 414 kPa for 6 hrs. Water flux of 100 ml was measured after every 15 min using digital weight machine and a stop watch. Water flux through the membranes declined initially

and attained a steady value after 3 to 4 hrs of compaction. After compaction, the compacted membranes were subjected to the evaluation of hydraulic permeability ($P_{com}$) and membrane hydraulic resistance ($R_{com}$). $P_{com}$ and $R_{com}$ was determined graphically from the slope of PWF and transmembrane pressure differential ($\Delta P$) (varying from 69 kPa - 345 kPa) plot using following equations [99]:

$$PWF = \frac{Q}{S \times \Delta t} = P_{com} \times \Delta P \quad (6.1)$$

$$R_{com} = \frac{\Delta P}{PWF} \quad (6.2)$$

UF experiments were carried out using 1000 mg/L of BSA solution at transmembrane pressure differential of 345 kPa. BSA solutions of concentration 1000 mg/L in phosphate buffer (0.5 M, pH 7.2) were prepared using deionized water. The pH of the feed solution was kept constant at 7.2, since a change in pH may increase the adsorptive fouling of the membranes [96]. Furthermore, intermolecular forces between BSA molecules and membranes will predominate and affect the efficiency of membranes if the pH of the solution changes [97]. During these experiments, the membrane flux was evaluated by measuring the amount of permeate collected after 1 hour. BSA concentration in both feed and permeate was determined using UV - Vis spectrophotometer at a wavelength of 278 nm. All permeation experiments were carried out using the experimental set up shown in Fig. 2.2.

## 6.2 Theoretical considerations

A schematic of various physical phenomena occurring during dip coating is shown in Fig. 6.1. As shown, when dip coating process was initiated, instantaneously CA solution tends to penetrate through the porous structure of support surface to yield an intermediate layer (Fig.

6.1b) [45]. This intermediate layer played an important role in membrane durability and bonding of the top layer with the ceramic support. The structural and morphological properties of the intermediate layer were largely dependent on the pore size and porosity of the support as well as concentration of CA used for dip coating. The growth of the CA top layer was anticipated after the formation of the intermediate layer [45]. CA top layer growth rate was also largely dependent on the CA concentration in the solution, structure and morphology of the intermediate layer [12, 15].

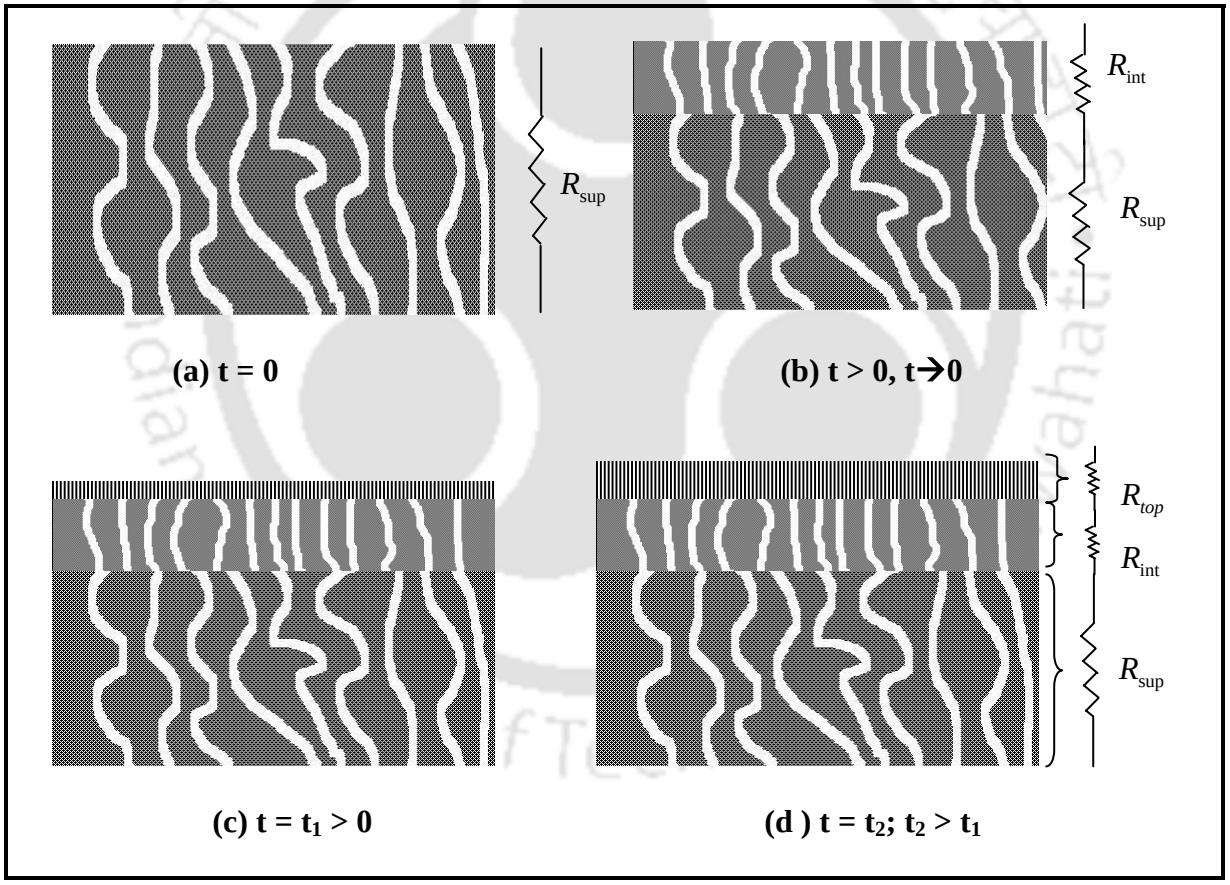


**Figure 6.1: A schematic representation for the formation of different layers during dip coating (a) support, (b) formation of intermediate layer, (c) formation of top layer and (d) growth of the top layer.**

$R_{com}$ was expressed as a function of two different resistances, resistance of support ($R_{sup}$) and resistance due to CA coating ($R_{coat}$) as

$$R_{com} = R_{sup} + R_{coat} \tag{6.3}$$

$R_{coat}$ can also be expressed as the sum of the intermediate layer resistances ($R_{int}$) and top layer resistance ($R_{top}$) as

$$R_{coat} = R_{int} + R_{top} \tag{6.4}$$

As only intermediate layer is created just after dipping the support in the solution ($t \to 0$, $t > 0$), the above expression can be written as

$$R_{coat} = R_{int} \quad \text{when } t \to 0 \tag{6.5}$$

The total resistance of the composite membrane may be expressed by combining Eqs. (6.3) and (6.4) as

$$R_{com} = R_{sup} + R_{int} + R_{top} \tag{6.6}$$

Now, various resistances in the above Eq. (6.6) may be expressed as functions of CA concentration and dipping time ($t$, s) as

$$R_{sup} \neq f_1(c,t), \qquad R_{int} = f_2(c),\ R_{top} = f_3(c,t)$$

Therefore, $R_{coat}$ can be expressed as

$$R_{coat} = f_2(c) + f_3(c,t) \tag{6.7}$$

Different resistances $R_{coat}$, $R_{int}$ and $R_{top}$ were determined using the following procedure:

1. Calculation of $R_{coat}$ using Eq. (6.4) from experimentally determined values of $R_{com}$ and $R_{sup}$.

2. Using the values of $R_{coat}$ for same CA concentration and varying dipping time a graph was plotted. The data points in the graph were fitted using suitable linear/nonlinear functions by regression analysis.
3. From the curve fit equation obtained from regression analysis, $R_{\text{int}}$ value was determined using Eq. (6.5) by extrapolating data points to $t = 0$.
4. The values of $R_{top}$ were calculated using Eq. (6.6).

During UF of BSA solutions, $R_{BSA}$ was evaluated using the following equation

$$R_{BSA} = R_{UF} - R_{\text{sup}} - R_{coat} \tag{6.8}$$

where $R_{UF}$ refers to the hydraulic resistance during UF experiments.

## 6.3 Results and discussion

In this section, results obtained from surface and flux characterization studies of fabricated membranes were discussed. The effect of dip coating parameters namely dipping time and CA solution concentration on membrane morphology, average pore size, effective porosity of the membranes, PWF, hydraulic resistance and BSA rejection studies were also presented.

### 6.3.1 Surface morphology

The broad intention behind the surface and cross sectional SEM study was to visualize various possible mechanisms involved in CA deposition on the ceramic support. Besides identifying surface defects, surface morphological study aimed to evaluate the effect of dip coating parameters on ceramic matrix blocking and CA top layer growth. Thereby, the competence of deposition conditions to yield composite membranes for MF and UF applications was assessed.

Figures 6.2a and 6.2b present the SEM image of top surface and cross section of ceramic support, respectively. It can be observed from Fig. 6.2a that the top surface of the support contains both macropores and mesopores. Figure 6.3 present SEM images of the top surface of composite membranes prepared by varying CA concentration (2 - 8 wt %) and dipping time (30 - 150 s). From the figure, it was observed that with an increase in both CA concentration and dipping time, the pore size of the membrane decreased. The SEM image of 2 wt % CA membrane (M-2-30) indicates that almost no change occurred to the porous structure in the membrane top surface. It could be further observed that the coverage of porous structure by CA increased with increasing dipping time from 30 s to 150 s. When the concentration of CA was increased to 4 %, the top surface consisting of both macropores and mesopores of support was totally covered by the CA layer and lead to the formation of a porous polymeric structure (M-4-30, M-4-90). The porous structure of the polymeric film was contributed by the evaporation of the solvent (acetone) from the membrane surface.

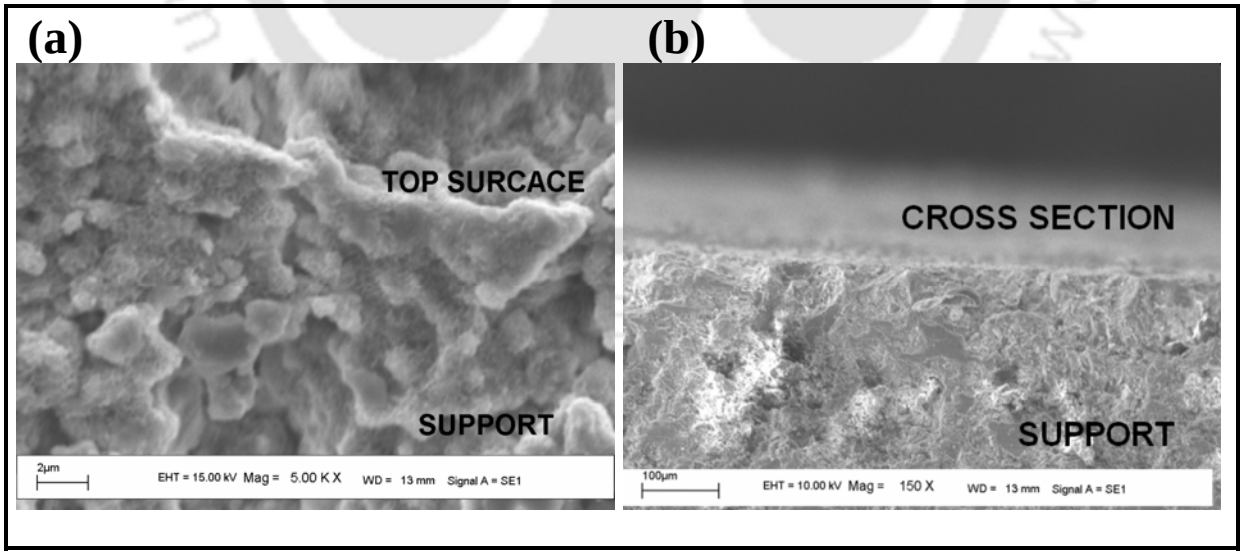


**Figure 6.2: SEM images of the ceramic support (a) top surface (Magnification: 5 KX) and (b) cross section (Magnification: 150 X).**

With an increase in dipping time from 30 to 150 s, the pore sizes of the membranes were observed to decrease very significantly due to deposition of more CA on the support. Formation of CA porous structure accounts for an increase in the effective membrane porosity of the membranes (M-4-30, M-4-90 and M-4-150) compared to the membranes prepared with 2 wt % CA concentration (M-2-30, M-2-90, M-2-150). This was attributed to the lack of formation of porous CA structure with 2 wt % CA solution concentrations. Finally, the membrane prepared with dipping time of 150 s (M-4-150) was observed to have the least pore sizes of all the membranes prepared at 4 wt % CA. Membranes prepared with 6 wt % CA concentration (M-6-30, M-6-90, M-6-150) indicated that a stable porous structure was formed. The pore sizes of the membranes were observed to be smaller than those obtained with 4 wt % CA concentration. With an increase in dipping time, the pore sizes were reduced further due to additional deposition of CA on the support. The membranes prepared with 8 wt % CA (M-8-30, M-8-90, M-8-150) were observed to possess lowest pore size among all the prepared membranes.

Figure 6.4 presents the cross sectional SEM images of the membrane prepared using varying CA solution concentrations (2 - 8 wt %) and dipping time (30 s - 150 s). Comparing the SEM image of ceramic support in Fig. 6.2b with SEM images of 2 wt % CA membranes (M-2-30, M-2-90, M-2-150), it could be observed that CA solution penetrates into the pores of the support due to very low solution viscosity and density (almost the same as the solvent). As a result, the porosity of the membranes was reduced. Further, SEM images indicate that the concentration was not enough to form a film on the support. With an increase in dipping time, more CA penetration occurs in the support as observed for membrane M-2-150. Therefore, CA solution contributes more towards the blocking of ceramic porous structure rather than

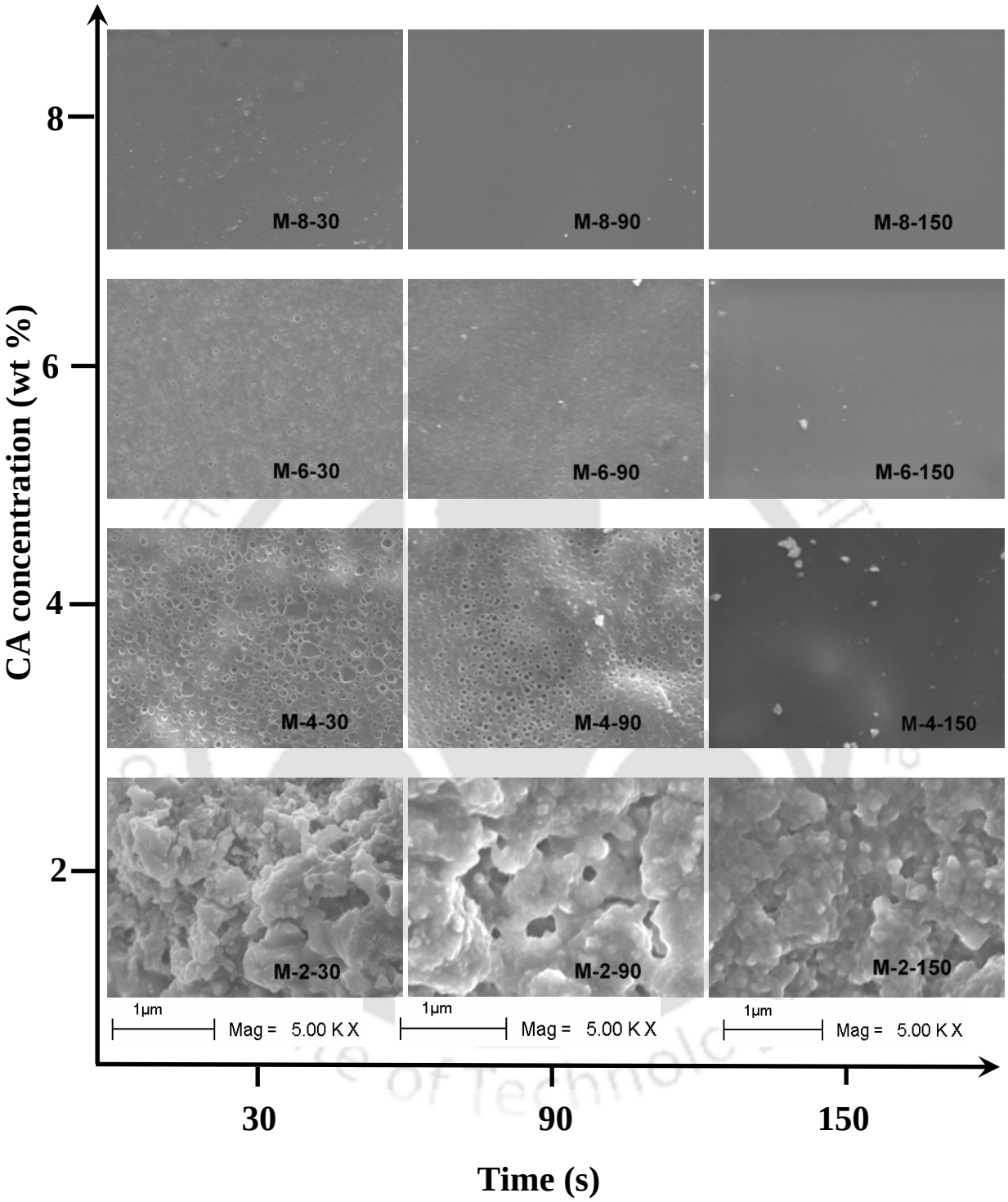


**Figure 6.3: Variation of top surface morphology with dipping time and CA concentration. (Magnification: 5 KX).**

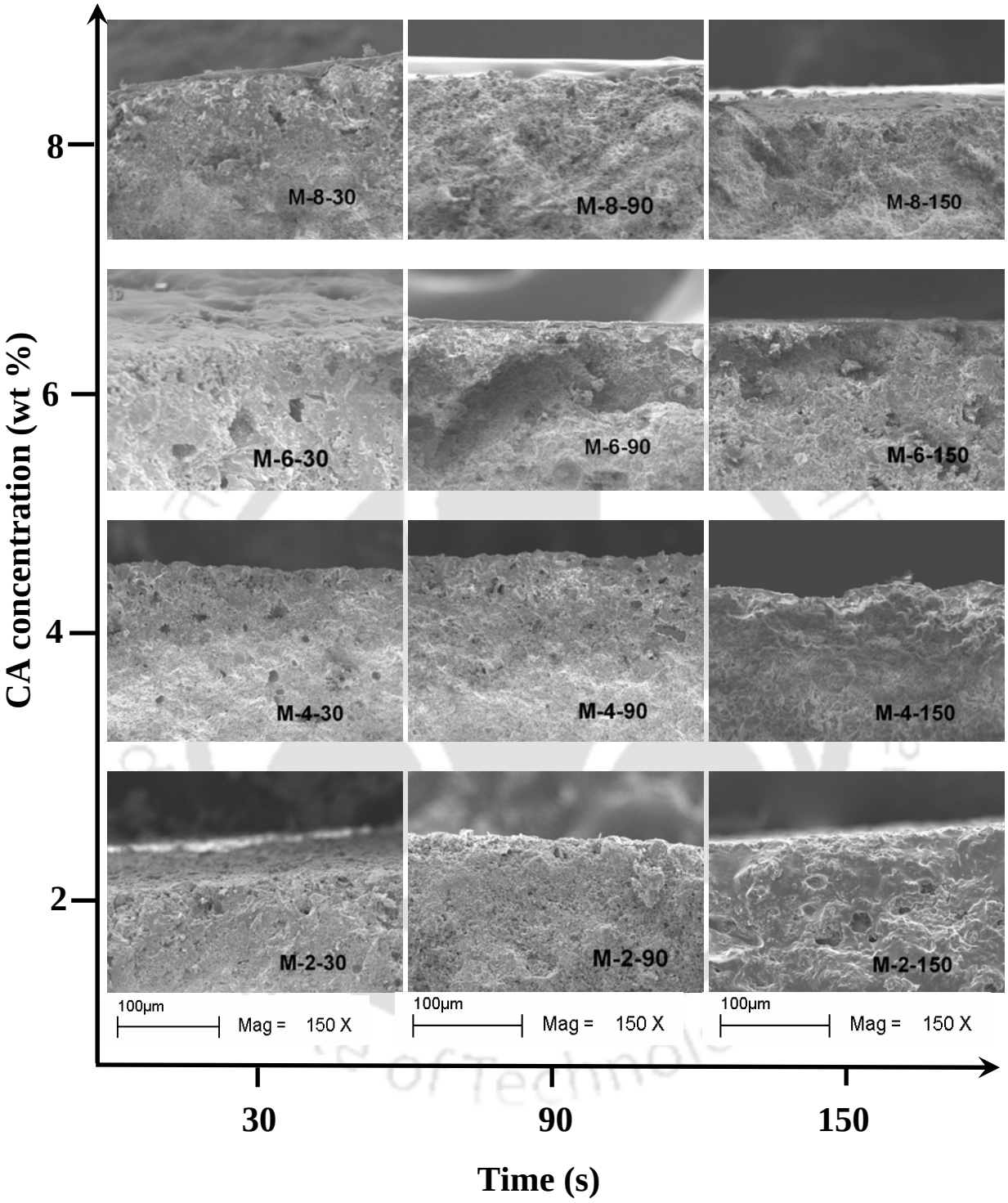


**Figure 6.4: Variation of cross-section morphology with dipping time and CA concentration. (Magnification: 150 X).**

creating a thin film on the top surface. SEM images for 4 wt % CA membrane (M-4-30, M-4-90 and M-4-150) shows similar trend like 2 wt % CA membranes. With an increase in dipping time, a tendency of creating film is observed. For dipping time of 150 s, a film like structure was formed on the top surface indicating the dominance of CA surface coverage over ceramic matrix blockage. The measured film thickness was about 0.6 μm. Due to less ceramic matrix blockage the effective porosity of the M-4-30, M-4-90 and M-4-150 membranes were more compared to M-2-30, M-2-90 and M-2-150 membranes. When the dip coating solution concentration was increased to 6 wt % CA, initially no film growth was observed for membrane M-6-30. With an increase in dipping times, a stable film was formed for M-6-90 and M-6-150. The measured film thickness for these membranes was 8 and 12 μm, respectively. With an increase in CA concentration in acetone, viscosity and density of the solution increased. Due to this, penetration tendency of the 8 wt % CA solution was less. As a result, less ceramic matrix blockage took place to obtain high effective porosity of the membranes compared to those prepared with 2 and 4 wt % CA concentrations. For 8 wt % CA membranes (M-8-30, M-8-90, M-8-150), a stable film growth was observed for all deposition times which increased with increasing deposition times. The measured film thickness of these membranes was 12, 22 and 32 μm for M-8-30, M-8-90 and M-8-150, respectively. Almost no penetration of the CA into the ceramic matrix was observed due to very high viscosity and density of the CA solution.

Based on these observations from SEM, it could be concluded that with an increase in CA concentration and dip coating time, the average pore size of the membranes decreases. This conclusion was in good agreement with results presented in the literature [98]. For the chosen ceramic support, CA concentrations varying from 6 to 8 wt % tend to be the optimal

combinations to yield UF membranes (pore diameter ranging between 10 nm to 100 nm) [3] with tailored pore size distributions. On the other hand, MF membranes (pore diameter >100 nm) [3] can be prepared using low to moderate concentrations of CA solution concentration (2 to 4 wt %). An increase in CA concentration was found to have profound effect in altering morphological properties than the dipping time, except for M-4-150 and M-6-30 where an increase in dipping time was found to yield similar effect as CA concentration.

### 6.3.2 Gas permeability

As discussed in chapter 2, various morphological parameters of the membranes such as pore size and effective porosity were determined with gas permeation experiments. Figures 6.5a - 6.5d show the variation of effective gas permeability factor ($K$) and average pressure ($P$) with $\Delta P$ (135 - 308 kPa) for all the membranes (2 - 8 wt % CA). Table 6.2 summarizes parameters evaluated from graphical analysis of average pressure ($P$) and effective gas permeability factor ($K$) data for all the membranes. As shown, the ceramic support grossly adopts viscous flux (77 - 84 %). It can be further observed that composite membranes fabricated with 2 wt % CA concentration also have morphological structure similar to that of the support with viscous flux contributing about 71 - 85 % to the total gas flux. This result was in good agreement with results observed from SEM analysis where almost no change in top surface morphology was observed for 2 wt % CA membranes. However, membranes prepared with 4 wt % CA concentration indicate a shift in the transport mechanism from viscous diffusion dominated domain (69 - 38 %) to Knudsen diffusion domain (31 to 62 %). Membranes fabricated with 6 and 8 wt % CA concentrations indicate Knudsen dominated transport properties of air where the percent contributions are 55 - 78 % and 64 - 86 %, respectively. This result was with good agreement with the results obtained in section 6.3.1

where the pore size of the membranes prepared with 6 and 8 wt % CA concentrations were in evaluated to be in the UF range.

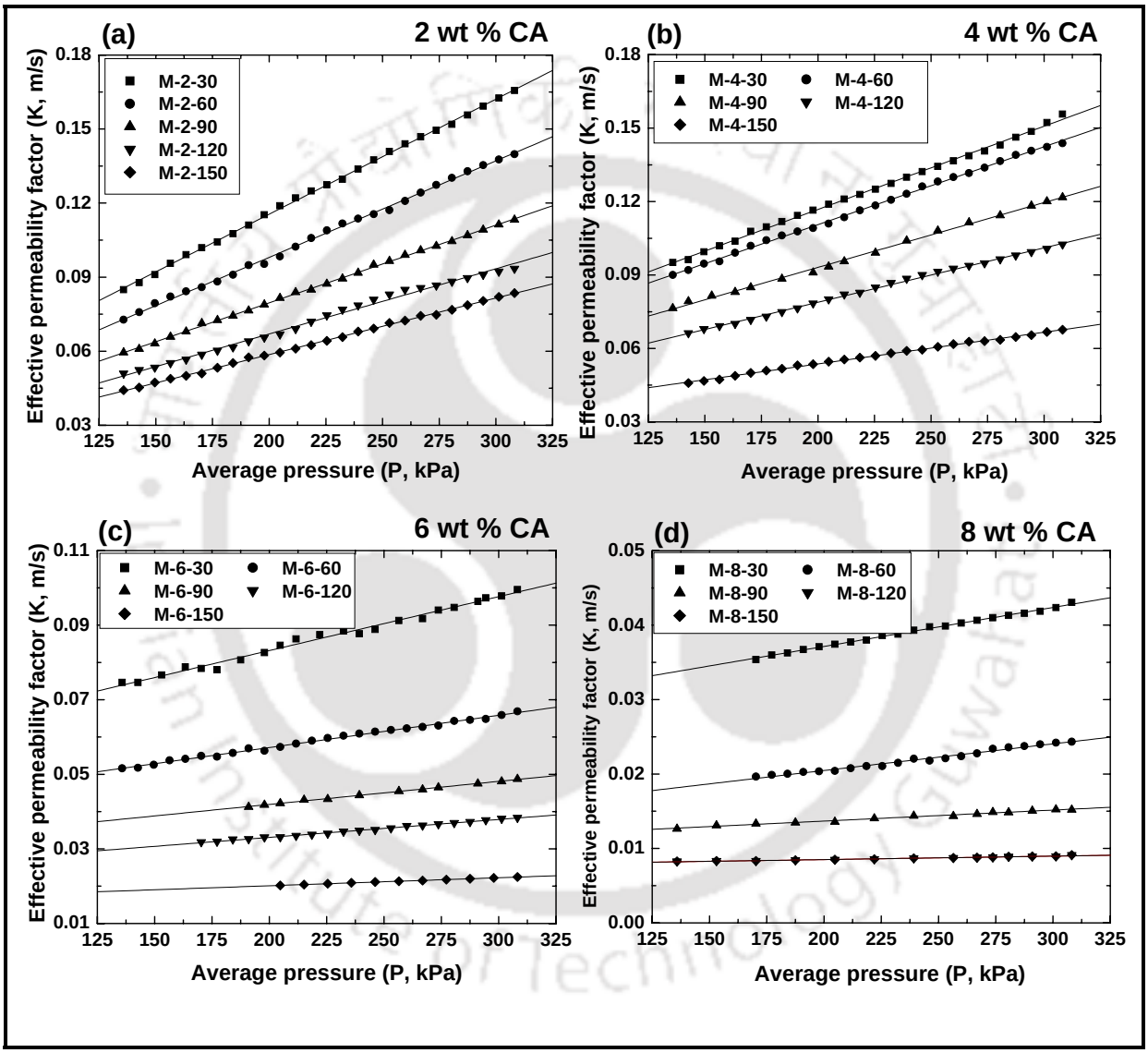


**Figure 6.5: Variation of effective permeability factor ( $K$ ) with average pressure ( $P$ ) for polymer-ceramic membranes fabricated with various CA solution concentrations (a) 2 wt % (b) 4 wt % (c) 6 wt % and (d) 8 wt %.**

**Table 6.2: Various membrane parameters evaluated from graphical analysis of gas permeation experiments.**

| Membrane name | Permeance at 206 kPa ($m^3/m^2.h.kPa$) | Slope (B) $\times 10^4$ (m/s.kPa) | Intercept (A) $\times 10^2$ (m/s) | Viscous flux (%) | Knudsen flux (%) |
|---|---|---|---|---|---|
| Support | 4.53 | 5.17 | 2.14 | 77-84 | 23-16 |
| M-2-30 | 4.23 | 4.66 | 2.22 | 74-87 | 26-13 |
| M-2-60 | 3.5 | 3.91 | 1.98 | 73-86 | 27-14 |
| M-2-90 | 2.9 | 3.15 | 1.66 | 72-85 | 28-15 |
| M-2-120 | 2.37 | 2.64 | 1.41 | 72-85 | 28-15 |
| M-2-150 | 2.11 | 2.29 | 1.28 | 71-85 | 29-15 |
| M-4-30 | 4.23 | 3.40 | 4.88 | 49-69 | 51-31 |
| M-4-60 | 2.92 | 3.18 | 4.69 | 48-67 | 52-33 |
| M-4-90 | 3.94 | 2.65 | 4.01 | 48-67 | 53-33 |
| M-4-120 | 3.32 | 2.21 | 3.61 | 45-65 | 55-35 |
| M-4-150 | 1.97 | 1.30 | 2.86 | 38-59 | 62-41 |
| M-6-30 | 3.01 | 1.45 | 5.42 | 27-46 | 73-55 |
| M-6-60 | 2.04 | 8.66 | 3.98 | 23-40 | 77-60 |
| M-6-90 | 1.53 | 6.18 | 2.96 | 24-39 | 76-61 |
| M-6-120 | 1.18 | 0.48 | 2.35 | 26-39 | 74-61 |
| M-6-150 | 0.72 | 0.22 | 1.58 | 22-30 | 78-70 |
| M-8-30 | 1.33 | 0.52 | 2.67 | 25-36 | 75-64 |
| M-8-60 | 0.75 | 0.29 | 1.55 | 21-36 | 79-64 |
| M-8-90 | 0.48 | 0.15 | 1.07 | 15-30 | 85-71 |
| M-8-120 | 0.30 | 0.075 | 0.70 | 14-25 | 86-75 |
| M-8-150 | 0.30 | 0.074 | 0.68 | 14-25 | 86-75 |

Figure 6.6a illustrates the variation of average pore size ($d_{g,com}$) of the membranes with different dipping time and CA concentration. Initially, the average pore size of the support was 560 nm. The average pore size of the CA composite membrane decreased to 487 nm when the support was subjected to dip coating at 2 wt % CA concentration and 30 s of

dipping time (M-2-30). With an increase in dipping time up to 150 s, the pore size of the membrane further decreased to 417 nm (M-2-150). Similar reduction trend in average pore size was observed when the support was dip coated with 4, 6 and 8 wt % CA solutions. The average pore size of the membrane varied between 162 - 106 nm for 4 wt %, 62 - 32 nm for 6 wt % and 46 - 25 nm for 8 wt % CA concentration solutions for a variation in dipping time from 30 s - 150 s.

Figure 6.6b illustrates the variation of effective porosity $(\varepsilon/q^2)_{com}$ of the membranes with varying dip time and CA concentrations. The effective porosity of the membrane was observed to reduce from 0.33 for support to 0.001 - 0.002 for 2 wt % CA membranes. The reduction of the porosity was due to the presence thin CA layer on the top surface of the membrane and blocking of the support porous structure as discussed in section 6.3.1.

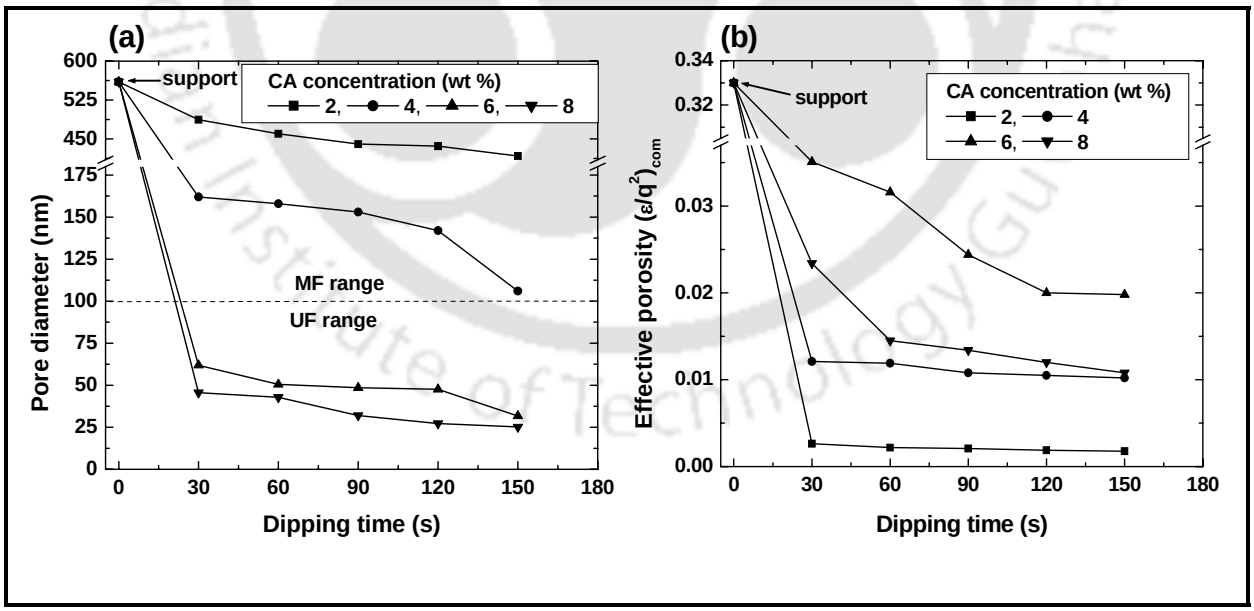


**Figure 6.6: Variation of (a) average pore diameter and (b) effective porosity of CA-ceramic composite membranes with CA concentration and dipping time.**

However, an increase in effective porosity of the membrane was observed when the CA concentration was increased up to 6 wt %. The effective porosity of the membrane varied between 0.012 - 0.01 for 4 wt % and 0.035 - 0.02 for 6 wt % CA concentrations with varying dipping time from 30 s - 150 s. The increase in effective porosity was due to the less amount of ceramic matrix blockage with an increase in CA concentration as discussed in section 6.3.1. However there was a reduction in the effective porosity of the membrane prepared using 8 wt % CA when compared to those with 6 wt % CA. This can be explained from the top surface and cross section SEM images of 6 and 8 wt % CA concentration membranes shown in Figs. 6.4 and 6.5. Cross section images inferred that all membranes have almost no ceramic matrix blockage in comparison to the cross section image of Fig. 3b. However, the top surface images infer that 8 wt % membranes contains less porosity in comparison to 6 wt % CA concentration membranes. The average pore size of the 6 wt % membrane varied from 62 nm (M-6-30) - 32 nm (M-6-150) as opposed to 46 nm (M-8-30) - 25 nm (M-8-150) for 8 wt % CA membranes. As a result, overall porous permeation areas for 6 wt % membranes were more than those for 8 wt % membranes. This indicated the optimality of 6 wt % CA concentration to yield membranes with good permeation characteristics.

### 6.3.3 Membrane compaction

The variation of pure water flux during compaction of different membranes prepared is shown in Figs. 6.7. From the figures, it can be observed that the PWF was initially high and declined gradually to reach a steady state value after 3 - 4 hours (depending upon CA concentration) for all the fabricated membranes. The reduction in PWF was due to the fact that the walls of the pores become closer, denser and uniform during compaction [3]. With an increase in dipping time and CA concentration, compaction factor calculated as ratio of initial pure water

flux (PWF) and final PWF of the membrane increased. This increase was due to an increase in both film thickness and number of voids in the porous structure.

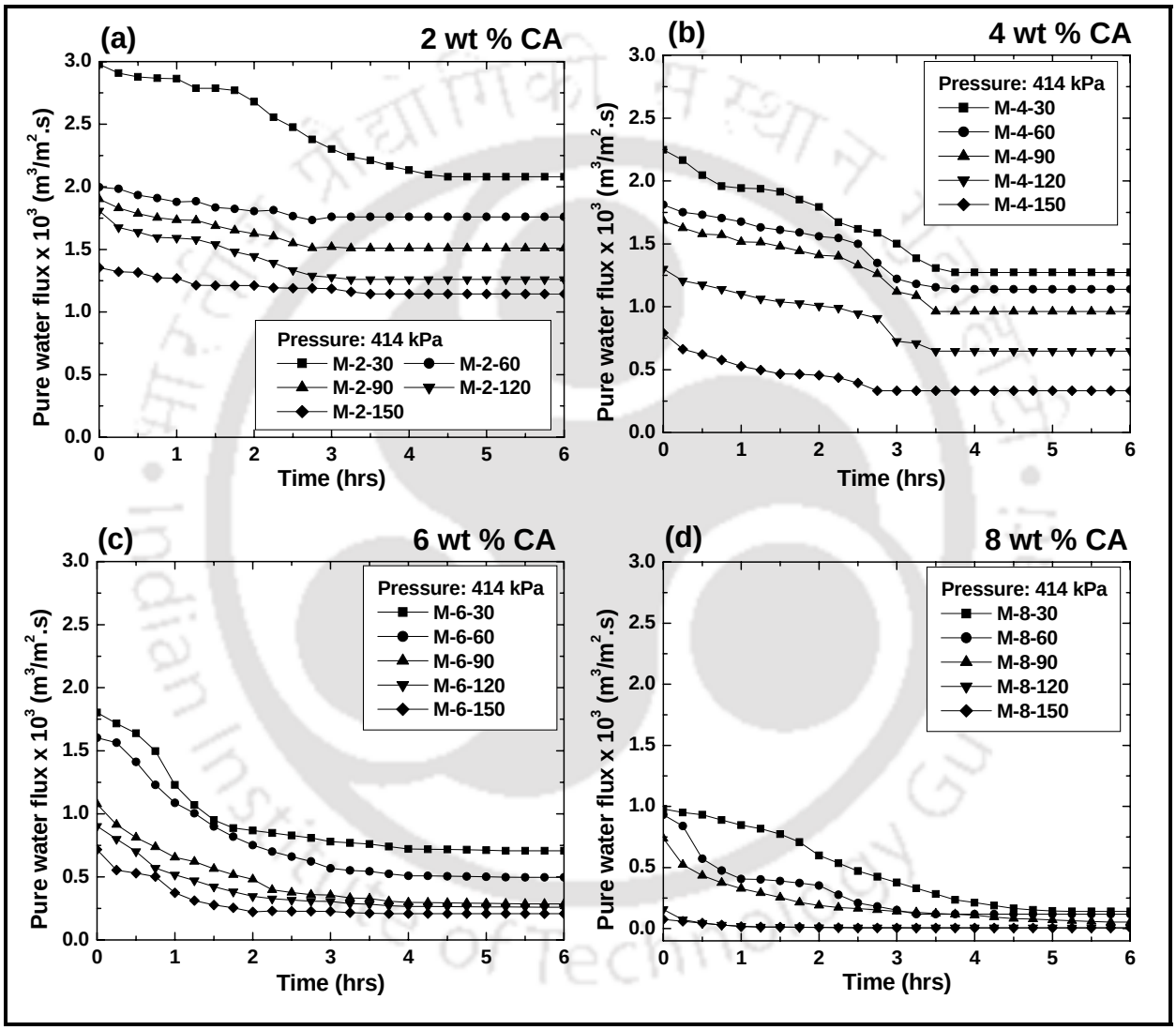


**Figure 6.7: Variation of pure water flux with time during compaction of CA coated composite membranes prepared from (a) 2 wt %, (b) 4 wt %, (c) 6 wt % and (d) 8 wt % CA solutions.**

### 6.3.4 Hydraulic permeability

The effect of dip coating parameters on the hydraulic permeability ($P_{com}$) of the prepared membranes is shown in Fig. 6.8. From the figure it can be inferred that for M-2-30 membrane, the decrease in $P_{com}$ was very less ($6.14\times10^{-6}$ - $4.98\times10^{-6}$ $m^3/m^2.s$). With an increase in dipping time as well as CA concentration $P_{com}$ decreases. This was due to the fact that, with an increase in both dipping time and CA concentration, the average pore size of the membrane decreases and top layer thickness increases.

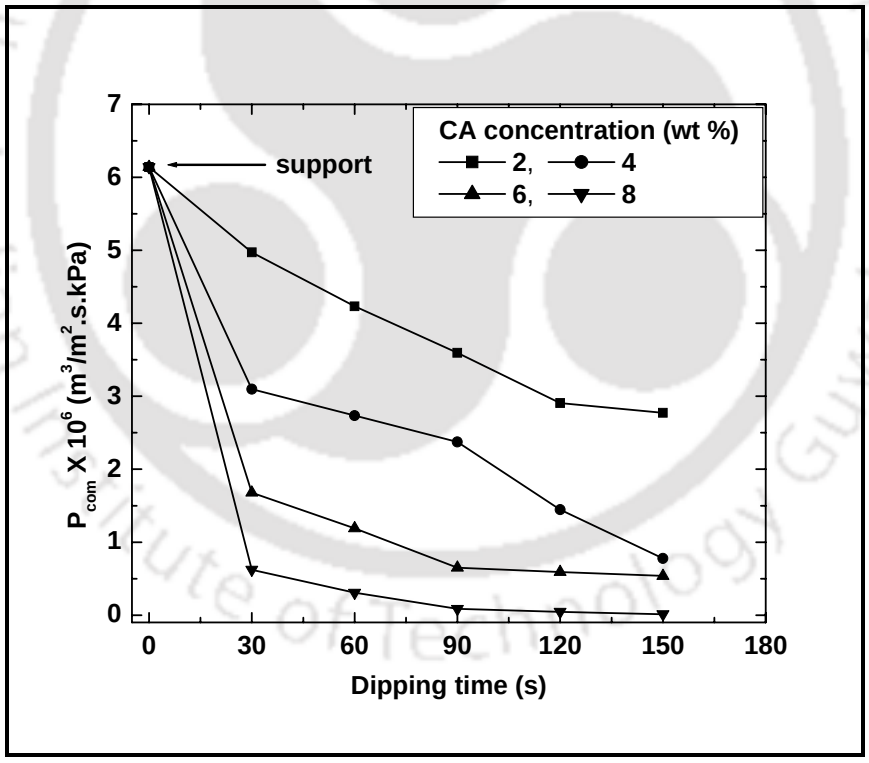


**Figure 6.8: Effect of CA concentration and dipping time on the hydraulic permeability of various composite membranes.**

### 6.3.5 Protein rejection

Figure 6.9 presents the variation of permeate flux and rejection (%) of BSA with dipping time for the membrane fabricated at 6 and 8 wt % CA membranes. As shown, the flux through the membrane decreased and percent BSA rejection increased with an increase in dipping time and CA concentration. When the dipping time was increased from 30 s (M-6-30) to 150 s (M-6-150), the membrane flux decreased from 212 - 43.9 $m^3/m^2.s$. Similarly, the membrane flux reduced from 58.9 - 12.2 $m^3/m^2.s$ for membranes prepared with 8 wt % CA solution concentrations with an increase in dip time from 30 to 150 s. The reduction in membrane flux and an increase in BSA rejection with an increase in dipping time were due to reduction in average pore size and porosity of the membranes. Percent BSA rejection was evaluated to vary from 5 % (M-6-30) to 42.5 % (M-6-150) for 6 wt % CA membranes and 20% (M-8-30) to 50 % (M-8-150) for 8 wt % CA membranes. Comparing the flux and BSA rejection

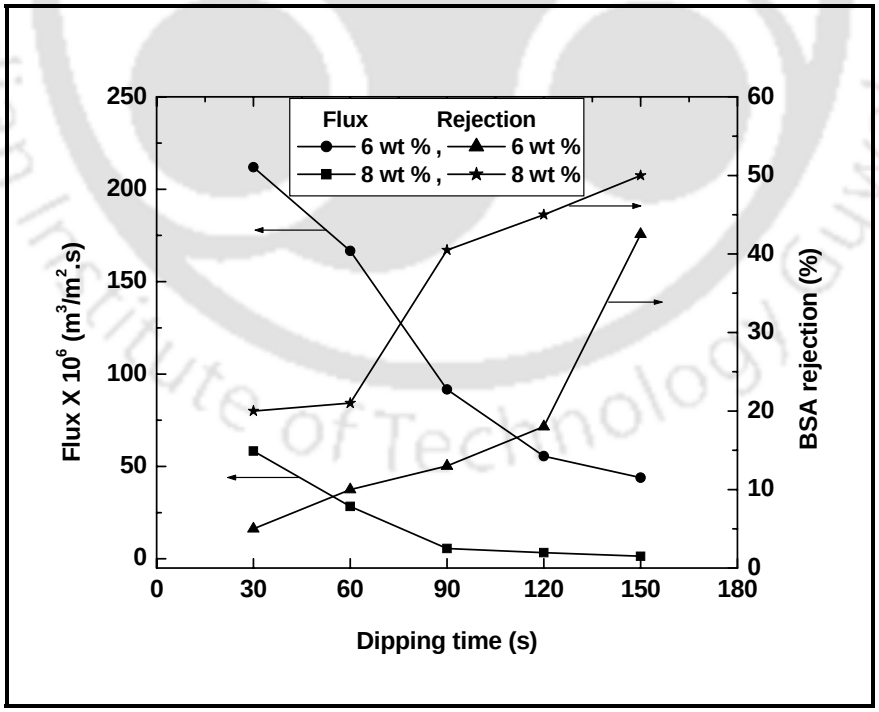


**Figure 6.9: Variation of permeate flux and BSA rejection with dip time for membranes fabricated using 6 and 8 wt % CA solutions.**

properties it could be concluded that membrane M-6-150 (pore size 32 nm, porosity 0.02) was the best membrane for the UF as it provided higher rejection properties as well as higher flux. For the membranes prepared with 2 and 4 wt % CA concentration negligible amount of BSA rejection was observed. This is justified because the average membrane pore sizes of those membranes (487 - 417 nm for 2 wt % CA and 162 - 106 nm for 4 wt % CA) are in the MF range.

### 6.3.6 Assessment of different hydraulic resistances

Based on measured PWF for different composite membranes and ceramic support, $R_{sup}$, $R_{com}$ and $R_{BSA}$ were determined using Eq. (6.2). Fig. 6.10a presents the variation of composite $R_{com}$ with varying dipping time for various concentration of CA solution (2 - 8 wt %). The total resistance of the composite membranes involved a nonlinear increase (from $2.01\times10^{6}$ - $72.28\times10^{6}$ $m^2$.s.kPa/$m^3$) with an increase in CA concentration and dipping time. Fig. 6.10b presents the variation of $R_{coat}$ with dipping time for different CA concentrations. The graphical trends illustrate that a semi log plot of $R_{coat}$ vs. $t$ follows straight line. This further confirmed that the CA film growth over ceramic support increases exponentially with increase in dipping time. Therefore, $R_{coat}$ was expressed as:

$$R_{coat} = Me^{at} \qquad (6.9)$$

Where, $M$ and $a$ are constants evaluated from linear regression analysis. Using the condition of Eq. 6.5 ($R_{coat} = R_{int}$, when $t \to 0$), the resistance of the intermediate layer was determined as $R_{int} = M$. The calculated values of $R_{int}$ and $a$ along with $R^2$ are presented in Table 6.3. Based on the values of $R_{coat}$ and $R_{int}$, $R_{top}$ was evaluated using Eq. (6.6). Fig. 6.10c presents

the variation of $R_{top}$ with varying CA concentration and dipping time. $R_{int}$ was found to vary from $0.323\times 10^6$ to $5.09 \times 10^6$ $m^2.s.kPa/m^3$ and $R_{top}$ varied from $0.089\times10^6$ to $71.6 \times10^6$ $m^2.s.kPa/m^3$. The observed trends for both the resistances indicate a nonlinear variation with the dip coating parameters.

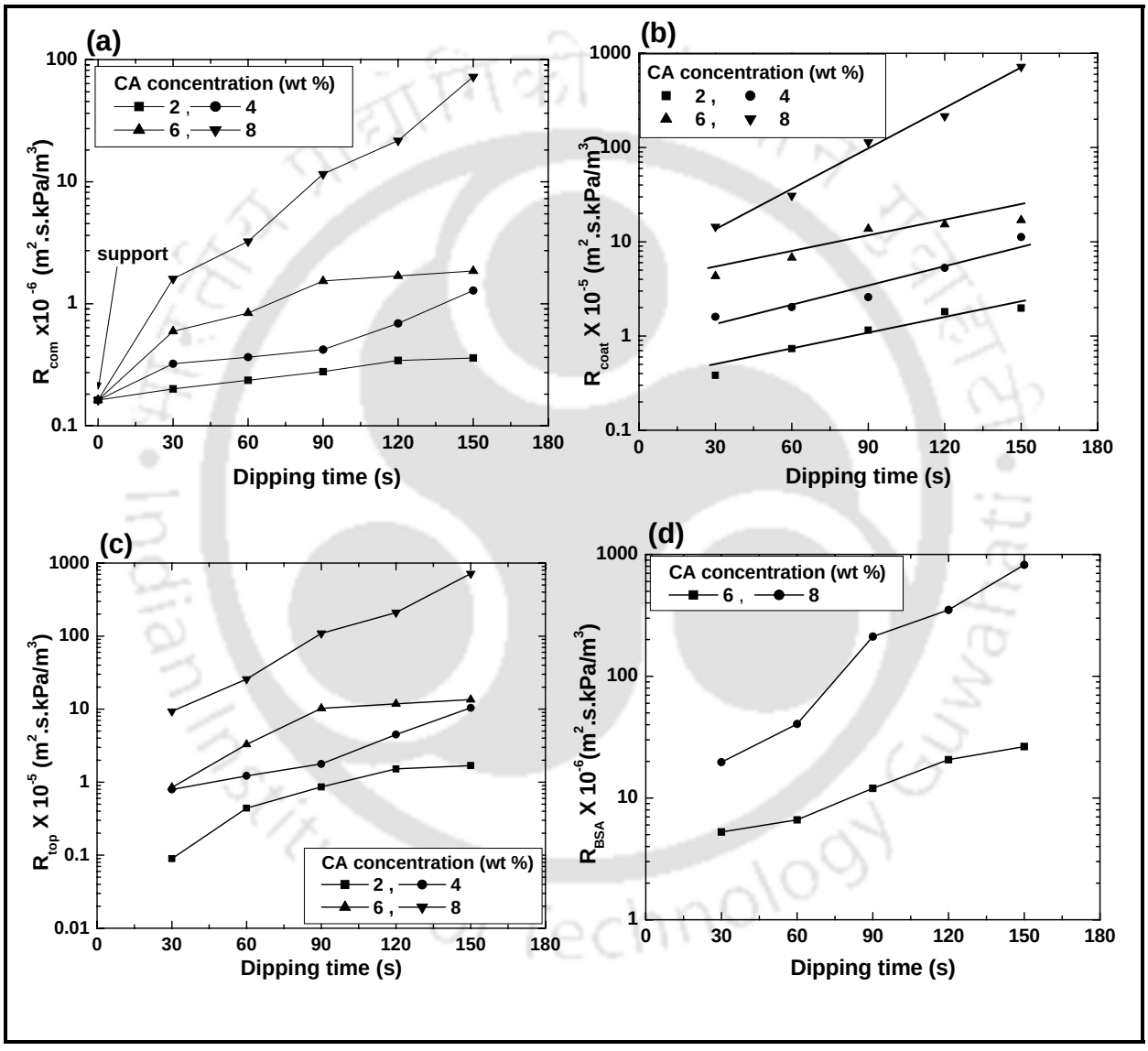


**Figure 6.10: Effect of CA concentration and dipping time on various membrane hydraulic resistances (a) total hydraulic resistance of the composite membrane, (b) coating layer hydraulic resistance, (c) top layer hydraulic resistance and (d) hydraulic resistance offered by BSA solution during UF experiments.**

**Table 6.3: Regression parameters for coating layer hydraulic resistance.**

| CA concentration (wt %) | $M \times 10^{-5}$ ($R_{int}$) ($m^2$.s.kPa/$m^3$) | $a$ ($s^{-1}$) | Correlation coefficient ($R^2$) |
|---|---|---|---|
| 2 | 0.32 | 0.014 | 0.95 |
| 4 | 0.91 | 0.0162 | 0.93 |
| 6 | 3.48 | 0.0118 | 0.89 |
| 8 | 5.09 | 0.0326 | 0.99 |

Figure 6.11 summarizes the percentage contributions of different resistances ($R_{sup}$, $R_{int}$ and $R_{top}$) for various composite membranes during water permeation experiments. It may be observed from the figure that for low CA concentration, $R_{sup}$ dominates the total resistance (varying from 81 % (M-2-30) to 45.1% (M-2-150)) and percent contribution of $R_{sup}$ to the overall hydraulic resistance decreases with increasing CA solution concentration. For highest CA concentration studied in this work (8 wt %), $R_{sup}$ was observed about 10.14 % (M-8-30) to 0.22 % (M-8-150). Similar trends were also observed for $R_{int}$. Contribution of $R_{int}$ varies from 14.6 % (M-2-30) to 8.13 % (M-2-150) for 2 wt % CA concentration and 31.7 % (M-8-30) to 0.7% (M-8-150) for 8 wt % CA concentration. However, an increase in the percent contribution of $R_{int}$ was observed at low dipping time of 30 s. This was due to an increase in CA concentration which enabled an increase in $R_{int}$ (Table 6.3) and hence its percent contribution also increased. The percent contribution of $R_{top}$ increased with increase in both concentration and dipping time. This was due to the fact that with an increase in dipping time as well as CA concentration, top layer film thickness increases and pore size decreases which resulted in the reduction of membrane permeability.

Figure 6.10d presents the resistance offered by BSA solution ($R_{BSA}$) during UF experiments (evaluated using Eq. (6.8)) for 6 and 8 wt % CA composite membranes. As shown, $R_{BSA}$ increased from 5.85× $10^6$ - 28.27 × $10^6$ $m^2$.s.kPa/$m^3$ for 6 wt % membrane and 21.27× $10^6$ - 893.56 × $10^6$ $m^2$.s.kPa/$m^3$ for 8 wt % membrane. This increase was due to the reduction in pore size of the membranes with an increase in CA concentration and dipping time. Table 6.4 presents the resistance offered by different layers of composite membrane during UF of BSA for 6 and 8 wt % CA composite membranes. It may be seen from the table that the resistance offered by the BSA solution over membrane surface ($R_{BSA}$) was significantly more in comparition to all other resistances for all the membranes.

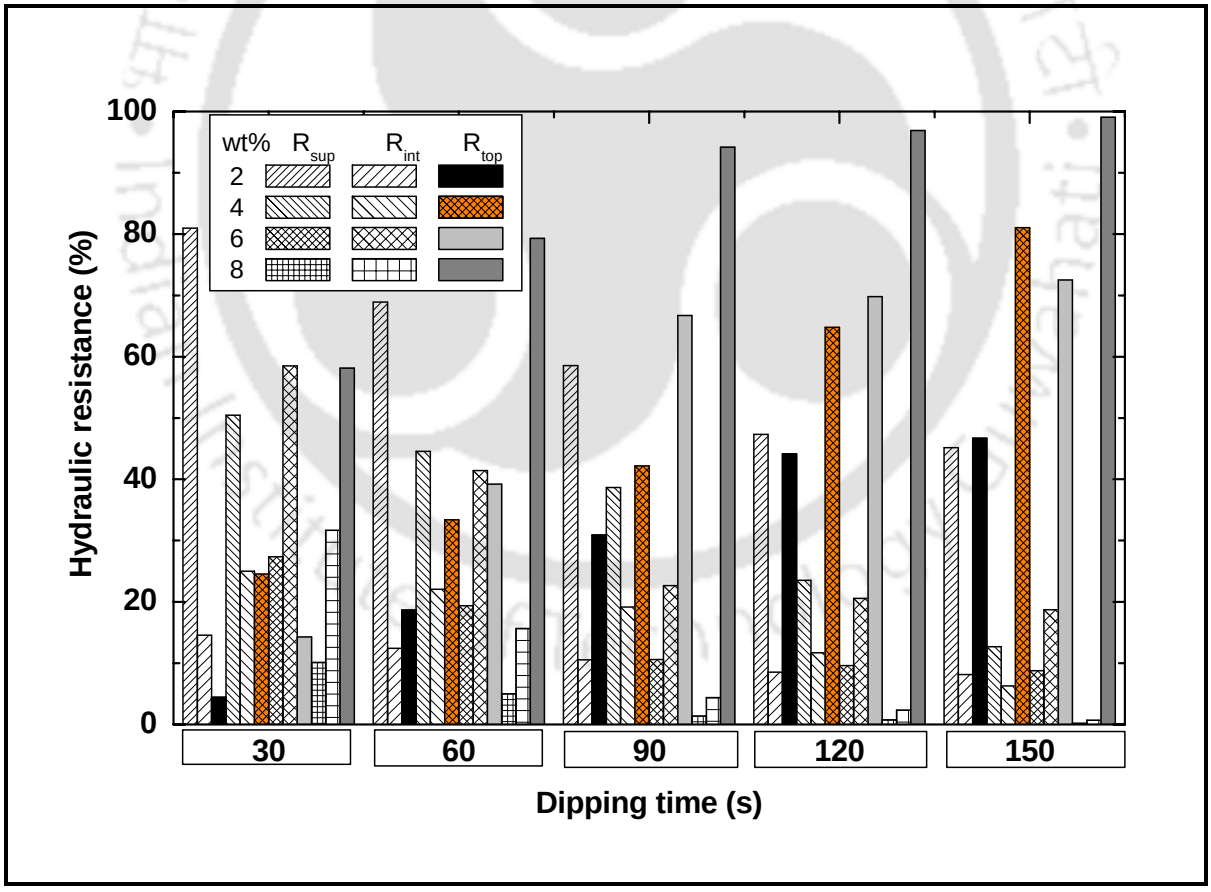


**Figure 6.11: Percent contribution of various hydraulic resistances to the total hydraulic resistance for all polymer-ceramic composite membranes.**

**Table 6.4: Percent contribution of various resistances offered by composite membranes during UF of BSA.**

| CA concentration (wt %) | Time (S) | $R_{sup}$ (%) | $R_{int}$ (%) | $R_{top}$ (%) | $R_{BSA}$ (%) | $R_{UF} \times 10^{-5}$ ($m^2$.s.kPa/$m^{3)}$ |
|---|---|---|---|---|---|---|
| 6 | 30 | 2.77 | 5.95 | 1.45 | 89.83 | 58.56 |
| | 60 | 2.19 | 4.68 | 4.43 | 88.70 | 74.46 |
| | 90 | 1.2 | 2.57 | 7.58 | 88.65 | 135.39 |
| | 120 | 0.73 | 1.56 | 5.29 | 92.42 | 223.39 |
| | 150 | 0.58 | 1.23 | 4.77 | 93.42 | 282.77 |
| 8 | 30 | 0.77 | 2.39 | 4.39 | 92.45 | 212.75 |
| | 60 | 0.37 | 1.16 | 5.88 | 92.59 | 438.02 |
| | 90 | 0.07 | 0.23 | 4.88 | 94.82 | 2233.90 |
| | 120 | 0.04 | 0.14 | 5.65 | 94.17 | 3723.17 |
| | 150 | 0.02 | 0.06 | 8.02 | 91.90 | 8935.61 |

The contributions of $R_{BSA}$ varied from 89.8 - 94.17 % of the total resistance ($R_{UF}$). These findings infer that the fabricated composite membranes do not offer significant hydraulic resistances during UF of BSA solution.

### 6.3.7 Phenomenological models for parameter dependency

This section presents the derivation of phenomenological models for the fabrication of composite membranes with dip coating method using the concept of hydraulic resistance of the polymeric film layer. The phenomenological models are conceptualized for the evaluation of parameter dependency either considering membrane properties or dip coating parameters. The primary goal behind the development of these empirical models was to provide insights into the contribution of various parameters to membrane morphology during dip coating.

### 6.3.7.1 Membrane parameters

The total hydraulic resistance of the composite membrane can be phenomenologically expressed as functions of support resistance, average pore size, effective porosity and thickness of the membrane and support as:

$$\frac{R_{com}}{R_{\sup}} = \left(\frac{d_{g,com}}{d_{g,\sup}}\right)^{bt}\left[\left(\frac{(\varepsilon/q^2)_{com}}{(\varepsilon/q^2)_{\sup}}\right)\right]^{d}\left(\frac{h_{com}}{h_{\sup}}\right)^{e} \tag{6.10}$$

The CA film thickness estimated from SEM analysis varied from 0.6 to 32 μm for a support thickness of the 4.5 mm. Therefore, the term $\left(h_{com}/h_{\sup}\right)^{e}$ tends to a value of unity ($h_{com} \approx h_{\sup}$). So, Eq. (6.10) can be expressed as

$$\frac{R_{com}}{R_{\sup}} = \left(\frac{d_{g,com}}{d_{g,\sup}}\right)^{bt}\left[\left(\frac{(\varepsilon/q^2)_{com}}{(\varepsilon/q^2)_{\sup}}\right)\right]^{d} \tag{6.11}$$

Where, $b$ and $d$ are constants that need to evaluated from regression studies. Hypothetically, the above expression can be analyzed from graphical trends presented in Figs. 6.6a, 6.6b and 6.10a. As indicated in these figures, with increasing CA concentration and dipping time, membrane hydraulic resistance increases (Fig. 6.10a) whereas the average membrane pore size decreases (Fig. 6.6a). However, the effective porosity was found to increase with increasing values of CA concentrations and decrease with increasing dipping times (Fig. 6.6b). Further, the phenomenological expression infers that when the composite membrane pore size and effective porosity approaches to that of the support, the total resistance of the membrane should approach the resistance measured for the ceramic support. Henceforth, the magnitude of parameters $b$ and $d$ quantifies the dependency of structural parameters ($d_{g,com}$, $d_{g,\sup}$, $(\varepsilon/q^2)_{com}$ and $(\varepsilon/q^2)_{\sup}$) on its transport properties. The evaluation of these

parameters was carried out with nonlinear regression technique using resistances ($R_{com}$ and $R_{\sup}$), average membrane pore sizes and effective porosity of the membrane for various CA concentrations, dipping time and support. All these parameters were obtained from liquid and gas permeation experiments.

Figure 6.12a illustrates the experimental and calculated values of $\left(R_{com}/R_{\sup}\right)$ for all four CA concentrations and dipping time used in this work. Table 6.5 summarizes the values of modeled parameters $b$ and $d$ along with the errors. From the figure it can be observed that the phenomenological empirical model equations used in this work evaluate membrane resistances with acceptable accuracy. It can be observed that, values of parameter $b$ varied from -0.0018 to -0.0143 and parameter $d$ varied from -0.0367 to -0.5467. Further, it can be observed that both parameters $b$ and $d$ depend upon the concentration of CA. Negative sign of these two parameters indicates that the ratio of pore diameter and effective porosity of the membrane and support would be $\left(\frac{d_{g,\sup}}{d_{g,com}}\right)$ and $\left(\frac{(\varepsilon/q^2)_{com}}{(\varepsilon/q^2)_{\sup}}\right)$ rather than $\left(\frac{d_{g,com}}{d_{g,\sup}}\right)$ and $\left(\frac{(\varepsilon/q^2)_{\sup}}{(\varepsilon/q^2)_{com}}\right)$ as the membrane resistance increases with a reduction in both average pore diameter and effective porosity of the membrane.

**6.3.7.2 Dip coating parameters**

As discussed in section 6.2, the resistance due to coating of the membrane was contributed by both intermediate layer and top layer resistance ($R_{coat} = R_{\text{int}} + R_{top}$). As observed from Table 6.3, $R_{\text{int}}$ was dependent only on CA concentration ($c$), where as $R_{top}$ was dependent on both

CA concentration ($c$) and dipping time ($t$) (Fig. 11b). Hence, $R_{top}$ should be regarded as a function of $c$ and $t$ together. With this hypothesis, Eq. (6.9) was further modified to yield a phenomenological expression to evaluate the resistance dependency of dip coating parameters:

$$R_{coat} = Nc^{f} e^{gct} \qquad (6.12)$$

The parameters, $N$, $f$ and $g$ needs to be evaluated by nonlinear regression analysis using calculated values of $R_{coat}$ for various values of $c$ and $t$. The magnitude of parameters $f$ and $g$ infer the dependency of $R_{coat}$ on both $c$ and $t$. Further, it can be noted here that the expression $Nc^{f}$ refers to $R_i$. Calculated values of the regressed parameters $N, f, g$ in Eq. (6.12) were shown in Table 6.6. The obtained values of $N$, $f$ and $g$ indicate that dip coating process was more critically influenced by solution concentrations rather than dipping time.

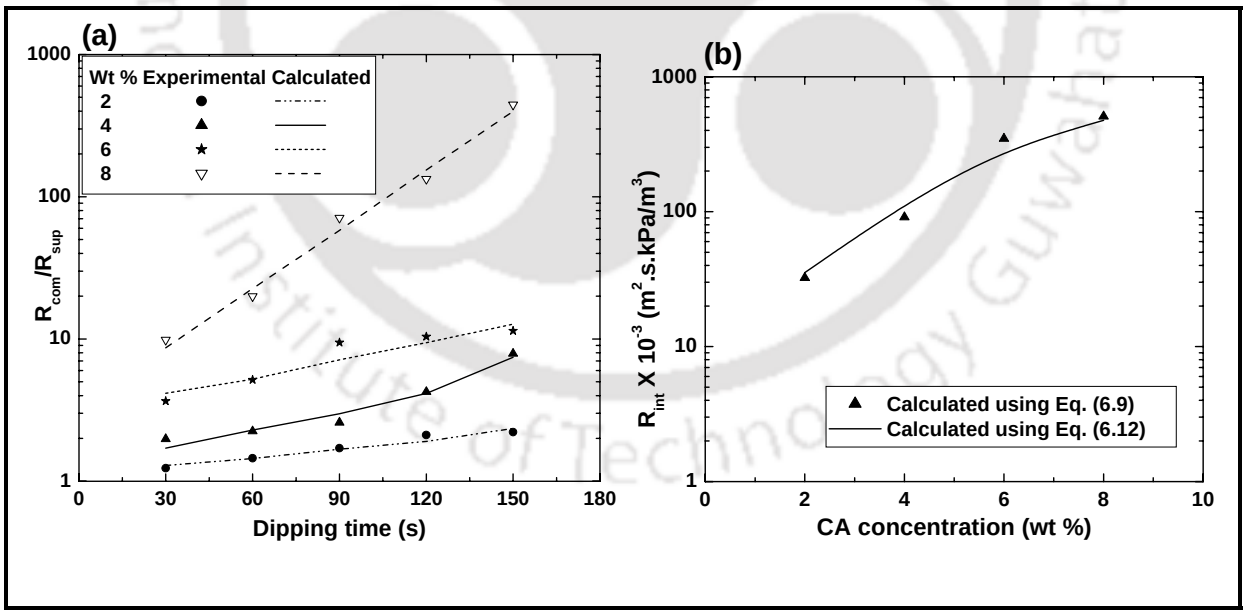


**Figure 6.12: Experimental and calculated values of (a) $\left(R_{com}/R_{\sup}\right)$ at various CA wt % concentrations and dipping times and (b) intermediate layer resistance using Eqs. (6.9) and (6.12).**

**Table 6.5: Regressed phenomenological model parameters of Eq (6.11).**

| CA concentration (wt %) | Parameter | | Error (%) | | | |
|---|---|---|---|---|---|---|
| | b | d | Maximum | Minimum | Average | RMS |
| 2 | -0.0143 | -0.0367 | 5.35 | 1.03 | 3.27 | 3.81 |
| 4 | -0.0072 | -0.0747 | 5.24 | 0.49 | 2.6 | 3.01 |
| 6 | -0.0018 | -0.6059 | 5.36 | 2.24 | 4.17 | 4.3 |
| 8 | -0.0090 | -0.5467 | 11.81 | 7.68 | 10.12 | 10.22 |

**Table 6.6: Regressed phenomenological model parameters of Eq (6.12).**

| Parameter | Value | Error (%) | | | |
|---|---|---|---|---|---|
| | | Maximum | Minimum | Average | RMS |
| N | 13061.21 | | | | |
| F | 1.7289 | 15.62 | 4.95 | 11.62 | 12.86 |
| g | 0.0024 | | | | |

Based on the regression analysis, calculated values of $R_i$ obtained from Eq. (6.9) and Eq. (6.12) were compared and shown in Fig. 6.12b. From the figure it can be observed that the phenomenological empirical model Eq. (6.12) evaluated intermediate layer resistance of the membrane with acceptable accuracy. The intermediate layer resistance was found to vary from $0.32 \times 10^5$ to $5.09 \times 10^5$ $m^2.s.kPa/m^3$ from Eq. (6.9) and $0.35 \times 10^5$ to $4.75 \times 10^5$ from Eq. (6.12), which were in the same range. The values of parameter $gc$ obtained from Eq. (6.12) (which varied from 0.0049 to 0.019) are also in same order with those obtained from Eq. (6.9) (which varied from 0.011 to 0.032).

**6.3.7.3 Error analysis**

To quantify the confidence levels of evaluated parameters, an error analysis was conducted for all regressed parameters ($b, d, N, f, g$). Table 6.5 and 6.6 presents results obtained from error analysis. As presented, the maximum and minimum error for parameter $b$ and $d$ (Eq. (6.11) were 11.81 % (M-8-120) and 0.49 % (M-4-60). The average error varied from 2.6 % (4 wt % CA) to 10.12 % (8 wt % CA). The RMS error calculated for Eq. (6.11) varied from 3.01 % to 10.22 %. Similar types of errors were also calculated for Eq. (6.12) where maximum and minimum error was 15.62 % and 4.96 %. The average and RMS error was 11.62 % and 12.85 % respectively, which confirms the validity of the proposed phenomenological models in the present study.

# Chapter 7:

# Conclusions and Scope of Future Work

# Conclusions and Scope of Future Work

*This chapter summarizes the inferences drawn from various works presented in this thesis. Also, some suggestions towards the scope for future research are outlined.*

## 7.1 Conclusions

This work dealt with the preparation, characterization and applications of inexpensive ceramic membranes as well as polymer-ceramic composite membranes. Two new inexpensive inorganic formulations constituting larger contents of inexpensive materials (85 % for composition A and 70 % for composition B) were identified to prepare defect free upper submicron range (0.5 - 1 μm) and lower submicron range (0.1 - 0.5 μm) ceramic membranes. Morphological characterization studies including SEM, TGA-DTA, XRD, gas and liquid permeation studies, porosity and structural density determination and finally corrosion resistance have indicated that the prepared membranes possessed desired properties for MF applications. The prepared ceramic membranes were used for the treatment of oily wastewater and mosambi juice clarification. The prepared ceramic membranes provide higher membrane fluxes, adequate product quality and lower fouling. The effective permeable area factor proved to provide good insights in due course of the analysis. Apart from this, cellulose acetate - ceramic composite membranes were prepared using a low cost kaolin based ceramic membrane support using dip coating technique. Composite membranes with variant morphology and transport properties were prepared by altering the dip coating parameters namely CA concentration in acetone and dipping time. Morphological study by SEM analysis, permeation characterization by both air and water were carried out to evaluate the general

characteristics of the membranes. Separation performance of membranes was verified by UF experiments using BSA solution. Phenomenological models were developed to evaluate the parameter dependency of membrane morphology as well as dip coating parameters on the hydraulic resistance of membranes. Valuable insights were gained from these model parameters which can be used for commercial polymer - ceramic composite membrane fabrication. The major conclusions obtained from this study are summarized below.

***Preparation and characterization of ceramic membranes***

1. Two new inorganic formulations were identified for the preparation of submicron range ceramic membranes. Inorganic precursor formulations in this work inferred that a defect free ceramic membrane can be fabricated with higher content of low cost materials and lower content of expensive precursors (only 15 % in composition A membranes and 30 % in composition B membranes).
2. TGA and XRD study inferred that the minimum sintering temperature for the chosen composition of materials was around 850 $^{o}$C for composition A and 800 $^{o}$C for composition B. These sintering temperature were well below the usual sintering temperature of 1100 - 1500 $^{o}$C , reported in various literatures.
3. SEM analysis inferred that the observable maximum pore size of the membranes was 5 μm for composition A membranes and 2 μm for composition B membranes. With increasing sintering temperature the average pore size of the membrane increased with a reduction in porosity. The average pore sizes of the membranes varied from 0.547 - 0.810 μm and 0.185 - 0.332 μm for composition A and composition B, respectively within the range of sintering temperatures considered in the present work.

4. The total porosity of membranes varied from 42 - 33 %, and 34.4 - 19.5 % for composition A membranes and composition B membranes, respectively. Corresponding variation in structural densities were 1260 - 1360 kg/$m^3$ and 1280 - 1540 kg/$m^3$.
5. Hydraulic permeability of the membranes varied from $19.44\times10^{-10}$ - $61.36\times10^{-10}$ $m^3/m^2$.s.Pa and $1.51\times10^{-10}$ - $6.33\times10^{-10}$ $m^3/m^2$.s.Pa for composition A membranes and composition B membranes, respectively within the various sintering temperatures ranges studied in this work.
6. Both hydraulic pore diameter and permeability of the membranes increased with an increase in sintering temperature.
7. Pore size distribution obtained from SEM image analysis was in good agreement with experimental results obtained from gas permeation analysis.
8. Chemical stability for membranes prepared using both the compositions were acceptable for real time applications (< 8% weight loss in both acid and base media).
9. Based on retail price of raw materials in laboratory scale, the cost of the membranes was estimated as 130 \$/$m^2$ (composition A) and 220 \$/$m^2$ (composition B). These prices were similar to the module cost of polymeric membrane (200 \$/$m^2$).

***Treatment of oily wastewater using prepared ceramic membrane***

1. A1 membrane exhibited 93.81 - 98.51 % oil rejection efficiency with a permeate flux of $10.54\times10^{-6}$ - $22.1\times10^{-6}$ $m^3/m^2$.s at various trans-membrane pressure drops ranging from 41.37 - 206.8 kPa after 30 minute of experimental run.
2. B3 membrane provided 98.8 % oil rejection and $7.46\times10^{-6}$ $m^3/m^2$.s permeate flux after 30 minutes of experimental run at 68.95 kPa trans-membrane pressure and 250 mg/L oil concentration.

3. For both membranes, permeate flux increased with an increase in operating pressure and reduced with an increase in initial oil concentration. On the other hand, oil rejection efficiency of the membrane increased with an increase in oil concentration and decreased with operating pressure.
4. For both membranes, experimental investigations confirmed that the prepared membrane can be used for the treatment of o/w emulsions to yield permeate streams with less than 5 mg/L oil concentration.
5. The decline in permeate flux were analyzed using various membrane pore blocking models. Analysis inferred that, for A1 membrane, permeate flux decline was initially (first 5 to 10 minutes depending on oil concentration) due to intermediate pore blocking and later due to formation of thin oily layer over the membrane surface (cake filtration). On the other hand, for B3 membrane, reduction in permeate flux was due to formation of thin oily layer over the membrane surface.
6. A comparative analysis among A1 and B3 membrane concluded that A1 membrane can be used to obtain higher permeate flux with slightly lower product quality than B3 membrane. Therefore, A1 membrane would be beneficial for industrial processing. If required, membrane B3 could be used to produce highest permeate quality.

***Microfiltration of mosambi juice using prepared ceramic membranes***

1. Pretreatment of juice primarily affects the colour, clarity, viscosity, AIS values. However, valuable parameters of the juice such as TSS (a measure of sugar content), acidity, pH and density do not get altered significantly.
2. During MF of mosambi juice, valuable properties of the juice (TSS, pH, acidity and density) did not vary significantly. However, significant reduction in colour, viscosity,

AIS and enhancement in clarity were observed due to the removal of pectic materials and they varied with $d_l$ and $\varepsilon_m$. For B3 membrane at $\Delta P$ of 137.90 kPa, clarity increased from 53.73 - 93.39 % for CJ and 67.87 - 98.98 % for ETCJ.

3. For composition A membranes (A1, A2, A3 and A4), permeate fluxes were observed to varied from 5.78 $\times 10^{-6}$ - 13.45 $\times 10^{-6}$ $m^3/m^2.s$ for CJ and 14.07 $\times 10^{-6}$ - 60.64$\times 10^{-6}$ $m^3/m^2.s$ for ETCJ at 82.7 kPa ($\Delta P$) with varying $\varepsilon_m d_l^{\,2}$ from 0.249 - 0.783 $\mu m^2$.
4. For B3 membrane, permeate flux decreased from 12.67$\times 10^{-6}$ - 5.94 $\times 10^{-6}$ $m^3/m^2.s$ for CJ and from 58.49$\times 10^{-6}$ - 22.62 $\times 10^{-6}$ $m^3/m^2.s$ for ETCJ at the end of 40 minutes of experimental run at $\Delta P$ of 137.90 kPa. This reduction in permeate flux was due to gel layer formation over the membrane surface.
5. Other phenomenological models were also studied for composition A membranes, to illustrate the dependency of total hydraulic resistance of membrane on $\varepsilon_m d_l^{\,2}$, $\Delta P$ and time ($t$). Based on experimental and theoretical investigations, membranes with $\varepsilon_m d_l^{\,2}$ of 0.443 $\mu m^2$ for CJ and 0.294 $\mu m^2$ for ETCJ and a $\Delta P$ value of 82.7 kPa were recommended for MF of mosambi juice.
6. The variation of cake filtration model constant ($k_c$) with ΔP was studied and modeled accordingly.
7. The long term storage study of the juice indicated that the membrane clarified juice can be stored in refrigerated condition for more than 30 days without significant change in juice quality.

8. The analysis of instantaneous initial fouling resistance ($R_f^0$) yielded significant insights to infer that $R_f^0$ contributed significantly to overall hydraulic resistance for CJ in contrast to ETCJ.
9. A comparative analysis among A1 and B3 membrane inferred that A1 membrane can be used to obtain higher permeate flux with slightly lower juice quality than B3 membrane. Therefore, A1 membrane would be beneficial for industrial processing. On the other hand, membrane B3 could be used to obtain best quality permeate juice.

***Preparation of cellulose acetate - ceramic composite membranes***

1. Ceramic composite membrane was found to be formed by blockage of ceramic support matrix (formation of intermediate layer) followed by deposition of CA over the intermediate layer (formation of top layer) during dip coating.
2. The average pore size of the membrane varied 487 - 417, 162 - 106, 62 - 32 and 46 - 25 nm for 2, 4, 6 and 8 wt % CA concentration solutions respectively with varying dipping time from 30 - 150 s.
3. Analysis inferred that the composite membrane prepared with 2 wt % and 4 wt % CA were suitable for MF applications and those with 6 wt % and 8 wt % were for UF applications.
4. During compaction study of membranes, PWF was initially high and declined gradually to reach a steady state value after 3 to 4 hrs for all prepared composite membranes.
5. The intermediate layer hydraulic resistance was evaluated to be nonlinearly dependent on the CA concentration only whereas the top layer resistance was found to be dependent on both dip coating parameters (CA concentration and dipping time).

6. The CA film growth rate was found to follow exponential trend with dip coating parameters.
7. Prepared membranes were used to separate BSA solution at 345 kPa pressure differential in batch mode of operation. Percent BSA rejection varied from 5 - 42.5 % for 6 wt % CA membranes and 20 - 50 % for 8 wt % CA membranes.
8. A resistance in series model was proposed to determine various resistances offered during UF of BSA solution. The analysis inferred that the fabricated composite membrane is useful for the industrial application since only 6 to 11 % of the total resistance was offered by these composite membranes during UF of BSA solution.
9. Phenomenological models were developed to evaluate the parameter dependency of membrane morphology as well as dip coating parameter on the hydraulic resistance of membranes.

## 7.2 Recommendations for future work

Research findings in this work provided a good number of insights with respect to fabrication and applications of comparatively low cost ceramic and polymer ceramic composite membranes. Few research areas for future work are presented as follows:

***Preparation of low cost inorganic membranes***

1. Preparation and characterization of bi-layered asymmetric membranes using simultaneous casting method. The membrane shall possess a top ceramic layer with narrow pore size distribution on a support with wider pore size distribution.
2. Preparation of environment responsive membranes using the prepared membranes.

3. To explore the effect of the variation in the selection and composition of inorganic pore forming agents ($CaCO_3$ and $Na_2CO_3$) on membrane morphological properties for both composition A and composition B membranes.
4. Studies upon the role of organic pore forming agents (such as poly ethylene glycol, poly vinyl alcohol) in influencing membrane morphology.
5. Preparation of UF symmetric ceramic membranes using low cost precursors.

***Microfiltration applications of low cost ceramic membranes***

1. Experimental investigations using cross-flow mode of operations for the MF of o/w emulsions as well as mosambi juice.
2. Microfiltration studies of industrial oily wastewaters.
3. Microfiltration studies for other types of juices such as orange, watermelon, pine apple, orange and sugarcane juices.
4. To study the influence of operating temperature upon the permeation characteristics of the membrane during oily wastewater treatment and mosambi juice clarification.
5. Pilot plant study for both the oily wastewater treatment and mosambi juice clarification using the prepared membranes.

***Polymer - ceramic composite membrane***

1. To study the influence of polymer type (hydrophobic / hydrophilic), solvent type and support morphology on the optimality of dip coating parameters.
2. To explore the role of pore forming agents (organic / inorganic) during dip coating.
3. To investigate the real time application for polymer-ceramic composite membrane.

# References

# *References*


1. H. P. Hsieh, Inorganic membranes for separation and reaction, Elsevier, Amsterdam, 1996.
2. M. Cheryan, Ultrafiltration and Microfiltration Handbook, Technomic Publishing Co. Inc. Lancaster, Pennsylvania, (1998).
3. M. Mulder, Basic Principles of Membrane Technology, Kluwer Academic Publishers, Dordrecht, (1991).
4. S. P. Nunes, K.V. Peinemann (Eds), Membrane Technology in the Chemical Industry, Wiley-VCH Verlag GmbH., (2001).
5. M. C. Porter, Handbook of industrial membrane technology, Noyes Publications, Westwood, New Jersey, U.S.A. (1989).
6. R. W. Baker, Membrane Technology and Applications, John Wiley & Sons Ltd, West Sussex, England, (2004).
7. S. Judd, B. Jefferson, Membranes for Industrial Wastewater Recovery and Re-use, Elsevier, Oxford OX5 lGB, UK, (2003).
8. R. S. Faibish, Y. Cohen, Fouling resistant ceramic supported polymer membranes for ultrafiltration of oil-in-water microemulsions, J. Membr. Sci., 185 (2001) 129 - 143.
9. Y. Matsumoto, M. Sudoh, Y. Suzuki, Preparation of composite UF membranes of sulfonated polysulfone coated on ceramics, J. Membr. Sci., 158 (1999) 55 - 62.
10. S. Sachdeva, A. Kumar, Synthesis and modeling of composite poly (styrene-co-acrylonitrile) membrane for the separation of chromic acid, J. Membr. Sci., 307 (2008) 37 - 52.

11. W. Yoshida, Y. Cohen, Ceramic-supported polymer membranes for pervaporation of binary organic/organic mixtures, J. Membr. Sci., 213 (2003) 145 - 157.

12. K. M. Song, W. H. Hong, Dehydration of ethanol and isopropanol using tubular type cellulose acetate membrane with ceramic support in pervaporation process, J. Membr. Sci., 123 (1997) 27 - 33.

13. X. Cao, T. Zhang, Q. T. Nguyen, Y. Zhang, Z. Ping, A novel hydrophilic polymer-ceramic composite membrane 1 Acrylic acid grafting membrane, J. Membr. Sci., 312 (2008) 15 - 22.

14. Y. Chen, F. Xiangli, W. Jin, N. Xu, Organic–inorganic composite pervaporation membranes prepared by self-assembly of polyelectrolyte multilayers on macroporous ceramic supports, J. Membr. Sci., 302 (2007) 78 - 86.

15. Y. Ki Hong, W. H. Hong, Influence of ceramic support on pervaporation characteristics of IPA/water mixtures using PDMS/ceramic composite membrane, J. Membr. Sci., 159 (1999) 29 - 39.

16. F. Xiangli, W. Wei, Y. Chen, W. Jin, N. Xu, Optimization of preparation conditions for polydimethylsiloxane (PDMS)/ceramic composite pervaporation membranes using response surface methodology, J. Membr. Sci., 311 (2008) 23 - 33.

17. H. Yanagishita, D. Kitamoto, K. Haraya, T. Nakane, T. Tsuchiya, N. Koura, Preparation and pervaporation performance of polyimide composite membrane by vapor deposition and polymerization (VDP), J. Membr. Sci., 136 (1997) 121 - 126.

18. Y. Yoshino, T. Suzuki, B. N. Nair, H. Taguchi, N. Itoh, Development of tubular substrates, silica based membranes and membrane modules for hydrogen separation at high temperature, J. Membr. Sci., 267 (2005) 8 - 17.

19. K. A. DeFriend, M. R. Wiesner,A. R. Barron, Alumina and aluminate ultra-filtration membranes derived from alumina nanoparticles, J. Membr. Sci., 224 (2003) 11 - 28.

20. J.M. Benito, A. Conesa, F. Rubio, M.A. Rodriguez, Preparation and characterization of tubular ceramic membranes for treatment of oil emulsions, J. Euro. Cer. Soci., 25 (2005) 1895 - 1903.

21. T. V. Gestel, C. Vandecasteele, A. Buekenhoudt, C. Dotremont, J. Luyten, R. Leysen, B. V. Bruggen, G. Maesc, Alumina and titania multilayer membranes for nanofiltration: preparation, characterization and chemical stability. J. Membr. Sci., 207 (2002) 73 - 89.

22. Y. H. Wang, T. F. Tian, X. Q.Liu, G. Y. Meng, Titania membrane preparation with chemical stability for very hash environments applications, J. Membr. Sci., 280 (2006) 261 - 269.

23. T. Tsuru, Inorganic porous membranes for liquid phase separation, Sep. Purif. Meth., 30 (2001) 191 -220.

24. C. Falamaki, M. Shafiee Afarani, A. Aghaie, Initial sintering stage pore growth mechanism applied to the manufacture of ceramic membrane supports, J. Europ. Cer. Soci., 24 (2004) 2285 - 2292.

25. S. Masmoudia, A. Larbot, H. El Feki, R. B. Amara, Elaboration and characterisation of apatite based mineral supports for microfiltration and ultrafiltration membranes, Cer. Inter., 33 (2007) 337-344.

26. N. Saffaj, S. Alami Younssi, A. Albizane, A. Messouadi, M. Bouhria, M. Persin, M. Cretin, A. Larbot, Elaboration and properties of $TiO_2$–$ZnAl_2O_4$ ultrafiltration membranes deposited on cordierite support, Sep. Purif. Technol., 36 (2004) 107 - 114.

27. I. Jedidi, S. Khemakhem, A. Larbot, R. B. Amar, Elaboration and characterization of fly ash based mineral supports for microfiltration and ultrafiltration membranes, Cer. Inter., 35 (2009) 2747 - 2753.

28. Y. Dong, X. Liu, Q. Ma, G. Meng, Preparation of cordierite-based porous ceramic micro-filtration membranes using waste fly ash as the main raw materials, J. Membr. Sci., 285 (2006) 173 - 181.

29. N. Saffaj, M. Persin, S. A. Younsi, A. Albizane , M. Cretin , A. Larbot, Elaboration and characterization of micro-filtration and ultra-filtration membranes deposited on raw support prepared from natural Moroccan clay: Application to filtration of solution containing dyes and salts, Appl. Clay Sci., 31 (2006) 110 - 119.

30. S. Khemakhem, A. Larbot, R. B. Amar, New ceramic microfiltration membranes from Tunisian natural materials: Application for the cuttlefish effluents treatment, Cer. Inter., 35 (2009) 55 - 61.

31. F. Bouzerara, A. Harabi, S. Achour, A. Larbot, Porous ceramic supports for membranes prepared from kaolin and doloma mixtures, J. Eur. Ceram. Soc., 26 (2006) 1663 - 1671.

32. A. Belouatek, N. Benderdouche, A. Addou, A. Ouagued, N. Bettahar, Preparation of inorganic supports for liquid waste treatment, Micropor. and Mesopor. Mater., 85 (2005) 163 - 168.

33. G. Chen, H. Q. W. Xing, N. Xu, Direct preparation of macroporous mullite supports for membranes by in situ reaction sintering, J. Membr. Sci., 318 (2008) 38 - 44.

34. B. K. Nandi, R. Uppaluri, M. K. Purkait, Preparation and characterization of low cost ceramic membranes for microfiltration applications, Appl. Clay Sci., 42 (2008) 102 - 110.

35. B. K. Nandi, B. Das, R. Uppaluri, M. K. Purkait, Preparation and characterization of inexpensive submicron range inorganic microfiltration membranes, Sep. Purif. Technol., (manuscript under review, 2009).

36. M. Kazemimoghadam, T. Mohammadi, Preparation of NaA zeolite membranes for separation of water/UDMH mixtures, Sep. Purif. Technol., 47 (2006) 173 - 178.

37. A. Huang, W. Yang, Enhancement of NaA zeolite membrane properties through organic cation addition, Sep. Purif. Technol., 61 (2008) 175 - 181.

38. A. Alem, H. Sarpoolaky, M. Keshmiri, Titania ultrafiltration membrane: Preparation, characterization and photocatalytic activity, J. Euro. Cer. Soci., 29 (2009) 629–635.

39. R. Das, B. K. Dutta, Permeation and Separation Characteristics of Supported Alumina and Titania Membranes, Sep. Sci. Technol., 34 (1999) 609 - 625.

40. A. Alem, H. Sarpoolaky, M. Keshmiri, Sol–gel preparation of titania multilayer membrane for photocatalytic applications, Cer. Inter., 35(2009) 1837 - 1843.

41. P. Aranda, W.J. Chen, C. R. Martin, Water transport across polystyrenesulfonate/ alumina composite membranes, J. Membr. Sci., 99 (1995) 185 - 195.

42. M. E. Rezac, W. J. Koros, Preparation of polymer-ceramic composite membranes with ultrathin defect-free separating layers, J. Appl. Polym. Sci., 46 (1992) 1927 - 1938.

43. Y. Gu, G. Meng, A Model for Ceramic Membrane Formation by Dip-coating, J. Eur. Cer. Soci., 19 (1999) 1961 - 1966.

44. A. A. Babaluo, M. Kokabi, M. Manteghian, R. Sarraf-Mamoory, A modified model for alumina membranes formed by gel-casting followed by dip-coating, J. Eur. Cer. Soci., 24 (2004) 3779 - 3787.

45. E. Lev¨anen, T. M¨antyl¨, P. Mikkola, J. B. Rosenholm, Layer Buildup on Two-Layered Porous Substrate by Dip-Coating: Modeling and Effect of Additives on Growth Rate, J. Coll. and Inter. Sci. 230 (2000) 186 - 184.

46. B. Chakrabarty, A. K. Ghoshal, M. K. Purkait, Ultrafiltration of stable oil-in-water emulsion by polysulfone membrane, J. Membr. Sci., 325 (2008) 427 - 437.

47. C. Ratlege, Mini review compilation biodegradation and biotransformations of oils and fats, J. Chem. Tech. Biotechnol., 55 (1992) 397 - 414.

48. A. Y. Hosny, Separating oil from oil-water emulsions by electroflotation technique, Sep. Technol., 6 (1996) 9 - 17.

49. A. E. Kayar, M. Hussein, A.A. Zatout, A.Y. Hosny, A. A. Amer, Removal of oil from stable oil-water emulsion by induced air floatation technique, Sep. Technol., 3 (1993) 25 - 31.

50. J. M. Benito, G. Rios, E. Ortea, E. Fernhdez, A. Cambiella, C. Pazos, J. Coca, Design and construction of a modular pilot plant for the treatment of oil-containing waste waters, Desalination, 147 (2002) 5 - 10.

51. D. Abdessemed, G. Nezzal, R. B. Aim, Coagulation-adsorption-ultrafiltration for wastewater treatment and reuse, Desalination, 131 (2000) 307 - 314.

52. M. Cheryan, N. Rajagopalan, Membrane processing of oily streams. Wastewater treatment and waste reduction, J. Membr. Sci., 151 (1998)13 - 28.

53. S. H. Lin, W.J. Lan, Waste oil/water emulsion treatment by membrane processes, J. Hazard. Mater., 59 (1998) 189 - 199.

54. A. Rezvanpoura, R. Roostaazada, M. Hesampour, M. Nystr¨om, C. Ghotbi, Effective factors in the treatment of kerosene–water emulsion by using UF membranes, J. Hazard. Mater., 161 (2009) 1216 - 1224.

55. J. Mueller, Y. Cen, R. H. Davis, Crossflow microfiltration of oily water, J. Membr. Sci., 129 (1997) 221 - 235.

56. P. Wang, N. Xu, J. Shi, A pilot study of the treatment of waste rolling emulsion using zirconia microfiltration membranes, J. Membr. Sci., 173 (2000) 159 - 166.

57. J. Zhong, X. Sun, C. Wang, Treatment of oily wastewater produced from refinery processes using flocculation and ceramic membrane filtration, Sep. Purf. Technol., 32 (2003) 93 - 98.

58. A. Lobo, A. Cambiella, J. M.Benito, C. Pazos, J. Coca, Ultrafiltration of oil-in-water emulsions with ceramic membranes: Influence of pH and crossflow velocity, J. Membr. Sci., 278 (2006) 328 - 334.

59. S. H. Hyun, G.T. Kim, Synthesis of ceramic microfiltration membranes for oil/water separation, Sep. Sci. Technol. 32 (1997) 2927 - 2943.

60. M. A. Rao, A. A. Vitali, Fruit Juice Concentration and Preservation, Handbook of Food Preservation, New York, (1999).

61. J. G. Brennan, Food Processing Handbook, Willy-VCH Verlag GmbH & Co. KGaA, (2006).

62. B. Sarkar, S. DasGupta, S. De, Cross-flow electro-ultrafiltration of mosambi (Citrus sinensis (L.) Osbeck) juice, J. Food Eng., 89 (2008) 241 - 245.

63. P. Rai, G. C. Majumdar, G. Sharma, S. Dass Gupta, S. De, Effect of various cutoff membranes on permeate flux and quality during filtration of mosambi (citrus sinensis (l.) Osbeck) juice, Food Bio. Pro., 84 (2006) 213 - 219.

64. D. F. Jesus, M. F. Leite, L. F. M. Silva, R. D. Modesta, V. M. Matta, L. M. C. Cabral, Orange (Citrus sinensis) juice concentration by reverse osmosis, J. Food Eng., 81 (2007) 287 - 291.

65. D.G. Lister, G. Maschio, I. Becchi, The Use of Membrane Processes in the Clarification of Orange and Lemon Juices, J. Food Eng., 21 (1994) 473 - 483.

66. L. Espamer, C. Pagliero, A. Ochoa, J. Marchese, Clarification of lemon juice using membrane process, Desalination 200 (2006) 565 – 567.

67. A. F. G. Bailey, A. M. Barbe, P.A. Hogan, R. A. Johnson, J. Sheng, The effect of ultrafiltration on the subsequent concentration of grape juice by osmotic distillation, J. Membr. Sci., 164 (2000) 195 - 204.

68. K. S Youn, J. H. Hong, D. H Bae, S. J. Kim, S. D. Kim, Effective clarifying process of reconstituted apple juice using membrane filtration with filter-aid pretreatment, J. Membr. Sci., 228 (2004) 179 - 186.

69. J. Yu, R.W. Lencki, Effect of enzyme treatments on the fouling behavior of apple juice during microfiltration, J. Food Eng., 63 (2004) 413 - 423.

70. G. T. Vladisavljevic, P. Vukosavljevic, B. Bukvic, Permeate flux and fouling resistance in ultrafiltration of depectic materialinized apple juice using ceramic membranes, J. Food Eng., 60 (2003) 241 - 247.

71. A. Cassano, E. Drioli, G. Galaverna, R. Marchelli, G. Di Silvestro, P. Cagnasso, Clarification and concentration of citrus and carrot juices by integrated membrane processes, J. Food Eng., 57 (2003) 153 - 163.

72. C. Chhaya, P. Rai, G.C. Majumdar, S. Dasgupta, S. De, Clarification of watermelon (citrullus lanatus) juice by microfiltration, J. Food Pro. Eng., 31 (2008) 768 - 782.

73. F. Vaillant, M. Cisse, M. Chaverri, A. Perez, M. Dornier, F. Viquez, C. D. Mayer, Clarification and concentration of melon juice using membrane processes, Inno. Food Sci. Emerg. Technol., 6 (2005) 213 - 220.

74. A. Cassano, M. Marchio, E. Drioli, Clarification of blood orange juice by ultrafiltration: analyses of operating parameters, membrane fouling and juice quality, Desalination, 212 (2007) 15 - 27.

75. L. M. J. Carvalho, I. M. Castro, C. A. B. Silva, A study of retention of sugars in the process of clarification of pineapple juice (Ananas comosus, L. Merril) by micro- and ultra-filtration, J. Food Eng., 87 (2008) 447 - 454.

76. P. Rai, G. C. Majumdar, S. DasGupta, S. De, Optimizing pectinase usage in pretreatment of mosambi juice for clarification by response surface methodology, J. Food Eng., 64 (2004) 397 - 403.

77. V. Jegatheesan, D. D. Phong, L. Shu, R. B. Aim, Performance of ceramic micro- and ultrafiltration membranes treating limed and partially clarified sugar cane juice, J. Membr. Sci., 327 (2009) 69 - 77.

78. S. T. D. Barros, C. M. G. Andrade, E. S. Mendes, L. Peres, Study of fouling mechanism in pineapple juice clarification by ultrafiltration, J. Membr. Sci., 215 (2003) 213 - 224.

79. J. S. Reed, Principles of Ceramics Processing, John Wiley & Sons, NewYork, (1995).

80. A. Potdar, A. sukla, A. Kumar, Effect of gas phase modification of analcime zeolite composite membrane on separation of surfactant by ultra-filtration, J. Membr. Sci., 210 (2002) 209 - 225.

81. B. Chakrabarty, A. K. Ghoshal, M. K. Purkait, SEM Analysis and Gas Permeability Test to Characterize Polysulfone Membrane Prepared with Polyethylene Glycol as Additive. J. Colloid Interf. Sci., 320 (2008) 245 - 253.

82. J. Marchese, C. L. Pagliero, Characterization of asymmetric polysulphone membranes for gas separation, Gas Sep. & Purif. 5 (1991) 215 - 221.

83. JCPDS (Joint Committee for Powder Diffraction Studies), Powder Diffraction File of Inorganic Phases, International Center for Diffraction Data, Swarthmore, PA, USA, (1997).

84. V. Balek, M. Murat, The emanation thermal analysis of kaolinite clay minerals. Thermochim. Acta., 282 - 283 (1996) 385 - 397.

85. Y. F. Chena, M. C. Wang, M. H. Hon, Phase transformation and growth of mullite in kaolin ceramics, J. Afri. Earth Sci., 46 (2006) 245 - 252.

86. M. C. Wang, N. C. Wu, M. H. Hon, Preparation of nepheline glass-ceramics dental porcelain, Materials Chemistry and Physics, 37 (1994) 370 - 375.

87. S. Tennison, Current hurdles in the commercial development of inorganic membrane reactors, Membrane Technology, 2000 (2000) 4 - 9.

88. V. C. Kandwal, K. M Agrawal, S. P. Nautiyal, H. U. Khan, Paraffin deposition and viscosity temperature behaviour of Assam crude oil, Petro. Sci. Technol., 18 (2000) 755 - 769.

89. H. M. Huotari, I. H. Huisman, G. Tragardh, Electrically enhanced crossflow membrane filtration of oily waste water using the membrane as a cathode, J. Membr. Sci., 156 (1999) 49 - 60.

90. J. Hermia, Constant pressure blocking filtration laws-application to power-law non-newtonian fluids, Trans. Inst. Chem. Eng. 60 (1982) 183 - 187.

91. B. Hu, K. Scott, Microfiltration of water in oil emulsions and evaluation of fouling mechanism, Chem. Eng. J., 136 (2008) 210 - 220.

92. P. Lipp, C. H. Lee, A.G. Fane and C. J. D. Fell, A fundamental study of the ultrafiltration of oil–water emulsions, J. Membr. Sci., 36 (1988) 161 - 177.

93. F. L. Hart, H. J. Fisher, Modern Food Analysis, Springer, Berlin, (1971).

94. H. D. Obermeyer, U. Kulozik, H. G. Kessler, Controlled deposit formation to influence the retention of solutes in reverse osmosis and ultrafiltration, Desalination, 90 (1993) 161 - 172.

95. A. B. Koltuniewicz, R. W. Field, T. C. Arnot, Cross-flow and dead-end microfiltration of oil-water emulsion. Part I: experimental study and analysis of flux decline, J. Membr. Sci., 102 (1995) 193 - 207.

96. K. M. Persson, V. Gekas, G. Trägårdh, Study of membrane compaction and its influence on ultrafiltration water permeability, J. Membr. Sci., 100(1995) 155 - 162.

97. J. Brinck, A. S. Jönsson, B. Jönsson and J. Lindau, Influence of pH on the adsorptive fouling of ultrafiltration membranes by fatty acid, J. Membr. Sci.,164 (2000) 187-194.

98. K. Boussu, C. Vandecasteele, B. Van der Bruggen, Study of the characteristics and the performance of self-made nanoporous polyethersulfone membranes, Polymer, 47 (2006) 3464 - 3476.

99. B. K. Nandi, R. Uppaluri, M. K. Purkait, Effects of dip coating parameters on the morphology and transport properties of cellulose acetate - ceramic composite membranes, J. Membr. Sci., 330 (2009) 246 - 258.

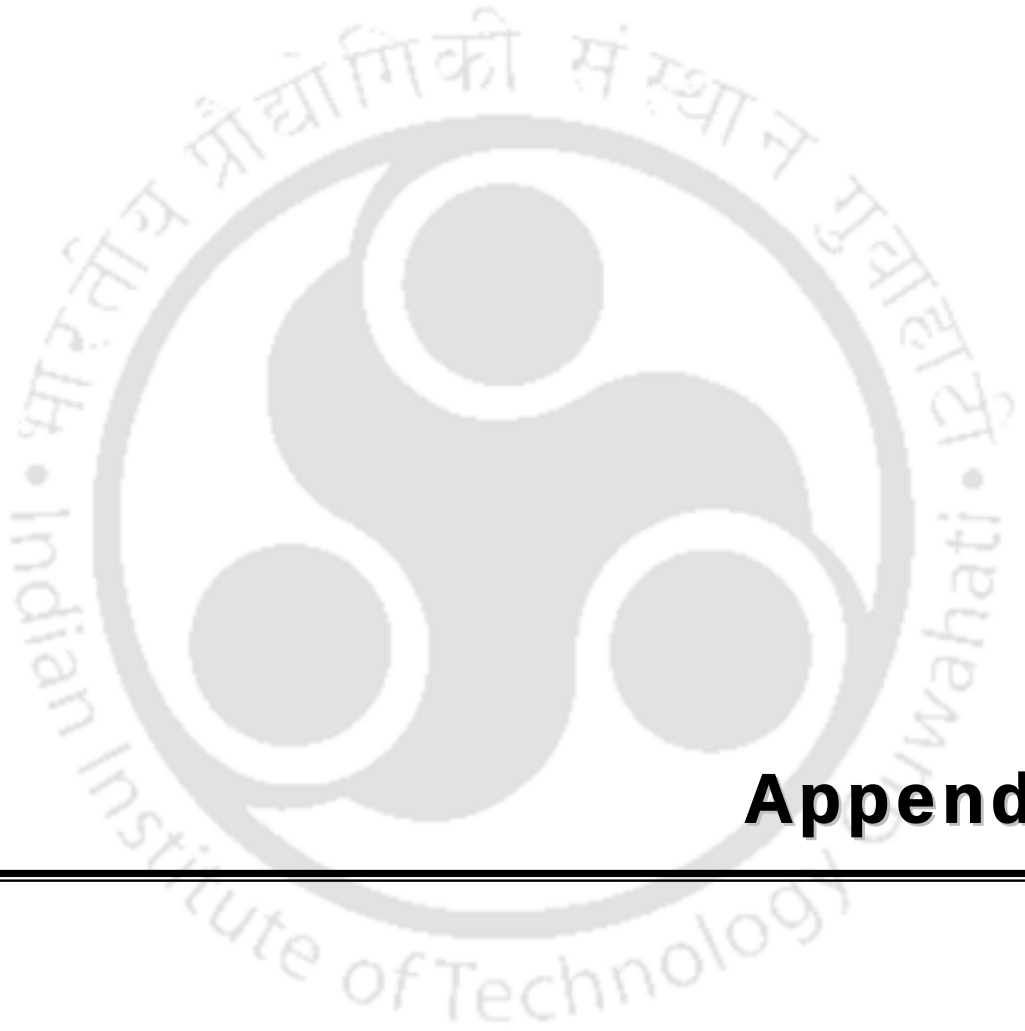

# Appendix

# Error analysis

For experimental investigations, it is common that always some differences exist between the sets of measured values at various time instances. Therefore, based on several experimental runs average values are usually reported. The confidence levels associated with the average values and measured values is often summarized in the form of an error analysis in scientific and technical reports. Error analysis determines the accuracy of calculations and reliability of the reported experimental data. Broadly, there exist two types of errors namely systematic error and random error. Systematic errors arise due to faulty assumptions and improper experimental measuring techniques. In this work, care was taken in eliminating systematic errors by appropriately designing the experiments and adopting well accepted methods for the analysis of data. On the other hand, random errors arise due to variation in the precision of measuring parameters. Usually, random errors are contributed by minor variations in successive measurements made by the experimentalist under nearly identical conditions. Therefore, random errors can not be eliminated. The aim of the error analysis section presented in this work is to quantify the magnitude of the random errors. In many experiments performed in this work, quantities were measured directly using digital instruments such as digital weight machine (balance), UV/Vis spectrophotometer, laser particle size analyzer and TGA. Therefore, significant amount of random error is not anticipated in these measurements.

## Error in the measurement of concentration

Concentrations of oil, BSA were measured using UV/Vis spectrophotometer. Calibration curves were prepared by measuring known values of concentrations of solute (oil/BSA). From

the calibration curves, it was observed that the standard deviation of the calculated value from actual value of concentration is more than 0.9931 for three different cases. Thus, every measurement of solution concentration is associated with a maximum error of 0.69 %, which is an insignificant value. On the other hand, TSS of juice was measured using digital refractometer, colour and clarity of mosambi juice was measured using UV/Vis spectrophotometer. These instruments provided measurements with four digit precision after the decimal and variation only in the fourth digit was observed during measurements. Therefore, the measurement errors in this case were about 0.1 - 0.01 %.

## Error in the measurement of permeate flux

The errors in the values of permeate flux are related to the errors in the measurements used to calculate those values. In this section, statistical analysis is used for estimation of the uncertainty associated with the values of permeate flux. Determination of standard deviation is generally considered to be one of the best methods to estimate the uncertainty which is based on the following method:

If $u_1$, $u_2$, ....., $u_N$ are the $N$ number results of the measurements of a particular quantity $u$, then the mean value of $u$ (i.e. $\bar{u}$), is defined as:

$$\bar{u} = \frac{u_1 + u_2 + \ldots\ldots\ldots\ldots + u_N}{N} = \frac{1}{N}\sum_{i=1}^{N} u_i \qquad \text{(E1)}$$

The uncertainty in the result is usually expressed as “root-mean-squared-deviation”, which is denoted as $\Delta u$, which is computed using the following equation:

$$\Delta u = \sqrt{\frac{(u_1 - \bar{u})^2 + (u_2 - \bar{u})^2 + \ldots\ldots\ldots\ldots + (u_N - \bar{u})^2}{N-1}} \qquad \text{(E2)}$$

For the characterization of all membranes, initially gas permeability experiments were conducted for the dry membrane followed with the pure water flux (PWF) experiments. Also, before and after each MF/UF experiment, membranes were cleaned thoroughly and PWF measurements were conducted. Uncertainties involved in the gas permeation experiments and PWF measurements are calculated using Eq. (E2). For A2 membrane, the associated uncertainities for both air permeance and PWF are presented in Table ER1. It was observed that the uncertainties were less than 1 % for all membranes.

**Table ER1: Values of uncertainties estimated in air permeance at 206.84 kPa and PWF measurements at 310 kPa trans-membrane pressure differential for A2 membrane.**

| Experiments | Run 1 | Run 2 | Run 3 | ū | $\Delta u$ | Uncertainties (%) |
|---|---|---|---|---|---|---|
| Air Permeance $\times 10^3$ ($m^3/m^2$.h.MPa) | 3.58 | 3.6 | 3.60 | 3.59 | 0.017 | 0.483 |
| PWF $\times 10^4$ ($m^3/m^2$.s) | 5.01 | 5.04 | 4.96 | 5.0 | 0.041 | 0.807 |

## International Journals:

1. B. K Nandi, R. Uppaluri, M. K. Purkait, Preparation and characterization of low cost ceramic membranes for microfiltration applications, App. Clay Sci., 42 (2008) 102 - 110.
2. B. K Nandi, R. Uppaluri, M.K. Purkait, Effects of dip coating parameters on the morphology and transport properties of cellulose acetate ceramic composite membranes, J. Membr. Sci., 330 (2009) 246 - 258.
3. B. K. Nandi, R. Uppaluri, M.K. Purkait, Treatment of oily waste water using low cost ceramic membrane: Flux decline mechanism and economic feasibility, Sep. Sci. Technol., 44 (2009) 2840 – 2869.
4. B. K. Nandi, B. Das, R. Uppaluri, M.K. Purkait, Microfiltration of Mosambi Juice using Low Cost Ceramic Membrane, J. Food Eng. 95 (2009) 597-605.

## Manuscripts communicated:

1. B. K. Nandi, B. Das, R. Uppaluri, M. K. Purkait, Preparation and characterization of inexpensive submicron range inorganic microfiltration membranes, Sep. Purif. Technol., (under review, 2009).
2. B. K. Nandi, R. Uppaluri, M.K. Purkait, Identification of optimal membrane morphological parameters during microfiltration of mosambi juice using low cost ceramic membranes, LWT - Food Sci. Technol., (under review, 2009).

3. B. K. Nandi, A. Moparthi, R. Uppaluri, M. K. Purkait, Treatment of Oily Wastewater Using Low Cost Ceramic Membrane: Comparative Assessment of Pore Blocking and Artificial Neural Network Models, Chem. Eng. Res. Des., (under review, 2009).
4. B. K. Nandi, R. Uppaluri, M. K. Purkait, Microfiltration of Stable Oil-in-water Emulsions using Kaolin based Ceramic Membrane and Evaluation of Fouling Mechanism, Chem. Eng. J., (under review, 2009)

## National Conference:

1. B.K. Nandi, R. Uppaluri, M.K.Purkait, "Preparation and characterization of low cost Microfiltration ceramic membrane" Indian Chemical Engineering Congress (CHEMCON-2007), 27 – 30 December, 2007, Kolkata, India.

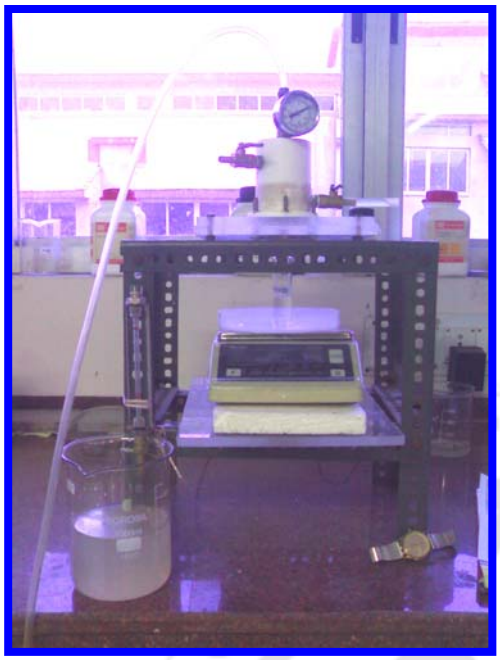

(a)

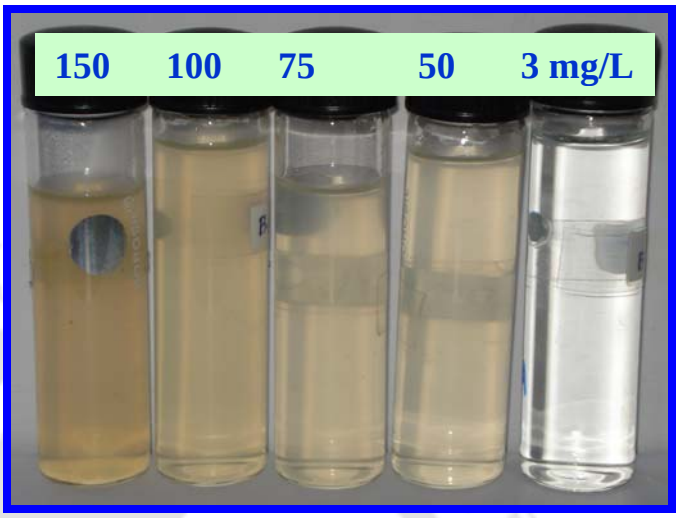


(b)

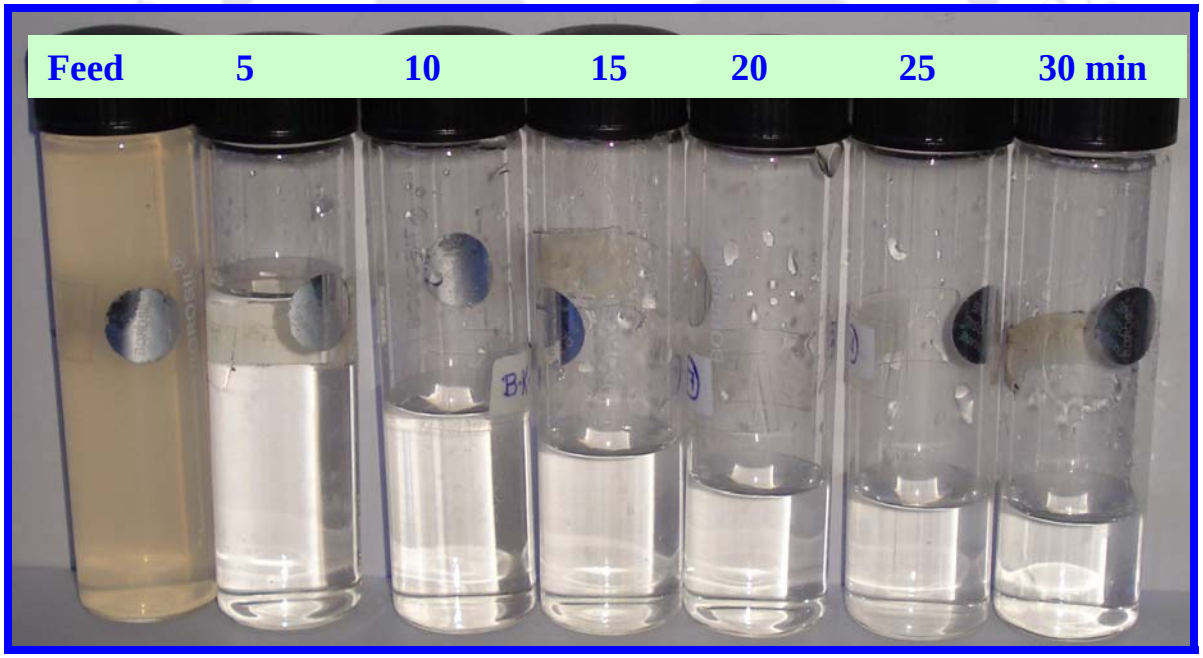


(c)

**(a) Experimental set up for MF of oil-in-water emulsions.**

**(b) Variation of oil concentration in emulsion.**

**(c) Variation of oil concentration and permeate flux with time.**

(a)

(b)

(c)


(d)

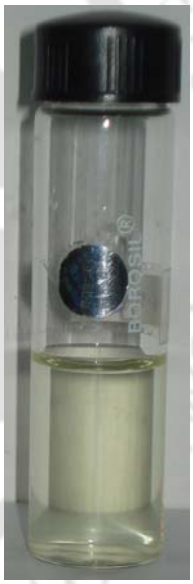

(e)

**(a) Experimental set up for MF of mosambi juice.**

**(b) FJ**

**(c) Centrifuged suspended particles.**

**(d) CJ.**

**(e) Permeate ETCJ.**

# Published papers

Available online at www.sciencedirect.com
ScienceDirect
Applied Clay Science 42 (2008) 102–110
Applied CLAY Science
www.elsevier.com/locate/clay

# Preparation and characterization of low cost ceramic membranes for micro-filtration applications

B.K. Nandi, R. Uppaluri *, M.K. Purkait *

*Department of Chemical Engineering, Indian Institute of Technology Guwahati, Guwahati, Assam-781039, India*

Received 16 August 2007; received in revised form 15 December 2007; accepted 18 December 2007
Available online 28 December 2007

**Abstract**

Contemporary research in ceramic composites for membrane applications targets the fabrication of stable low cost micro-filtration range membranes. This work reports the fabrication of stable low cost mesoporous membranes deploying subsequent formulations based on kaolin and other suitable low cost materials such as quartz, sodium carbonate, calcium carbonate, boric acid and sodium metasilicate. Incidentally, the processing temperature in this work is about 850–1000 °C instead of 1100 °C which is the usual sintering temperature for inorganic membrane fabrication. The membranes casted as circular disks (52.5 mm diameter and 4.5 mm thickness) were subjected for characterization studies using TGA, XRD, SEM analysis, to evaluate the effect of maximum sintering temperature on membrane structure, porosity and mechanical integrity. Pore size distribution, porosity, average pore size of the membrane along with permeation experiments with both water and air is carried out to study the membrane performance. The average pore size of the membrane is observed to increase from 550 nm to 810 nm when sintering temperature increases from 850 °C to 1000 °C. However, with the increase in temperature from 850 °C to 1000 °C, the membrane porosity is reduced (from 42% to 33%) and flexural strength is increased (from 3 to 8 MPa). The membrane corrosion resistance is found to be unaltered with processing temperature. Based on raw-material prices, the membrane cost is estimated to be \$130/m$^2$. Henceforth, these low cost membranes with good membrane properties are suggested for cheaper application in chemical and biochemical processes using micro-filtration and ultra-filtration techniques.


*Keywords:* Kaolin; Micro-filtration; Inorganic membrane; Sintering; Low cost ceramic membrane

## 1. Introduction

In the past two decades, significant advances in membrane technology research are already reported. Numerous applications have been proposed of which micro-filtration and ultra-filtration are critical technologies in chemical and biochemical processing that are regarded economically competitive due to the availability of membranes with higher flux and lower process cost. Existing and continuing research in membrane technology aims to extend the horizons of membranes for high temperature processing (Sourirajan, 1970; Yoshino et al., 2005) and corrosive feed stocks (Wang et al., 2006) for which ceramic membrane development is targeted. These membranes are found to be capable for high temperature, corrosive and high pressure applications with good durability (Sourirajan, 1970; Meares, 1976; Cuperus and Nijhuis, 1993; DeFriend et al., 2003; Yoshino et al., 2005; Wang et al., 2006).

The preparation of inorganic symmetric and composite membranes is focused towards fundamental research on the combinatorial impact of the type of inorganic precursors on the morphology, stability and porous texture of the inorganic matrix. In addition, the aspiring feature of such research is to find optimal formulations of different ingredient to yield a thermally and chemically stable membrane with good separation characteristics.

Early research in inorganic membrane fabrication is focused towards the utilization of α-alumina which is an expensive precursor to fabricate the membrane (DeFriend et al., 2003; Yoshino et al., 2005). Research at a later stage, involved the utilization of inorganic materials such as γ-alumina, zirconia,

* Corresponding authors. Tel.: +91 361 2582260/62; fax: +91 361 2582291.
*E-mail addresses:* ramgopalu@iitg.ernet.in (R. Uppaluri), mihir@iitg.ernet.in (M.K. Purkait).

0169-1317/$ - see front matter © 2008 Elsevier B.V. All rights reserved.
doi:10.1016/j.clay.2007.12.001

titania and silica (Tsuru, 2001; Falamaki et al., 2004; Yoshino et al., 2005; Wang et al., 2006). Nonetheless, the cost of these precursors remains to be significantly high and therefore significantly contributes to the operating cost of membrane modules for industrial applications. To circumvent the issue of membrane cost, recent research in the fabrication of inorganic membranes is focused towards the utilization of cheaper raw materials such as apatite powder (Masmoudia et al., 2007), fly ash (Saffaj et al., 2004), natural raw clay (Saffaj et al., 2005, 2006), dolomite, kaolin (Almandoza et al., 2004; Bouzerara et al., 2006). Of these inorganic precursors, kaolin appears to be an important inexpensive raw material that can be studied for the fabrication of stable micro-filtration range inorganic membranes at a lesser cost. Potdar et al. (2002) and Neelakandan et al. (2003) have provided optimal inorganic formulations (based on dry basis) using kaolin (12.7 wt.%), ball clay (16.1 wt.%), quartz (23.6 wt.%), feldspar (5.1 wt.%), $CaCO_3$ (28.1 wt.%) and pyrophallite (14.3 wt.%) for the fabrication of micro-filtration range inorganic membranes. Of these precursors, quartz, feldspar and pyrophallite could be regarded as expensive materials when compared to kaolin, ball clay and calcium carbonate. In a similar approach, Belouatek et al. (2005) have reported optimal inorganic formulations (based on dry basis) using clay (21 wt.%), kaolin (35 wt.%), feldspar (20 wt.%) and sand (24 wt.%) for fabricating inorganic supports capable for liquid waste treatment. Incidentally, the sintering temperature of this work is about 1100 °C. Of these ingredients reported by the authors, only feldspar can be regarded as an expensive raw material compared to the others i.e., clay, kaolin and sand.

A critical review of the above publications and other relevant research findings convey the following conclusions for the fabrication of inorganic membranes based on kaolin. Firstly, there is a need to develop alternate formulations that could provide a breakthrough to the development of inorganic composite membranes without using expensive inorganic precursors. Secondly, if a ceramic membrane is prepared by using expensive inorganic precursor formulation; such formulation should report the small quantities of expensive inorganic precursors and larger quantities of inexpensive inorganic precursors. Thirdly, the fabrication of the inorganic membrane with a processing temperature below 1000 °C needs to be experimentally tested and verified. The reduction in maximum sintering temperatures to values below 1000 °C would be beneficial for additional cost reduction of membrane fabrication process. Fourthly, the prepared ceramic membrane should provide excellent combination of thermal, mechanical and chemical stability in addition to good separation characteristics.

This work reports the fabrication of ceramic membrane using inorganic materials such as quartz, sodium carbonate, calcium carbonate, boric acid and sodium metasilicate in addition to kaolin. Apart from this, the inorganic precursor formulation reflects to lower contents of expensive materials such as quartz (15 wt.%). Further, this work reports a higher contents of kaolin (40 wt.%), and calcium carbonate (25 wt.%) which are usually regarded as inexpensive precursors along with sintering temperature below 1000 °C. Structural and morphological study of the membrane is done to evaluate the general characteristics of the fabricated ceramic membrane. Both liquid and gas permeation experiments are carried out to evaluate the membrane performance. Mechanical and chemical stability study of the membrane is also performed to verify its application in highly corrosive medium. Finally, the cost analysis of the prepared membranes is done to compare the membrane along with other similar membrane available in market.

## 2. Experimental

### 2.1. Raw materials

This work utilizes six common inorganic raw materials such as kaolin, quartz, calcium carbonate, sodium carbonate, boric acid and sodium metasilicate. Different raw materials used in this work for the fabrication of inorganic membrane serve for different functional attributes. Kaolin provides low plasticity and high refractory properties to the membrane. Quartz contributes for mechanical and thermal stability of the membrane. Regulation of porous texture in the ceramic is realized by calcium carbonate which under sintering conditions would dissociate into CaO and release $CO_2$ gas. The path taken by the released $CO_2$ gas thereby creates the porous texture of the inorganic membrane and contributes to the membrane porosity during the sintering process. On the other hand, sodium carbonate and boric acid acts as a colloidal agent and improves dispersion properties of the inorganic precursors thereby addressing homogeneity in the membrane structure. Boric acid also increases membrane mechanical strength by the formation of metallic metaborates at sintering temperatures. In a similar way, sodium metasilicate acts as binder by creating silicate bonds among the elements to induce higher mechanical strength in the ceramic membrane (Reed, 1995; Saffaj et al., 2005).

Kaolin and sodium metasilicate are obtained from CDH India. Quartz is collected from Research Lab Fine Chem Industry, India. All other inorganic precursors such as calcium carbonate, boric acid, sodium carbonate are obtained from Merck India. All these raw materials used for inorganic fabrication are graded at least 99.5% pure and used without further purification.

Major constituents of kaolin are alumina silicates with the following chemical composition (by wt.%) $SiO_2$: 46.5%, $Al_2O_3$: 39.5% and $H_2O$: 14%. Spectrum obtained from X-ray diffraction (D8 ADVANCE, Bruker Axs) analysis of kaolin sample is illustrated in Fig. 1. The XRD spectrum is matched with the JCPDS data base file (PDF-01-089-6538) which indicates that the kaolin used in our work is ideal kaolinite ($Al_2Si_2O_5(OH)_4$). Particle size distribution analysis (Mastersizer 2000, Malvern) of major inorganic materials such as kaolin, calcium carbonate and quartz used for the membrane fabrication process are shown in Fig. 2. The figure shows that almost 90% of the particles having diameter below 10 μm. The average particle size of kaolin, calcium carbonate and quartz are 2.37 μm, 4.108 μm and 8.4 μm, respectively.

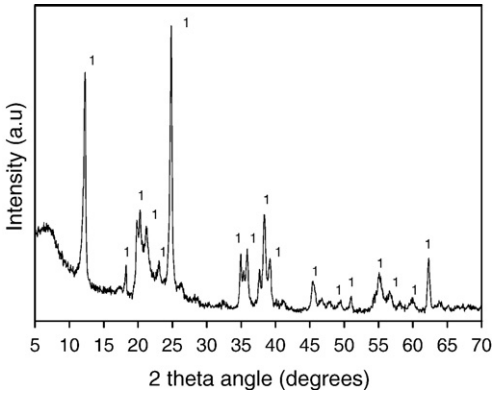


Fig. 1. XRD diagram of kaolin powder. 1; kaolinite (PDF-01-089-6538).

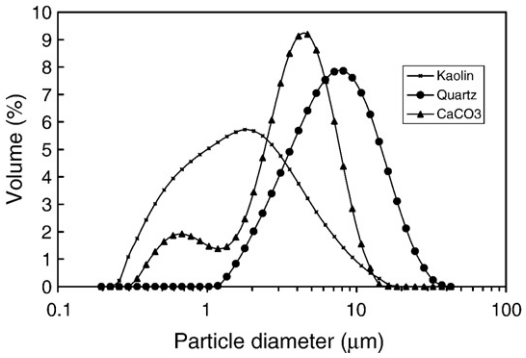


Fig. 2. Particle size distribution for different raw materials.

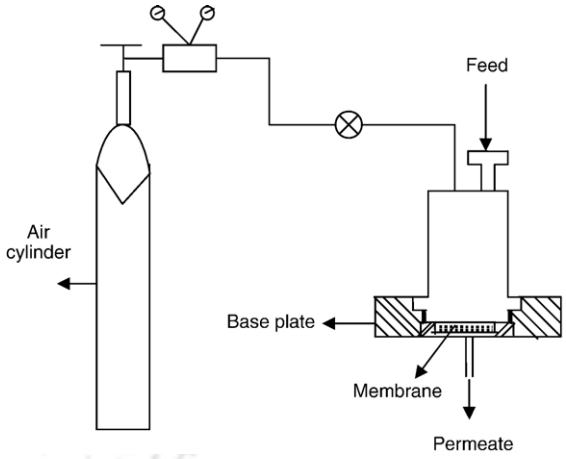


Fig. 3. Experimental setup for the permeation experiments.

### 2.2. Membrane preparation

The membrane fabrication process is initialized by thorough mixing of dry inorganic raw materials (Table 1) followed by addition of distilled water to prepare a paste. The paste is then cast over gypsum in the shape of a circular compact disk (55 mm diameter and 5 mm thickness) using a SS316 ring of 55 mm inner diameter and 5 mm thickness. Subsequently, the ring is carefully removed and the paste is kept under distributed pressure of 2 kg for 24 h to prevent the propagation deformation and drive homogeneity in the inorganic matrix. The paste is then subjected to two different sequential heat treatment steps. Firstly, the circular mold is dried at room temperature for 24 h. After that it is dried at 100 °C for 12 h in a hot air oven followed by drying at 250 °C for 24 h. During the transition from 100 °C to 250 °C, low heating rate is maintained in order to eliminate the induction of thermal stresses generated due to loss of moisture. The second heat treatment step involves the heating of the membrane from 250 °C to desired sintering temperature at a heating rate of 2 °C/min. Then the membrane is kept for 5 h for sintering. Sintering of membranes at four different temperature 850 °C, 900 °C, 950 °C and 1000 °C are done to verify the effect of sintering temperature on the membrane properties. Subsequent cooling of the membrane is conducted by atmospheric cooling procedure adopted by switching off the muffle furnace that is previously maintained at desired sintering temperature. After sintering, membranes achieved hard, rigid and porous texture. Finally, the fabricated membrane is polished with silicon carbide abrasive paper (C-220) to obtain a smooth, flat micro-filtration membrane of diameter 52.5 mm and thickness 4.5 mm.

### 2.3. Characterization techniques

Characterization techniques involves the structural characterization of the membrane by thermogravimetric analysis (TGA), differential thermal analysis (DTA), XRD and morphological study by scanning electron microscope (SEM), permeation experiments by water and air, chemical and mechanical stability. TGA and DTA of the sample mixture are conducted (TGA SDTA 851$^e$, Mettler Toledo) to identify the various thermal transformations of the material during sintering condition. XRD analysis of the inorganic membrane is conducted to evaluate the extent of phase transformations.

Table 1
Composition of raw materials used for the fabrication of inorganic membrane

| Material | Composition wet basis (wt.%) | Composition dry basis (wt.%) |
|---|---|---|
| Kaolin | 29.63 | 40 |
| Quartz | 11.11 | 15 |
| Calcium carbonate | 18.52 | 25 |
| Sodium carbonate | 7.40 | 10 |
| Boric acid | 3.71 | 5 |
| Sodium metasilicate | 3.71 | 5 |
| Water | 25.92 | 0 |



Scanning electron microscopy (LEO 1430VP, Oxford) is carried out to analyze the presence of possible defects and estimate the membrane pore size. A BET surface analyzer (SA 3100, Beckman Coulter) is used to measure nitrogen adsorption isotherm at 77 K. Before measurement, the sample is degassed using Helium at 553 K for 3 h.

The micropores and mesopores are obtained from the adsorption isotherms. The estimation of average membrane pore size from SEM micrographs is carried out using ImgeJ software (Version 1.37). The open porosity of the membrane is evaluated using Archimedes method with water as the wetting liquid. The membrane performance and presence of defects in the interior portion of the membranes is evaluated using both liquid (water) and gas (air) flux characterization. For liquid and gas permeation experiments a laboratory made permeation setup of capacity 125 ml is used. The setup (as shown in Fig. 3) used for this experiment consists a Teflon tubular cell with a flat circular Teflon base plate which contains the membrane housing. The deionized water is filled in the tubular section from the top. The membrane is placed in a Teflon casing and sealed with epoxy resin and then place in the membrane housing provided on the base plate. The cell is pressurized with compressed air. Liquid permeate flow rate is measured using a digital weight machine. For air permeation experiments the outlet is connected to a gas flow meter for measuring the gas flow rate for various trans-membrane pressure drop of air. The hydraulic permeability and the corresponding pore diameter of the membranes are also determined. All permeation experiments are conducted at a temperature of 25 °C.

Chemical (or corrosion) resistivity of the membrane is evaluated by subjecting the membrane to concentrated HCl and concentrated NaOH solution. EDX analysis of the membranes before and after corrosion test is done to verify any change in elemental composition. The mechanical strength of the membranes is tested in a three point bending load method (H 1000K-S, Hounsfield). All these quantitative experiments are conducted for at least four different membrane samples prepared for evaluating the general membrane performance and characteristics.

## 3. Results and discussion

### 3.1. Structural characterization

#### 3.1.1. Thermogravimetric analysis

The objective of thermal analysis is to identify temperature regimes where predominant weight losses (and hence transformations) occur in the membrane. Thereby, an understanding could be developed for analyzing the effect of various temperature regimes on the porous structure, pore diameter and mechanical strength of the membrane. Fig. 4 presents the TGA and DTA of the powder mixture when subjected to

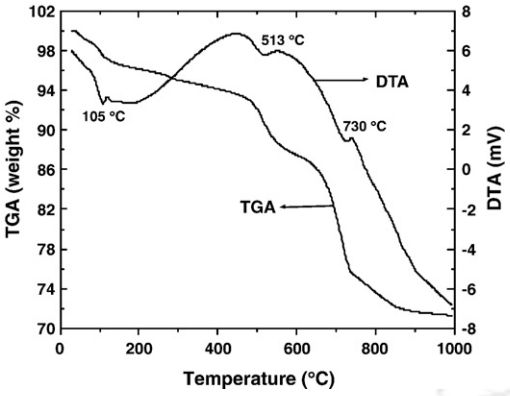


Fig. 4. TGA–DTA curves.

thermogravimetric analysis by heating the dry inorganic mixture in a α-alumina crucible from room temperature to 1000 °C at a heating rate of 10 °C/min.

The figure conveys that a highly non-linear variation exists due to the presence of complex phase transformations and interactions. The total weight loss of the sample is observed to 28.5%. About 2.5% weight loss is observed below 105 °C due to the removal of weakly bonded water molecules in the sample mixture. This specific water loss is characterized by an endothermic peak at 105 °C in the DTA curve. The weight loss of the sample between 105 and 400 °C is around 4%, which can be correlated with the pre-dehydration process of kaolin and dehydration of crystal water of boric acid. The pre-dehydration process of kaolin takes place as a result of the reorganization of the octahedral layer, first occurring at the OH of the surface (Balek and Murat, 1996). The second endothermic peak in the DTA curve is corresponding to the loss of structural hydroxyl groups at 513 °C due to the transformation of kaolinite to metakaolinite according to the following reaction (Chena et al., 2006).

$$Al_2O_3{\cdot}2SiO_2{\cdot}2H_2O(\text{kaolinite}) \rightarrow Al_2O_3{\cdot}2SiO_2(\text{metakaolinite}) + 2H_2O \quad (1)$$

The formation of $CO_2$ (and hence enhancement of the porous structure of the membrane) occurred at 730 °C corresponding to a weight loss of 10% in the temperature regime of 663 °C to 745 °C due to calcinations of $CaCO_3$ in this temperature regime. Calcinations of $Na_2CO_3$ starts at temperature 800 °C and ended in temperature 843 °C which corresponds to very minute loss of mass in this temperature range in TGA curve.

These two calcinations temperature regimes are individually verified by conducting TGA analysis of $CaCO_3$ and $Na_2CO_3$ samples. The sample corresponded to very insignificant weight loss above 843 °C as conveyed by the TGA curve. This result infers that minimum sintering temperature for the membrane fabrication should be above 843 °C.

### 3.1.2. Phase characterization by XRD analysis

From the TGA–DTA analysis it is observed that above sintering temperature of 843 °C almost no significant weight loss occurred. To verify this hypothesis XRD analysis of membrane structure at temperature higher than 843 °C is done. Fig. 5 summarizes XRD graphs for four different samples calcined at 25 °C, 850 °C, 900 °C and 1000 °C for 5 h in muffle furnace. The observation of peaks and trends in the XRD graphs convey that the inorganic mixture originally consisted of kaolinite, quartz and inyoite as main components. The XRD graph obtained for the sample calcined at 850 °C depicts that peaks corresponding to kaolinite are disappeared due to conversion of kaolinite to metakaolinite. In this regard, it could be pointed out that the formation of metakaolinite is illustrated by TGA–DTA curve trends explained in the previous sub-section at a temperature of 513 °C. The other phases that appear are nephiline and quartz. Nephiline ($Na_2O$, $Al_2O_3$, $2SiO_2$) is produced by the reaction of sodium oxide ($Na_2O$) and metakaolinite at temperature at 850 °C (Wang et al., 1994). A critical observation of the peaks at higher temperature revels that no other significant phase transformation occurs above 850 °C to 1000 °C. This signifies that the membrane skeletal structure constitutes mainly metakaolinite, quartz and nephiline. From the XRD analysis it also can be concluded that the sintering temperature of 850 °C is sufficient for membrane fabrication. All XRD diffractogram graphs indicate no change in the peak trends corresponding to quartz thereby inferring that quartz phase is not at all affected by sintering of inorganic materials within the temperature considered in this work. Therefore the sintering temperature above 850 °C is considered in this work.

### 3.1.3. Surface morphology

Fig. 6 illustrates SEM pictures for the membrane sintered at four different temperatures considered in this work. All the membranes showed a surface with rough morphological structure. The ceramic substrates sintered at lower temperature (850 °C and 900 °C) show highly porous structure (Fig. 6a and b). The membrane sintered at 950 °C and 1000 °C are more consolidated (Fig. 6c and d) due to the fact that for sintering temperatures over 900 °C the particles agglomerate together creating more dense ceramic body. As a result the porosity of the membrane decreases with increase in sintering temperature. A superficial observation of the SEM indicates that the membrane did not have any pinholes cracks and the maximum observable pore size of the surface is

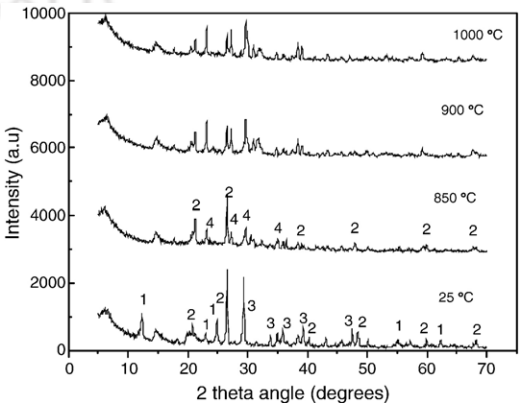


Fig. 5. X-ray diffraction patterns of the sample mixture sintered at different temperature. 1: kaolinite (PDF-01-089-6538), 2: quartz (PDF-01-075-0443), 3: inyoite (PDF-00-006-0361), 4: nephiline (PDF-00-019-1176).

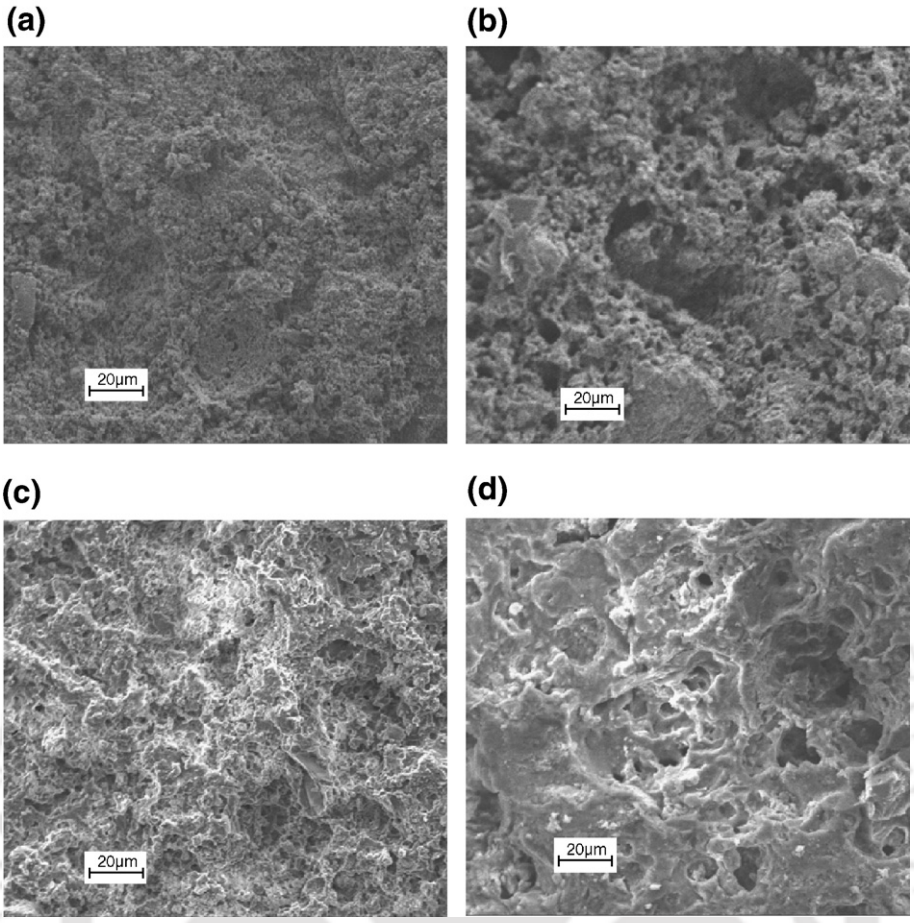


Fig. 6. SEM photographs of the prepared micro-filtration membrane surface sintered at (a) 850 °C, (b) 900 °C, (c) 950 °C and (d) 1000 °C.

about 5 μm. These attributes of the membrane make it suitable for micro-filtration applications.

*3.1.4. Pore size analysis based on SEM*

Individual pore diameters are measured for about 500 pores using ImgeJ software for different pores visible in the SEM (Pugazhenthi and Kumar, 2004). Since pore size distribution and average pore size distribution values are critically dependent on the sampling procedure, five SEM pictures are evaluated using the software. These micrographs are taken from the randomly selected sections of the membrane. These ensure that the pore size distribution represent the existing porous texture of the membrane.

Fig. 7 presents the pore size distribution summarizing the evaluated values of percentage pore numbers with respect to different pore diameters. The area average pore diameter ($d_s$) from SEM analysis of the membrane is evaluated by assuming cylindrical porous texture of the membrane as:

$$d_s = \left[\frac{\sum_{i=1}^{n} n_i d_i^2}{\sum_{i=1}^{n} n_i}\right]^{0.5} \quad (2)$$

where, $n$ is the number of pores, $d_i$ is the pore diameter (μm) of $i$th pore. The average pore diameters of membranes are determined as 0.55, 0.70, 0.78 and 0.81 μm for membranes sintered at 850 °C, 900 °C, 950 °C, 1000 °C respectively that correspond to micro-filtration range ceramic membrane. It can be observed from Fig. 7 that the pore size distribution is closely related to the sintering temperature. For all the sintering temperatures the maximum no of pores (65–75%) are in the range of 0.3–0.6 μm. The mean pore size of the membranes rises with an increase in the sintering temperature, and the pore

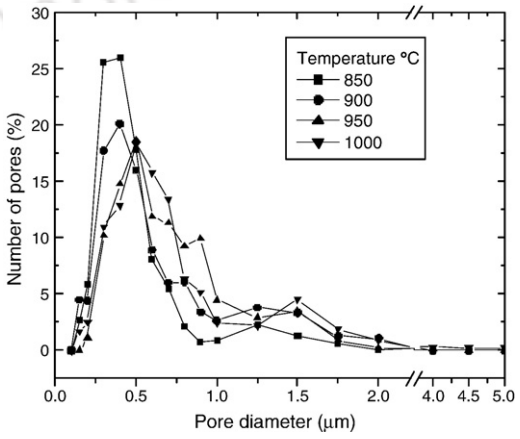


Fig. 7. Pore size distribution of the prepared micro-filtration membranes sintered at various temperatures as determine from SEM micrographs.

size distribution broadens at the same time. This is partly due to the growth of grains lead to the formation of large pores and elimination of small pores when the membranes are sintered at higher temperature.

### 3.2. Permeation experiments

#### 3.2.1. Liquid permeation

The inorganic membranes are subjected to liquid permeation test using deionized water in batch mode operation. The hydraulic permeability ($L_h$), average pore diameter and porosity of the membrane are determined experimentally. Trans-membrane pressure drop for water permeation tests is maintained at 0–250 kPa (micro-filtration range). Before using each fresh membrane, membrane compaction has been conducted using deionized water at a trans-membrane pressure of 310 kPa (which is higher than the maximum operating pressure for the set of experiments conducted). During these experiments, the membrane flux was observed to be high initially and reduced to the steady value after 2 h of operation for all the membranes. At the beginning of compaction flux is $9.6\times10^{-5}$ $m^3$ $m^{-2}$ s which reaches to a steady state value of $7.2\times10^{-5}$ $m^3$ $m^{-2}$ s at the end of compaction for the membrane sintered at 900 °C. The permeation tests involve the measurement of permeates liquid volume as a function of time at specific values of trans-membrane pressure drop. The flux of liquid is measure at an interval of 10 s to verify the variation of flux with time. These experiments are performed until the total liquid permeate collected is 80 ml at a specific pressure differential. Physical observations during liquid permeation tests confirmed that the flow rate did not vary during the 10 s intervals. The hydraulic permeability ($L_h$) and average pore radius ($r_l$) of the membrane can be estimated according to the following expression (Almandoza et al., 2004)

$$J = \frac{n\pi r^4 \Delta P}{8\mu l} = L_h \Delta P \tag{3}$$

where $J$ ($m^3 m^{-2}$ $s^{-1}$) is the liquid flux through the membrane, $\Delta P$ (kPa) is the trans-membrane pressure drop across the membrane, $\mu$ is the viscosity of water, $l$ is pore length, $\varepsilon$ ($=n\pi r^2$) is the porosity of the membrane. The average pore radius ($r_l$) of the membrane is then evaluated by assuming presence of cylindrical pores in the membrane matrix using the following equation deduced from Eq. (3) as

$$r_l = \left[\frac{8\mu l L_h}{\varepsilon}\right]^{0.5}. \tag{4}$$

The porosity ($\varepsilon$) of the membrane is determined by the pycnometric method using water as wetting liquid. Figs. 8 and 9 summarize the structural density, porosity, hydraulic permeability and average pore diameter of the membranes varying with sintering temperature. Fig. 8 shows the variation of membrane porosity and structural density of membrane with varying sintering temperature. The membrane porosity decreases from 42% to 33% where as structural density increases from 1.26 ml/g to 1.36 ml/g when sintering temperature varies from 850 °C to 1000 °C. This is due to the fact that increase in sintering temperature densification of the porous structure occurs and thereby allows for an increase in structural density and decrease in the membrane porosity. Fig. 9 shows that variation of pore diameter and permeability of the membrane with sintering temperature. As shown, average pore diameter of the membrane increases with increasing sintering temperature due to which membrane permeability also increases. Similar trends are reported in literature (Saffaj et al., 2005; Bouzerara et al., 2006) for the other type of clay based inorganic membrane fabrication.

#### 3.2.2. Gas permeation

The qualitative analysis of SEM and the quantitative analysis of liquid permeation studies conveyed the presence of only macropores in the membrane structure. The presence of micropores and their contribution is not clear from these analyses.

Therefore, gas permeation experimentation is adopted to observe the role and contribution of microporous membrane structure to the overall membrane flux.

Based on these gas permeation data, two different membrane characteristics namely average pore radius ($r_g$) and effective porosity $\left(\frac{\varepsilon}{q^2}\right)$ can be estimated according to the expression (Marchese and Pagliero, 1991)

$$K = 2.133\frac{r_g v}{l}\frac{\varepsilon}{q^2} + 1.6\frac{r_g^2}{l\eta}\frac{\varepsilon}{q^2}p \tag{5}$$

where $P$ is the average pressure on the membrane, $v$ (m/s) is the molecular mean velocity of the gas, $l$ (m) is the pore length, $q$ is the tortuosity, $\eta$ (Pa s) is the viscosity of gas, $K$ (m/s) is the effective permeability factor evaluated as

$$K = \frac{QP_2}{S\Delta P} \tag{6}$$

where, $S$ ($m^2$) is the permeable area of the membrane, $Q$ ($m^3$/s) is the volumetric flow rate, $P_2$ is the membrane pressure at permeate side and $\Delta P$ is the trans-membrane pressure drop.

In Eq. (5), the first term corresponds to Knudsen permeance and the second term corresponds to the viscous permeance. Therefore, Eq. (5) can be represented as a straight line in a graph

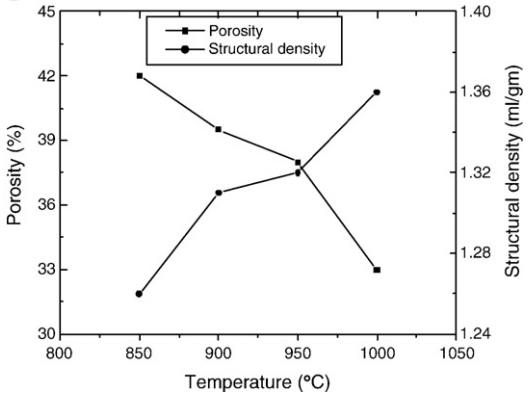


Fig. 8. Porosity and structural density of membranes sintered at various temperatures.

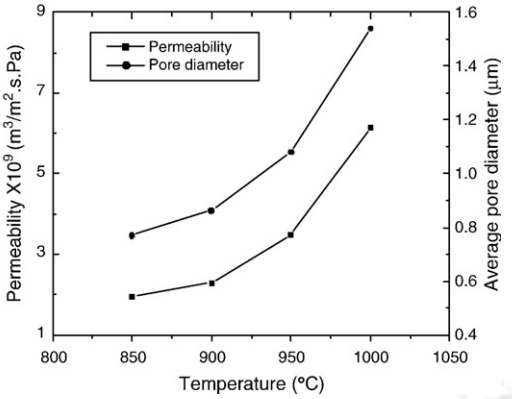


Fig. 9. Hydraulic permeability and average pore size of membranes sintered at various temperatures.

drawn between $K$ and $P$ and the slope and intercept of this line represents viscous and Knudsen permeability of the membrane respectively. Henceforth the values of the slope and intercept obtained from the graph can be used to evaluate the percentage contribution of pores (and pore sizes) that contribute towards viscous and Knudsen flow transport mechanisms. In other words, gaseous flux characterization of the ceramic can yield qualitative information with respect to the pore size distribution applicable for the contribution of Knudsen or viscous flow regimes towards the overall membrane flux. The average pore radius ($r_g$) of the membrane can be evaluated using the slope ($A$) and intercept ($B$) of the generated graph expressed as

$$r_g = 1.333\frac{B}{A}v\eta. \quad (7)$$

Fig. 10 presents the variation of flux with average pressure $P$ varying from 120–240 kPa for different membranes. The measured gas permeance of different membranes are $2.08\times10^3$, $3.34\times10^3$, $3.59\times10^3$ and $4.53\times10^3$ m$^3$ m$^{-2}$ h$^{-1}$ MPa$^{-1}$ at trans-membrane pressure drop of 0.206 MPa for sintering temperature of 850 °C, 900 °C, 950 °C and 1000 °C, respectively. Table 2

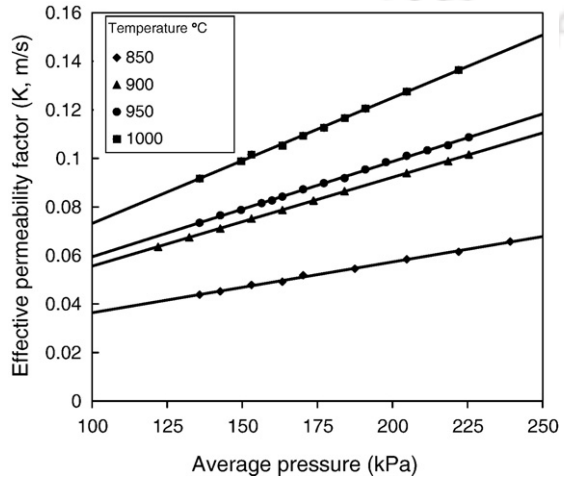


Fig. 10. Air permeability vs. mean pressure for the different membranes.

Table 2
Various parameters evaluated from graphical analysis of trans-membrane gaseous flux data

| Sintering temperature (°C) | Intercept $(A)\times10^2$ (m/s) | Slope $(B)\times10^7$ (m/s Pa) | Pore diameter (nm) | Porosity $\left(\frac{\varepsilon}{q^2}\right)$ | Viscous flux (%) | Knudsen flux (%) |
|---|---|---|---|---|---|---|
| 850 | 1.55 | 2.09 | 313 | 0.477 | 65–76 | 35–24 |
| 900 | 1.89 | 3.66 | 449 | 0.405 | 70–81 | 30–19 |
| 950 | 2.02 | 3.93 | 452 | 0.428 | 73–82 | 27–18 |
| 1000 | 2.14 | 5.17 | 560 | 0.368 | 77–84 | 23–16 |

summarizes parameters evaluated from graphical analysis of trans-membrane flux data. As shown in the table, the average pore diameter of the membrane obtained from theoretical analysis of permeation varies from 0.31 to 0.56 μm. In this regard, measured pore radius from SEM analysis could be observed to be varies from 0.55 μm to 0.81 μm which is also closer to the value evaluated from liquid permeation data. The table also summarizes effective porosity factor values ranging from 0.477 to 0.368 that truly represent and contribute to the membrane transport. In this regard, it can be observed that the constant average porosity of the membrane is about 0.42 to 0.33 which is close to the predicted value of the effective porosity. Henceforth, the assumption of cylindrical pores in the calculation procedure is justified with the fact that tortuosity is close to one. However, the most important aspect of gas permeation data is the ability to judge how much percentage of trans-membrane flux is accounted due to Knudsen diffusion effect and viscous diffusion effect. Table 2 infers that for membrane sintered at 900 °C of the air flux, viscous diffusion contributes 70 to 81% to the total flux conveying that about 70 to 81% of the pores in the membrane have pore sizes well above the regime where Knudsen diffusion dominates (1 to 20 nm).

The existence of micropores in the membrane structure is further confirmed by surface analysis using BET method. Pore size distribution obtained from BET data is in the range of 3.65 to 148 nm. The membrane sintered at 900 °C consists of 53.8% of micropores are in the range of 3.65 to 10 nm and 25.63% of the micropores are in the range 10–20 nm. Similar pore size distribution trends are observed for membranes sintered at other temperatures. Hence hypothesis deduced from gas permeation characteristics is also confirmed by $N_2$ adsorption/desorption isotherm analysis.

A similar observation can be made from the permeation analysis of other membranes where it is found that viscous flux contributes 65 to 84% of the total flux. These results therefore illustrate that the pore size distribution reported earlier in this work is almost well agreed. The Knudsen flow regime and hence pores in the range 1 to 20 nm represent only 20 to 30% of the pore size contributing to the transport mechanism.

With respect to the observable trends of gaseous flux data, it is reasonable to argue that gaseous flux characterization predicts smaller average pore radius than that obtained from liquid flux characterization using liquid such as water or mercury. This is due to the fact that liquid permeation detects not only actual pores but also other non-interconnected voids of the porous matrix. However, since hydraulic permeability involves the transport of liquid through pores accountable for micro-filtration

Table 3
EDX analysis of the membrane materials sintered at 900 °C before and after corrosion test

| Elements | Membrane (wt.%) | Membrane after acid corrosion test (wt.%) | Membrane after base corrosion test (wt.%) |
|---|---|---|---|
| Oxygen | 49.24 | 48.55 | 50.26 |
| Sodium | 7.96 | 7.21 | 8.43 |
| Aluminum | 11.84 | 12.60 | 11.32 |
| Silicon | 14.82 | 16.45 | 14.43 |
| Calcium | 16.14 | 15.19 | 15.56 |

process, the most appropriate average pore size of the membrane could be inferred from liquid flux data but not gaseous flux data. Gaseous flux characterization enables one to evaluate the percentage distribution of micropores of varying sizes and their contribution to the overall transport behavior of the membrane. These results agree with the experimental data reported in the literature (Almandoza et al., 2004).

### 3.3. Physical characterization

#### 3.3.1. Chemical stability

The micro-filtration membrane sintered at different temperature is tested for their corrosion resistance using NaOH solution (pH 13) and HCl (pH 1.5). The membranes are subjected to chemical resistance measurement by measuring its weight after leaving it in contact with the above solutions for seven consecutive days at atmospheric conditions and evaluating the net weight loss after drying the membrane. Further, porosity measurements before and after acid or alkali treatment are conducted in order to verify any change in the porosity when the membrane is exposed to corrosive environment. For all sintering temperatures the weight loss of membrane during these tests is not significant and is less than 4%. However, 8% increase in membrane porosity is observed for both HCl and NaOH for all the membranes. EDX analysis of the membranes before and after corrosion test for the ceramic membrane sintered at 900 °C is shown in Table 3.

It can be inferred from the table that the elemental composition of the membrane is almost the same in both the acid and basic media. Similar type of data is obtained for the other sintering temperature. Therefore, the observed trends in weight loss and EDX analysis during corrosion tests convey that the membrane possesses excellent corrosion resistance and is suitable for micro-filtration applications involving acidic and basic media. Similar trend of chemical resistance is reported for kaolin (Wang et al., 1994) and for apatite (Saffaj et al., 2004) based low cost membranes.

#### 3.3.2. Mechanical strength

The mechanical strength of the prepared membranes is performed using the three points bending strength method. The flexural strength of the membranes at different sintering temperature is shown in Fig. 11. As presented in the figure, it can be seen that the flexural strength increases (3 MPa at 850 °C) with increasing sintering temperature (8 MPa at 1000 °C). The increase in mechanical strength is attributed to the densification of the clay materials with increasing sintering temperature of the samples. This result is in good agreement with the trends found in literature (Saffaj et al., 2004; Bouzerara et al., 2006).

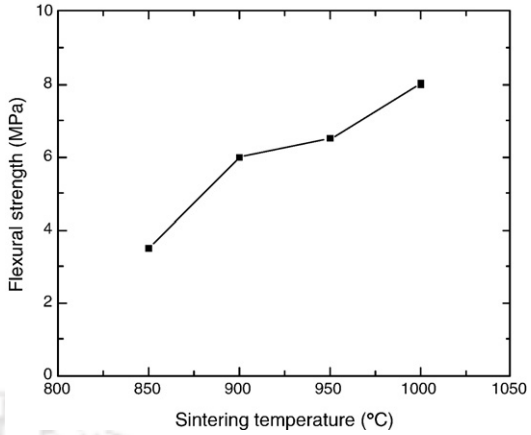


Fig. 11. Mechanical strength of membranes sintered at various temperatures.

## 4. Membrane cost

Industrially competitive aspect of membrane technology lies in its cost. Conventional polymeric membranes available for industrial scale operation cost around $50–200/m$^2$ (Bhide and Stern 1991). However, often inorganic membranes are quoted to be at least 10 times expensive than the polymeric membranes and their cost is projected to be around $500–1000/m$^2$ (Koros and Mahajan, 2000). An α-alumina ceramic symmetric membrane tubes with 1000–6000 nm costs in the similar range of $500–1000/m$^2$ (Céramiques Techniques, 2007). While manufacturing cost for tubular membranes could be higher due to the inherent complexity in homogenous tubular mold preparation, the higher cost of α-alumina cannot be ruled out for these ceramic membranes. Based on the unit costs of raw materials used for preparing the inorganic membrane in this work (Table 4), the manufacturing cost of the inorganic membrane is evaluated to be $130/m$^2$. Including manufacturing and shipment costs, the

Table 4
Cost analysis of fabricated membrane from the unit cost of raw materials

| Raw material | Weight (kg)×$\frac{3}{10}$ | Unit price ($/kg)[a] |
|---|---|---|
| Feldspar | – | 80 |
| Pyrophallite | – | 35 |
| Kaolin | 8 | 5 |
| Quartz | 3 | 64 |
| $CaCO_3$ | 5 | 4.2 |
| $Na_2CO_3$ | 2 | 4.6 |
| Boric acid | 1 | 5.6 |
| Sodium meta-silicate | 1 | 8.4 |
| Dry inorganic formulation (0.02 kg for one disk shaped dry membrane of 4.5 mm thickness and 52.5 mm diameter) | 20 | $130/m$^2$ |

[a] Prices are taken from the catalog of the corresponding company as mentioned in Section 2.1.

average cost of the inorganic membrane for industrial applications based on bulk production methods would be closer to the value of $200/m$^2$ that is often quoted for polymeric membrane configurations for gaseous separation in industrial systems (Bhide and Stern 1991). In comparison, the ceramic symmetric membranes made with α-alumina cost around $500/m$^2$ and stainless steel asymmetric membranes cost around $3000/m$^2$ (Mott Metallurgical Corporation, 2007). Therefore, it can be inferred from cost analysis that the inorganic membrane based on kaolin would be closer to the cost of the polymeric membranes deployed for industrial configurations and could be slightly expensive than the modules prepared with polymeric membranes owing to the costs involved in manufacturing and bare module costs. The reported value of the membrane cost is conceptual in nature and may vary significantly depending on the fouling characteristics, on time performance and long term stability of the ceramic membrane in process applications. However, corrosion resistance and mechanical strength data presented in this work instill confidence in the long term performance and hence the projected membrane cost is anticipated to be close to the reported value.

## 5. Conclusions

A new inorganic formulation is tested for the fabrication of defect-free inorganic micro-filtration ceramic membranes with average pore diameters varying from 550–810 nm. In addition to formulations [18, 19] this study indicates that a defect-free ceramic membrane can be fabricated with higher contents kaolin (40%) and lower contents of expensive precursors such as quartz (15%). Thermal characterization and XRD study inferred that the appropriate sintering temperature for the chosen composition of materials is around 850 °C. The observable maximum pore size of the membranes is 5 μm. The distribution of pore sizes based on SEM and physical interpretation is in good agreement with experimental results and only 20–30% of the porous structure contributes towards Knudsen flow regime during the transport studies. The membranes provided good mechanical strength (3 to 8 MPa flexural strength) and chemical stability (<8% weight loss in both acid and base media). The approximate cost of the membrane is equal to the module cost of polymeric membrane ($200/m$^2$). These results provide significant opportunities to develop ceramic micro-filtration membranes with flexible pore sizes for industrial applications.

## References


Almandoza, M.C., Marchese, J., Prádanos, P., Palacio, L., Hernández, A., 2004. Preparation and characterization of non-supported micro-filtration membranes from aluminosilicates. J. Membr. Sci. 241, 95–103.

Balek, V., Murat, M., 1996. The emanation thermal analysis of kaolinite clay minerals. Thermochim. Acta 282–283, 385–397.

Belouatek, A., Benderdouche, N., Addou, A., Ouagued, A., Bettahar, N., 2005. Preparation of inorganic supports for liquid waste treatment. Microporous Mesoporous Mater. 85, 163–168.

Bhide, B.D., Stern, S.A., 1991. A new evaluation of membrane processes enrichment of air. II. Effects of economic membrane properties. J. Membr. Sci. 62, 37–58.

Bouzerara, F., Harabi, A., Achour, S., Larbot, A., 2006. Porous ceramic supports for membranes prepared from kaolin and doloma mixtures. J. Eur. Ceram. Soc. 26, 1663–1671.

Céramiques Techniques & Industrielles, SA, France, 2007. http://perso.orange.fr/ctisa.

Chena, Y.F., Wang, M.C., Hon, M.H., 2006. Phase transformation and growth of mullite in kaolin ceramics. J. Afr. Earth Sci. 46, 245–252.

Cuperus, F.P., Nijhuis, H.H., 1993. Applications of membrane technology to food processing. Trends Food Sci. Technol. 4, 277–286.

DeFriend, K.A., Wiesner, M.R., Barron, A.R., 2003. Alumina and aluminate ultra-filtration membranes derived from alumina nanoparticles. J. Membr. Sci. 224, 11–28.

Falamaki, C., Shafiee, A.M., Aghaie, A., 2004. Initial sintering stage pore growth mechanism applied to the manufacture of ceramic membrane supports. J. Eur. Ceram. Soc. 24, 2285–2292.

Koros, W.J., Mahajan, R., 2000. Pushing the limits on possibilities for large scale gas separation: which strategies? J. Membr. Sci. 175, 181–196.

Marchese, J., Pagliero, C.L., 1991. Characterization of asymmetric polysulphone membranes for gas separation. Gas Sep. Purif. 5, 215–221.

Masmoudia, S., Larbot, A., Feki, H.E., Amara, R.B., 2007. Elaboration and characterisation of apatite based mineral supports for microfiltration and ultrafiltration membranes. Ceram. Int. 33, 337–344.

Meares, P., 1976. Membrane Separation Processes. Elsevier, Amsterdam.

Mott Metallurgical Corporation, USA, 2007. http://www.mottcorp.com).

Neelakandan, C., Pugazhenthi, G., Kumar, A., 2003. Preparation of NOx modified PMMA–EGDM composite membrane for the recovery of chromium (VI). Eur. Poly. J. 39, 2383–2391.

Potdar, A., Sukla, A., Kumar, A., 2002. Effect of gas phase modification of analcime zeolite composite membrane on separation of surfactant by ultrafiltration. J. Membr. Sci. 210, 209–225.

Pugazhenthi, G., Kumar, A., 2004. Enzyme membrane reactor for hydrolysis of olive oil using lipase immobilized on modified PMMA composite membrane. J. Membr. Sci. 228, 187–197.

Reed, J.S., 1995. Principles of Ceramics Processing. John Wiley & Sons, NewYork.

Saffaj, N., Younssi, S.A., Albizane, A., Messouadi, A., Bouhria, M., Persin, M., Cretin, M., Larbot, A., 2004. Preparation and characterization of ultrafiltration membranes for toxic removal from wastewater. Desalination 168, 259–263.

Saffaj, N., Persin, M., Younssi, S.A., Albizan, A., Bouhria, M., Loukili, H., Dacha, H., Larbot, A., 2005. Removal of salts and dyes by low $ZnAl_2O_4$–$TiO_2$ ultra-filtration membrane deposited on support made from raw clay. Sep. Purif. Technol. 47, 36–42.

Saffaj, N., Persin, M., Younsi, S.A., Albizane, A., Cretin, M., Larbot, A., 2006. Elaboration and characterization of micro-filtration and ultra-filtration membranes deposited on raw support prepared from natural Moroccan clay: application to filtration of solution containing dyes and salts. Appl. Clay Sci. 31, 110–119.

Sourirajan, S., 1970. Reverse Osmosis. Logos Press, London.

Tsuru, T., 2001. Inorganic porous membranes for liquid phase separation. Sep. Purif. Methods 30, 191–220.

Wang, M.C., Wu, N.C., Hon, M.H., 1994. Preparation of nepheline glass-ceramics dental porcelain. Mater. Chem. Phys. 37, 370–375.

Wang, Y.H., Tian, T.F., Liu, X.Q., Meng, G.Y., 2006. Titania membrane preparation with chemical stability for very hash environments applications. J. Membr. Sci. 280, 261–269.

Yoshino, Y., Suzuki, T., Nair, B.N., Taguchi, H., Itoh, N., 2005. Development of tubular substrates, silica based membranes and membrane modules for hydrogen separation at high temperature. J. Membr. Sci. 267, 8–17.

*Separation Science and Technology*, 44: 2840–2869, 2009

ISSN: 0149-6395 print/1520-5754 online
DOI: 10.1080/01496390903136004

Taylor & Francis
Taylor & Francis Group



# Treatment of Oily Waste Water Using Low-Cost Ceramic Membrane: Flux Decline Mechanism and Economic Feasibility

**B. K. Nandi, R. Uppaluri, and M. K. Purkait**
Department of Chemical Engineering, Indian Institute of Technology Guwahati, Guwahati, Assam, India

**Abstract:** This work addresses the applicability of different membrane pore blocking models for the prediction of flux decline mechanisms during dead end microfiltration (MF) of stable oil-in-water (o/w) emulsions using relatively low-cost ceramic membranes. Circular disk type membranes (52.5 mm diameter and 4.5 mm thickness) were prepared by the paste method using locally available low-cost inorganic precursors such as kaolin, quartz, calcium carbonate, sodium carbonate, boric acid, and sodium metasilicate. Characterization of the prepared membrane was done by SEM analysis, porosity determination, and pure water permeation through the membrane. Hydraulic pore diameter, hydraulic permeability, and hydraulic resistance of the membrane was evaluated as 0.7 μm, $1.94 \times 10^{-6}\,m^3/m^2 \cdot s \cdot kPa$ and $5.78 \times 10^{11}\,m^2/m^3$, respectively. The prepared membrane was used for the treatment of synthetic stable o/w emulsions of 40 and 50 mg/L crude oil concentration in batch mode with varying trans-membrane pressure differentials ranging from 41.37 to 165.47 kPa. The membrane exhibited 96.97% oil rejection efficiency and $21.07 \times 10^{-6}\,m^3/m^2 \cdot s$ permeate flux after 30 min of experimental run at 165.47 kPa trans-membrane pressure for 50 mg/L oil concentration. Different pore blocking, models such as complete pore blocking, standard pore blocking, intermediate pore blocking and cake filtration were used to gain insights into the nature of membrane fouling during permeation. The observed trends for flux decline data convey that the decrease in permeate flux was initially due to intermediate pore blocking (during 1 to 10 minutes of

Received 8 December 2008; accepted 12 May 2009.
Address correspondence to R. Uppaluri or M. K. Purkait, Department of Chemical Engineering, Indian Institute of Technology Guwahati, Guwahati 781039, India. Tel.: +91-361-2582262; Fax: 91-361-2582291. E-mail: ramgopalu@iitg.ernet.in or mihir@iitg.ernet.in

experimental run) followed with cake filtration (during 10 to 30 minutes of experimental run). Based on retail prices of the inorganic precursors, the membrane cost was estimated to be 130 $/m$^2$. Finally, preliminary process economic studies for a single stage membrane plant were performed for the application of the prepared membrane in industrial scale treatment of o/w emulsions. A process economics study inferred that the annualized cost of the membrane plant would be 0.098 $/m$^3$ feed for treating 100 m$^3$/day feed with oil concentration of 50 mg/L.

**Keywords:** Ceramic membrane, microfiltration, oily wastewater, pore blocking, process economics



## INTRODUCTION

Various process industries such as petroleum refineries, petrochemical industries, metallurgical, transportation, and food processing industries produce large volumes of oily wastewater with oil concentrations of 50 to 1000 mg/L. Existing tolerance limits of total oil and grease concentrations in wastewater streams is 10 mg/L (1). To achieve the desired discharge limits, among various alternative plausible technologies, membrane technology has been found to be very promising due to various advantages such as lower capital cost, higher separation factors, compact design, and the elimination of other chemical and mechanical treatment units. Recent research indicates that both polymeric membranes as well as ceramic membranes can be applied for the treatment of o/w emulsions (2). However, during filtration, polymeric membranes are susceptible to fouling and degradation and eventually need to be replaced frequently. As a result the operating cost increases significantly (2). In addition, each polymeric membrane has its own solvent compatibility and weakness to specific chemicals present in the permeating liquid. For instance, cellulose acetate membranes are severely affected by the presence of chlorine and solvents such as acetone and aniline (3). On the other hand, due to high chemical, thermal, and mechanical stability, ceramic membranes appear to more promising for the treatment of o/w emulsions for industrial scale operation. One of the limitations for industrial application of the ceramic membrane is their cost, which is significantly higher (2000 to 4000 $/m$^2$ (4)) than polymeric membranes (50 to 200 $/m$^2$ (3)). The higher cost of ceramic membranes is due to the utilization of expensive inorganic precursors such as alumina and zirconia and higher sintering temperature (more than 1100°C) during membrane fabrication (5,6). This is also due to the fact that higher sintering temperatures demand higher electrical energy and hence operating costs. In addition, higher sintering temperatures may also give rise to

enhancement in furnace power specifications and hence the installed costs. Therefore, higher sintering temperatures translate to higher membrane fabrication costs.

To circumvent the higher costs of inorganic membranes, existing and ongoing research in the preparation of low-cost inorganic membranes is quite challenging as the use of low-cost inorganic precursors as well as the low sintering temperature (below 1000°C) may deteriorate the membrane performance, lifetime, and ultimately affect their edge over the polymeric membranes. Fortunately, many literatures do indicate that kaolin-based membranes have the ability to serve as low-cost substitutes when compared to costly alumina and zirconia membranes. Belouatek et al. (7), and Almandoza et al. (8), have prepared kaolin-based ceramic membrane applicable for microfiltration (MF) or ultrafiltration (UF) applications. However, the sintering temperature used in these works was more than 1100°C. As a result, the cost of the inorganic membrane is anticipated to be higher due to higher sintering temperatures, even though inexpensive raw materials were utilized. Therefore, there exists a necessity to address the fabrication of stable inexpensive ceramic membranes that involves both cheaper precursors and lower sintering temperatures (lower than 1000°C), to further existing research trends in cheaper ceramic membrane filters.

Most of the literatures that report the treatment of oily wastewaters address technological solutions for feed oil concentrations ranging 500 to 2000 mg/L (2). These feed systems consist of unstable oil droplets of droplet sizes higher than 50 μm and hence their removal is easily achievable (9). However, lower droplet sizes (less than 10 μm) exist for feeds with oil concentrations below 100 mg/L. These sub-micron range oil droplets have been reported to be highly stable and their separation is anticipated to be a challenging one (10). Therefore, it is very likely that the oil concentrations in discharged process wastewater streams from effluent treatment plants fail to comply with the allowable discharge limits of 10 mg/L (1). For such complicating scenarios, ceramic membrane technology could provide technological solutions. To the best of our knowledge, the applicability of low cost ceramic membranes to treat wastewaters consisting of oil concentration below 100 mg/L and their economic feasibility has not been studied to date. This work attempts to address these issues using a low-cost MF ceramic membrane.

The objective of this work was to identify competent, low-cost inorganic precursor formulation that can yield ceramic membrane using a sintering temperature below 1000°C to yield an inexpensive ceramic membrane. Different low-cost inorganic raw materials such as kaolin,

quartz, calcium carbonate, sodium carbonate, boric acid, and sodium metasilicate were used for the preparation of the ceramic membrane. The sintering temperature was kept below 900°C to minimize the cost of the fabrication process without affecting the performance of the membranes. The cost of the fabricated ceramic membranes was estimated to be 130 $/m$^2$ based on the retail price of inorganic precursors. Subsequently, the membrane cost was assumed to be 400 $/m$^2$ including fabrication and module costs, which is significantly comparable to that of the conventional polymeric membranes (50–200 $/m$^2$) and far lower than other commercially available ceramic membranes (2000–4000 $/m$^2$). Structural, morphological, and pure water flux (PWF) study of the prepared membrane was carried out to evaluate the general characteristics of the fabricated ceramic membrane. PWF experiments were carried out to evaluate different membrane parameters such as hydraulic permeability, hydraulic pore diameter, and porosity of the membrane. Prepared inexpensive inorganic membrane was used to verify the separation of o/w emulsions capability with low concentrations (40 and 50 mg/L). Permeate flux decline was analyzed using various flux decline models to get an insight into the nature of membrane fouling during filtration. Finally, preliminary studies on the cost of the prepared membranes along with the process economics of the membrane for a single stage membrane plant was adopted to evaluate the economic competitiveness of the prepared membrane in industrial scale treatment systems. Thereby, we wish to promote further the applicability of ceramic membrane technology in challenging industrial scenarios.



## EXPERIMENTAL

### Raw Materials

This work utilized six common inorganic raw materials such as kaolin (CDH, India), quartz (Research Lab Fine Chem Industry, India), calcium carbonate (Merck India), sodium carbonate (Merck India), boric acid (Merck India), and sodium metasilicate (SD Fine Chem Ltd., India). All these raw materials used for inorganic fabrication were graded at least 99.5% pure and were used without any further purification. Different raw materials used in this work for the fabrication of inorganic membrane served for different functional attributes. Kaolin provided low plasticity and high refractory properties to the membrane. Quartz contributed to the mechanical and thermal stability of the membrane. Regulation of porous texture in the ceramic was realized by calcium carbonate which

under sintering conditions would dissociate into CaO and release $CO_2$ gas. The path taken by the released $CO_2$ gas thereby created the porous texture of the inorganic membrane and contributed to the membrane porosity during the sintering process. Boric acid increased membrane mechanical strength by the formation of metallic metaborates at sintering temperatures. Boric acid and sodium carbonate also act as colloidal agents and improved the dispersion properties of the inorganic precursors thereby addressing homogeneity in the membrane structure. In a similar way, sodium meta-silicate acted as a binder by creating silicate bonds among the elements to induce higher mechanical strength in the ceramic membrane (11).

Two major clay materials namely kaolin and quartz used for the membrane fabrication process were characterized using X-ray diffraction analysis (Make: Bruker Axs; Model: D8 ADVANCE) and particle size distribution analysis (Make: Malvern; Model: Mastersizer 2000). The XRD spectrum of the clay materials matched with the JCPDS database file PDF-01-089-6538 and PDF-01-075-0443 for kaolin and quartz. The results obtained from particle size analysis of clay materials infers that particle size of the kaolin varied from 18.67 to 0.224 μm and 37.24 μm to 1.18 μm for quartz. The average particle size of kaolin and quartz were 2.37 and 8.4 μm, respectively.

## Membrane Fabrication

The ceramic micrifiltration (MF) membrane was prepared from a clay mixture with the composition as kaolin (8 g), quartz (3 g), calcium carbonate (5 g), sodium carbonate (2 g), boric acid (1 g) and sodium metasilicate (1 g). Subsequently, the raw materials were mixed with 7 g of distilled water to prepare a paste. Details of the preparation method are shown in Fig. 1. The paste was molded in the form of a circular disk on a gypsum surface by using an SS 316 ring of 55 mm internal diameter and 5 mm thickness. Then the disk type mold was dried at room temperature for 24 hours, at 100°C for 12 hours and at 250°C for 24 hours for complete removal of loose moisture. Subsequently, the membrane was sintered at 850°C for 5 hours with a heating rate of 2°C per minute. A sintering temperature of 850°C was chosen based on thermogravimetric analysis of the clay mixture, where no major phase transformation was observed above 843°C (12). After sintering, the membranes achieved a hard, rigid, and porous texture. Eventually, the membrane was polished with silicon carbide abrasive paper (C-220) to obtain a smooth, flat MF membrane of diameter 52.5 mm and thickness 4.5 mm. Finally, the membrane was cleaned in a sonicator for 15 minutes to remove loose

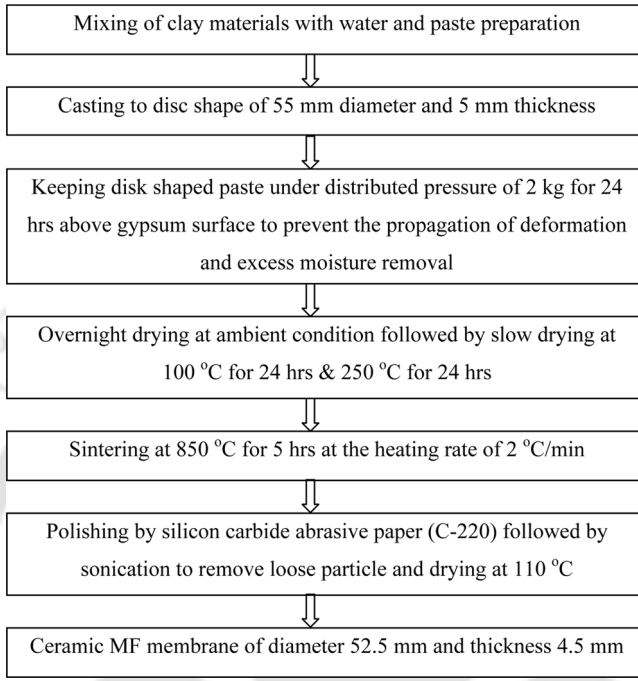


***Figure 1.*** Block diagram for the preparation of ceramic membrane from raw materials.

particles from the membrane, dried at 120°C, and was ready for the MF experiment.

## Characterization Techniques

The prepared membrane was characterized by scanning electron microscopy (SEM) analysis, total porosity determination, and hydraulic permeability determination using pure water permeation through the membrane. Scanning electron microscopy (Make: Oxford; Model: LEO 1430VP) was carried out to analyze the presence of possible defects and estimate the membrane pore size. The estimation of the average membrane pore size ($d_s$) from SEM micrographs was carried out using ImageJ software (Version 1.40) (13). The open porosity of the membrane was evaluated using the Archimedes method with water as the wetting liquid. Pure water flux (PWF) permeation experiments were carried out for the determination of the hydraulic permeability ($P_m$), hydraulic pore diameter ($d_l$) of the membrane.

## Experimental Set-Up

A schematic of the experimental set-up used for both air and water permeation experiments is presented in Fig. 2. The set-up constitutes a Teflon tubular cell (125 ml capacity) with a flat circular Teflon base plate that houses the composite membrane. Membranes were kept in the Teflon casing and sealed with epoxy resin. For air permeation experiments the outlet was connected to a gas flow meter for measuring the gas flow rate for various trans-membrane pressure drop of air. For pure water flux and o/w emulsions the feed (deionized water and o/w emulsions) was filled in the tubular section from the top. The cell was pressurized with compressed air. The liquid permeate flow rate was measured using a digital weight machine. The membrane diameter was 52.5 mm and effective membrane area was $1.66 \times 10^{-3}\,m^2$. Before using each fresh membrane, compaction of the membrane was performed using deionized water at a transmembrane pressure of 310 kPa (which is higher than the maximum operating pressure for the set of experiments conducted). During these experiments, the membrane flux was observed to be high initially and reduced to a near steady value after two hours of operation for all the membranes.

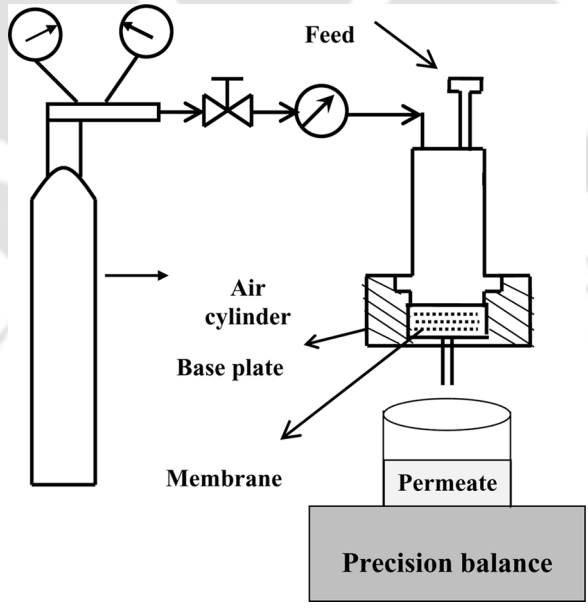


*Figure 2.* Schematic of the experimental set-up.

## Preparation of Oil-in-Water Emulsions

Crude oil collected from Guwahati Refinery, Indian Oil Corporation Limited (IOCL), India, was used without any treatment to prepare synthetic o/w emulsions. The crude oil was obtained from Assam crude oil reservoirs. Assam crude is typically characterized to possess a high degree of aromatic and wax content (14). Oil-in-water emulsions were prepared using distilled water and crude oil by placing the o/w mixture in a sonicator tank (Make: Elmasonic; Model: S30H) for 15 hours at a temperature of 25°C. The disappearance of the oily layer on the water surface confirmed the achievement of emulsification process during sonication. No surfactant was added externally to stabilize the emulsion as the natural surfactants present in the crude oil were sufficient to yield a highly stable emulsion. The onset of the stable emulsion was further tested by measuring the droplet size distribution, the absorbance at 235 nm wavelength, the pH, and the viscosity of the emulsions regularly. After a time period of two weeks, coalescence of the oil droplets were observed that lead to the formation of a thin oil film on the water surface. Similar observations were also found by Huotari et al. (15). Therefore, all MF experiments were done with emulsions prepared within 10 days. Droplet sizes and their distribution of the prepared o/w emulsions were measured using a laser particle size analyzer (Make: Malvern; Model: Mastersizer 2000). The droplet sizes of the emulsion were observed to vary between 0.04 μm to 10 μm. The average droplet sizes of the emulsions were 0.52 and 0.56 μm for emulsions prepared with 40 and 50 mg/L oil concentration, respectively.

## Microfiltration of Oil-in-Water Emulsion

Microfiltration experiments of the synthetic oil-in-water (o/w) emulsions were carried out in an unstirred batch MF cell using two different concentrations of oil (40 and 50 mg/L). Four different trans-membrane pressures differential ($\Delta P$) of 41.37, 82.74, 124.11, and 165.47 kPa are used to observe the effect of $\Delta P$ on the permeate flux and oil rejection efficiency. The feed concentration of oil was measured before each MF run. The permeate was collected at an interval of 5 minutes for the determination of permeate oil concentration. The permeate flux was calculated at an interval of 1 minute using an electronic balance place at the bottom of the MF cell. Further, all MF experiments were conducted at room temperature

(~25°C). The permeate flux ($J$, $m^3/m^2 \cdot s$) and the percent oil rejection ($R$) were evaluated using the following expressions:

$$J = \frac{V}{A \times \Delta t} \tag{1}$$

$$R = \left(1 - \frac{C_P}{C}\right) \times 100 \tag{2}$$

Where $A$ ($m^2$) is the effective membrane area, $V$ ($m^3$) is the volume of permeate, $\Delta t$ (s) is the sampling time, $C$ (mg/L) and $C_P$ (mg/L) are the concentration of oil in the feed and permeate, respectively. The oil concentrations in the permeate and the feed were determined using a UV-Vis spectrophotometer (Make: Perkin Elmer Precisel; Model: Lambda 35) by measuring absorbance at a wave length of 235 nm where maximum absorbance was observed (10). After each experimental run, the membranes were cleaned with "Surfexcel," a laboratory detergent solution. The pure water flux (PWF) of each membrane was verified before and after cleaning the membrane. The difference between the PWF of cleaned membrane and fresh membrane was found to be negligible. All these quantitative experiments were conducted for at least four different membrane samples in order to confirm the average membrane performance characteristics. The maximum uncertainty in all measurements was within the range of ±5%.

## Analysis of Fouling Mechanism

Hermia (16) developed four empirical models for dead-end filtration based on constant pressure filtration laws that correspond to four basic types of flux decline mechanisms: complete blocking, intermediate blocking, standard blocking and cake filtration (Fig. 3). During constant pressure dead end MF, initial permeate flux mainly depends on the membrane resistance. As microfiltration proceeds, different phenemona take place across the membrane structure such as, adsorption of oil droplets on ceramic matrix causing blocking of pores, oil cake deposition and concentration polarization. All these phenomena contribute to the overall resistance of the membrane and as a result MF permeation process could involve a transition from a membrane resistance-limited regime to a pore blocking resistance-limited or a cake resistance-limited regime. Thereby, the evaluations of parameters associated to these four basic models of flux decline enable physical insights and comprehensions upon the most appropriate mechanisms applicable for the process.

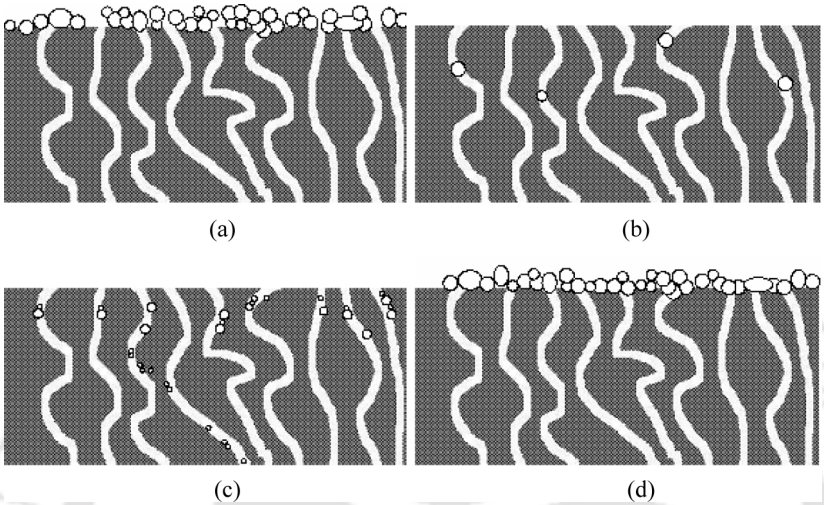


***Figure 3.*** Schematic representation of blocking mechanism (a) Intermediate pore blocking, (b) Complete pore blocking, (c) Standard pore blocking and (d) Cake filtration.



## Intermediate Pore Blocking Model

This model considers that one membrane pore is not necessarily blocked by one oil droplet and some oil droplets may settle over others. The non-blocked membrane surface diminishes with time and hence the probability of blocking a membrane pore reduces by oil droplet continuously with time. Intermediate blocking occurs when the oil droplet size is similar to the membrane pore size. Therefore, oil droplets are expected to obstruct a membrane pore entrance without blocking the pore completely (Fig. 3a). The permeate flux decline model based on the intermediate blocking mechanism is expressed as (3,17)

$$J = J_0(1 + K_I\ AJ_0t)^{-1} \tag{3}$$

## Complete Pore Blocking Model

According to this model, it is assumed that each oil droplet arriving at the membrane surface participates in blocking by pore sealing and the oil droplets never settle over another that has been previously deposited on the membrane surface. The permeate flux through the

unblocked pores is unaffected and hence the fractional reduction in the permeate flux is equal to the fractional reduction in the membrane surface area corresponding to unblocked pores. This type of fouling occurs when the size of the oil droplets is greater than the size of the membrane pores. Therefore, pore blocking takes place over the membrane surface and not inside the membrane pores (Fig. 3b). Applicable flux decline expression for complete pore blocking model is presented as (3,17)

$$J = J_0 \exp(-k_b t) \tag{4}$$

Standard Pore Blocking Model

This model considers that oil droplets enter the membrane pores and deposit over the pore walls due to the irregularity of the pore passages, thereby reducing the membrane pore volume. Some oil droplets are not simply deposited over the internal surface of the membrane pores since they are adsorbed over the pore walls. This type of fouling is caused by oil droplets smaller than the membrane pore size and pore blocking occurs inside the membrane pores. As a result, the volumes of membrane pores decreases proportionally to the filtered permeate volume (Fig. 3c). The decrease in the volume of membrane pores with time is equal to the decrease in their cross section. The permeate flux expression for standard pore blocking model is expressed as (3,17)

$$J = J_0 \left(1 + 0.5 K_S (A J_0)^{0.5} t\right)^{-2} \tag{5}$$

Cake Filtration Model

Cake filtration usually occurs when particles larger than the average pore size accumulate on the membrane surface, forming a "cake" (Fig. 3d). With time the cake grows and provides an additional porous barrier through which the liquid must permeate. As a result, the cake may increase the particle removal efficiency of the membrane; however, it also increases the membrane resistance and subsequently diminishes flux. The permeate flux for this case is expressed as (3,17)

$$J = J_0 \left(1 + 2 K_S (A J_0)^2 t\right)^{-2} \tag{6}$$

Identification of Fouling Mechanism

A linearized representation of Eqs. (3) – (6) is shown below:

a) Intermediate pore blocking model: $J^{-1} = J_0^{-1} + k_i t$ (7)

b) Complete pore blocking model: $\ln(J^{-1}) = \ln(J_0^{-1}) + k_b t$ (8)

c) Standard pore blocking model: $J^{-0.5} = J_0^{-0.5} + k_s t$ (9)

d) Cake filtration model: $J^{-2} = J_0^{-2} + k_c t$ (10)

where $k_i = K_I A$, $k_b$, $k_s = 0.5 K_S A^{0.5}$ and $k_c = 2K_C A^2$ are the system parameters relating to intermediate pore blocking, complete pore blocking, standard pore blocking, and cake filtration model, respectively. Therefore, a plot of $J^{-1}$ vs. $t$, $\ln(J^{-1})$ vs. $t$, $J^{-0.5}$ vs. $t$ and $J^{-2}$ vs. $t$ shall be a straight line with slope of $k_i$, $k_b$, $k_s$, $k_c$ and y-intercept of $J_0^{-1}, \ln(J_0^{-1})$, $J_0^{-0.5}$ and $J_0^{-2}$ for intermediate pore blocking, complete pore blocking, standard pore blocking, and cake filtration model, respectively. The appropriate applicability of these models can be confirmed by comparing the values of coefficient of correlation ($R^2$) obtained from the linear regression analysis as well as error analysis between experimental and calculated flux data.

## Process Economics

In general, the total cost of a membrane-based process is evaluated as the sum of different cost components such as cost of the membranes, pumps, pipes and valves, electrical and instrumentation, tanks and frames, and other miscellaneous items (including buildings, electrical supply, treated water storage, and pumping, etc.). However, as the aim of the present study was a conceptual cost-based economic study, different establishment costs (buildings, electrical supply, treated water storage, and pumping etc.) were ignored and only the cost of the membrane, the pump (used to energize stream from feed tank to higher pressure membrane chamber), and the operating cost of the pump (electricity) were considered in this study. The main focus of this study was to find the effect of membrane cost, operating pressure, and feed concentration on the total operating cost of the plant. Annualized cost of the membrane ($Q_{Amem}$, \$/year), pump ($Q_{Apump}$, \$/year) and operating cost of the pump ($Q_{AOpump}$, \$/year) were estimated using the

**Table 1.** Different model equations for the cost estimation (20)

| Item | Expressions | Eq. no |
|---|---|---|
| Membrane area | $A_{mem} = \frac{Q_F \times \theta}{J_{ss}},\ J_{SS} = f(\Delta P)$ | (11,12) |
| Annualized cost of membrane module | $Q_{Amem} = \frac{(A_{mem})^{0.8} \times Q_{mem} \times i \times (i+1)^{L_M}}{(i+1)^{L_M} - 1}$ | (13) |
| Pump cost | $Q_{pump} = I \times f_1 \times f_2 \times L \times 81.27 \times (C \times \Delta P)^{0.39}$ | (14) |
| Annualized cost of the pump | $Q_{Apump} = \frac{Q_{pump} \times i \times (i+1)^{L_p}}{(i+1)^{L_p} - 1}$ | (15) |
| Work done by the pump | $W = \Delta Z \times g + \frac{v^2}{2} + \frac{\Delta P}{\rho}, v = \frac{Q_F}{\frac{\pi}{4} d_{pipe}^2}$ | (16, 17) |
| Energy required by the pump | $E = \left(\frac{W \times Q_F \times \rho_E}{\beta}\right)$ | (18) |
| Annualized operating cost of the pump | $Q_{AOpump} = E \times 24 \times 300 \times Q_E$ | (19) |
| Total annualized cost of the plant | $Q_{total} = Q_{Amem} + Q_{Apump} + Q_{AOpump}$ | (20) |
| | $Q_{total} = f(C, \Delta P, \theta, Q_F, Q_{mem})$ | (21) |

correlation provided by Sethi and Wiesner (18) and are summarized in Table 1.

The annualized cost of the membrane ($Q_{Amem}$, \$/year) was evaluated as a function of the membrane area ($A_{mem}$, $m^2$) required to obtain the desired permeate flux, the module cost of the membrane ($Q_{mem}$, \$/$m^2$), and the life span ($L_M$, years) of the membrane. The annualized pump cost ($Q_{AOpump}$, \$/$m^2$) was calculated as functions of the update factor ($I$), the labor factor ($L$), the construction material factor ($f_1$), the suction pressure correction factor ($f_2$), the feed concentration ($C$), and the trans-membrane pressure differential ($\Delta P$). The operating cost of the membrane plant was evaluated as a function of the power (energy, $E$, kW) required by the pump to provide necessary flow rate and trans-membrane pressure differential. Finally, the total annualized cost of the plant ($Q_{total}$) was evaluated as the sum of the cost of the membrane unit ($Q_{Amem}$), the cost of pump ($Q_{Apump}$), and the operating cost of the pump ($Q_{AOpump}$) and was a function of $C$, $\Delta P$, $\theta$, $Q_F$, $Q_{mem}$ where other parameters were assumed to be constant. In the present study, $Q_{total}$ were optimized as a single variable function of $\Delta P$ for feed oil concentration of 50 mg/L and varying steady feed flow rate of 1 to 100 $m^3$/day. Details of the other parameters used in this work are summarized in Table 2. Relevant update factors have been considered to report costs based on the prices of year 2008.

**Table 2.** Different design and operating parameters used for process optimization and economic analysis (20)

| Parameter | Values |
|---|---|
| Feed flow rate ($Q_F$, $m^3$/day) | 1 to 100 |
| Stage cut ratio ($\theta$) | 0.8 |
| Height between pump and membrane ($\Delta Z$, m) | 3 |
| Density of feed ($\rho_F$, Kg/$m^3$) | 1000 |
| Acceleration due to gravity ($g$, m/$s^2$) | 9.81 |
| Efficiency of pump ($\beta$) | 0.6 |
| Update factor ($I$) | 2.28 |
| Factor to adjust for pump construction material ($f_1$) | 1.5 |
| Factor to adjust for suction pressure range ($f_2$) | 1 |
| Factor used to incorporate labor costs ($L$) | 1.4 |
| Annual interest rate ($i$) | 0.1 |
| Membrane cost ($Q_M$, \$/$m^2$) | 400 |
| Membrane life ($L_M$, years) | 5 |
| Pump life ($L_P$, years) | 10 |
| Energy cost ($Q_E$, \$/kWh) | 0.1 |
| Diameter of pipe ($d_{pipe}$, m) | 0.05 |



## RESULTS AND DISCUSSION

### Characterization of the Membrane

#### SEM Analysis

Figure 4a shows the SEM image of the prepared membrane. The membrane shows a surface with highly porous, rough morphological structure. A superficial observation of the image indicates that the membrane did not have any defects such as pinholes and cracks. The maximum observable pore size of the surface is about 2.5 μm. Individual pore diameters of the membrane using ImageJ software (Version 1.40) was measured from these types of five images taken from randomly selected locations of the membrane and the average pore diameter and pore size distribution were evaluated. The area average pore diameter ($d_s$) from SEM analysis of the membrane was evaluated by assuming cylindrical porous texture of the membrane as

$$d_s = \left[ \frac{\sum_{i=1}^{n} n_i d_i^2}{\sum_{i=1}^{n} n_i} \right]^{0.5} \tag{22}$$

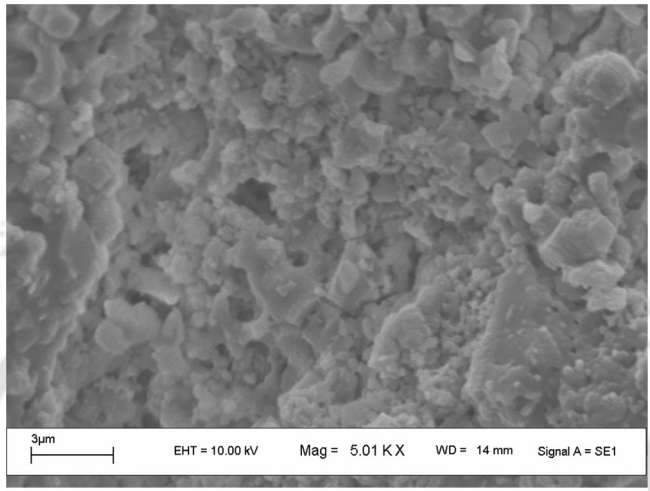


(a)

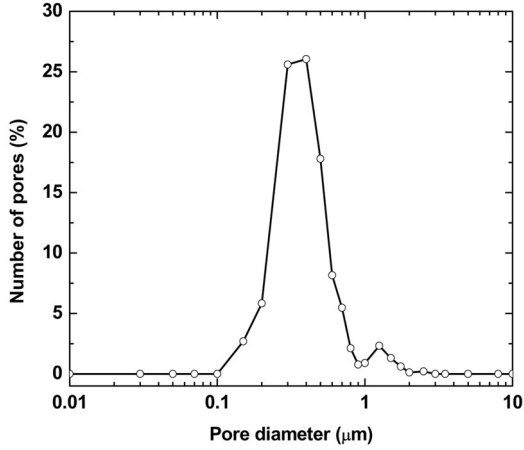


(b)

***Figure 4.*** (a) SEM image of the prepared membrane; (b) Pore size distribution of the prepared membrane obtained from the image analysis.

Where, $n$ is the number of pore, $d_i$ is the pore diameter (µm) of $i$th pore.

Figure 4b presents the pore size distribution summarizing the evaluated values of percentage pore numbers with respect to different pore diameters. The figure illustrates that about 50% of the pores had a pore diameter in the range of 0.3 to 0.5 µm. The maximum and

minimum pore sizes of the membrane were 2.5 μm (0.2%) and 0.15 μm (2.7 %). Average pore diameter of the membrane (calculated using Eq. (22)) was 0.55 μm.

## Hydraulic Permeability, Pore Diameter, and Resistance of the Membrane

The hydraulic permeability ($P_m$), pore diameter ($d_l$) and resistance of the membrane ($R_m$) were evaluated by assuming the presence of cylindrical pores in the membrane matrix using the following expressions (19)

$$PWF = \frac{Q}{S \cdot \Delta t} = P_m \cdot \Delta P \tag{23}$$

$$d_l = 2 \times \left[\frac{8 \times \mu \times l \times P_m}{\varepsilon}\right]^{0.5} \tag{24}$$

$$R_m = \frac{\Delta P}{PWF} \tag{25}$$

Where $PWF$ ($m^3\,m^{-2}\,s^{-1}$) is the liquid flux through the membrane, $\Delta P$ (kPa) is the trans-membrane pressure drop across the membrane, $\mu$ is the viscosity of water, $l$ is pore length, and $\varepsilon = (n \times \pi \times r_l^2)$ is the total porosity of the membrane. The porosity ($\varepsilon$) of the membrane determined by the pycnometric method using water as wetting liquid was 0.42. The hydraulic permeability of the membrane and corresponding membrane resistance determined from pure water permeation experiment was $1.94 \times 10^{-9}\,m^3/m^2.s.Pa$ and $5.78 \times 10^{11}\,m^2/m^3$. The hydraulic pore diameter calculated from PWF data using Eq. (24) was 0.7 μm which is slightly higher than the pore diameter calculated from SEM analysis. However, this type of deviation is always observed in membrane pore size determination using different techniques and the results are in good agreement with those reported in literature for kaolin-based membrane (8) as well as for polymeric membranes (13).

## Microfiltration of Oil-in-Water Emulsion

### Effect of Trans-Membrane Pressure and Feed Concentration on Permeate Flux

Figure 5 shows the permeate flux profiles for 50 mg/L crude oil feed concentration with respect to the permeation time for different

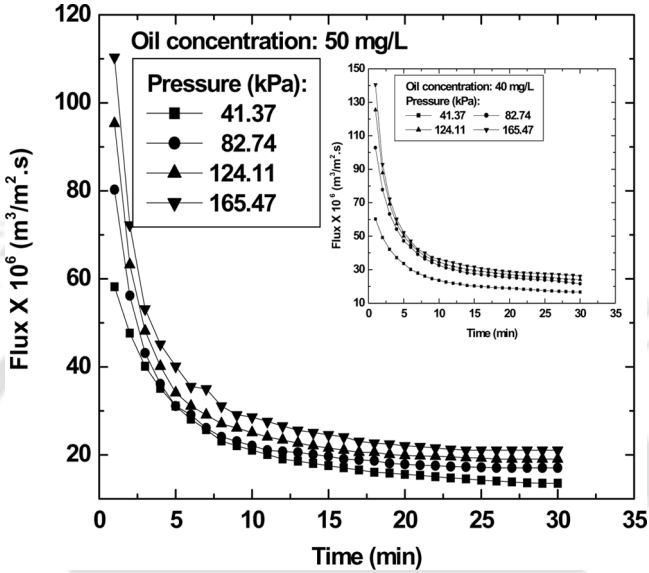


***Figure 5.*** Variation of permeate flux for with time at different trans-membrane pressure. Initial oil concentration: 50 mg/L.

trans-membrane pressure drop (41.37, 82.74, 124.11, and 165.47 kPa). From the figure, it was observed that the permeate flux declined sharply within the initial 10 to 15 minutes of operation and becomes gradual thereafter. The permeate flux decreases from $58.2 \times 10^{-6}$ to $13.6 \times 10^{-6}\,m^3/m^2 \cdot s$ within 30 minutes of experimental run at a trans-membrane pressure drop of 41.37 kPa. This decline in flux with time was due to pore blocking of the ceramic porous structure and formation of the thin oily film layer over the membrane surface. It is also observed that the permeate flux increases with increase in trans-membrane pressure. From the figure it may be observed that as the permeate flux increased from $58.2 \times 10^{-6}$ to $110.4 \times 10^{-6}\,m^3/m^2 \cdot s$ when $\Delta P$ was increased from 41.37 to 165.47 kPa. An increase in permeate flux with $\Delta P$ was due to the higher driving force across the membrane. Similar flux decline trends with trans-membrane pressure and operating time were also observed for 40 mg/L oil concentrations (inset of Fig. 5). The permeate flux was observed to increased with decrease in oil concentration. This was because of the fact that with an increase in feed concentration, adsorptive resistances as well as thin film hydraulic resistances increased and hence the permeate flux decreased.

## Effect of Trans-Membrane Pressure and Feed Concentration on Oil Rejection

Figure 6 shows the percent rejection of crude oil with time at four different trans-membrane pressure drops for a feed oil concentration of 50 mg/L. It can be observed from the figure that the rejection efficiency of the membrane slightly increased from 96.9 (5 minute) to 97.3% (30 minute) in the due course of MF test at $\Delta P$ of 41.37 kPa. Also, the rejection efficiency was observed to be slightly lower at 165.47 kPa (95.7 to 97%). Similar trends were also observed for oil concentrations of 40 mg/L where the rejection efficiency was varied from 94.9% (41.37 kPa, 5 min) to 95.8% (165.47 kPa, 30 min) studied in this work (inset of Fig. 6). A decrease in the oil rejection efficiency with a reduction in oil concentration was due to the lower droplet size of the oil at lower concentration. A reduction in the oil rejection efficiency with increase in $\Delta P$ is argued according to the hypothesis that higher pressures facilitate the enhancement of wetting and coalescence of oil droplets, thereby imposing some oil droplets to pass through the membrane pores and reach the permeate stream. The increase in oil-rejection efficiency with

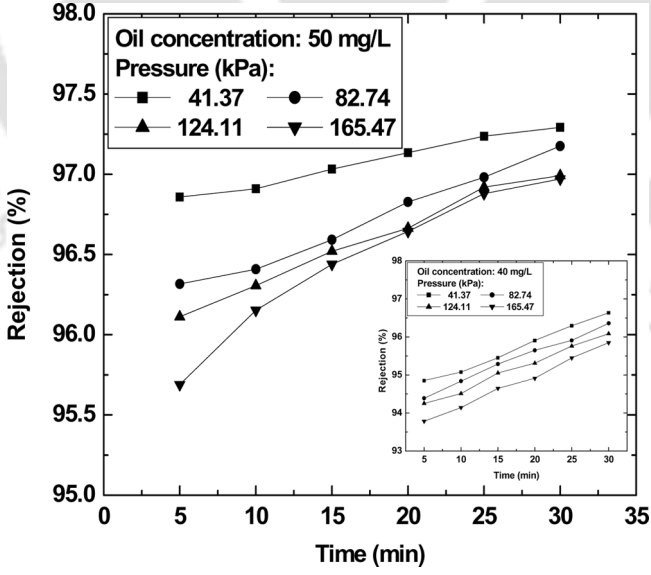


***Figure 6.*** Variation of oil rejection efficiency with time at different trans-membrane pressure. Initial oil concentration: 50 mg/L.

time was due to the reduction of the pore diameter of the membrane as a result of the adsorption of oil droplets in the membrane pores.

## Analysis of Membrane Fouling Mechanism

Figures 7 and 8 show the plot of different membrane pore blocking models for both initial oil concentrations (40 and 50 mg/L). The plots correspond to various models such as intermediate filtration ($J^{-1}$ vs. $t$ as outlined by (Eq. 7)), complete pore blocking ($\ln(J^{-1})$ vs. $t$ as outlined in Eq. (8)), standard pore blocking ( $J^{-0.5}$ vs. $t$ as outlined by Eq. (9)), and cake filtration models ($J^{-2}$ vs. $t$ as outlined in Eq. (10)). From these figures, it can be observed that the decline in permeate flux can be explained using cake filtration models as the plot of $J^{-2}$ vs. $t$ (Figs. 7d

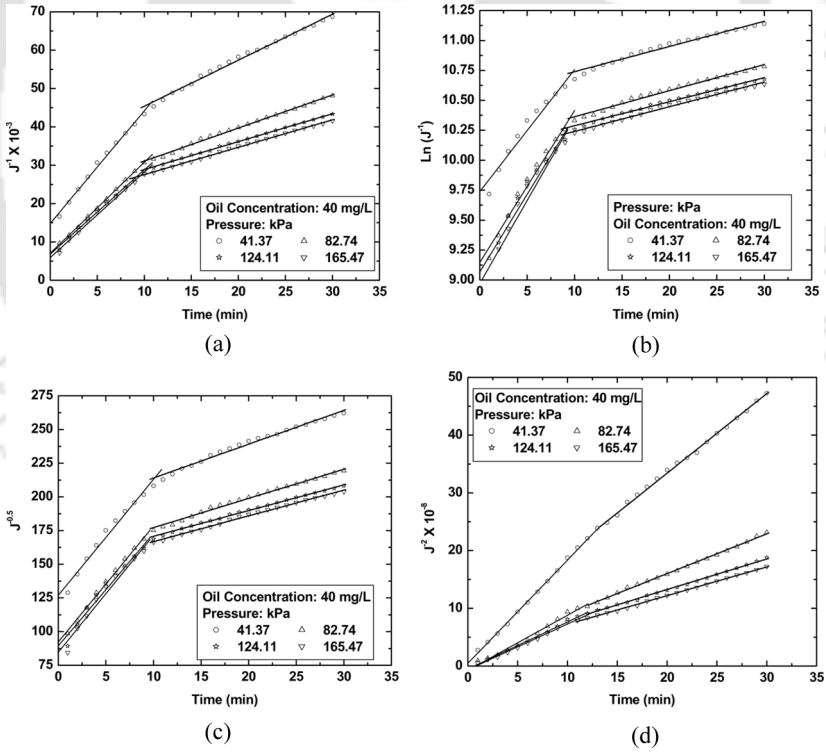


***Figure 7.*** Linear plot of permeate flux vs. time for different pore blocking models (7,19). Initial oil concentration: 40 mg/L. (a) $J^{-1}$ vs. $t$, (b) $\ln(J^{-1})$ vs. $t$, (c) $J^{-0.5}$ vs. $t$, (d) $J^{-2}$ vs. $t$.

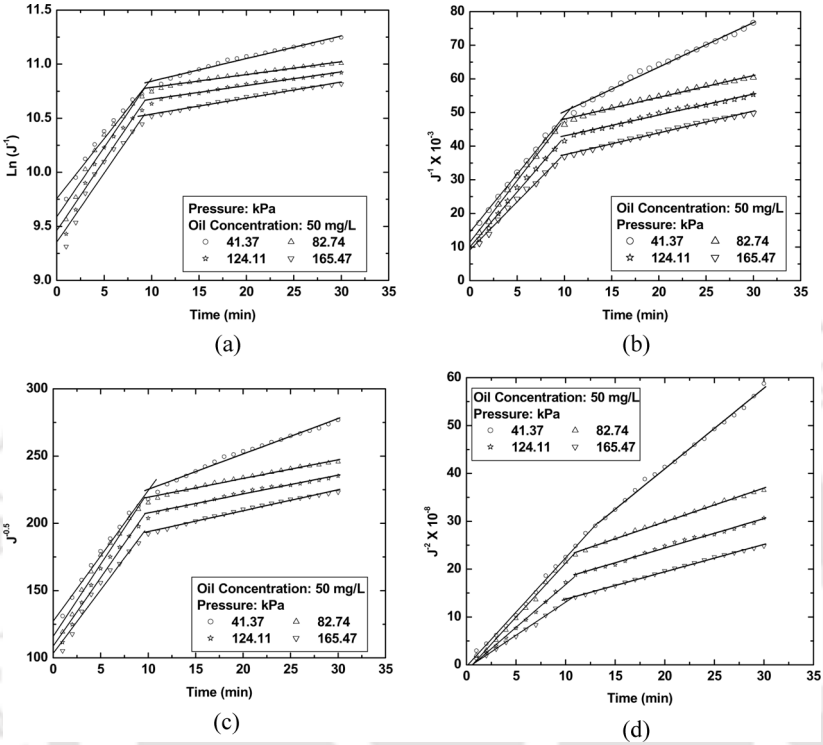


***Figure 8.*** Linear plot of permeate flux vs. time for different pore blocking models (7,19). Initial oil concentration: 50 mg/L. (a) $J^{-1}$ vs. $t$, (b) $\ln(J^{-1})$ vs. $t$, (c) $J^{-0.5}$ vs. $t$, (d) $J^{-2}$ vs. $t$.

and 8d) gives the best linear fitness. However, a careful observation of the plots indicates that, two different distinct filtration regimes of initial 10 minutes and the rest. It signifies that the flux decline with time occurs through two different pore blocking mechanisms. A similar type of result was also observed during MF of o/w emulsions with a polymeric membrane (17). Henceforth, the experimental flux data was further analyzed separately in the two time regimes, namely the initial regime (during the first 10 minutes of MF) and the later regime (10 to 30 minutes of MF) to identify the most competent combinations of models in both the regimes. Using the linear regression analysis the slope, intercept, as well as correlation coefficients of all the permeate flux data were calculated and summarized in Tables 3a, 3b, and 3c, respectively.

For the initial regime (during the first 10 minutes of MF), it can be critically observed in Table 3b that there exists a negative intercept for

**Table 3a.** Calculated values of slopes obtained from linear regression analysis of different membrane pore blocking models (Eqs. (7–10))

| Concentration of oil (mg/L) | Pressure (kPa) | Complete pore blocking ($k_b$) | | Standard pore blocking ($k_S$) | | Intermediate pore blocking ($k_i$) | | Cake filtration ($k_C$) $\times 10^{-7}$ | |
|---|---|---|---|---|---|---|---|---|---|
| | | Initial regime | Final regime | Initial regime | Final regime | Initial regime | Final regime | Initial regime | Final regime |
| 40 | 41.37 | 0.102 | 0.021 | 8.60 | 2.51 | 2940 | 1199 | 17.86 | 13.79 |
| | 82.74 | 0.127 | 0.022 | 8.59 | 2.16 | 2372 | 862 | 9.55 | 6.88 |
| | 124.11 | 0.129 | 0.020 | 8.34 | 1.91 | 2200 | 726 | 8.15 | 5.29 |
| | 165.47 | 0.138 | 0.021 | 8.67 | 1.91 | 2230 | 713 | 7.92 | 4.98 |
| 50 | 41.37 | 0.111 | 0.021 | 9.70 | 2.63 | 3447 | 1323 | 22.70 | 16.85 |
| | 82.74 | 0.129 | 0.012 | 10.73 | 0.39 | 3662 | 648 | 22.60 | 7.07 |
| | 124.11 | 0.130 | 0.013 | 10.18 | 1.40 | 3268 | 623 | 17.88 | 6.15 |
| | 165.47 | 0.128 | 0.015 | 9.44 | 1.55 | 2855 | 650 | 13.86 | 5.72 |

**Table 3b.** Calculated values of intercept obtained from linear regression analysis of different membrane pore blocking models (Eqs. (7–10))

| Concentration of oil (mg/L) | Pressure (kPa) | Complete pore blocking ($\ln(J_0^{-1})$) | | Standard pore blocking ($J_0^{-0.5}$) | | Intermediate pore blocking ($J_0^{-1}$) | | Cake filtration ($J_0^{-2}$) $\times 10^{-7}$ | |
|---|---|---|---|---|---|---|---|---|---|
| | | Initial regime | Final regime | Initial regime | Final regime | Initial regime | Final regime | Initial regime | Final regime |
| 40 | 41.37 | 9.738 | 10.529 | 126.92 | 188.93 | 14797 | 33402 | 4.84 | 58.28 |
| | 82.74 | 9.147 | 10.145 | 92.36 | 155.57 | 7054 | 22465 | −7.5 | 22.42 |
| | 124.11 | 9.067 | 10.087 | 89.41 | 151.65 | 6791 | 21624 | −5.12 | 26.56 |
| | 165.47 | 8.971 | 10.035 | 84.76 | 147.62 | 5909 | 20421 | −6.38 | 22.40 |
| 50 | 41.37 | 9.757 | 10.632 | 127.25 | 198.97 | 14458 | 37066 | 33.35 | 72.39 |
| | 82.74 | 9.588 | 10.666 | 115.95 | 205.59 | 11449 | 41562 | 13.33 | 157.27 |
| | 124.11 | 9.461 | 10.549 | 108.75 | 193.75 | 10038 | 36814 | 10.98 | 121.15 |
| | 165.47 | 9.354 | 10.390 | 103.35 | 178.33 | 9162 | 30920 | 7.6 | 79.95 |

**Table 3c.** Observed values of correlation coefficient ($R^2$) obtained linear regression analysis of permeate flux data for different membrane pore blocking models (Eqs. (7–10))

| Concentration of oil (mg/L) | Pressure (kPa) | Complete pore blocking | | Standard pore blocking | | Intermediate pore blocking | | Cake filtration | |
|---|---|---|---|---|---|---|---|---|---|
| | | Initial regime | Final regime | Initial regime | Final regime | Initial regime | Final regime | Initial regime | Final regime |
| 40 | 41.37 | 0.956 | 0.981 | 0.979 | 0.988 | 0.993 | 0.993 | 0.997 | 0.998 |
| | 82.74 | 0.978 | 0.987 | 0.995 | 0.993 | 0.999 | 0.996 | 0.978 | 0.998 |
| | 124.11 | 0.936 | 0.994 | 0.974 | 0.997 | 0.994 | 0.999 | 0.990 | 0.998 |
| | 165.47 | 0.930 | 0.991 | 0.971 | 0.995 | 0.993 | 0.998 | 0.991 | 0.999 |
| 50 | 41.37 | 0.963 | 0.980 | 0.984 | 0.987 | 0.995 | 0.992 | 0.992 | 0.997 |
| | 82.74 | 0.943 | 0.986 | 0.973 | 0.989 | 0.991 | 0.992 | 0.992 | 0.996 |
| | 124.11 | 0.943 | 0.984 | 0.974 | 0.987 | 0.993 | 0.989 | 0.994 | 0.993 |
| | 165.47 | 0.937 | 0.986 | 0.971 | 0.990 | 0.991 | 0.993 | 0.993 | 0.998 |

the cake filtration model. As the negative intercept values signify negative initial permeate flux, so this model cannot be applicable for the flux decline and henceforth is ignored in the subsequent analysis of flux decline for the initial regime. Further, it can be also observed in Table 3c for the same regime that the $R^2$ values for all other models (standard pore blocking, complete pore blocking, and intermediate pore blocking) is in appreciable range (0.95 to 0.99). To further analyze the applicability of various models, the percent error of experimental flux and predicted permeate flux using slope and intercept values for those models were calculated and analyzed. The percent error of the permeate flux was calculated using the standard equation as:

$$Error(\%) = \left(\frac{J_{Experimental} - J_{Calculated}}{J_{Experimental}}\right) \times 100 \qquad (26)$$

Figure 9a shows the result obtained from error analysis for experimental condition of 40 mg/L initial oil concentration and 124.11 kPa trans-membrane pressure drop. Based on the observations from Fig. 9a, it can be inferred that intermediate pore blocking model is the most appropriate model to account for the flux decline mechanism during the initial regime, with the lowest error (−0.0003 to 0.21%). Similar observations were also observed for other experimental conditions also.

Similarly, for the later regime (10 to 30 minutes of MF), it can be observed in Table 3b that none of the models indicate negative intercepts and hence $R^2$ and error analysis need to be conducted to evaluate the most appropriate model. Based on observed values of $R^2$ in Table 3c, it can be inferred that all the four models indicated good fitness ($R^2 > 0.99$). Figure 9b shows the result obtained from error analysis for experimental condition of 50 mg/L initial oil concentration and 82.74 kPa trans-membrane pressure drop. Based on the observations from Fig. 9b, it can be inferred that the cake filtration model is the most appropriate to represent the flux decline during the later regime (10 to 30 minutes of MF), with the lowest error (−0.11 to 1.16%). Therefore, based on the physical observation as well as the fitness of the cake filtration model, the thin layer of oil droplets formed during the membrane process can be conveniently represented using a cake layer model.

Figure 10 presents a parity plot between experimental and calculated flux based on the combinations of the two most appropriate models in the initial and later regimes. As shown, a good fitness between experimental and evaluated values is observed and henceforth, the suggested model combination is herewith inferred to be applicable for the analysis,

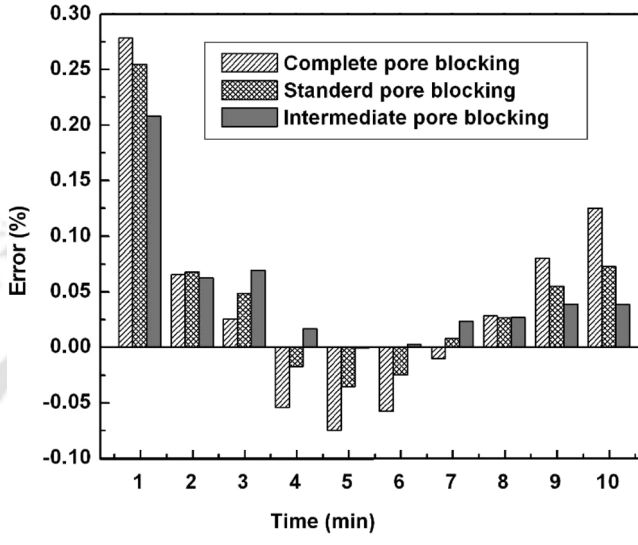


(a)

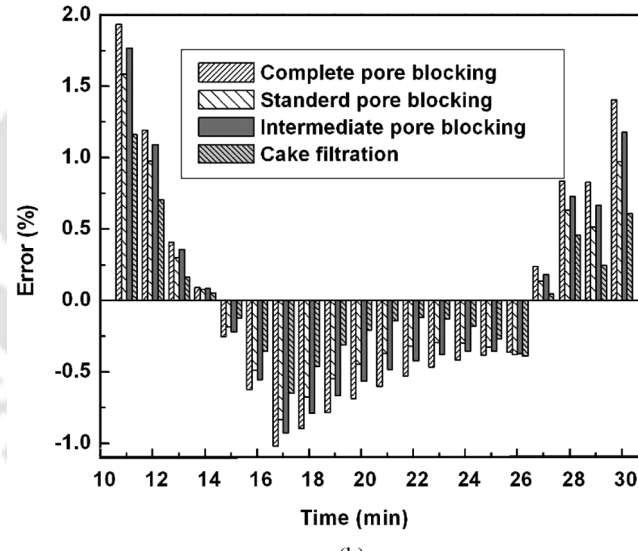


(b)

***Figure 9.*** (a) Variation of error (%) with time for the initial regime. Initial oil concentration: 40 mg/L and trans-membrane pressure: 124.11 kPa; (b) Variation of error (%) with time for the initial regime. Initial oil concentration: 50 mg/L and trans-membrane pressure: 82.74 kPa.

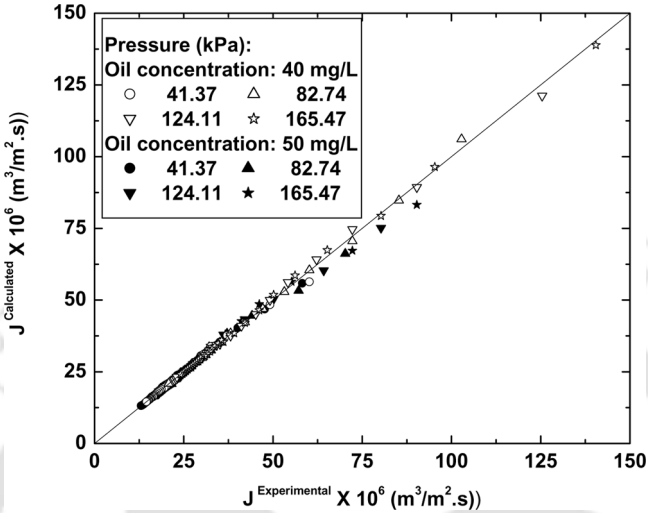


*Figure 10.* Parity plot of experimental and calculated permeate flux using combination of intermediate pore blocking and cake filtration model.

design, planning, and scheduling of time-dependent MF processes for oil-water emulsion separation in the process industries.

## Membrane Cost

The industrially competitive aspect of membrane technology lies in its cost. Based on the unit costs of raw materials used for preparing the inorganic membrane in this work (Table 4), the manufacturing cost of the inorganic membrane was evaluated to be 130 $/m$^2$. Including manufacturing and shipment costs, the average cost of the inorganic membrane for industrial applications based on bulk production methods would be closer to the value of 400 $/m$^2$. Contemporary elemental costs of various polymeric membranes and $\alpha$-alumina ceramic symmetric membrane varies form 50 to 200 $/m$^2$ (3) and 2000 to 4000 $/m$^2$ (4), respectively. Therefore, it can be inferred from the cost analysis that the inorganic membrane based on kaolin would be closer to the cost of the polymeric membranes deployed for industrial configurations (as retail cost is much higher than industrial production cost). However, the reported value of the membrane cost is conceptual in nature and may vary significantly depending on the fouling characteristics, on time performance, and

**Table 4.** Cost analysis of fabricated membrane from the unit cost of raw materials

| Material | Weight (gm) | Unit price ($/kg*) | Cost contribution ($/kg mixture) |
|---|---|---|---|
| Kaolin (PDF-01-089-6538) | 8 | 5 | 2 |
| Quartz ($SiO_2$) (PDF-01-075-0443) | 3 | 64 | 9.6 |
| Calcium carbonate ($CaCO_3$) | 5 | 4.2 | 1.05 |
| Sodium carbonate ($Na_2CO_3$) | 2 | 4.6 | 0.46 |
| Boric acid ($H_3BO_3$) | 1 | 5.6 | 0.28 |
| Sodium metasilicate ($Na_2SiO_3 \cdot 9H_2O$) | 1 | 8.4 | 0.42 |
| Water | 7 | – | |
| Total 50 numbers of membranes with surface area of 0.108 $m^2$ (0.02 kg dry mixture/membrane of 4.5 mm thickness and 52.5 mm diameter). So the cost of the membrane is 13.81 $/0.108 $m^2 \approx 130$ $/$m^2$ | | | 13.81 ($/kg dry mixture) |

*Prices taken from the catalog of the corresponding company as mentioned in experimental section.

long-term stability of the ceramic membrane in particular process applications.

## Economic Feasibility

Table 5 presents a variation of the total optimum cost for the treatment of o/w emulsions with feed oil concentration 50 mg/L for varying feed rate. The module cost of cheaper inorganic membrane (including module and installed costs) reported in this work was taken as 400 $/$m^2$ with an

**Table 5.** Cost contribution of the pump, membrane and operating cost with respect to total cost of the process for different feed rate

| Feed ($m^3$/day) | Operating pressure (kPa) | Total cost ($/$m^3$ feed) | Cost contribution (%) | | |
|---|---|---|---|---|---|
| | | | Pump | Membrane | Operating |
| 1 | 66.43 | 0.425 | 44.60 | 54.37 | 1.03 |
| 10 | 119.05 | 0.189 | 30.89 | 65.52 | 3.60 |
| 25 | 139.46 | 0.143 | 24.85 | 69.74 | 5.41 |
| 50 | 151.37 | 0.118 | 20.42 | 72.55 | 7.03 |
| 100 | 159.05 | 0.098 | 16.32 | 74.90 | 8.78 |

assumption that the overall membrane cost would be higher than the materials cost of 130 $/m$^2$. As the ceramic membrane offers excellent chemical and fouling resistance, the life span of the membrane was assumed to be 5 years. Permeate flux data after 30 minutes of experimental run were assumed as steady the permeate flux ($J_{ss}$). Subsequently, $J_{ss}$ was observed to vary linearly with operating pressure and a suitable correlation for both feed oil concentrations were developed and used in Eq. (11) for the evaluation of the required membrane area ($A_{mem}$). In addition, optimization methodology using a genetic algorithm was applied to yield optimal combinations of the membrane area and the pressure differential ($\Delta P$).

From Table 5, it can be inferred that the total annualized cost for the treatment of 100 $m^3$/day feed rate will be around 0.098 $/$m^3$ feed with the optimal operating pressure of 159.05 kPa. Further, it can also be observed that with an increase in the feed capacity (from 1 to 100 $m^3$/day), the cost contribution due to the pump to the overall cost reduced from 44.6 to 16.32% whereas the cost of the membrane increased from 54.37 to 74.9%. The lower contribution of the pump cost to the overall cost is anticipated due to lower optimal trans-membrane pressure differentials for the chosen case. The increase in the operating cost of the plant was observed to be insignificant when compared to the fixed costs of the membrane and pump. A further reduction in the membrane process system cost is anticipated, as the existing steady-state data were based on the dead end MF and not the cross-flow mode of operation. Therefore, based on these observations, it can be inferred that the ceramic membrane based process systems appear to be promising for industrial scale application.

## CONCLUSIONS

This work reports an inexpensive ceramic precursor formulation utilizing locally available low-cost inorganic raw materials such as kaolin, quartz, calcium carbonate, sodium carbonate, boric acid, and sodium metasilicate. The average pore size of the prepared ceramic membrane was 0.55 μm with a total porosity of 42%. Based on the retail price of raw materials cost of membranes was estimated to be 130 $/$m^2$. The membrane shows 97.3% oil rejection efficiency with $13.6 \times 10^{-6}$ $m^3/m^2 \cdot s$ permeate flux after 30 min of experimental run at 41.37 kPa trans-membrane pressure and 50 mg/L oil concentration. A decline in the permeate flux has been analyzed using different pore blocking models. A decrease in the permeate flux was initially due to (1 to 10 minute) intermediate pore blocking and later (10 to 30 minute) due to

cake filtration. Process economics studies for a single stage membrane permeation unit infers that the total optimal cost of the membrane permeation unit was estimated to be 0.098 $/m$^3$ feed for processing 100 m$^3$/day feed of 50 mg/L feed oil concentration and was dominated by the membrane cost. Henceforth, the newly prepared ceramic membrane is suggested for application in oily wastewater treatment using suitable MF/UF techniques.

## REFERENCES


1. Bevis, A. (1992) The treatment of oily water by coalescing. *Filtr. Sep.*, 295.
2. Cheryan, M.; Rajagopalan, N. (1998) Membrane processing of oily streams. Wastewater treatment and waste reduction. *J. Membr. Sci.*, *151*: 13.
3. Cheryan, M. (1998) *Ultrafiltration and microfiltration handbook*; Techno. Pub. Co. Inc.
4. Tennison, S. (2000) Current hurdles in the commercial development of inorganic membrane reactors. *Membrane Technology*, *2000* (128): 4.
5. Das, R.; Dutta, B. K. (1999) Permeation and separation characteristics of supported alumina and titania membranes. *Sep. Sci. Technol.*, *34* (4): 609.
6. Saffaj, N.; Persin, M.; Younsi, S.A.; Albizane, A.; Cretin, M.; Larbot, A. (2006) Elaboration and characterization of micro-filtration and ultra-filtration membranes deposited on raw support prepared from natural Moroccan clay: Application to filtration of solution containing dyes and salts. *Appl. Clay Sci.*, *31*: 110.
7. Belouatek, A.; Benderdouche, N.; Addou, A.; Ouagued, A.; Bettahar, N. (2005) Preparation of inorganic supports for liquid waste treatment. *Micropor. and Mesopor. Mater.*, *85*: 163.
8. Almandoza, M.C.; Marchese, J.; Prádanos, P.; Palacio, L.; Hernández, A. (2004) Preparation and characterization of non-supported micro-filtration membranes from aluminosilicates. *J. Membr. Sci.*, *241*: 95.
9. Gryta, M.; Karakulski, K. (1999) The application of membrane distillation for the concentration of oil-water emulsions. *Desalination*, *121*: 23.
10. Chakrabarty, B.; Ghoshal, A.K.; Purkait, M.K. (2008) Ultrafiltration of stable oil-in-water emulsion by polysulfone membrane. *J. Membr. Sci.*, *325*: 427.
11. Reed, J.S. (1995) *Principles of Ceramics Processing*; John Wiley & Sons: NewYork.
12. Wang, M.C.; Wu, N.C.; Hon, M.H. (1994) Preparation of nepheline glass-ceramics dental porcelain. *Materials Chemistry and Physics*, *37*: 370.
13. Chakrabarty, B.; Ghoshal, A.K.; Purkait, M.K. (2008) SEM analysis and gas permeability test to characterize polysulfone membrane prepared with polyethylene glycol as additive. *J. Colloid Interf. Sci.*, *320*: 245.

14. Kandwal, V.C.; Agrawal, K.M.; Nautiyal, S.P.; Khan, H.U. (2000) Paraffin deposition and viscosity temperature behaviour of Assam crude oil. *Petro. Sci. Technol.*, *18*: 755.
15. Huotari, H.M.; Huisman, I.; Tragardh, H.G. (1999) Electrically enhanced crossflow membrane filtration of oily waste water using the membrane as a cathode. *J. Membr. Sci.*, *156*: 49.
16. Hermia, J. (1982) Constant pressure blocking filtration laws–Application to power-law non-newtonian fluids. *Trans. Inst. Chem. Eng.*, *60*: 183.
17. Hu, B.; Scott, K. (2008) Microfiltration of water in oil emulsions and evaluation of fouling mechanism. *Chem. Eng. J.*, *136*: 210.
18. Sethi, S.; Wiesner, M.R. (2000) Simulated cost comparisons of hollow-fiber and integrated nanofiltration configurations. *Wat. Res.*, *34*: 2589.
19. Mulder, M. (1991) *Basic Principles of Membrane Technology*; Kluwer Academic Publishers: Dordrecht.

Journal of Food Engineering 95 (2009) 597–605

Contents lists available at ScienceDirect

Journal of Food Engineering

journal homepage: www.elsevier.com/locate/jfoodeng

# Microfiltration of mosambi juice using low cost ceramic membrane

B.K. Nandi, B. Das, R. Uppaluri *, M.K. Purkait *

*Department of Chemical Engineering, Indian Institute of Technology Guwahati, Guwahati 781039, Assam, India*

ARTICLE INFO

*Article history:*
Received 16 April 2009
Received in revised form 5 June 2009
Accepted 14 June 2009
Available online 21 June 2009

*Keywords:*
Mosambi
Ceramic membrane
Microfiltration
Pore blocking model
Low cost

ABSTRACT

This work reports on microfiltration (MF) studies of mosambi juice using low cost ceramic membrane prepared from locally available inorganic precursors. Characterization of the prepared membrane was done by SEM analysis, porosity determination and pure water permeation experiments. The average pore diameter, total porosity and hydraulic resistance of the membrane were evaluated as 0.285 μm, 23.6% and $9.26 \times 10^{11}$ $m^2/m^3$, respectively. Dead-end MF experiments were performed for both centrifuged mosambi juice (CJ) and enzyme treated centrifuged mosambi juice (ETCJ). It was observed that after MF, important properties like TSS, pH, acidity and density of both CJ and ETCJ were almost unaffected. However, significant improvement in juice colour, clarity and AIS was observed. It was also observed that the clarified juice can be stored in refrigerated condition for more than 30 days without significant change in juice quality. Different membrane pore blocking models were used to analyze the observed permeate flux decline.



## 1. Introduction

Ultrafiltration (UF) and microfiltration (MF) of mosambi (Sarkar et al., 2008; Rai et al., 2005a,b, 2006), orange (Lister et al., 1994), lemon (Espamer et al., 2006), grape (Bailey et al., 2000), apple (Youn et al., 2004; Yu and Lencki, 2004; Vladisavljevic et al., 2003), carrot (Cassano et al., 2003), water melon (Chhaya et al., 2008; Vaillant et al., 2005), blood orange (Cassano et al., 2007) and pineapple (Carvalho et al., 2008) juice had been studied by many investigators. Amongst several beverage processing sectors, citrus fruits constituting orange, lemon, pineapple and mosambi are prominent due to their wider availability, low cost as well as high nutrition value to human health. Citrus fruits primarily constitute both lower molecular weight compounds (such as sugar, acid, salt, flavor, aroma compounds, etc.) as well as higher molecular weight polysaccharides (such as pectic material cellulose, hemicellulose, etc.) in addition to haze causing proteins and microorganisms. The presence of pectic material and protein in fruit juice is responsible for cloudiness and post bottling haze formation as well as their fermentation during long storage (Cheryan, 1998). The objective of clarification of fruit juice using membrane filtration is to eliminate the high molecular weight pectic material and its derivatives and retain low molecular weight solutes (valuable for human health) such as sucrose, acid, salt, aroma and flavor compounds in the clarified juice (Cheryan, 1998).

Recently, much work has been reported with respect to the clarification of citrus fruits using membrane technology. Rai et al. (2004) identified optimal conditions (pectinase concentration: 0.0004 w/v%, heating temperature: 42 °C, duration: 100 min,) for enzymatic treatment of mosambi juice. Amongst several treatment methods, the authors indicated that, enzymatic treatment followed by bentonite addition provided the highest permeate flux (23 L/$m^2$ h at 414 kPa and 1200 rpm in a stirred cell) using 50,000 molecular weight cut-off polyamide (polymeric) membranes. Cassano et al. (2007) conducted UF of blood orange juice using commercial tubular polyvinylidenefluoride (PVDF) membranes. They observed that with an increase in operating temperature from 21 °C to 25 °C, 12% increase in permeate flux occurred. Recently, Sarkar et al. (2008) studied electric field assisted UF of mosambi juice using polyethersulfone membranes. They observed that the application of electric field reduced membrane fouling and increased permeate flux without significant change in juice quality.

A critical insight into the above literatures infers that mainly polymeric membranes have been studied for mosambi juice and other citrus juice clarification studies. This is due to the fact that polymeric membranes are inexpensive in comparison with the ceramic membrane and are very easy to use. However, the major drawback of polymeric membrane is their low corrosion resistance in acidic media and hence they possess lesser life cycle times for juice processing applications. For any industrial application, the lifespan of membrane is always a major issue. Many varieties of fruit juices are acidic in nature with pH in the range of 3–5. Henceforth, though experimental studies indicate the successful applicability of polymeric membranes for juice processing applications, industrialization of membrane technology for juice processing

* Corresponding authors. Tel.: +91 361 2582260/2582262; fax: +91 361 2582291.
*E-mail addresses:* ramgopalu@iitg.ernet.in (R. Uppaluri), mihir@iitg.ernet.in (M.K. Purkait).

0260-8774/$ - see front matter © 2009 Elsevier Ltd. All rights reserved.
doi:10.1016/j.jfoodeng.2009.06.024

**List of symbols**

| | | | |
|---|---|---|---|
| $J$ | permeate flux ($m^3/m^2$ s) | $\Delta P$ | trans-membrane pressure (kPa) |
| $J_0$ | initial permeate flux ($m^3/m^2$ s) | $Q$ | volume of permeate ($m^3$) |
| $k_b$ | complete blocking model constant (Eq. (2)) ($s^{-1}$) | $R^2$ | square of correlation coefficient (dimension less) |
| $k_c$ | cake filtration model constant (Eq. (5)) ($s.m^{-2}$) | $R_m$ | intrinsic membrane resistance ($m^2/m^3$) |
| $k_C^{CJ}$ | cake filtration model constant for centrifuged juice (Eq. (6)) (s $m^{-2}$) | $R_t^0$ | instantaneous total resistance of the membrane during MF ($m^2/m^3$) |
| $k_C^{ETCJ}$ | cake filtration model constant for enzyme treated centrifuged juice (Eq. (7)) (s $m^{-2}$) | $R_f^0$ | instantaneous fouling resistance of the membrane during MF ($m^2/m^3$) |
| $k_i$ | intermediate pore blocking model constant (Eq. (4)) ($m^{-1}$) | $S$ | permeable area of membrane ($m^2$) |
| $k_s$ | standard pore blocking model constant (Eq. (3)) ($m^{-0.5}$ $s^{-0.5}$) | $T$ | sampling time (s) |
| | | $\mu_p$ | viscosity of permeate (kPa s) |

has not been promising so far. For these circumstances, the usage of ceramic membranes with high corrosion resistance in both acidic as well as basic media is rendered to be more beneficial, especially in the citrus juice sector. One of the striking limitations of ceramic membranes is their higher cost (1600 $/m^2$) in comparison with the polymeric membranes (50–200 $/m^2$ (Cheryan, 1998)). The higher cost of ceramic membranes is due to the utilization of expensive inorganic precursors such as alumina and zirconia and higher sintering temperature (more than 1100 °C) during membrane fabrication. Therefore, the development of low cost ceramic membranes is envisaged by utilizing low cost inorganic precursors and lower sintering temperatures. Also, to the best of our knowledge the applicability of low cost ceramic membranes for the clarification (MF) of mosambi juice has not been studied till date.

In this work, low cost ceramic membrane has been prepared using different low cost inorganic precursors such as kaolin, quartz, feldspar, sodium carbonate, boric acid and sodium metasilicate. Structural, morphological and pure water flux (PWF) studies of the prepared membrane were carried out to evaluate the general characteristics of the fabricated ceramic membrane. Dead-end MF of centrifuged mosambi juice (CJ) as well as enzyme treated mosambi juice (ETCJ) was carried out using the prepared membrane. The effect of enzyme treatment on the permeate flux as well as permeate quality and stability for long term storage of the clarified mosambi juice was also investigated. Different physio-chemical properties of the juice such as colour, clarity, pH, citric acid content, total soluble solid (TSS), alcohol insoluble solid (AIS) were measured before and after the MF experiments to study the effect of clarification on the properties of juice. Different membrane pore blocking models are used to identify the most prominent flux decline mechanism. Finally, the stability of the clarified juice for long term storage was studied by keeping the clarified juices up to 30 days in refrigerated condition.

## 2. Experimental

### 2.1. Preparation of ceramic membrane

The ceramic membrane was prepared using kaolin (CDH, India), quartz (Research Lab Fine Chem Industry, India), Feldspar (National Chemicals, India), sodium carbonate (Merck India), boric acid (Merck India) and sodium metasilicate (SD Fine Chem Ltd, India) as raw materials. All raw materials used for membrane fabrication were graded at least 99.5% pure and were used without any further purification. For the membrane preparation kaolin (10 g), quartz (3 g), feldspar (3 g), sodium carbonate (2 g), boric acid (1 g) and sodium metasilicate (1 g) were mixed with 7 g of distilled water to yield a paste. The paste was then molded in the form of a circular disk on a gypsum surface by using a stainless steel 316 ring of 55 mm internal diameter and 5 mm thickness. Then the disk type mold was dried at room temperature for 24 h, at 100 °C for 12 h and at 250 °C for 24 h for complete removal of loose moisture. Subsequently, the membrane was sintered at 900 °C for 5 h with a heating rate of 2 °C per minute. After sintering, membrane becomes hard, rigid and porous texture. Eventually, the membrane was polished with silicon carbide abrasive paper (C-220) to obtain a smooth, flat membrane of diameter 52.5 mm and thickness 4.5 mm. Finally, the membrane was cleaned in a sonicator for 15 min to remove loose particles from the membrane and dried at 120 °C. The cost of the prepared membrane was calculated using laboratory scale retail price of the precursors. An estimated cost of 220 $/m^2$ was obtained from this calculation. However, considering other issues such as scale of fabrication and bulk prices of the commodities, the membrane cost is anticipated to reduce further and reach similar values (50–200 $/m^2$) to that of the polymeric membranes. Further, details on the fabrication method and laboratory scale retail prices of raw materials were summarized elsewhere (Nandi et al., 2008).

### 2.2. Preparation of mosambi juice

Mosambi fruits (sweet orange, *Citrus sinensis* (*L.*) *Osbeck*) of proper maturity and ripeness were purchased from the local market and used for juice extraction. The juice was extracted from depulped fruits in a manually operated screw type juice extractor. Pectinase (SRL, India) with activity 3.5 units/mg (proteins Lowry) was used for enzymatic treatment of mosambi juice. The extracted juice was centrifuged (Make: Eltek, Model: TC 8100 D, India) at 4000 rpm for 20 min to prepare the centrifuged juice (CJ). The enzyme treated centrifuged juice (ETCJ) was prepared by pretreatment of mosambi juice with pectinase followed by centrifugation at 4000 rpm for 20 min. The centrifugation speed and duration was determined from a trial and error method to remove maximum amount of suspended solids from the juice (highest clarity and minimum colour. The enzymatic pretreatment of the juice was carried out by heating the juice at 42 °C temperature for 100 min with enzyme concentration of 0.0004 w/v%. Subsequently, the suspension was heated to 90 °C for 5 min in a water bath to inactivate the remaining enzyme in the juice. Finally, the juice was cooled to ambient temperature (25 °C) and centrifuged at 4000 rpm for 20 min.

### 2.3. Microfiltration studies

Dead-end MF experiments were carried out in a membrane permeation cell of capacity 300 ml with varying trans-membrane pressure drops of 137.9, 206.8, 275.8 and 344.7 kPa for both CJ

and ETCJ. The experimental setup (Fig. 1) consisted of a stainless steel tubular cell with a flat circular stainless steel base plate which holds the membrane housing. The membrane was placed on a stainless steel casing and sealed with epoxy resin and then place in the membrane housing provided on the base plate. The membrane diameter was $5.25 \times 10^{-2}$ m and effective membrane area was $1.66 \times 10^{-3}$ m$^2$. The cell was pressurized with compressed air. Before using each fresh membrane, compaction of membrane was performed using deionised water at a trans-membrane pressure of 414 kPa (which is higher than the maximum operating pressure for the set of experiments conducted). During compaction, the pure water flux was observed to be high initially and reduced to the steady value after two hours of operation. Permeate flux and intrinsic membrane resistance of the membrane was determined using standard equation:

$$J = \frac{Q}{S \cdot \Delta t} = \frac{\Delta P}{\mu_p \cdot R_m} \quad (1)$$

After each MF experiment, cleaning of the membrane was carried out to regain the membrane permeability. After MF experiment, a thick gel layer was observed over the membrane surface. For cleaning of the membrane, the SS casing containing the membrane was removed from the set up. Then the membrane surface was cleaned with soft nylon brush and washed with tap water. Subsequently, the membrane was kept in a sonicator for 15 min to remove loose particles inside the membrane pores. Finally, the membrane was fixed in the experimental set up and 50 mL alkaline solution (0.02 N NaOH) was passed through the membrane at 137.90 kPa. After this cleaning procedure, it was observed that the membrane regained more than 98% of pure water flux of the fresh membrane.

### 2.4. Analytical methods

Particle size distributions of fresh juice (FJ), CJ and ETCJ samples were measured using a laser particle size analyzer (Make: Malvern; Model: Mastersizer 2000, UK). All juice samples (FJ, CJ, ETCJ and permeate of CJ, ETCJ) were analyzed for colour, clarity, soluble solids, pH, acidity, viscosity, density and alcohol insoluble solids (AIS). Colour and clarity of the juice were evaluated by measuring the absorbance at 420 nm and transmittance at 660 nm, respectively using a UV/Vis spectrophotometer (Make: Perkin Elmer Precisel; Model: Lambda 35, USA) (Rai et al., 2006). TSS was determined (in °Brix) using a digital refractometer (Make: Atago; Model: DR-A1, India). The pH of the samples was measured using a water and soil analysis kit (Make: VSI Electronics, Model: VSI-06D1, India). Acidity measurements were carried out by titrating 10 mL of the juice sample with 0.1 N NaOH until the solution pH reaches to 8.2 and expressed as wt% anhydrous citric acid equivalent. Viscosity of the juice samples was measured using a glass Oswald capillary viscometer (Make: Pisco: Model: D 30797, India). The density was measured using 25 mL pycnometer. AIS were used as a measure of pectic material in the juice and AIS were measured by mixing 20 g juice with 300 mL of 80% methanol solution and simmering for 30 min. Subsequently, the solution was filtered and the residue was again washed with 80% alcohol solution followed by drying at 100 °C for 2 h. After drying, the final residue was weighed and expressed as AIS in wt% (Hart and Fisher, 1971).

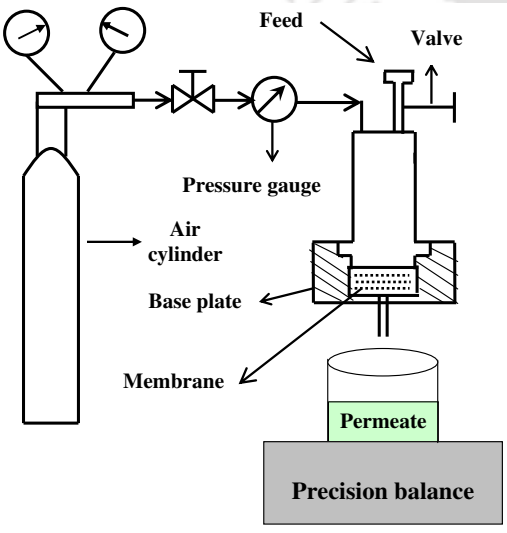


**Fig. 1.** Schematic of experimental setup for the microfiltration experiments.

## 3. Theory of membrane fouling mechanism

Hermia (1982) proposed four empirical models to present membrane fouling mechanisms in dead-end filtration based on constant pressure: complete pore blocking, standard pore blocking, intermediate pore blocking and cake filtration. Complete pore blocking occurs when the sizes of the solute particles are greater than the size of the membrane pores. As a result pore blocking occurs over the membrane surface and not inside the membrane pores. Standard pore blocking hypothesizes that the particles enter the membrane pores and deposit over the pore walls due to the irregularity of pore passages, thereby reducing the membrane pore volume. This type of fouling is caused by particles smaller than the membrane pore size and pore blocking occurs inside the membrane pores. Thereby, the volumes of membrane pores decrease proportionally to the filtered permeate volume. Intermediate blocking occurs when the solute particle size is similar to the membrane pore size. In this model, it is assumed that a membrane pore is not necessarily blocked by the solute molecules and some particles may settle over others. Therefore, the non-blocked membrane surface area diminished with time and some molecules are expected to obstruct the membrane pore entrance without blocking the pore completely. Cake filtration corresponds to a scenario where particles larger than the average pore size accumulate on the membrane surface thus forming a "cake". Thereby, the cake grows with time and provides an additional porous barrier (and hence hydraulic resistance) to the permeating liquid. Various pore blocking models can be represented using the following linearized expressions as:

$$\text{(a) Complete pore blocking : } \ln(J^{-1}) = \ln(J_0^{-1}) + k_b t \quad (2)$$

$$\text{(b) Standard pore blocking : } J^{-0.5} = J_0^{-0.5} + k_s t \quad (3)$$

$$\text{(c) Intermediate pore blocking : } J^{-1} = J_0^{-1} + k_i t \quad (4)$$

$$\text{(d) Cake filtration : } J^{-2} = J_0^{-2} + k_c t \quad (5)$$

Therefore, a plot of $\ln(J^{-1})$ vs. $t$, $J^{-0.5}$ vs. $t$, $J^{-1}$ vs. $t$ and $J^{-2}$ vs. $t$ shall be a straight line with slope of $k_b$, $k_s$, $k_i$ and $k_c$, with y-intercept of $\ln(J_0^{-1})$, $J_0^{-0.5}$, $J_0^{-1}$ and $J_0^{-2}$ for complete pore blocking, standard pore blocking, intermediate pore blocking and cake filtration model, respectively. The appropriate fitness and competence of various fouling models can be confirmed by comparing the values of coefficient of correlation ($R^2$) obtained from the linear regression analysis.

## 4. Results and discussion

### 4.1. Characterization of the membrane

The prepared membrane was characterized using scanning electron microscopy (SEM) analysis, total porosity determination

and hydraulic permeability determination using pure water permeation through the membrane. Table 1 summarizes the different properties of the membrane. SEM analysis (Make: Oxford; Model: LEO 1430VP, UK) was carried out to analyze the presence of possible defects on the membrane surface and estimate the membrane pore size. Fig. 2 shows the SEM image of the prepared membrane. The membrane shows a surface with highly porous, rough morphological structure. A critical observation of the image indicates that the membrane did not have any defects such as pinholes and cracks. The maximum observable pore size of the surface was about 2 μm. Individual pore diameters of the membrane was measured using ImageJ software (Version 1.40) for the determination of average pore diameter and pore size distribution. For this, five images taken from randomly selected locations of the membrane were used. The area average pore diameter ($d_s$) from SEM analysis of the membrane was evaluated by assuming cylindrical porous texture of the membrane as 0.285 μm. The open porosity of the membrane was evaluated using Archimedes method with water as the wetting liquid. Estimated value of total porosity was 23.6%. Intrinsic membrane resistance ($R_m$) was calculated as $9.26 \times 10^{11}$ m$^2$/m$^3$ from the pure water flux (PWF) permeation experiments and were calculated using Eq. (1). Further details with respect to the characterization techniques were discussed elsewhere (Nandi et al., 2008).

### 4.2. Particle size distribution

Fig. 3 shows the particle size distribution of fresh juice (FJ), centrifuged juice (CJ) and enzyme treated centrifuged juice (ETCJ). As indicated by the profiles, a multimodal distribution of suspended particles and pectic materials was apparent for all juice categories. For FJ, bimodal distribution was observed. About 30% particles were observed to possess particle sizes between 0.038 and 8.15 μm and about 70% particles within the range of 21.43–590.25 μm. The average particle size of FJ sample was evaluated to be 170 μm. During centrifugation, particles with bigger sized (21.43–590.25 μm) were completely removed as the particle sizes ranging from 21.43 to 590.25 μm are not visible in the particle size distribution profiles corresponding to both CJ and ETCJ. Also, the observed particle size distributions for CJ and ETCJ indicate that some smaller sized particles were removed during centrifugation. This may be due to the agglomeration of the smaller particles to form bigger particles that are removed during centrifugation.

The average particle size for CJ was evaluated as 0.818 μm with 17.15% of the particles within the range 1.78–8.15 μm and 71.66% of the particles within the range 0.038–0.39 μm. After enzyme treatment, volume of particles between 1.78 and 8.15 μm reduced to 4.5% and particles ranging 0.038–0.39 μm increased to 86.02% (as observed from ETCJ profile). This was due to the hydrolysis of pectic molecules by the enzyme that facilitates splitting of bigger particles to yield smaller particles. As a result, the average particle size of ETCJ reduced to 0.365 μm. With regards to the average pore diameter of the membrane (0.285 μm) it is worthy to note that the average particle size of CJ and ETCJ samples is higher than the average membrane pore size. Therefore, it is expected that the membrane would remove almost all the pectic materials of CJ and ETCJ during MF.

**Table 1**
Properties of used ceramic membrane.

| Properties | Value |
|---|---|
| Membrane permeable area (m$^2$) | $1.66 \times 10^{-3}$ |
| Thickness (m) | $4.5 \times 10^{-3}$ |
| Average pore diameter from SEM analysis (μm) | 0.285 |
| Percent pores with pore diameters between 0.1 and 0.3 μm (From SEM analysis) | 82.67 |
| Hydraulic pore diameter (μm) | 0.51 |
| Intrinsic membrane resistance, $R_m$ (m$^2$/m$^3$) | $9.26 \times 10^{11}$ |
| Total porosity | 23.6% |

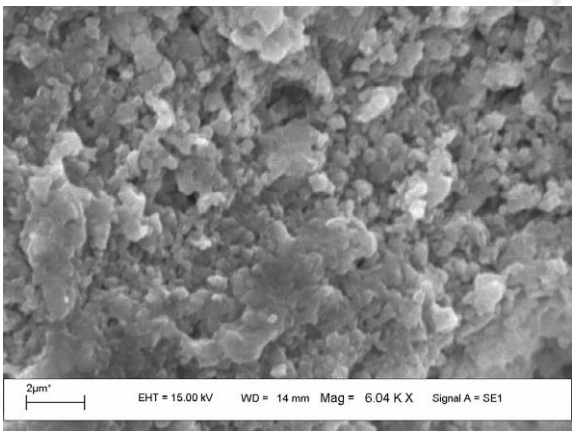


**Fig. 2.** SEM image of the prepared ceramic membrane.

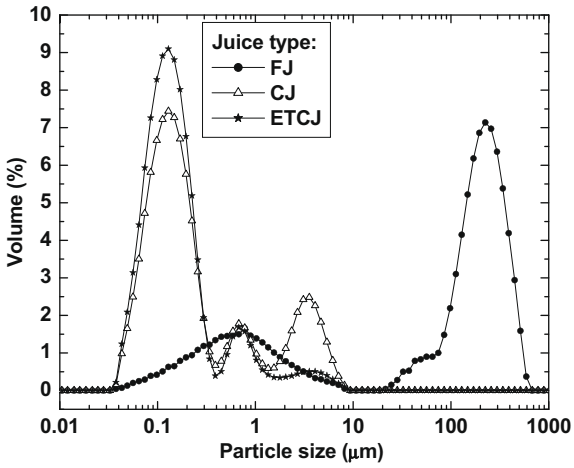


**Fig. 3.** Particle size distribution of different juice samples.

### 4.3. Effect of pretreatment on juice

Table 2 summarizes various physio-chemical properties such as colour, clarity, TSS, acidity (as citric acid), pH, density, viscosity and AIS for FJ, CJ and ETCJ. From the table it can be inferred that the pretreatment of juice primarily affects the colour, clarity, viscosity, AIS values. On the other hand, valuable parameters of the juice such as TSS (a measure of sugar content), acidity, pH and density do not altered significantly. It may be observed from the table that substantial improvement in the colour, clarity and viscosity were observed for CJ and ETCJ when compared with those corresponding to FJ. This was due to the removal of coloured suspended particles from the juice. Colour of the juice decreased (from 4.5 of FJ to 0.69 for CJ and 0.48 for ETCJ) and clarity increased (from 0.18% to 53.73% for CJ and 67.87% for ETCJ). Due to the same reason, the viscosity also decreased (from 3.56 mPa s of FJ to 1.61 for CJ and 1.56 mPa s for ETCJ). The removal of pectic materials by enzyme treatment is further supported by the AIS values (0.34 wt% for CJ and 0.2 wt% for ETCJ). A minute reduction in the juice density was observed after pretreatment, which is attributed to the elimination of bigger suspended particles during centrifugation and enzyme treatment. The reduction in juice viscosity and AIS during pretreatment is advantageous for subsequent clarification by MF

**Table 2**
Physico-chemical properties of fresh and pre-treated mosambi juice.

| Juice type | Colour ($A_{420}$) | Clarity (%$T_{660}$) | TSS (°Brix) | Citric acid (wt%) | pH | Density (g/cm$^3$) | Viscosity (mPa S) | AIS (wt%) |
|---|---|---|---|---|---|---|---|---|
| FJ | 4.50 | 0.18 | 9.2 | 0.84 | 3.79 | 1.04 | 3.56 | 0.92 |
| CJ | 0.69 | 53.73 | 9.1 | 0.84 | 3.80 | 1.038 | 1.61 | 0.34 |
| ETCJ | 0.48 | 67.87 | 9.1 | 0.84 | 3.80 | 1.037 | 1.56 | 0.2 |

as they will enhance the permeate flux. Further, these variations in parameters also contribute towards longer life cycle of the membrane due to reduced fouling at lower concentrations of pectic material in the juice.

### 4.4. Microfiltration of juice

Figs. 4 and 5 present permeate flux decline profiles for CJ and ETCJ, respectively at different trans-membrane pressures differential ($\Delta P$) of 137.9, 206.8, 275.8 and 344.7 kPa. From both the figures, it can be observed that permeate flux declined sharply within the initial phase of 5–10 min and becomes gradual thereafter. Decline in flux with time was due to pore blocking of ceramic porous structure and gel layer formation over the membrane surface by pectic materials present in the juice. The permeate flux decreased from $12.67 \times 10^{-6}$ to $5.65 \times 10^{-6}$ m$^3$/m$^2$ s for CJ and from $58.49 \times 10^{-6}$ to $21.45 \times 10^{-6}$ m$^3$/m$^2$ s for ETCJ at the end of 45 min of experimental run at $\Delta P$ of 137.9 kPa. From the figures it may also be observed that permeate flux increased with increase in $\Delta P$. The initial permeate flux increases from $12.67 \times 10^{-6}$ to $33.15 \times 10^{-6}$ m$^3$/m$^2$ s for CJ and $58.49 \times 10^{-6}$ to $117 \times 10^{-6}$ m$^3$/m$^2$ s for ETCJ when $\Delta P$ was increased from 137.9 to 344.74 kPa. An increase in permeate flux with $\Delta P$ was due to the higher driving force across the membrane. Also, the permeate flux was higher for ETCJ compared to the CJ. This was due to the presence of higher amounts of pectic materials in the CJ (causing higher amount of gel layer formation) as well as higher viscosity of the centrifuged juice. The observed flux data using the ceramic membrane have been found to be better than those obtained using polymeric membranes. The ceramic membrane provided a flux decline of $138.6 \times 10^{-6}$ to $20 \times 10^{-6}$ m$^3$/m$^2$ s within 45 min of experimental run for a trans-membrane pressure differential of 137.9–44.7 kPa which is comparable to the flux reported by Rai et al. (2006) using polymeric membranes ($250 \times 10^{-6}$ to $1.94 \times 10^{-6}$ m$^3$/m$^2$ s at 138 kPa within 27 min of experimental run). Further, the polymeric membranes provided 98% reduction in the flux due to fouling phenomena which is quite high in comparison to the ceramic membrane (84%). In other words, the ceramic membrane performed better than the polymeric membrane.

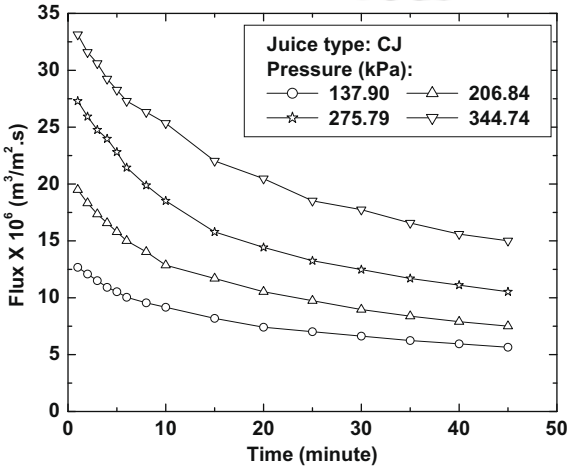


**Fig. 4.** Variation of permeate flux with time at different trans-membrane pressure for centrifuged mosambi juice (CJ).

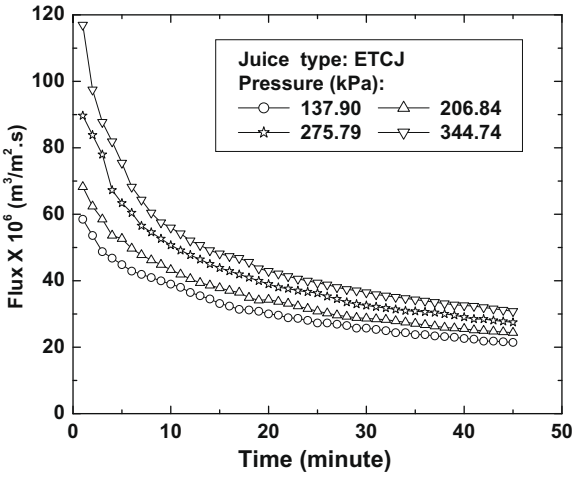


**Fig. 5.** Variation of permeate flux with time at different trans-membrane pressure for enzyme treated mosambi juice (ETCJ).

### 4.5. Identification of competent flux decline mechanism

The identification of competent flux decline mechanism is very important for any MF processes. The decline in permeate flux during dead-end MF of juice has been analyzed using different membrane pore blocking models as discussed in Section 3. Figs. 6 and 7 illustrate the fitness of different pore blocking models corresponding to flux data for CJ and ETCJ juice, respectively. A critical observation of scatter trends in Fig. 6a–c and 7 indicate that two linear trends are adopted during the duration of the MF experimental runs. Therefore, these trends indicate that there exist two different paradigms of fouling phenomena that correspond to the initial 4–5 min of the MF run and the rest for all experimental investigations. In order to visualize the most competent fouling phenomena during the initial phase of 5 minutes membrane performance, the correlation coefficients ($R^2$) have been evaluated by considering all models namely complete pore blocking, standard pore blocking, intermediate pore blocking and cake filtration. Amongst these models, it was found that the fitness of intermediate pore blocking and cake filtration models varied between 0.989 to 0.999 and 0.98 to 0.989, respectively with variation in juice type (CJ and ETCJ) and trans-membrane pressure. On the other hand, for the second regime (from 5 to 45 min of experimental run), cake filtration model $R^2$ values have always been found to be highest (0.998). Therefore, it is herewith inferred that intermediate pore blocking followed with cake filtration represent the most competent combination of fouling mechanisms for the observed membrane flux decline. Since it will be also convenient to identify a single most competent model to represent the entire flux decline regime, the $R^2$ values of all four models have been as well compared. It has been observed that the cake filtration model provided the best values of $R^2$

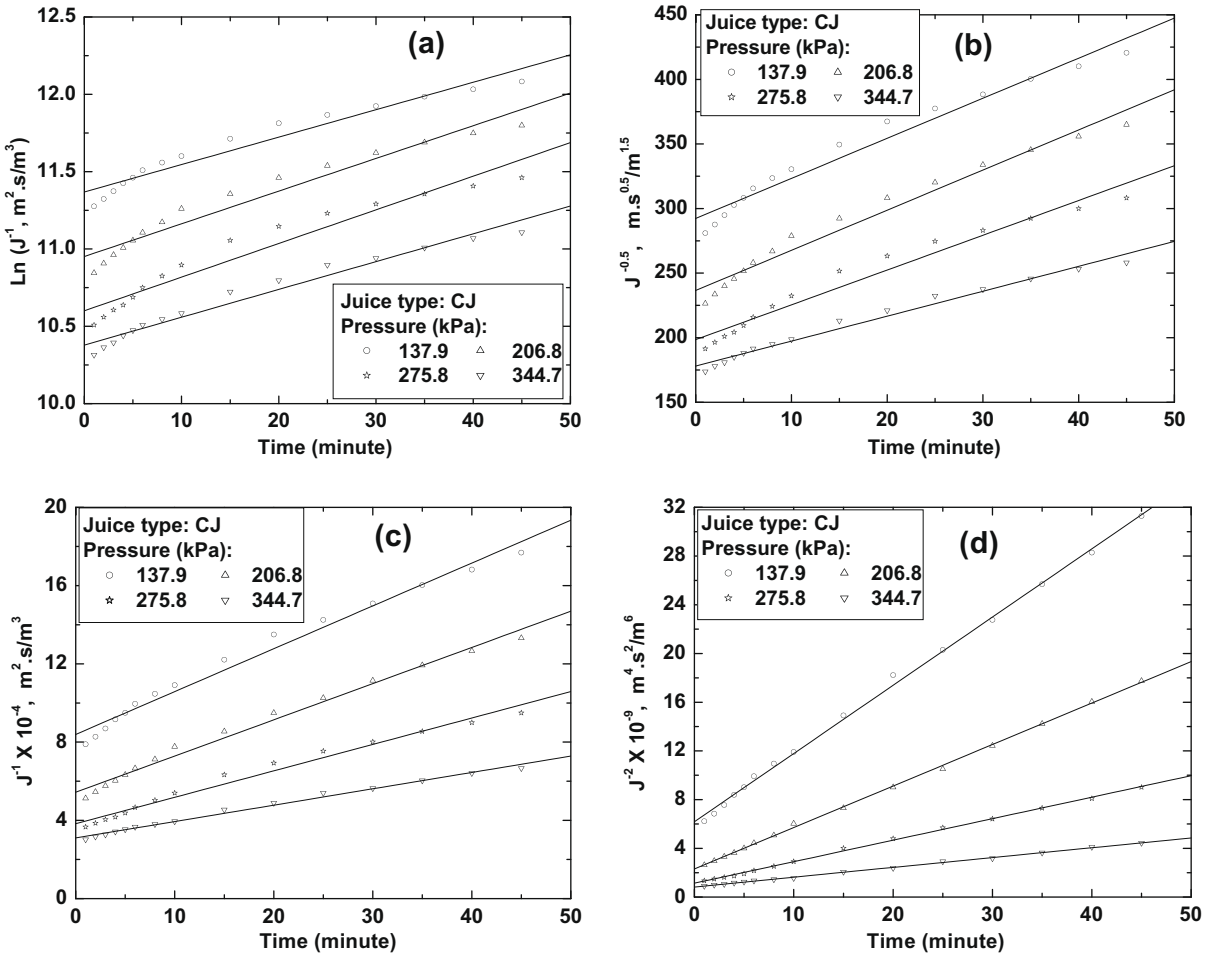


**Fig. 6.** Linearized plot of permeate flux vs. time for different pore blocking models for centrifuged mosambi juice (CJ). (a) complete pore blocking model, (b) standard pore blocking model, (c) intermediate pore blocking model, (d) cake filtration model.

(0.998). Since the variation in $R^2$ for single model (cake filtration) and combination model (intermediate pore blocking followed with cake filtration) have been found to be insignificant, it has been finally inferred that cake filtration could also represent the pertinent flux decline phenomena. Table 3 summarizes different model parameters (slope, intercept and correlation coefficient) of complete pore blocking, standard pore blocking, intermediate filtration and cake filtration models for CJ and ETCJ. An overall observation of the Fig. 6a–d inferred that all models fit with the experimental data within acceptable accuracy. However, a critical observation inferred that Fig. 6d represents the observed flux decline trends better than all other models. To confirm the fitness of the models, correlation coefficients ($R^2$) of different models summarized in Table 3 were used as a basis. As presented, $R^2$ values varied from 0.942 to 0.967 for complete pore blocking, 0.965–0.982 for standard pore blocking, 0.982–0.992 for intermediate filtration and 0.998 to 0.999 for cake filtration model. As cake filtration model provided the highest values of $R^2$, this model was identified as the best fitted model to represents the flux decline mechanism for CJ. Similar analysis was also carried out for ETCJ to evaluate the best suited flux decline model (Fig. 7a–d). It can be inferred from the Fig. 7a–d and corresponding $R^2$ (Table 3) values that the flux decline due cake filtration was the best fitted model to represent the fouling mechanism associated to the MF of ETCJ.

According to the definitions and physical significance of Hermia's model parameters expressed in Eqs. (2)–(5), magnitude of $k_b$, $k_s$, $k_i$ and $k_c$ values refers to severity of fouling. Table 3 indicates that for both CJ and ETCJ, $k_c$ decreases with an increase in $\Delta P$, thereby inferring that the fouling of membrane reduces with an increase in $\Delta P$. This was due to several reasons. Firstly, higher $\Delta P$ enables lower adsorption of non-permeating molecules on the walls of the membrane pores due to the higher liquid velocity through the membrane pores. Secondly, due to higher driving force ($\Delta P$), some of the blocked pores get cleaned by permeating liquid. This was further confirmed by the reduction in the overall quality of permeate juice (color, clarity, viscosity and AIS in Table 5) due to the passage of higher amount of pectic materials at higher $\Delta P$. The comparison of $k_c$ values obtained for CJ and ETCJ further indicates that lower $k_c$ values exist for ETCJ. This is due to lower concentration of pectic material in ETCJ when compared to CJ. Fig. 8 presents the variation of $k_c$ with $\Delta P$ that can be suitably correlated using linear expressions:

$$k_c^{CJ} = 8.948 \times 10^8 - 2.562 \times 10^6 \Delta P \quad R^2 = 0.989 \tag{6}$$

$$k_c^{ETCJ} = 5.686 \times 10^7 - 1.090 \times 10^5 \Delta P \quad R^2 = 0.996 \tag{7}$$

within the pressure range $137.9 \leqslant \Delta P \leqslant 344.7$.

Using the values of $J_0^{-2}$ summarized in Table 3, the initial instantaneous fouling resistance of the membrane ($R_f^0$) during MF was calculated as:

$$J_0 = \frac{\Delta P}{\mu_p (R_t^0)} = \frac{\Delta P}{\mu_p (R_m + R_f^0)} \tag{8}$$

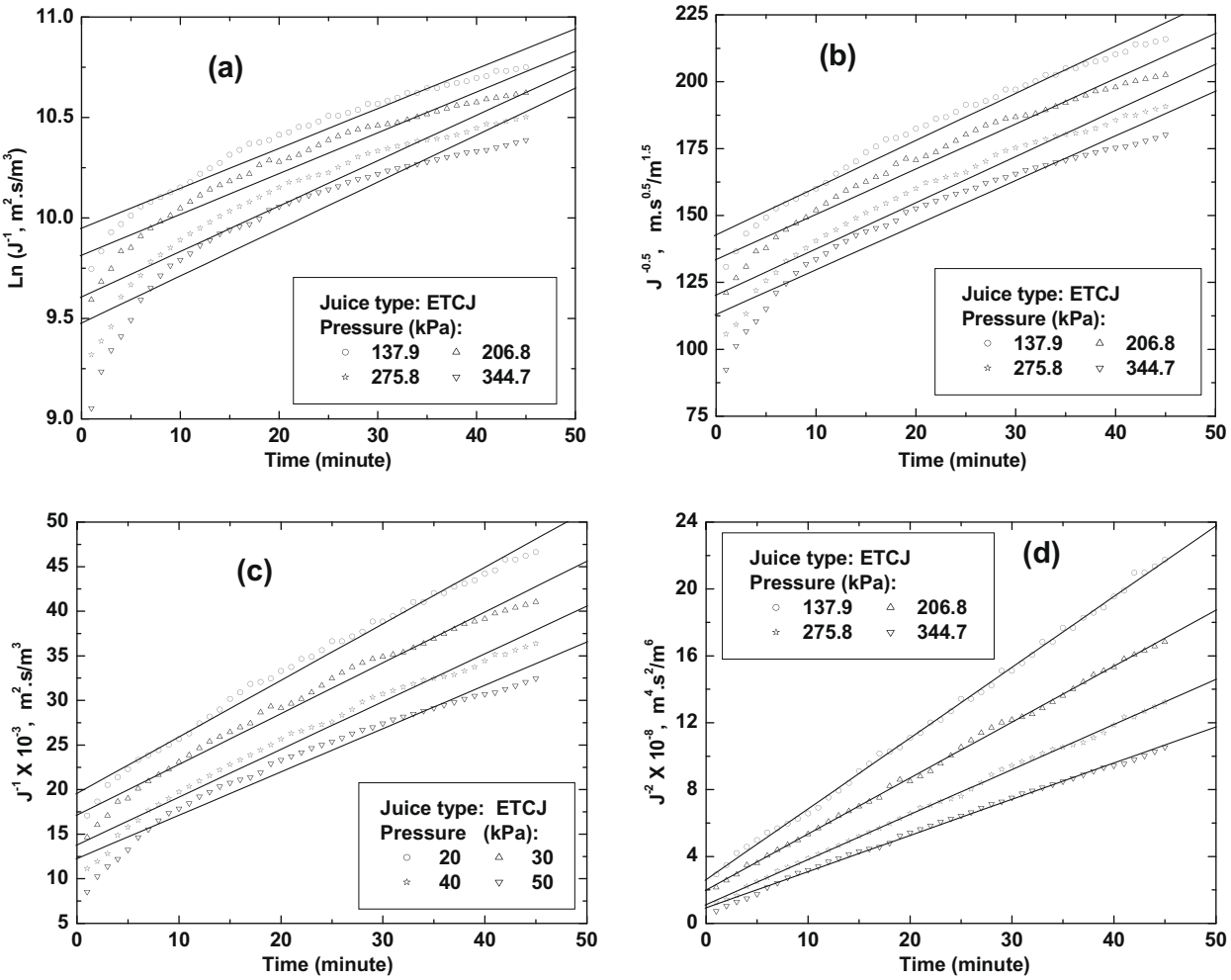


**Fig. 7.** Linearized plot of permeate flux vs. time for different pore blocking models for enzyme treated centrifuged mosambi juice. (a) complete pore blocking model, (b) standard pore blocking model, (c) intermediate pore blocking model, (d) cake filtration model.

**Table 3**
Summary of parameters associated to various pore blocking models.

| Juice type | Pressure (kPa) | Complete pore blocking | | | Standard pore blocking | | | Intermediate pore blocking | | | Cake filtration | | |
|---|---|---|---|---|---|---|---|---|---|---|---|---|---|
| | | $k_b \times 10^2$ | $\ln(J_0^{-1})$ | $R^2$ | $k_S$ | $J_0^{0.5}$ | $R^2$ | $k_i$ | $J_0^{-1} \times 10^{-4}$ | $R^2$ | $k_C \times 10^{-7}$ | $J_0^{-2} \times 10^{-8}$ | $R^2$ |
| CJ | 137.9 | 1.77 | 11.37 | 0.947 | 3.10 | 292.33 | 0.967 | 2190 | 8.39 | 0.983 | 56.01 | 61.87 | 0.998 |
| | 206.8 | 2.11 | 10.95 | 0.950 | 3.11 | 236.57 | 0.973 | 1851 | 5.44 | 0.988 | 34.04 | 23.12 | 0.999 |
| | 275.8 | 2.17 | 10.60 | 0.942 | 2.69 | 198.51 | 0.965 | 1351 | 3.83 | 0.982 | 17.65 | 11.44 | 0.999 |
| | 344.7 | 1.80 | 10.38 | 0.967 | 1.93 | 178.04 | 0.982 | 836 | 3.10 | 0.992 | 8.06 | 8.27 | 0.999 |
| ETCJ | 137.9 | 1.98 | 9.95 | 0.944 | 1.76 | 142.78 | 0.970 | 634 | 1.96 | 0.987 | 4.23 | 2.62 | 0.999 |
| | 206.8 | 2.03 | 9.81 | 0.931 | 1.69 | 133.54 | 0.961 | 570 | 1.71 | 0.982 | 3.35 | 2.00 | 0.999 |
| | 275.8 | 2.26 | 9.61 | 0.904 | 1.73 | 120.26 | 0.946 | 536 | 1.38 | 0.975 | 2.70 | 1.12 | 0.998 |
| | 344.7 | 2.34 | 9.48 | 0.866 | 1.67 | 113.03 | 0.920 | 486 | 1.23 | 0.959 | 2.16 | 0.93 | 0.997 |

**Table 4**
Variation of total and initial instantaneous fouling resistance with pressure during MF of mosambi juice.

| Juice type | Pressure (kPa) | $R_t^0 \times 10^{-11}$ (m$^2$/m$^3$) | $R_f^0 \times 10^{-11}$ (m$^2$/m$^3$) | % $R_m$ | % $R_f^0$ |
|---|---|---|---|---|---|
| CJ | 137.9 | 74.81 | 65.55 | 12.38 | 87.62 |
| | 206.8 | 68.59 | 59.33 | 13.50 | 86.50 |
| | 275.8 | 64.32 | 55.06 | 14.40 | 85.60 |
| | 344.7 | 64.40 | 55.14 | 14.38 | 85.62 |
| ETCJ | 137.9 | 15.71 | 6.45 | 58.94 | 41.06 |
| | 206.8 | 20.60 | 11.34 | 44.95 | 55.05 |
| | 275.8 | 20.54 | 11.28 | 45.09 | 54.91 |
| | 344.7 | 23.39 | 14.13 | 39.58 | 60.42 |

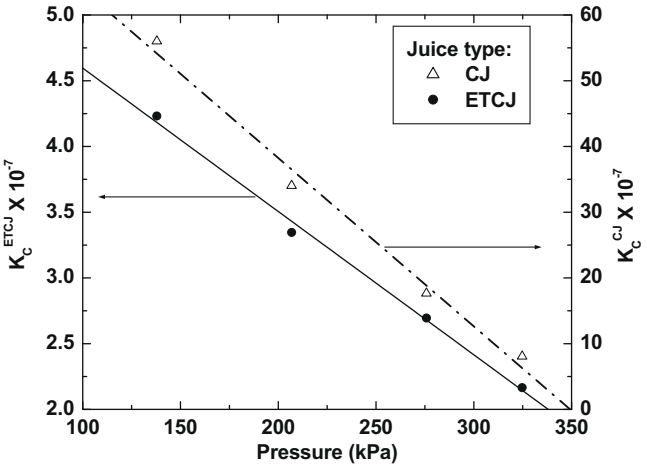


**Fig. 8.** Variation of cake filtration constant ($k_c$) with pressure.

In the above expression, $R_f^0$ corresponds to the fouling membrane resistance due to the membrane fouling at zero time. This hydraulic resistance was due to the presence of both soluble and insoluble solids in the feed juice and henceforth relates to the magnitude of the instantaneous initial fouling of the membrane. Subsequently, $R_t^0$ and $R_f^0$ were evaluated from Eq. (8) using $R_m$ values summarized in Table 1. Table 4 summarizes the variation of instantaneous fouling resistance ($R_f^0$) with $\Delta P$ and its percentage contribution to the instantaneous total resistance ($R_t^0$). As shown, percent contribution $R_f^0$ varies from 85.6 to 87.6% for CJ and 41–60% for ETCJ. Higher values of $R_f^0$ for CJ were due to the presence of higher amounts of pectic material compounds in CJ when compared to that in ETCJ.

### 4.6. Permeate quality after filtration

Table 5 presents various physio-chemical properties of clarified CJ and ETCJ. It can be observed from the table that, there was significant improvement in the colour and clarity of the mosambi juice after filtration. Colour decreases from 0.69 of FJ to 0.0953 for CJ and from 0.48 to 0.0232 for ETCJ. Clarity increases from 53.73 to 93.39% for CJ and 67.87–98.98% for ETCJ. This was due to the removal of pectic materials present in juice. 100% removal of AIS content was observed for ETCJ. However, negligible amount of AIS was found in permeate of CJ. Viscosity decreased from 1.61 to 1.45 mPa s and 1.56–1.42 mPa s for CJ and ETCJ, respectively. The reduction of viscosity was due to the removal of pectic materials in the juice. However, the valuable properties of the juices such as pH, soluble solids, acidity, density does not vary significantly for both CJ and ETCJ. These findings agree with the results reported in the literature for the mosambi juice clarification using polymeric membrane (Rai et al., 2006). Therefore, low cost ceramic membrane can be recommended for the mosambi juice processing.

### 4.7. Long term stability

Stability of juice without substantial variation in its physio-chemical properties during long term storage is always a significant factor for the characterization of processes involved in juice

**Table 5**
Physico-chemical properties of clarified mosambi juice after MF.

| Juice type | Pressure (kPa) | Colour ($A_{420}$) | Clarity (%$T_{660}$) | TSS (°Brix) | Citric acid (wt%) | pH | Density (g/cm$^3$) | Viscosity (mPa S) | AIS (wt%) |
|---|---|---|---|---|---|---|---|---|---|
| CJ | 137.9 | 0.0953 | 93.39 | 9.1 | 0.80 | 3.87 | 1.03 | 1.45 | 0.04 |
| | 206.8 | 0.1016 | 93.16 | 9.1 | 0.81 | 3.84 | 1.03 | 1.45 | 0.04 |
| | 275.8 | 0.1049 | 92.97 | 9.1 | 0.81 | 3.84 | 1.03 | 1.46 | 0.05 |
| | 344.7 | 0.1162 | 92.56 | 9.1 | 0.81 | 3.84 | 1.03 | 1.46 | 0.05 |
| ETCJ | 137.9 | 0.0232 | 98.98 | 9.1 | 0.78 | 3.9 | 1.03 | 1.42 | Nil |
| | 206.8 | 0.0342 | 98.61 | 9.1 | 0.81 | 3.85 | 1.03 | 1.43 | Nil |
| | 275.8 | 0.0512 | 98.01 | 9.1 | 0.81 | 3.85 | 1.03 | 1.43 | Nil |
| | 344.7 | 0.0586 | 97.08 | 9.1 | 0.81 | 3.85 | 1.03 | 1.43 | Nil |

**Table 6**
Summary of physio-chemical properties obtained for various juice samples during long term stability analysis.

| Juice type | Day | Colour ($A_{420}$) | Clarity (%$T_{660}$) | TSS (°Brix) | Citric acid (wt%) | pH | Density (g/cm$^3$) |
|---|---|---|---|---|---|---|---|
| CJ | 1st | 0.69 | 53.73 | 9.1 | 0.84 | 3.80 | 1.038 |
| | 7th | 0.59 | 63.54 | 8.6 | 0.87 | 3.75 | 1.035 |
| | 15th | 1.231 | 56.85 | 8.2 | 0.90 | 3.65 | 1.033 |
| | 21st | 1.865 | 30.28 | 7.6 | 0.96 | 3.5 | 1.032 |
| | 30th | 2.464 | 21.56 | 7.3 | 1.01 | 3.4 | 1.031 |
| CJ permeate (137.9 kPa) | 1st | 0.095 | 93.39 | 9.1 | 0.80 | 3.87 | 1.03 |
| | 7th | 0.123 | 91.25 | 9 | 0.81 | 3.85 | 1.03 |
| | 15th | 0.239 | 89.31 | 8.9 | 0.82 | 3.82 | 1.03 |
| | 21st | 0.098 | 87.62 | 8.8 | 0.84 | 3.79 | 1.03 |
| | 30th | 0.134 | 85.82 | 8.7 | 0.86 | 3.75 | 1.03 |
| ETCJ | 1st | 0.48 | 67.87 | 9.1 | 0.84 | 3.80 | 1.037 |
| | 7th | 0.59 | 63.54 | 9 | 0.85 | 3.78 | 1.036 |
| | 15th | 0.89 | 60.85 | 8.8 | 0.87 | 3.75 | 1.036 |
| | 21st | 0.99 | 58.54 | 8.6 | 0.88 | 3.72 | 1.035 |
| | 30th | 1.231 | 56.85 | 8.4 | 0.89 | 3.67 | 1.034 |
| ETCJ permeate (137.9 kPa) | 1st | 0.023 | 98.98 | 9.1 | 0.78 | 3.9 | 1.03 |
| | 7th | 0.035 | 91.25 | 9.1 | 0.79 | 3.88 | 1.03 |
| | 15th | 0.056 | 90.03 | 9.0 | 0.80 | 3.87 | 1.03 |
| | 21st | 0.072 | 89.82 | 9.0 | 0.81 | 3.86 | 1.03 |
| | 30th | 0.086 | 89.51 | 9.0 | 0.81 | 3.86 | 1.03 |

processing. To observe the stability of the valuable parameters of clarified juices for long term storage, 500 mL of CJ, ETCJ, permeate obtained with $\Delta P$ of 137.9 kPa for CJ and ETCJ were kept in refrigerated condition for 30 days. During storage, important parameters of the juice like colour, clarity, TSS, pH, citric acid and density were measured. Table 6 shows the obtained results for the juice samples. From the table it can be observed that overall quality of the CJ and ETCJ degrade with time, with higher degradation rate for CJ. For example, TSS decreases from 9.1 to 7.3 for CJ and 8.4 for ETCJ during 30 days of storage. This was due to the presence of pectic materials in the juice that undergo fermentation even when kept in refrigerated storage conditions. The fermentation reactions enable a significant variation in the sugar concentration (indicated as °Brix) of the juice along with the alteration in colour, clarity, and pH. The degradation in these properties was found to be higher for CJ due to the higher amount of pectic materials (AIS) in the juice.

After membrane clarification, permeate samples corresponding to both CJ and ETCJ have been found to be more stable than CJ and ETCJ samples. During 30 days of storage, variation of juice properties is found to be negligible for ETCJ permeate, where as small variation for CJ permeate was observed. Since all pectic materials were removed during MF, significant contribution of fermentation reactions to alter the juice quality has not been observed for ETCJ permeate. However, for CJ permeate samples, negligible amount of AIS were present in the permeate juice (0.04%) and some contributions from fermentation reactions to alter the juice quality slightly were observed. These observations further justify deploying enzymatic treatment of the mosambi juice before MF based clarification to substantially enhance the juice quality and stability.

## 5. Conclusions

This work addressed the applicability of low cost ceramic membranes for mosambi juice microfiltration. The inexpensive ceramic membrane was prepared using locally available low cost inorganic raw materials such as kaolin, quartz, feldspar, sodium carbonate, boric acid and sodium metasilicate. Prepared membrane was characterized using SEM analysis, porosity determination and pure water permeation through the membrane. The average pore diameter, total porosity and hydraulic resistance of the membrane were evaluated as 0.285 μm, 23.6% and $9.26 \times 10^{11}$ $m^2/m^3$, respectively. Based on raw material retail price, the cost of the membrane was evaluated as 220 $\$/m^2$. The membrane exhibited a permeate flux of $5.65 \times 10^{-6}$ and $21.45 \times 10^{-6}$ $m^3/m^2$ s after 45 min of experimental run at 137.9 kPa trans-membrane pressure drop for CJ and ETCJ, respectively. Different important physio-chemical properties of mosambi juice such as colour, clarity, total soluble solids (TSS), pH, acidity, density and AIS were measured before and after MF experiments. During enzymatic treatment as well as UF, valuable properties of the juice (TSS, pH, acidity, density) do not vary significantly. However significant decrease in colour, viscosity, AIS and increase in clarity were observed during enzymatic treatment as well as MF due to the removal of pectic materials. The decline in permeate flux was analyzed using different membrane pore blocking models. Cake filtration model was identified as the best suited model. The variation of cake filtration model constant ($k_c$) with $\Delta P$ was also studied. The analysis of instantaneous initial fouling resistance ($R_f^0$) yielded significant insights to infer that $R_f^0$ contributed significantly to overall hydraulic resistance for CJ in contrast to ETCJ. Finally, the stability of the clarified juice for long term storage study were also verified and it was observed that permeate of ETCJ can be stored in refrigerated condition for more than 30 days without significant change in juice quality. Henceforth, enzyme treatment is strongly recommended prior to juice MF to enhancing the life cycle of the membrane and competence of membrane based juice processing. In summary, this work infers that low cost ceramic membranes are promising for mosambi juice processing.

## References


Bailey, A.F.G., Barbe, A.M., Hogan, P.A., Johnson, R.A., Sheng, J., 2000. The effect of ultrafiltration on the subsequent concentration of grape juice by osmotic distillation. Journal of Membrane Science 164, 195–204.

Carvalho, L.M.J., Castro, I.M., Silva, C.A.B., 2008. A study of retention of sugars in the process of clarification of pineapple juice (Ananas comosus, L. Merril) by micro- and ultra-filtration. Journal of Food Engineering 87, 447–454.

Cassano, A., Drioli, E., Galaverna, G., Marchelli, R., Silvestro, G.D., Cagnasso, P., 2003. Clarification and concentration of citrus and carrot juices by integrated membrane processes. Journal of Food Engineering 57, 153–163.

Cassano, A., Marchio, M., Drioli, E., 2007. Clarification of blood orange juice by ultrafiltration: analyses of operating parameters, membrane fouling and juice quality. Desalination 212, 15–27.

Cheryan, M., 1998. Ultrafiltration and Microfiltration Handbook. Techno Pub. Co. Inc..

Chhaya, C., Rai, P., Majumdar, G.C., Dasgupta, S., De, S., 2008. Clarification of watermelon (*citrullus lanatus*) juice by microfiltration. Journal of Food Process Engineering 31, 768–782.

Espamer, L., Pagliero, C., Ochoa, A., Marchese, J., 2006. Clarification of lemon juice using membrane process. Desalination 200, 565–567.

Hart, F.L., Fisher, H.J., 1971. Modern Food Analysis. Springer, Berlin.

Hermia, J., 1982. Constant pressure blocking filtration laws-application to power-law non-newtonian fluids. Trans. Inst. Chem. Eng. 60, 183–187.

Lister, D.G., Maschio, G., Becchi, I., 1994. The use of membrane processes in the clarification of orange and lemon juices. Journal of Food Engineering 21, 473–483.

Nandi, B.K., Uppaluri, R., Purkait, M.K., 2008. Preparation and characterization of low cost ceramic membranes for microfiltration applications. Applied Clay Science 42, 102–110.

Rai, P., Majumdar, G.C., Sharma, G., DassGupta, S., De, S., 2006. Effect of various cut-off membranes on permeate flux and quality during filtration of mosambi (citrus sinensis (l.) Osbeck) juice, Food and Bioproducts Processing, 84, 213–219.

Rai, P., Majumdar, G.C., DasGupta, S., De, S., 2004. Optimizing pectinase usage in pretreatment of mosambi juice for clarification by response surface methodology. Journal of Food Engineering 64, 397–403.

Rai, P., Majumdar, G.C., Dasgupta, S., De, S., 2005. Quantification of flux decline of depectic materialinized mosambi (citrus sinensis[l.] osbeck) juice using unstirred batch ultrafiltration, Journal of Food Process Engineering, 28, 359–377.

Rai, P., Majumdar, G.C., Dasgupta, S., De, S., 2005b. Understanding ultrafiltration performance with mosambi juice in an unstirred batch cell. Journal of Food Process Engineering 28, 166–180.

Sarkar, B., DasGupta, S., De, S., 2008. Cross-flow electro-ultrafiltration of mosambi (Citrus sinensis (L.) Osbeck) juice. Journal of Food Engineering 89, 241–245.

Vaillant, F., Cisse, M., Chaverri, M., Perez, A., Dornier, M., Viquez, F., Mayer, C.D., 2005. Clarification and concentration of melon juice using membrane processes. Innovative Food Science and Emerging Technologies 6, 213–220.

Vladisavljevic, G.T., Vukosavljevic, P., Bukvic, B., 2003. Permeate flux and fouling resistance in ultrafiltration of depectic materialinized apple juice using ceramic membranes. Journal of Food Engineering 60, 241–247.

Youn, K.S., Hong, J.H., Bae, D.H., Kim, S.J., Kim, S.D., 2004. Effective clarifying process of reconstituted apple juice using membrane filtration with filter-aid pretreatment. Journal of Membrane Science 228, 179–186.

Yu, J., Lencki, R.W., 2004. Effect of enzyme treatments on the fouling behavior of apple juice during microfiltration. Journal of Food Engineering 63, 413–423.

Journal of Membrane Science 330 (2009) 246–258

Contents lists available at ScienceDirect

Journal of Membrane Science

journal homepage: www.elsevier.com/locate/memsci

# Effects of dip coating parameters on the morphology and transport properties of cellulose acetate–ceramic composite membranes

B.K. Nandi, R. Uppaluri*, M.K. Purkait*

*Department of Chemical Engineering, Indian Institute of Technology Guwahati, Guwahati 781039, Assam, India*

ARTICLE INFO

*Article history:*
Received 6 June 2008
Received in revised form 31 October 2008
Accepted 29 December 2008
Available online 16 January 2009

*Keywords:*
Composite membrane
Cellulose acetate
Resistances in series model
Hydraulic resistance
Dip coating
Phenomenological model

ABSTRACT

This work presents the fabrication of cellulose acetate (CA)–ceramic composite membranes using dip coating technique. Ceramic supports used in this work were prepared from kaolin with an average pore size of 560 nm and total porosity of 33%. The dip coating parameters studied experimentally were the concentration of CA solution (varying from 2 wt% to 8 wt%) in acetone and dipping time (varying from 30 s to 150 s). The fabricated composite membranes were characterized using scanning electron microscope, gas permeation, pure water flux and ultrafiltration (UF) experiments using bovine serum albumin (BSA). It was observed that the membrane prepared with 2 wt% and 4 wt% CA were suitable for microfiltration applications and those with 6 wt% and 8 wt% were for ultrafiltration applications. Theoretical investigation was conducted to know the macroporous and mesoporous structure of the prepared membranes using Knudsen and viscous permeability analysis of air. A resistance in series model was applied to identify different resistances responsible for the flux decline. Phenomenological models were proposed to illustrate the dependency of hydraulic resistance of membrane on the structural parameters such as average pore size, effective porosity as well as dip coating parameters like dipping time and concentration of CA. It was found that, the growth rate of CA film on the ceramic support followed exponential growth law with respect to dipping time. The total hydraulic resistance of the membrane was evaluated to be inversely proportional to the ratio of pore sizes of top layer and ceramic support. The resistance due to the CA film was found to be depended to the order of 1.73 with respect to concentration of CA. An increase in the concentration of CA was found to be more effective than dipping time to reduce the membrane pore size.



## 1. Introduction

Polymer–ceramic composite membranes characterized with superior combinations of structural integrity, fouling resistance, flux and selectivity have been reported for the ultrafiltration (UF) [1–3] and pervaporation (PV) [4–8] applications. These membranes constitute a polymer skin layer consisting of polysulfone [2], styrene acrylonitrile [3], polyvinyl acetate (PVAc), polyvinyl pyrrolidone (PVP) [4], cellulose acetate (CA) [5], polydimethylsiloxane (PDMS) [8,9] and ceramic supports with nominal pore sizes of 200–2000 nm made from kaolin [3], alumina [4] and zirconia [9].

Despite many notable merits, the industrial competitiveness of polymer–ceramic composite membranes has not been largely addressed. The principle reason for the lack of industrial sustenance is the high cost of the ceramic supports that varies between 1600$/m$^2$ [10] and 20,000$/m$^2$ [11]. These costs are about three to four orders of magnitude compared to the cost of the polymeric thin film membrane, having cost in the range of 5–10$/m$^2$ [11]. The cost of the ceramic support accounting to about one to two orders of magnitude to the cost of the polymeric films is anticipated to enhance industrial sustainability and is hence the object of concern in this study. There are several methods available for the preparation of composite membrane like spray coating [3], grafting [4], spin coating [5], self assembly [7], dip coating [9] and vapor deposition [12]. Among these methods dip coating method is simple, inexpensive and most desirable choice for industrial applications.

Numerous articles have been published using dip coating technique for the preparation of ceramic–ceramic, polymer–ceramic and polymer–polymer composite membranes. In the field of polymer–ceramic composite membrane, Matsumoto et al. [2] has prepared sulfonated polysulfone–ceramic composite membrane suitable for UF. Song and Hong [5] fabricated cellulose acetate–ceramic membrane using dip coating and rotation drying technique using a ceramic support with surface average pore size of 100 nm and CA concentration of 20% which was tested for

* Corresponding authors. Tel.: +91 361 2582260/2582262; fax: +91 361 2582291.
*E-mail addresses:* ramgopalu@iitg.ernet.in (R. Uppaluri), mihir@iitg.ernet.in (M.K. Purkait).

0376-7388/$ – see front matter © 2009 Elsevier B.V. All rights reserved.
doi:10.1016/j.memsci.2008.12.071

the dehydration of ethanol and isopropanol. Ki Hong and Hong [8] prepared PDMS–ceramic membrane by dip coating method using 20–30 wt% polymer concentrations on a ceramic support having average pore size of 370 nm and applied it for the PV of IPA/water mixture. Similarly, Sachdeva and Kumar [3], Xiangli et al. [9], Aranda et al. [13], Rezac and Koros [14] prepared polymer–ceramic composite membranes using different polymer precursors and commercial ceramic supports for preparing membranes to suit UF and PV applications. These works infer that an optimal combination of preparation conditions such as polymer solution concentration, dipping time and cross linking agent concentration (if any) yields better composite membrane. Further, membrane permeance or hydraulic resistance was taken as an index to quantify the polymer/ceramic film growth rate and thereby identify optimal combinations of membrane porosity, film thickness and average pore size. Gu and Meng [15], Babaluo et al. [16] and Levänen et al. [17] presented mathematical models supported with experimentation to conclude that the ceramic film growth rate (or membrane hydraulic resistance) on a ceramic support was proportional to the square root of dipping time. Xiangli et al. [9] presented nonlinear models to express the flux (and hence hydraulic resistance) and selectivity of the polymer–ceramic composite membrane as functions of dip coating parameters such as polymer concentration, cross linking agent concentration and dip coating time using response surface methodology. However, the physical mechanisms that occur during dip coating process have not been analyzed quantitatively to evaluate their contribution towards the properties of the composite membrane such as morphology and transport properties.

A critical review of the above publications and other relevant research findings convey the following conclusions for the fabrication of polymeric ceramic composite membranes. Firstly, use of low cost ceramic support rather than using alumina based costly support should be encouraged to minimize the cost of the composite membrane suitable for industrial competence. Secondly, membrane preparation method needs to be simple, inexpensive with minimal instrumentation without compensating on the desired precision. So dip coating technique may be a better choice compared to other alternative method such as polymer grafting, spin coating. Dip coating technique also provides opportunities to explore the impact of coating parameters such as polymer concentration in solution and dipping time during the fabrication of composite membrane to obtain membrane with specific pore diameter. So research in this direction should be encouraged. Finally, conceptual phenomenological models have to be developed that enable to quantify the dependency of membrane morphology on ceramic as well as dip coating parameters. These approaches could identify potential pathways for furthering the industrial competitiveness of the polymeric ceramic composite membranes.

This work reports the fabrication of CA–ceramic composite membranes using dip coating method. Low cost ceramic supports were prepared using kaolin as raw material. Quantitative as well as qualitative assessment of the dip coating process and membrane performance during UF experiment was carried out. Surface and flux characterization were conducted to evaluate the effect of dip coating parameters (CA concentration in solution and dipping time) on the structure and morphology of the fabricated membrane. A resistance in series model was proposed to evaluate the magnitude of different resistances offered by the different structural layers of the composite membrane during UF of BSA. Finally, phenomenological models were developed to evaluate the dependency of various membrane parameters such as average pore size, effective porosity of the membrane as well as dip coating parameters namely dipping time and CA concentration of the solution on the total hydraulic resistance.



**Table 1**
Composition of raw materials and their cost used for the fabrication of ceramic support.

| Material | Composition (wt%) | | Unit price ($/kg)[a] |
|---|---|---|---|
| | Wet basis | Dry basis | |
| Kaolin | 29.63 | 40 | 5 |
| Quartz | 11.11 | 15 | 64 |
| Calcium carbonate | 18.52 | 25 | 4.2 |
| Sodium carbonate | 7.40 | 10 | 4.6 |
| Boric acid | 3.71 | 5 | 5.6 |
| Sodium metasilicate | 3.71 | 5 | 8.4 |
| Water | 25.92 | 0 | – |
| Support of 4.5 mm thickness and 52.5 mm diameter | 0.027 kg | 0.02 kg | 130$/m$^2$ |

[a] Prices are taken from the catalog of the corresponding company as mentioned in Section 2.1.

## 2. Experimental

### 2.1. Raw materials

Cellulose acetate (molecular weight 30 kDa and acetyl content 39.8 wt%) was procured from Loba Chemicals Ltd., India. Acetone, solvent used for dissolving cellulose acetate was purchased from Merck India. Bovine serum albumin (BSA) with molecular weight of 69 kDa was purchased from SRL Chemicals Ltd., India. The raw materials were graded at least 99.5% pure and used without any further purification.

### 2.2. Preparation of composite membrane

Table 1 summarizes the composition and cost of the corresponding raw materials for the preparation of the ceramic support. Details methods for the preparation of the ceramic support were reported in our earlier publication [18]. Ceramic microfiltration (MF) membranes of 52.5 mm diameter and 4.5 mm thickness with the average surface pore size of 560 nm and total porosity of 33% were used in this work as support. The cost of these support materials was calculated to be 130$/m$^2$. CA solution was prepared by dissolving CA flakes of 2 g, 4 g, 6 g, and 8 g in 100 ml acetone separately in a stopper conical flask of 250 ml capacity. The mixtures were stirred using a magnetic stirrer for 24 h to ensure uniform and complete dissolution of cellulose acetate in acetone. Prior to the dip coating process, the ceramic supports were kept in acetone for 3 h to displace air bubbles present in the membrane porous structure and restrict the penetration of CA solution into the membrane pores during dip coating. Surfaces other than the top surface of the support were covered using Teflon tape to prevent CA deposition. Coating of CA over the support was carried out by dipping the support in the CA solution with dipping time varying from 30 s to 150 s. After coating process, the composite membranes were kept on a flat glass surface at ambient temperature for 24 h to yield a thin coating of CA on the ceramic support. During this time, acetone of the top layer evaporates and thereby contributes to the pore formation and hence membrane morphology and separation capabilities [3]. The composite membrane thus prepared constituted a ceramic support that was dominated with macroporous structure and a CA top layer that was dominated with mesoporous and microporous structure. Finally, the composite membrane was dried at 45 °C for 3 h in a hot air oven to accomplish complete removal of acetone from the membrane structure. The nomenclature of various composite membranes fabricated with varying CA concentration in acetone (2–8 wt%) and dipping time (30–150 s) are presented in Table 2.

**Table 2**
Nomenclature of different fabricated composite membranes.

| Time (s) | CA concentration (wt%) | | | |
|---|---|---|---|---|
| | 2 | 4 | 6 | 8 |
| 30 | M-2-30 | M-4-30 | M-6-30 | M-8-30 |
| 60 | M-2-60 | M-4-60 | M-6-60 | M-8-60 |
| 90 | M-2-90 | M-4-90 | M-6-90 | M-8-90 |
| 120 | M-2-120 | M-4-120 | M-6-120 | M-8-120 |
| 150 | M-2-150 | M-4-150 | M-6-150 | M-8-150 |

### 2.3. Characterization methods

Characterization techniques involve the structural characterization of the support and composite membranes by scanning electron microscope (SEM), flux characterization using gas (air) and liquid (water) permeation, compaction study and solute rejection experiments using BSA. SEM analysis were carried out using scanning electron microscope (Make: Oxford; Model: LEO 1430VP) for the evaluation of membrane morphology, presence of surface/cross-sectional defects such as pinholes and cracks (if any) and estimation of membrane thickness for those cases where substantial films were deposited (more than 500 nm). Air flux characterization aims to quantify membrane morphological parameters such as average pore size and porosity that contribute to transport. Pure water flux (PWF) characterization is anticipated to provide insight into the physical effects of dip coating parameters on liquid transport properties as well as solute rejection properties during UF experiment.

A schematic of experimental set up used for both air and water permeation experiment is presented in Fig. 1. The set up constitutes a Teflon tubular cell (125 ml capacity) with a flat circular Teflon base plate that houses the composite membrane. Membranes were kept in the Teflon casing and sealed with epoxy resin. Effective membrane permeation area was 15.9 $cm^2$. During air permeation experiments transmembrane pressure differentials ranging from 69 kPa to 414 kPa was applied. Air flow rate through the membrane was measured using a gas flow meter.

The membrane compaction study conducted for all membranes was aimed to achieve rigid porous structure and size in the membranes to accomplish consistency in hydraulic characterization tests. During compaction, the cell was initially filled with 110 ml deionized water and pressurized at 414 kPa for 6 h. Water flux of 100 ml was measured after every 15 min using digital weight machine and a stop watch. Water flux through the membranes declines initially and attained a steady value after 3–4 h of compaction. After the compaction, the compacted membranes were subjected to the evaluation of hydraulic permeability ($P_m$) and membrane hydraulic resistance ($R_m$). $P_m$ was determined graphically from the slope of PWF and transmembrane pressure differential ($\Delta P$) (varying from 69 kPa to 345 kPa) plot. PWF, $P_m$ and $R_m$ of the membrane were evaluated using the following expressions [19]:

$$\text{PWF} = \frac{Q}{S\,\Delta t} = P_m\,\Delta P \tag{1}$$

$$R_m = \frac{\Delta P}{\text{PWF}} \tag{2}$$

UF experiments were carried out using 1000 mg/l of BSA solution at transmembrane pressure differential of 345 kPa. BSA solutions of concentration 1000 mg/l in phosphate buffer (0.5 M, pH 7.2) were prepared using deionized water. The pH of the feed solution was kept constant at 7.2, since a change in pH may increase the adsorptive fouling of the membranes [20]. Furthermore, intermolecular forces between BSA molecules and membranes will predominate and affect the efficiency of membranes if the pH of the solution changes [21]. During these experiments, the membrane flux was evaluated by measuring the amount of permeate collected after 1 h. BSA concentration in both feed and permeate was determined using UV–vis spectrophotometer (Make: Perkin Elmer Precisel; Model: Lambda-35) at a wavelength of 278 nm. Percent rejection by the membranes was evaluated as

$$R\ (\%) = \frac{C_f - C_p}{C_f} \times 100 \tag{3}$$

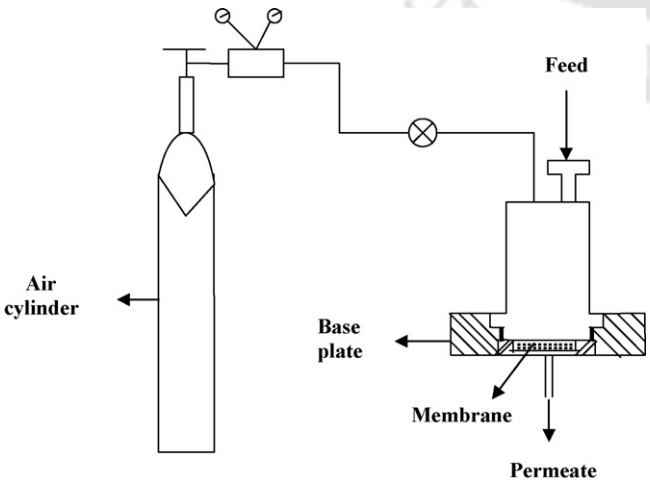


**Fig. 1.** Experimental setup for permeation experiments.

## 3. Theoretical considerations

### 3.1. Gas transport through the membrane

The average pore size and effective porosity of the membrane were determined by gas (air) permeation experiments. Population of macropores (pore diameter > 50 nm) and mesopores (pore diameter < 50 nm) [22] in the membrane top layer were also determined through this experiment. Results obtained from gas transport studies were suggested to be in agreement with those evaluated from analytical methods such as mercury porosimetry and water permeation method [23]. Average pore radius ($r$) and effective porosity ($\varepsilon/q^2$) of the membrane were determined using the following expressions [24]:

$$K = 2.133\frac{rv}{l}\frac{\varepsilon}{q^2} + 1.6\frac{r^2}{l\eta}\frac{\varepsilon}{q^2}P \tag{4}$$

$$K = \frac{WP_2}{S\ \Delta P} \tag{5}$$

In Eq. (4), the first term corresponds to Knudsen permeance and the second term corresponds to the viscous permeance. Eq. (4) was represented as a straight line in a graph drawn between $K$ and $P$. The slope and intercept of this line represents viscous and Knudsen permeability of the membrane, respectively. Henceforth the values of the slope and intercept obtained from the graph were used to evaluate the percentage contribution of pores (and pore sizes) that contribute towards viscous and Knudsen flow transport through the membrane. In other words, gaseous flux characterization of the membrane may yield qualitative information with respect to the pore size distribution applicable for the contribution of Knudsen or viscous flow regimes towards the overall membrane flux. The average pore radius of the membrane was evaluated using the intercept ($A$) and slope ($B$) and of the generated graph expressed as

$$r = 1.333\frac{B}{A}v\eta \tag{6}$$

where $A = 2.133(rv/l)(\varepsilon/q^2)$ and $B = 1.6(r^2/l\eta)(\varepsilon/q^2)$.

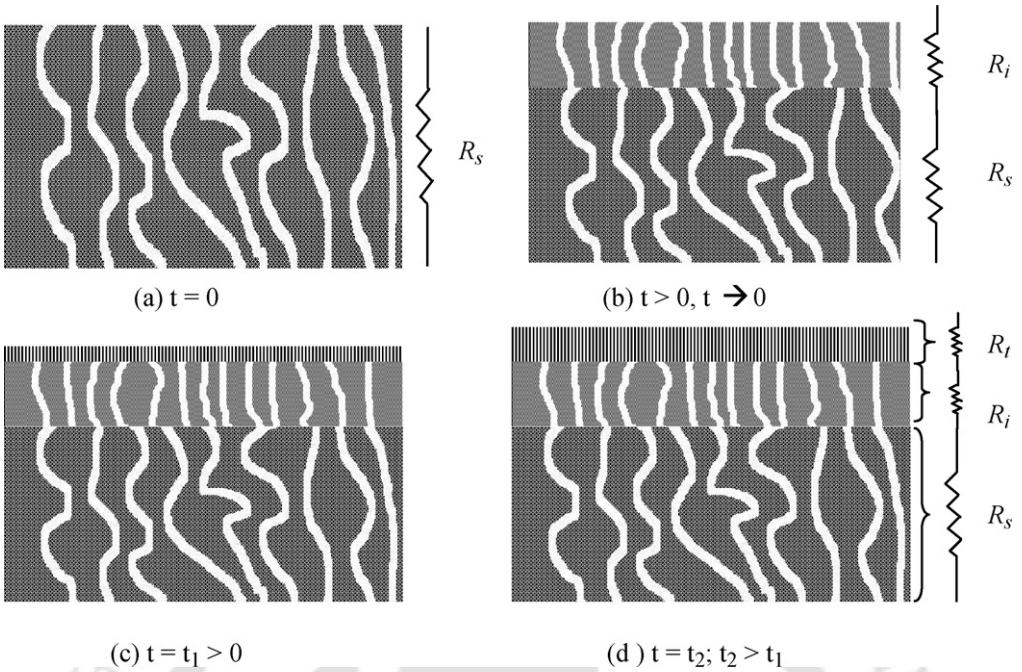


**Fig. 2.** Formation of different layers during dip coating. $R_s$: resistance of the support; $R_i$: resistance of the intermediate layer; $R_t$: resistance of the top layer; $t$: time of dip coating. (a) $t = 0$, (b) $t > 0$, $t \to 0$, (c) $t = t_1 > 0$ and (d) $t = t_2$; $t_2 > t_1$.

### 3.2. Hydraulic resistances

Fig. 2 presents a schematic of various physical phenomena occurring during dip coating. As shown, when dip coating process was initiated, instantaneously CA solution tends to penetrate through the porous structure of support surface to yield an intermediate layer (Fig. 2b) [17]. This intermediate layer played an important role in membrane durability and bonding of the top layer with the ceramic support. The structural and morphological properties of the intermediate layer were largely dependent on the pore size and porosity of the support as well as concentration of CA used for dip coating. The growth of the CA top layer was anticipated after the formation of the intermediate layer [17]. CA top layer growth rate was also largely dependent on the CA concentration in the solution, structure and morphology of the intermediate layer [5,8]. $R_m$ was expressed as a function of two different resistances, resistance of support ($R_s$) and resistance due to CA coating ($R_c$) as

$$R_m = R_s + R_c \tag{7}$$

$R_c$ can also be expressed as the sum of the intermediate layer resistances ($R_i$) and top layer resistance ($R_t$) as

$$R_c = R_i + R_t \tag{8}$$

As just after dipping the support in the solution ($t \to 0$, $t > 0$) only intermediate layer is created, so

$$R_c = R_i, \quad \text{when } t \to 0 \tag{9}$$

Total resistance of the composite membrane may be expressed by combining Eqs. (7) and (8) as

$$R_m = R_s + R_i + R_t \tag{10}$$

Now, various resistances in the above Eq. (10) may be expressed as functions of CA concentration and dipping time ($t$, s) as

$$R_s \neq f_1(c, t), \qquad R_i = f_2(c), \qquad R_t = f_3(c, t)$$

So $R_c$ can be expressed as

$$R_c = f_2(c) + f_3(c, t) \tag{11}$$



Different resistances $R_c$, $R_t$ and $R_i$ were determined using the following procedure:

(1) Calculation of $R_c$ using Eq. (8) from experimentally determined values of $R_m$ and $R_s$.
(2) Using the values of $R_c$ of same CA concentration and varying dipping time a graph was plotted. The data points in the graph were fitted in suitable linear/nonlinear curve by regression analysis.
(3) From the curve fit equation obtain from regression analysis $R_i$ value were determined using Eq. (9) by extrapolating data points to $t = 0$.
(4) The values of $R_t$ were calculated using Eq. (10).

$R_{BSA}$ was evaluated using the following equation:

$$R_{BSA} = R_{UF} - R_s - R_c \tag{12}$$

## 4. Results and discussion

In this section, results obtained from surface and flux characterization studies of fabricated membranes are discussed. The effect of dip coating parameters namely dipping time and CA solution concentration on membrane morphology, average pore size, effective porosity of the membranes, PWF, hydraulic resistance and BSA rejection studies are also presented.

### 4.1. Surface morphology

The broad intention behind the surface and cross-sectional SEM study was to visualize various possible mechanisms involved in CA deposition on the ceramic support. Besides identifying surface defects, surface morphological study aimed to evaluate the effect of dip coating parameters on ceramic matrix blocking and CA top layer growth. Thereby, the competence of deposition conditions to yield composite membranes for MF and UF applications was assessed.

Fig. 3a and b presents the SEM image of top surface and cross-section of ceramic support, respectively. It can be observed from Fig. 3a that the top surface of the support contains both the macropores and mesopores. Fig. 4 presents SEM images of the top surface

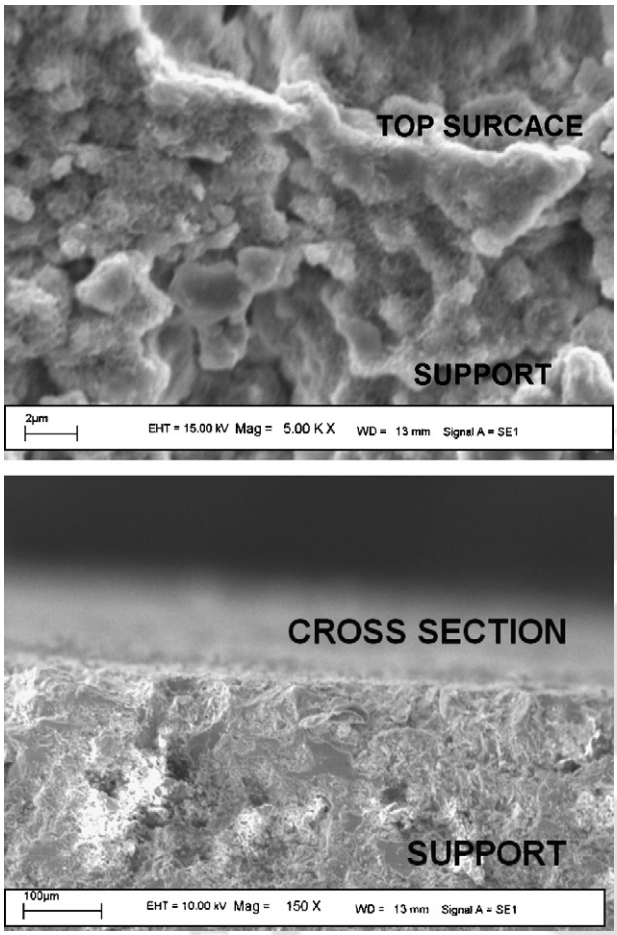


**Fig. 3.** SEM images of uncoated ceramic support: (a) top surface (magnification: 5000×) and (b) cross-section (magnification: 150×).

of composite membranes prepared by varying CA concentration (2–8 wt%) and dipping time (30–150 s). From the figure it was observed that with increase in both CA concentration and dipping time, the pore size of the membrane decreases. The SEM image of 2 wt% CA membrane (M-2-30) indicates that almost no change occurred to the porous structure in the membrane top surface. It could be further observed that the coverage of porous structure by CA increased with increasing dipping time from 30 s to 150 s. When the concentration of CA was increased to 4%, the top surface consisting of both macropores and mesopores of support was totally covered by the CA layer and create a porous polymeric structure (M-4-30 and M-4-90). The porous structure of the polymeric film was contributed by the evaporation of the solvent (acetone) from the membrane surface. With increase in dipping time from 30 s to 150 s, the pore sizes of the membranes were observed to decrease very significantly due to deposition of more CA on the support. Formation of CA porous structure accounts for an increase in the effective membrane porosity of the membranes (M-4-30, M-4-90 and M-4-150) compared to the membranes prepared with 2 wt% CA concentration (M-2-30, M-2-90 and M-2-150). This was attributed to the lack of formation of porous CA structure with 2 wt% CA solution concentrations. Finally, the membrane prepared with dipping time of 150 s (M-4-150) was observed to having the least pore sizes of all the membranes prepared at 4 wt% CA concentration. Membranes prepared with 6 wt% CA concentration (M-6-30, M-6-90 and M-6-150) indicated that a stable porous structure was formed. The pore sizes of the membranes were observed to be smaller than those obtained with 4 wt% CA concentration. With increase in dipping time the pore sizes were reduced further due to further deposition of CA on the support. The membranes prepared with 8 wt% CA (M-8-30, M-8-90 and M-8-150) were observed to possess lowest pore size among all the prepared membranes.

Fig. 5 presents the cross-sectional SEM images of the membrane prepared using varying CA solution concentration (2–8 wt%) and dipping time (30–150 s). Comparing the SEM image of ceramic support in Fig. 3b with SEM images of 2 wt% CA membranes (M-2-30, M-2-90 and M-2-150) it could be observed that CA solution penetrates into the pores of the support due to very low solution viscosity and density (almost the same as the solvent). As a result the porosity of the membranes was reduced. Further, SEM images indicate that the concentration is not enough to form a film on the support. With increase in deposition times, more CA penetration occurs in the support as observed for membrane M-2-150. Therefore CA solution contributes more towards the blocking of ceramic porous structure rather than creating a thin film on the top surface. SEM images for 4 wt% CA membrane (M-4-30, M-4-90 and M-4-150) shows similar trend like 2 wt% CA membranes. With increase in dipping time a tendency of creating film is observed. For dipping time of 150 s, a film like structure was formed on the top surface indicating the dominance of CA surface coverage over ceramic matrix blockage. The measured film thickness was about 0.6 μm. Due to less ceramic matrix blockage the effective porosity of the M-4-30, M-4-90 and M-4-150 membranes were more compared to M-2-30, M-2-90 and M-2-150 membranes. When the dip coating solution concentration was increased to 6 wt% CA, initially no film growth was observed for membrane M-6-30. With increase in dipping times, a stable film was formed for M-6-90 and M-6-150. The measured film thickness for these membranes was 8 μm and 12 μm, respectively, with increase in CA concentration in acetone, viscosity and density of the solution increases. Due to this, penetration tendency of the 8 wt% CA solution was less. As a result, less ceramic matrix blockage took place to obtain high effective porosity of the membranes compared to those prepared with 2 wt% and 4 wt% CA concentrations. For 8 wt% CA membranes (M-8-30, M-8-90 and M-8-150), a stable film growth was observed for all deposition times which increased with increasing deposition times. The measured film thickness of these membranes was 12 μm, 22 μm and 32 μm for M-8-30, M-8-90 and M-8-150, respectively. Almost no penetration of the CA into the ceramic matrix was observed due to very high viscosity and density of the CA solution.

Based on these observations from SEM, it could be concluded that with increase in CA concentration and dip coating time, the average pore size of the membranes decreases. This conclusion was in good agreement with results presented in literature [25]. For the chosen ceramic support, CA concentrations varying from 6 wt% to 8 wt% tend to be the optimal combinations to yield UF membranes (pore diameter ranging between 10 nm and 100 nm) [22] with tailored pore size distributions. On the other hand, MF membranes (pore diameter > 100 nm) [22] can be prepared using low to moderate concentrations of CA solution concentration (2–4 wt%). An increase in CA concentration was found to have profound effect in altering morphological properties than the dipping time, except for M-4-150 and M-6-30 where an increase in dipping time was found to yield similar effect as CA concentration.

### 4.2. Gas permeability

Different morphological parameters of the membranes such as pore size and effective porosity were determined from the gas permeation experiment [23]. Fig. 6a shows the variation of effective permeability factor ($K$) and average pressure ($P$) varying from 135 kPa to 308 kPa for 4 wt% CA membranes. Similar types of plot were obtained for other CA concentration membranes (figure not shown). Table 3 summarizes parameters evaluated from graphical analysis of average pressure ($P$) and effective permeability factor

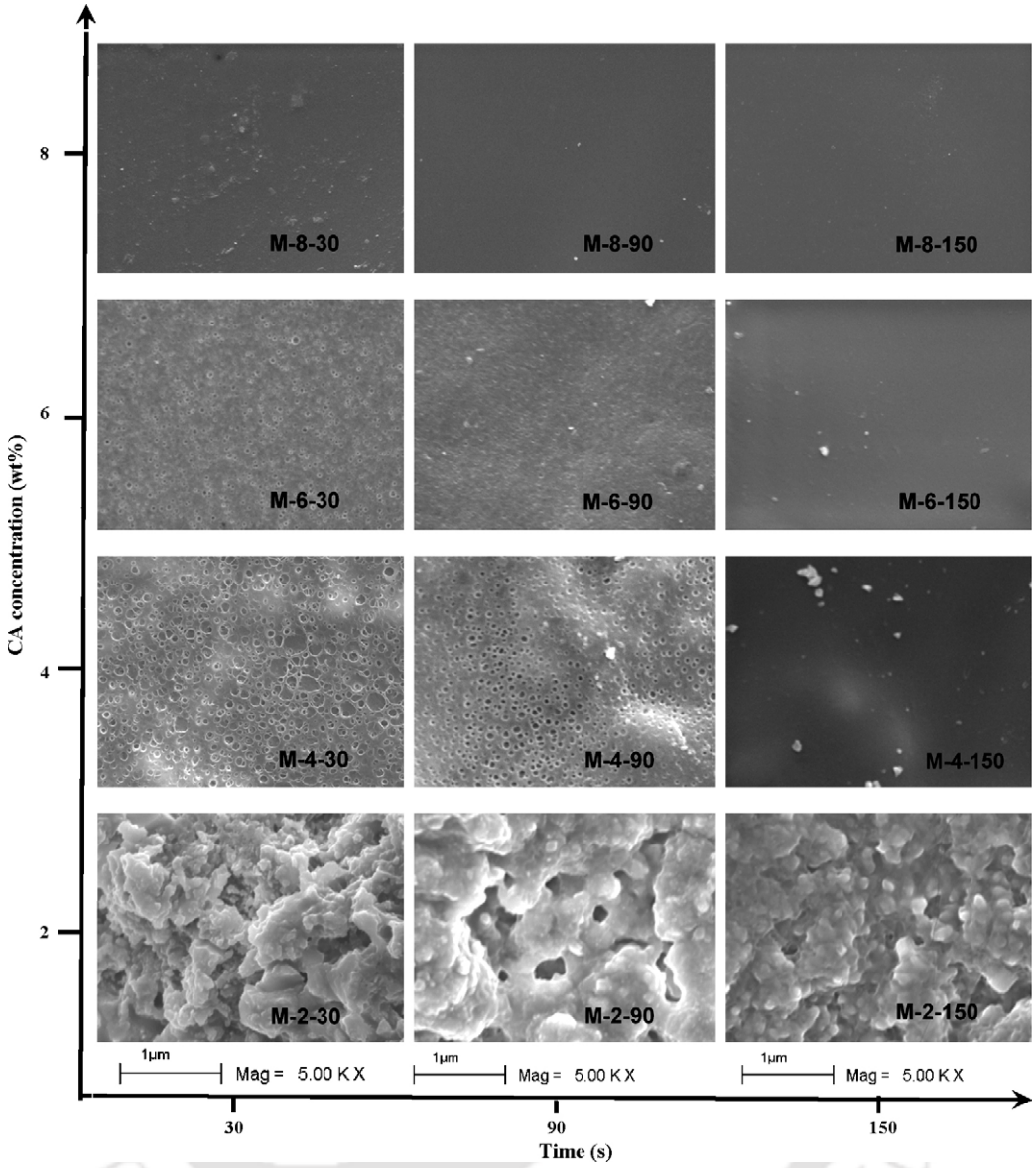


**Fig. 4.** SEM images of top surface of different composite membranes (magnification: 5000×).

**Table 3**
Various parameters evaluated from graphical analysis of gas permeation result.

| Membrane name | Permeance at 206 kPa ($m^3/(m^2\ h\ kPa)$) | Slope ($B$) ($\times 10^4$ m/(s kPa)) | Intercept ($A$) ($\times 10^2$ m/s) | Viscous flux (%) | Knudsen flux (%) |
|---|---|---|---|---|---|
| Support | 4.53 | 5.17 | 2.14 | 77–84 | 23–16 |
| M-2-30 | 4.23 | 4.66 | 2.22 | 74–87 | 26–13 |
| M-2-60 | 3.5 | 3.91 | 1.98 | 73–86 | 27–14 |
| M-2-90 | 2.9 | 3.15 | 1.66 | 72–85 | 28–15 |
| M-2-120 | 2.37 | 2.64 | 1.41 | 72–85 | 28–15 |
| M-2-150 | 2.11 | 2.29 | 1.28 | 71–85 | 29–15 |
| M-4-30 | 4.23 | 3.40 | 4.88 | 49–69 | 51–31 |
| M-4-60 | 2.92 | 3.18 | 4.69 | 48–67 | 52–33 |
| M-4-90 | 3.94 | 2.65 | 4.01 | 48–67 | 53–33 |
| M-4-120 | 3.32 | 2.21 | 3.61 | 45–65 | 55–35 |
| M-4-150 | 1.97 | 1.30 | 2.86 | 38–59 | 62–41 |
| M-6-30 | 3.01 | 1.45 | 5.42 | 27–46 | 73–55 |
| M-6-60 | 2.04 | 8.66 | 3.98 | 23–40 | 77–60 |
| M-6-90 | 1.53 | 6.18 | 2.96 | 24–39 | 76–61 |
| M-6-120 | 1.18 | 0.48 | 2.35 | 26–39 | 74–61 |
| M-6-150 | 0.72 | 0.22 | 1.58 | 22–30 | 78–70 |
| M-8-30 | 1.33 | 0.52 | 2.67 | 25–36 | 75–64 |
| M-8-60 | 0.75 | 0.29 | 1.55 | 21–36 | 79–64 |
| M-8-90 | 0.48 | 0.15 | 1.07 | 15–30 | 85–71 |
| M-8-120 | 0.30 | 0.075 | 0.70 | 14–25 | 86–75 |
| M-8-150 | 0.30 | 0.074 | 0.68 | 14–25 | 86–75 |

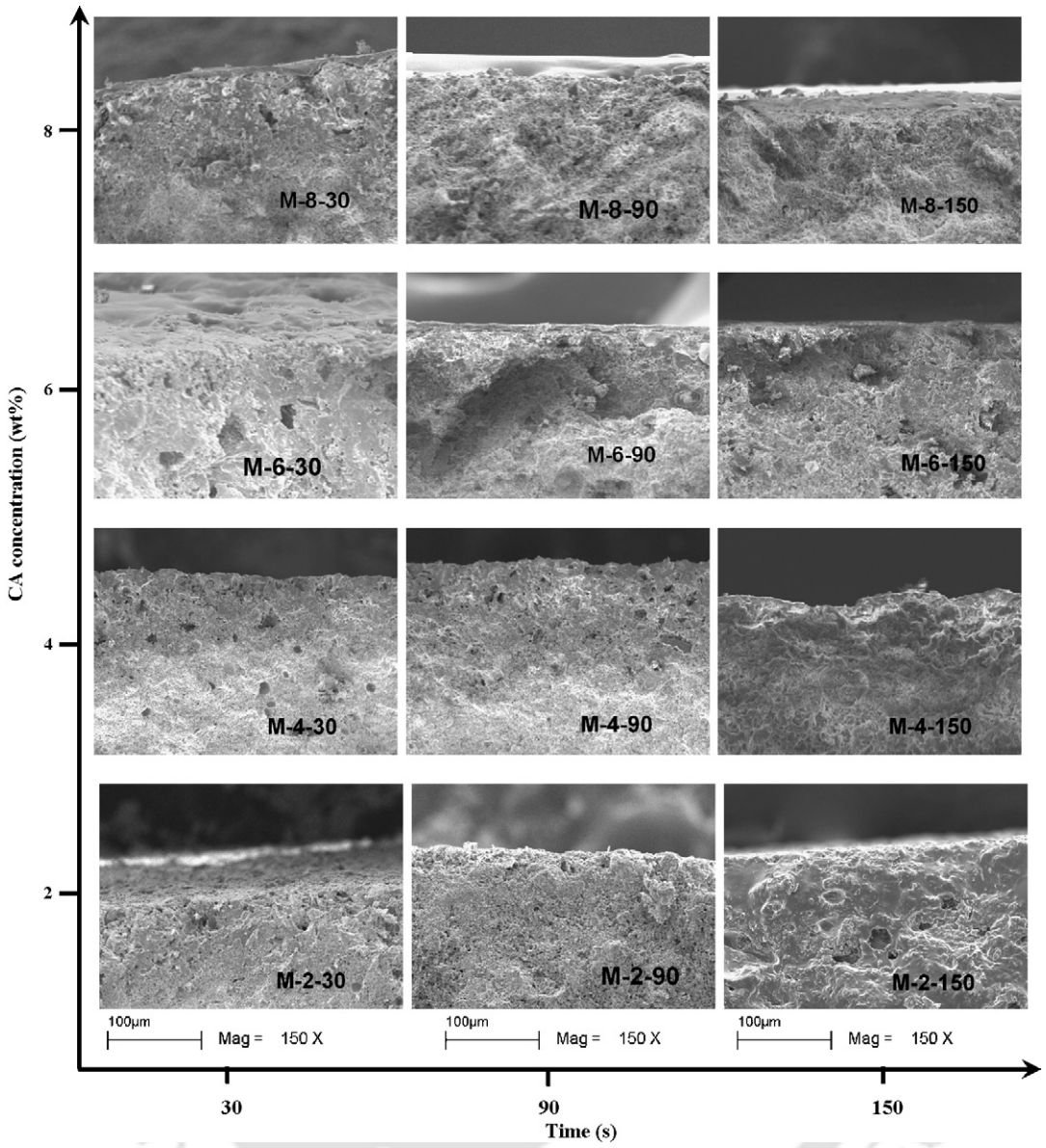


**Fig. 5.** SEM images of cross-section of different composite membranes (magnification: 150×).

($K$) data for all the membranes. As shown, the ceramic support grossly adopts viscous flux (77–84%). It can be further observed that composite membranes fabricated with 2 wt% CA concentration also have similar morphological structure like that of the support with viscous flux contributing about 71–85% to the total gas flux. This result was in good agreement with result observed from SEM analysis where almost no change in top surface morphology was observed for 2 wt% CA membranes. However, membranes prepared with 4 wt% CA concentration indicate a shift in the transport mechanism from viscous diffusion dominated domain (69–38%) to Knudsen diffusion domain (31–62%). Membranes fabricated with 6 wt% and 8 wt% CA concentration show Knudsen dominated transport properties of air where the percent contribution are 55–78% and 64–86%, respectively. This result was with good agreement with result obtained in Section 4.1 where the pore size of the membranes prepared with 6 wt% and 8 wt% CA concentrations were in the UF range.

Fig. 6b illustrates the variation of average pore size ($d_p$) of the membranes with different dipping time and CA concentration. Initially, the average pore size of the support was 560 nm. The average pore size of the CA composite membrane decreased to 487 nm when the support was subjected to dip coating at 2 wt% CA concentration and 30 s of dipping time (M-2-30). With increase in dipping time up to 150 s, the pore size of the membrane further decreased to 417 nm (M-2-150). Similar trend of reduction in average pore size was observed when the support was dip coated with 4 wt%, 6 wt% and 8 wt% CA solutions. The average pore size of the membrane varied between 162 nm and 106 nm for 4 wt%, 62–32 nm for 6 wt% and 46–25 nm for 8 wt% CA concentration solutions and dipping time varying from 30 s to 150 s.

Fig. 6c illustrates the variation of effective porosity ($\varepsilon/q^2$) of the membranes with varying dip time and CA concentrations. The effective porosity of the membrane was observed to reduce from 0.33 for support to 0.001–0.002 for 2 wt% CA membranes. The reduction of the porosity was due to the presence of thin CA layer on the top surface of the membrane and blocking of porous structure of the support as discussed in Section 4.1. However, an increase in effective porosity of the membrane was observed when the CA concentration was increased up to 6 wt%. The effective porosity of the membrane varied between 0.012 and 0.01 for 4 wt% and 0.035–0.02

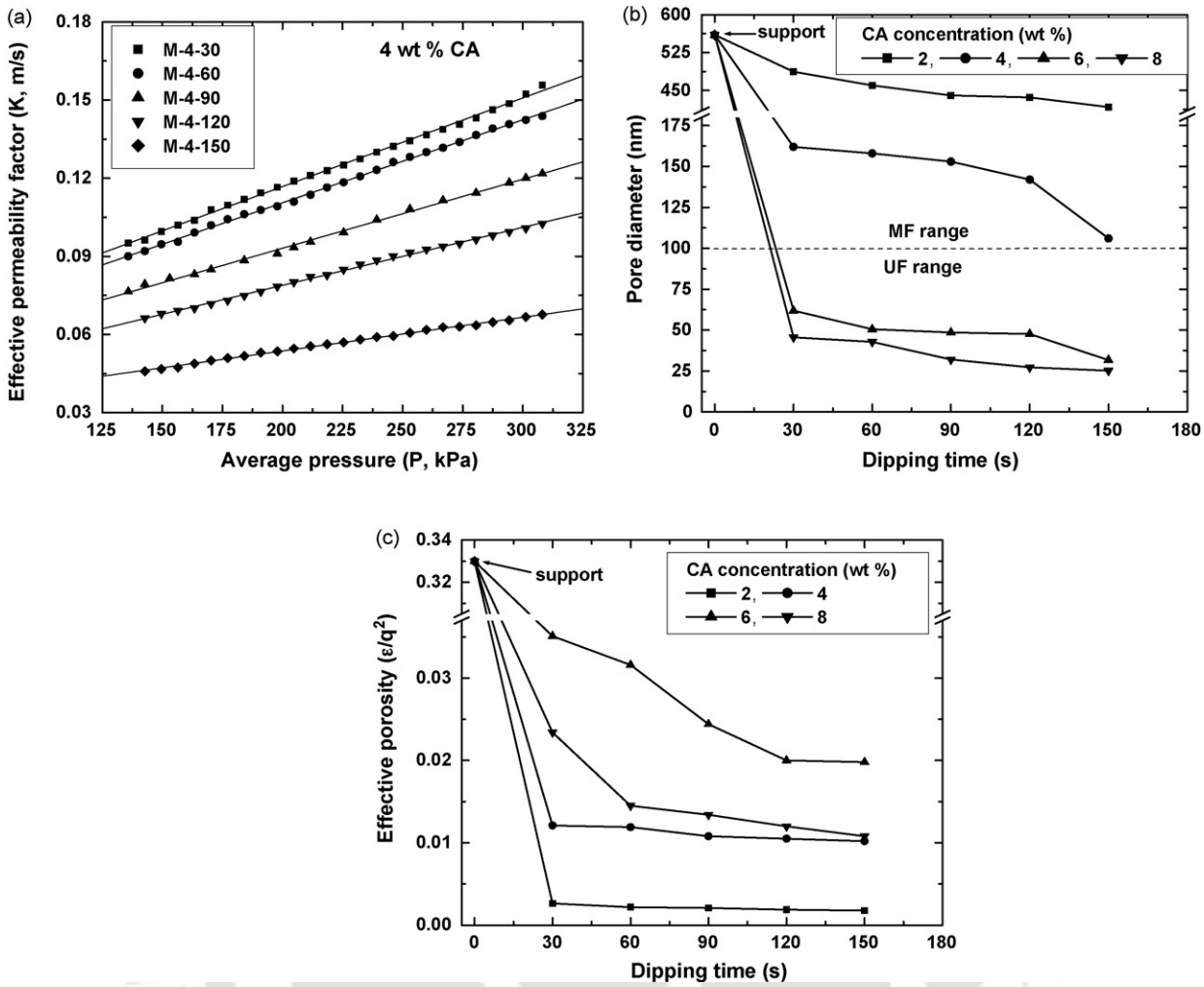


**Fig. 6.** (a) Variation of effective permeability factor ($K$) with average pressure ($P$) for 4 wt% CA membranes. Variation of (b) average pore diameter and (c) effective porosity of the composite membrane with varying CA concentration and dipping time.

for 6 wt% CA concentrations with varying dipping time from 30 s to 150 s. The increase in effective porosity was due to the less amount of ceramic matrix blockage with increase in CA concentration as discussed in Section 4.1. However there was a decrease in the effective porosity of the membrane prepared using 8 wt% CA compared to 6 wt% CA membranes. This can be explained from the top surface and cross-sectional SEM images of 6 wt% and 8 wt% CA concentration membranes shown in Figs. 4 and 5. Cross-sectional images inferred that all the membranes have almost no ceramic matrix blockage compare to cross-section image of Fig. 3b. But the top surface images shows that 8 wt% membranes contains less porosity compare to 6 wt% CA concentration membranes. The average pore size of the 6 wt% membrane varied from 62 nm (M-6-30) to 32 nm (M-6-150) as opposed to 46 nm (M-8-30) to 25 nm (M-8-150) for 8 wt% CA membranes. As a result overall porous permeation area for 6 wt% membranes are more compared to 8 wt% membranes.

### 4.3. Membrane compaction

Fig. 7 presents pure water compaction profiles for different membranes prepared in this work. From the figure it can be observed that the PWF was initially high and declined gradually to reach a steady state value after 3–4 h for all the fabricated membranes. The reduction in PWF was due to the fact that the walls of the pores become closer, denser and uniform during compaction [22]. With increase in dipping time and CA concentration, compaction factor calculated as ratio of initial PWF and final PWF of the membrane was increased. This increase was due to increase in film thickness as well as number of voids in the porous structure.

### 4.4. Hydraulic permeability

Fig. 8 shows the effect of dip coating parameters on the hydraulic permeability ($P_m$) of the prepared membranes. From the figure it can be infered that for M-2-30 membrane decrease in $P_m$ was very less ($6.14 \times 10^{-6}$–$4.98 \times 10^{-6}$ $m^3/(m^2\,s)$). With increase in dipping time as well as CA concentration $P_m$ decreases. This was due to the fact that, with increase in both dipping time and CA concentration, the average pore size of the membrane decreases and top layer thickness increases.

### 4.5. Protein rejection

Fig. 9 presents the variation of permeate flux and rejection (%) of BSA with dipping time for the membrane fabricated at 6 wt% and 8 wt% CA membranes. As shown, the flux through the membrane decreased and percent BSA rejection increased with an increase in dipping time and CA concentration. The membrane flux decreased from 212 $m^3/(m^2\,s)$ to 43.9 $m^3/(m^2\,s)$ when the dipping time was increased from 30 s (M-6-30) to 150 s (M-6-150). Similarly, the membrane flux reduced from 58.9 $m^3/(m^2\,s)$ to 12.2 $m^3/(m^2\,s)$ for membranes prepared with 8 wt% CA solution concentrations with

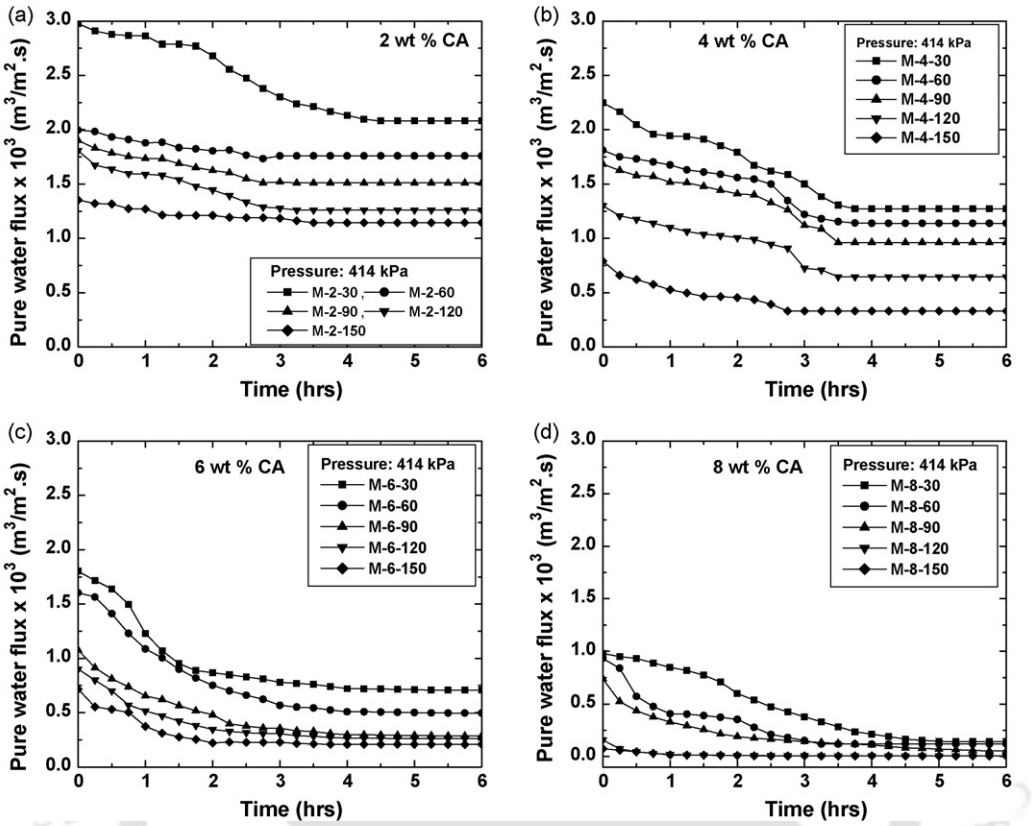


**Fig. 7.** Variation of PWF with time during compaction of CA coated composite membranes: (a) 2 wt% CA, (b) 4 wt% CA, (c) 6 wt% CA and (d) 8 wt% CA.

an increase in dip time from 30 s to 150 s. The reduction in membrane flux and an increase in BSA rejection with increase in dipping time was due to decrease in average pore size and porosity of the membranes. Percent BSA rejection was evaluated to vary from 5% (M-6-30) to 42.5% (M-6-150) for 6 wt% CA membranes and 20% (M-8-30) to 50% (M-8-150) for 8 wt% CA membranes. Comparing the flux and BSA rejection properties it could be concluded that membrane M-6-150 (pore size 32 nm, porosity 0.02) was the best membrane for the UF as it provides higher rejection properties as well as higher flux compared to other membrane. For the membranes prepared with 2 wt% and 4 wt% CA concentration negligible amount of BSA rejection was observed. This is justified because the average membrane pore sizes of those membranes (487–417 nm for 2 wt% CA and 162–106 nm for 4 wt% CA) are in the MF range.

### 4.6. Different resistances

Based on measured PWF for different composite membranes and ceramic support, $R_s$, $R_m$ and $R_{BSA}$ were determined using Eq. (2). Fig. 10 presents the variation of composite $R_m$ with varying dipping time for various concentration of CA solution (2–8 wt%). The total resistance of the composite membranes involved a nonlinear increase with increase in CA concentration and dipping time ranging from $2.01 \times 10^6$ m$^2$ s kPa/m$^3$ to $72.28 \times 10^6$ m$^2$ s kPa/m$^3$. Fig. 11a presents the variation of $R_c$ with dipping time for different CA con-

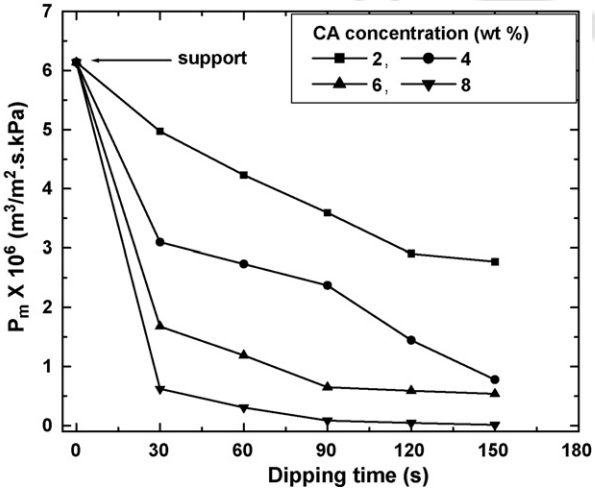


**Fig. 8.** Effect of CA concentration and dipping time on the hydraulic permeability of different composite membranes.

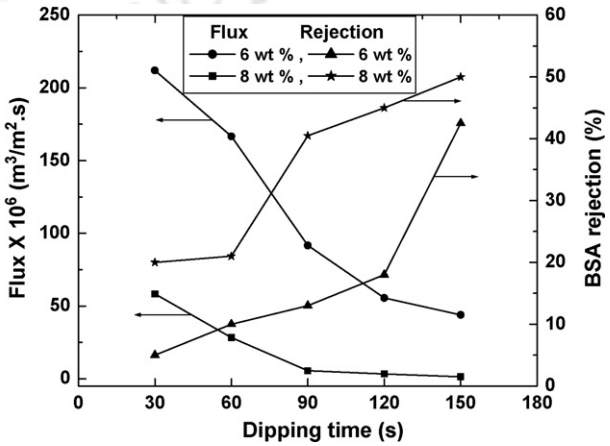


**Fig. 9.** Permeate flux and BSA rejection profile for membrane fabricated at 6 wt% and 8 wt% CA concentrations at different dipping time.

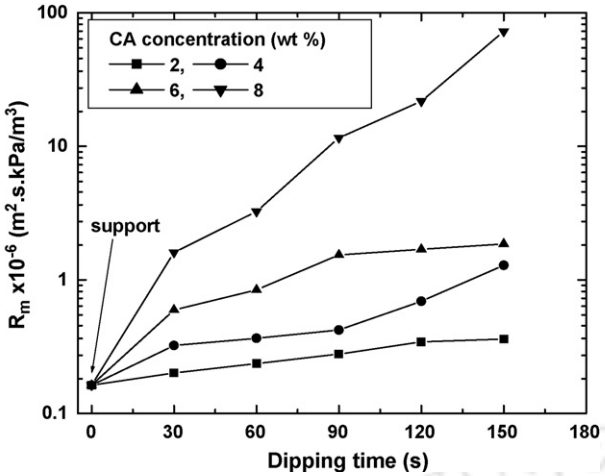


**Fig. 10.** Effect of CA concentration and dipping time on the membrane resistance ($R_m$) of different composite membranes.

centrations. The graphical trends illustrate that a semi log plot of $R_c$ vs. $t$ follows straight line. This further confirms that the CA film growth over ceramic support increases exponentially with increase in dipping time. Therefore, $R_c$ was expressed as

$$R_c = Me^{at} \quad (13)$$

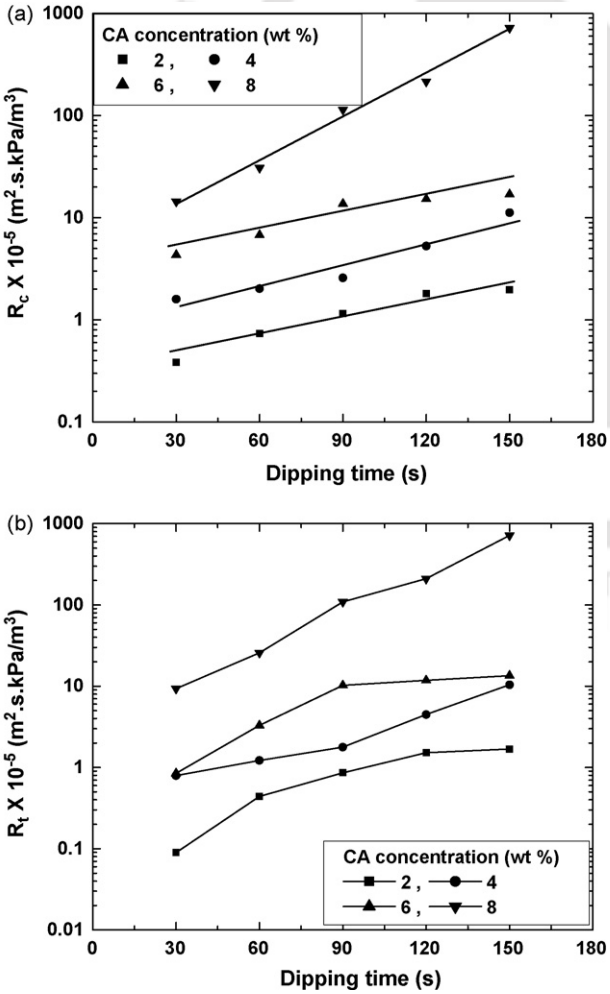


**Fig. 11.** Effect of CA concentration and dipping time on the (a) coating resistance ($R_c$) and (b) top layer resistance ($R_t$) of different composite membranes.

**Table 4**
Regression parameters for coating layer hydraulic resistance.

| CA concentration (wt%) | $M = R_i$ ($\times 10^{-5}$ m$^2$ s kPa/m$^3$) | $a$ (s$^{-1}$) | Square of correlation coefficient ($R^2$) |
|---|---|---|---|
| 2 | 0.32 | 0.014 | 0.95 |
| 4 | 0.91 | 0.0162 | 0.93 |
| 6 | 3.48 | 0.0118 | 0.89 |
| 8 | 5.09 | 0.0326 | 0.99 |

where $M$ and $a$ are constant, evaluated from linear regression analysis. Using the condition of Eq. (9) ($R_c = R_i$, when $t \to 0$) resistance of the intermediate layer was determined as $R_i = M$. The calculated values of $R_i$, $a$ along with correlation coefficient ($R^2$) are presented in Table 4. Based on the values $R_c$ and $R_i$, $R_t$ was evaluated using Eq. (10). Fig. 11b presents the variation of $R_t$ with varying CA concentration and dipping time. $R_i$ was found to vary from $0.323 \times 10^6$ m$^2$ s kPa/m$^3$ to $5.09 \times 10^6$ m$^2$ s kPa/m$^3$ and $R_t$ varied from $0.089 \times 10^6$ m$^2$ s kPa/m$^3$ to $71.6 \times 10^6$ m$^2$ s kPa/m$^3$. The observed trends for both the resistances illustrate the nonlinear variation with the dip coating parameters.

Fig. 12 summarizes the percentage contributions of different resistances ($R_s$, $R_i$ and $R_t$) of different composite membranes during water permeation experiment. It may be observed from the figure that for low CA concentration $R_s$ dominates the total resistance varying from 81% (M-2-30) to 45.1% (M-2-150) and percent contribution of $R_s$ to the overall hydraulic resistance decreases with increasing CA solution concentration. For highest CA concentration studied in this work (8 wt%) $R_s$ was observed about 10.14% (M-8-30) to 0.22% (M-8-150). Similar trend was also observed for $R_i$. Contribution of $R_i$ varies from 14.6% (M-2-30) to 8.13% (M-2-150) for 2 wt% CA concentration and 31.7% (M-8-30) to 0.7% (M-8-150) for 8 wt% CA membrane. However, an increase in the percent contribution of $R_i$ was observed at low dipping time of 30 s. This was due to the increase in CA concentration. With increase in CA concentration $R_i$ increase (Table 4) as a result its percent contribution also increases. Percent contribution of $R_t$ increases with increase in both concentration and dipping time. This was due to the fact that with increase in dipping time as well as CA concentration top layer film thickness increases and pore size decreases which resulted in the reduction of membrane permeability.

Fig. 13 presents the resistance offered by BSA solution ($R_{BSA}$) during UF experiment calculated using Eq. (12) for 6 wt% and 8 wt% CA composite membranes. As shown, $R_{BSA}$ increases from $5.85 \times 10^6$ m$^2$ s kPa/m$^3$ to $28.27 \times 10^6$ m$^2$ s kPa/m$^3$ for 6 wt% membrane and $21.27 \times 10^6$–$893.56 \times 10^6$ m$^2$ s kPa/m$^3$ for 8 wt% membrane. This increase was due to the decrease in pore size of

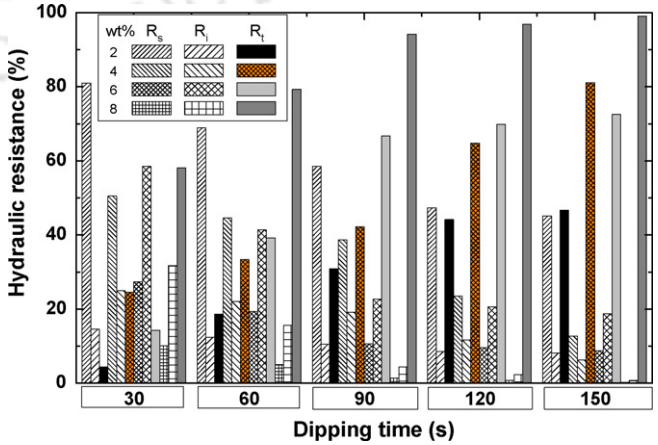


**Fig. 12.** Percent contribution of different resistances offered by composite membranes fabricated at different CA concentration and dipping time.

**Table 5**
Percent contribution of different resistances offered by composite membranes fabricated at different CA concentration and dipping time during UF of BSA.

| CA concentration (wt%) | Time (s) | $R_s$ (%) | $R_i$ (%) | $R_t$ (%) | $R_{BSA}$ (%) | $R_{UF}$ ($\times 10^{-5}$ m$^2$ s kPa/m$^3$) |
|---|---|---|---|---|---|---|
| 6 | 30 | 2.77 | 5.95 | 1.45 | 89.83 | 58.56 |
| | 60 | 2.19 | 4.68 | 4.43 | 88.70 | 74.46 |
| | 90 | 1.2 | 2.57 | 7.58 | 88.65 | 135.39 |
| | 120 | 0.73 | 1.56 | 5.29 | 92.42 | 223.39 |
| | 150 | 0.58 | 1.23 | 4.77 | 93.42 | 282.77 |
| 8 | 30 | 0.77 | 2.39 | 4.39 | 92.45 | 212.75 |
| | 60 | 0.37 | 1.16 | 5.88 | 92.59 | 438.02 |
| | 90 | 0.07 | 0.23 | 4.88 | 94.82 | 2233.90 |
| | 120 | 0.04 | 0.14 | 5.65 | 94.17 | 3723.17 |
| | 150 | 0.02 | 0.06 | 8.02 | 91.90 | 8935.61 |

the membranes with increase in CA concentration as well as dipping time. Table 5 summarizes the different resistances offered by 6 wt% and 8 wt% CA composite membranes during UF of BSA.

Table 5 presents the resistance offered by different layers of composite membrane during UF of BSA calculated using Eq. (12) for 6 wt% and 8 wt% CA composite membranes. It may be seen from the table that the resistance offered by the BSA solution over membrane surface ($R_{BSA}$) was more compared to all other resistances for all the membranes. The contributions of $R_{BSA}$ varied from 89.8% to 94.17% of the total resistance ($R_{UF}$). These findings infer that the fabricated composite membranes do not offer significant hydraulic resistances during UF of BSA solution.

### 4.7. Phenomenological models for parameter dependency

This section presents the derivation of phenomenological models for the fabrication of composite membranes with dip coating method using the concept of hydraulic resistance of the polymeric film layer. The phenomenological models are conceptualized for the evaluation of parameter dependency either considering membrane properties or dip coating parameters. The primary goals behind the development of these empirical models are to provide insights into the contribution of various parameters to membrane morphology during dip coating.

#### 4.7.1. Membrane parameters

The total hydraulic resistance of the composite membrane can be phenomenologically expressed as functions of support resistance, average pore size, effective porosity and thickness of the membrane and support as

$$\frac{R_m}{R_s} = \left(\frac{d_{p,m}}{d_{p,s}}\right)^{bt} \left[\left(\frac{(\varepsilon/q^2)_m}{(\varepsilon/q^2)_s}\right)\right]^{d} \left(\frac{h_m}{h_s}\right)^{e} \tag{14}$$

The CA film thickness estimated from SEM analysis were varied from 0.6 μm to 32 μm compared to the thickness of the support (4.5 mm). Therefore, the term $(h_m/h_s)^e$ tends to a value of unity ($h_m \approx h_s$). So, Eq. (14) can be expressed as

$$\frac{R_m}{R_s} = \left(\frac{d_{p,m}}{d_{p,s}}\right)^{bt} \left[\left(\frac{(\varepsilon/q^2)_m}{(\varepsilon/q^2)_s}\right)\right]^{d} \tag{15}$$

where $b$ and $d$ are constants to be evaluated numerically. Hypothetically, the above expression can be analyzed from graphical trends presented in Figs. 6b, 6c and 10. As indicated in these figures, with increasing CA concentration and dipping time, membrane hydraulic resistance increases (Fig. 10) whereas the average membrane pore size decreases (Fig. 6b). However, the effective porosity was found to increase with increasing values of CA concentrations and decrease with increasing dipping times (Fig. 6c). Further, the phenomenological expression infers that when the composite membrane pore size and effective porosity approaches to that of the support, the total resistance of the membrane should approach the resistance measured for the ceramic support. Henceforth, the magnitude of parameters $b$ and $d$ quantifies the dependency of structural parameters ($d_{p,m}$, $d_{p,s}$, $(\varepsilon/q^2)_m$ and $(\varepsilon/q^2)_s$) on its transport properties. The evaluation of these parameters was carried out with nonlinear regression technique using resistances ($R_m$ and $R_m$), average membrane pore sizes and effective porosity of the membrane for different CA concentration and dipping time and support, obtained from liquid and gas permeation experiments.

Fig. 14a illustrates the experimental and calculated values of ($R_m/R_s$) for all the four CA concentrations and dipping time used in this work. Table 6a summarizes the values of modeled parameters $b$ and $d$ along with the errors. From the figure it can be observed that the phenomenological empirical model equations used in this work evaluate membrane resistances with acceptable accuracy. Values of parameter $b$ varies from −0.0018 to −0.0143 whereas the parameter $d$ varies from −0.0367 to −0.5467. Further, it can be observed that both parameters $b$ and $d$ depends on the concentration of CA. Negative sign of these two parameters indicates that the ratio of pore diameter and effective porosity of membrane and support

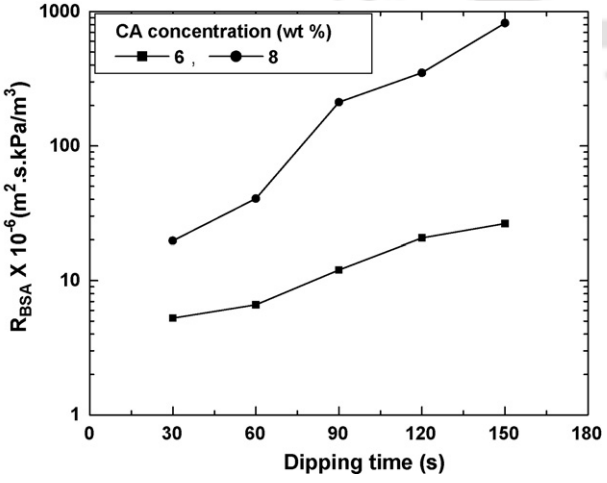


**Fig. 13.** Effect of CA concentration and dipping time on the resistance offered by BSA ($R_{BSA}$) solution during ultrafiltration experiment using different composite membranes.

**Table 6a**
Regressed phenomenological model parameters of Eq. (15).

| Concentration | Parameter | | Error (%) | | | |
|---|---|---|---|---|---|---|
| | $b$ | $d$ | Maximum | Minimum | Average | RMS |
| 2 | −0.0143 | −0.0367 | 5.35 | 1.03 | 3.27 | 3.81 |
| 4 | −0.0072 | −0.0747 | 5.24 | 0.49 | 2.6 | 3.01 |
| 6 | −0.0018 | −0.6059 | 5.36 | 2.24 | 4.17 | 4.3 |
| 8 | −0.0090 | −0.5467 | 11.81 | 7.68 | 10.12 | 10.22 |

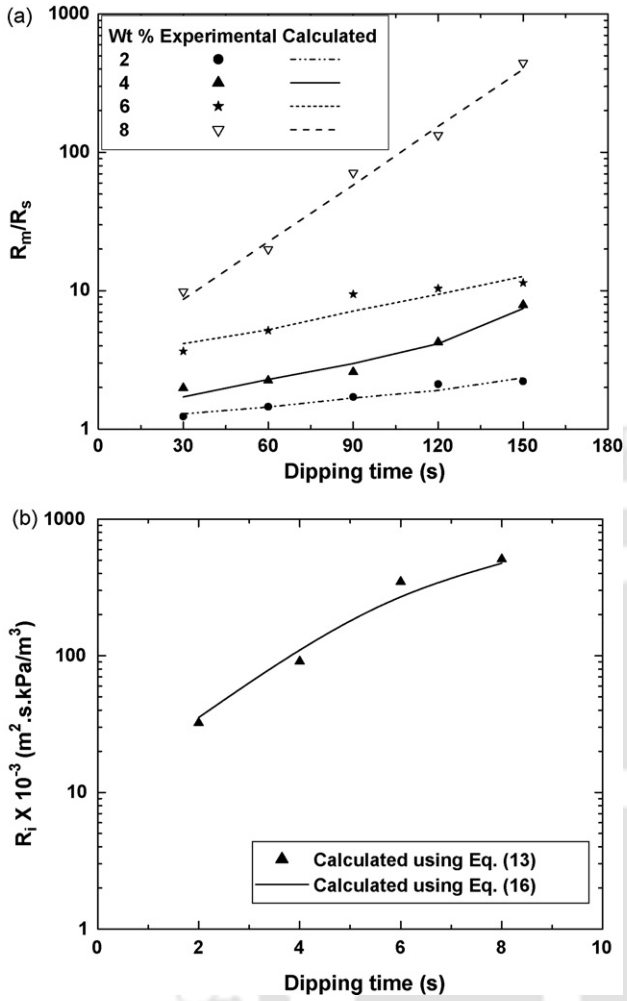


**Fig. 14.** (a) Experimental and calculated values of ($R_m/R_s$) for different CA concentrations varying dipping time. (b) Comparison between calculated values of intermediate layer resistance ($R_i$) using Eqs. (13) and (16).

would be ($d_{p,s}/d_{p,m}$) and $((\varepsilon/q^2)_m/(\varepsilon/q^2)_s)$ rather than ($d_{p,m}/d_{p,s}$) and $((\varepsilon/q^2)_s/(\varepsilon/q^2)_m)$ as the membrane resistance increases with decrease in both average pore diameter and effective porosity of the membrane.

*4.7.2. Dip coating parameters*

As discussed in Section 3.2, the resistance due to coating of the membrane was the sum of intermediate layer resistance and top layer resistance ($R_c = R_i + R_t$). As observed from Table 4, $R_i$ was dependent only on CA concentration ($c$), whereas $R_t$ were dependent on both CA concentration ($c$) and dipping time ($t$) (Fig. 11b). So, $R_t$ should be regarded as a function of $c$ and $t$ together. With this hypothesis, Eq. (13) was further modified to yield a phenomenological expression to evaluate the resistance dependency of dip coating parameters:

$$R_c = Nc^f e^{gct} \tag{16}$$

The parameters, $N$, $f$ and $g$ needs to be evaluated by nonlinear regression analysis using calculated values of $R_c$ at different $c$ and $t$. The magnitude of parameters $f$ and $g$ infer the dependency of $R_c$ on both $c$ and $t$. Further, it can be noted here that the expression $Nc^f$ refers to $R_i$. Calculated values of the regressed parameters $N$, $f$, $g$ corresponding to Eq. (16) are shown in Table 6b. The obtained values of $N$, $f$, and $g$ indicate that dip coating process is more critically influenced by solution concentrations rather than

**Table 6b**
Regressed phenomenological model parameters of Eq. (16).

| Parameter | Value | Error (%) | | | |
|---|---|---|---|---|---|
| | | Maximum | Minimum | Average | RMS |
| $N$ | 13,061.21 | | | | |
| $F$ | 1.7289 | 15.62 | 4.95 | 11.62 | 12.86 |
| $g$ | 0.0024 | | | | |

dipping time. Based on the regression analysis, calculated values of $R_i$ obtained from Eqs. (13) and (16) was compared and shown in Fig. 14b. From the figure it can be observed that the phenomenological empirical model Eq. (16) evaluate intermediate layer resistance of the membrane was with acceptable accuracy. The intermediate layer resistance was found to vary from $0.32 \times 10^5$ m$^2$ s kPa/m$^3$ to $5.09 \times 10^5$ m$^2$ s kPa/m$^3$ from Eq. (13) and $0.35 \times 10^5$ to $4.75 \times 10^5$ from Eq. (16), which are in the same range. The values of parameter $gc$ obtained from Eq. (16) (varies from 0.0049 to 0.019) are also in same order with those obtained from Eq. (13) (varies from 0.011 to 0.032).

*4.7.3. Error analysis*

To quantify the confidence levels of evaluated parameters, an error analysis was conducted for all regressed parameters ($b$, $d$, $N$, $f$ and $g$). Tables 6a and 6b present results obtained from error analysis. As presented, the maximum and minimum error for parameters $b$ and $d$ (Eq. (15)) were 11.81% (M-8-120) and 0.49% (M-4-60) for all cases with an average error varying from 2.6% (4 wt% CA) to 10.12% (8 wt% CA). The RMS error calculated for Eq. (15) varies from 3.01% to 10.22%. Similar types of errors were also calculated for Eq. (16) where maximum and minimum error was 15.62% and 4.96%. Average and RMS error was 11.62% and 12.85%, respectively, which confirms the validity of the proposed phenomenological models in the present study.

## 5. Conclusions

Though numerous articles have addressed the fabrication of polymer–ceramic composite membranes, this work was dovetailed towards extending the conceptual barriers of polymer–ceramic composite membranes. Cellulose acetate–ceramic composite membranes were prepared using a low cost kaolin based ceramic membrane support using dip coating technique. Effect of dip coating parameters namely CA concentration (varying from 2 wt% to 8 wt%) in acetone and dipping time (varying from 30 s to 150 s) on the prepared membranes were studied. Morphological study, gas (air) and liquid (water) permeation study and UF experiments using BSA solution were performed in detail. Average pore size and effective porosity for different composite membrane were determined from the gas permeation data. Analysis shows that the composite membrane prepared with 2 wt% and 4 wt% CA were suitable for MF applications and those with 6 wt% and 8 wt% were for UF applications. Different resistances of the composite membrane were analyzed using permeation experiments data. Ceramic composite membrane was found to be formed by blockage of ceramic support matrix (formation of intermediate layer) followed by deposition of CA over the support (formation of top layer). The intermediate layer hydraulic resistance was evaluated to be nonlinearly dependent on the CA concentration only whereas the top layer resistance was found to be dependent on both the parameters of dip coating. The CA film growth rate was found to follow exponential trend with dip coating parameters. Fabricated membranes were used to separate BSA solution at 345 kPa pressure differential in batch mode of operation. The flux and rejection characteristics of different membranes were investigated. A resistance in series model was proposed to determine different resistances offered during UF

of BSA solution. The analysis inferred that, the fabricated composite membrane may be useful for the industrial application since only 6–11% of the total resistance offered by these composite membranes during UF of BSA solution. Finally, phenomenological models were developed to evaluate the parameter dependency of membrane morphology as well as dip coating parameter on the hydraulic resistance of membranes. These research findings are anticipated to further strengthen precision in polymer–ceramic composite membranes technology and pave the way for rapid commercialization in the near future.

## Nomenclature

*List of symbols*

| | |
|---|---|
| $A$ | intercept of Eq. (4) (m/s) |
| $B$ | slope of Eq. (4) (m/(s kPa)) |
| $c$ | concentration of CA in acetone (wt%) |
| $C_f$ | concentration of BSA in feed (mg/L) |
| $C_p$ | concentration of BSA in permeate (mg/L) |
| $d_{p,m}$ | pore diameter of composite membrane (m) |
| $d_{p,s}$ | pore diameter of support (m) |
| $f_1, f_2, f_3$ | functions |
| $h_m$ | total thickness of composite membrane (m) |
| $h_s$ | total thickness of support (m) |
| $K$ | effective permeability factor (m/s) |
| $l$ | length of the pore (m) |
| $P$ | average pressure (kPa) |
| PWF | Pure water flux, ($m^3/(m^2\,s)$) |
| $P_m$ | hydraulic permeability, ($m^3/(m^2\,s\,kPa)$) |
| $\Delta P$ | transmembrane pressure drop (kPa) |
| $P_2$ | membrane pressure at permeate side (kPa) |
| $Q$ | quantity of permeate ($m^3$) |
| $R_{BSA}$ | resistance offered by BSA film ($m^2\,s\,kPa/m^3$) |
| $R_c$ | resistances due to CA coating ($m^2\,s\,kPa/m^3$) |
| $R_i$ | resistances offered by intermediate layer ($m^2\,s\,kPa/m^3$) |
| $R_m$ | hydraulic resistance of composite membrane ($m^2\,s\,kPa/m^3$) |
| $R_s$ | resistance of the support ($m^2\,s\,kPa/m^3$) |
| $R_t$ | resistances offered by the top layer ($m^2\,s\,kPa/m^3$) |
| $R_{UF}$ | total hydraulic resistance during UF ($m^2\,s\,kPa/m^3$) |
| $r$ | average pore radius of membrane (m) |
| $S$ | effective membrane area ($m^2$) |
| $v$ | molecular mean velocity of the gas (m/s) |
| $W$ | volumetric flow rate, ($m^3/s$) |
| $(\varepsilon/q^2)_m$ | effective porosity of the composite membrane |
| $(\varepsilon/q^2)_s$ | effective porosity of the support |
| $\eta$ | viscosity of gas (kPa s) |

## References


[1] R.S. Faibish, Y. Cohen, Fouling resistant ceramic supported polymer membranes for ultrafiltration of oil-in-water microemulsions, J. Membr. Sci. 185 (2001) 129.
[2] Y. Matsumoto, M. Sudoh, Y. Suzuki, Preparation of composite UF membranes of sulfonated polysulfone coated on ceramics, J. Membr. Sci. 158 (1999) 55.
[3] S. Sachdeva, A. Kumar, Synthesis and modeling of composite poly(styrene-co-acrylonitrile) membrane for the separation of chromic acid, J. Membr. Sci. 307 (2008) 37.
[4] W. Yoshida, Y. Cohen, Ceramic-supported polymer membranes for pervaporation of binary organic/organic mixtures, J. Membr. Sci. 213 (2003) 145.
[5] K.M. Song, W.H. Hong, Dehydration of ethanol and isopropanol using tubular type cellulose acetate membrane with ceramic support in pervaporation process, J. Membr. Sci. 123 (1997) 27.
[6] X. Cao, T. Zhang, Q.T. Nguyen, Y. Zhang, Z. Ping, A novel hydrophilic polymer–ceramic composite membrane. 1. Acrylic acid grafting membrane, J. Membr. Sci. 312 (2008) 15.
[7] Y. Chen, F. Xiangli, W. Jin, N. Xu, Organic–inorganic composite pervaporation membranes prepared by self-assembly of polyelectrolyte multilayers on macroporous ceramic supports, J. Membr. Sci. 302 (2007) 78.
[8] Y. Ki Hong, W.H. Hong, Influence of ceramic support on pervaporation characteristics of IPA/water mixtures using PDMS/ceramic composite membrane, J. Membr. Sci. 159 (1999) 29.
[9] F. Xiangli, W. Wei, Y. Chen, W. Jin, N. Xu, Optimization of preparation conditions for polydimethylsiloxane (PDMS)/ceramic composite pervaporation membranes using response surface methodology, J. Membr. Sci. 311 (2008) 23.
[10] N. Singh, M. Cherya, Process Design, Economic analysis of a ceramic membrane system for microfiltration of corn starch hydrolysate, J. Food Eng. 38 (1998) 57.
[11] Sterlitech Corporation, USA, http://www.sterlitech.com/ (May 2008).
[12] H. Yanagishita, D. Kitamoto, K. Haraya, T. Nakane, T. Tsuchiya, N. Koura, Preparation and pervaporation performance of polyimide composite membrane by vapor deposition and polymerization (VDP), J. Membr. Sci. 136 (1997) 121.
[13] P. Aranda, W.J. Chen, C.R. Martin, Water transport across polystyrenesulfonate/alumina composite membranes, J. Membr. Sci. 99 (1995) 185.
[14] M.E. Rezac, W.J. Koros, Preparation of polymer–ceramic composite membranes with ultrathin defect-free separating layers, J. Appl. Polym. Sci. 46 (1992) 1927.
[15] Y. Gu, G. Meng, A model for ceramic membrane formation by dip-coating, J. Eur. Ceram. Soc. 19 (1999) 1961.
[16] A.A. Babaluo, M. Kokabi, M. Manteghian, R. Sarraf-Mamoory, A modified model for alumina membranes formed by gel-casting followed by dip-coating, J. Eur. Ceram. Soc. 24 (2004) 3779.
[17] E. Levänen, T. Mäantyl, P. Mikkola, J.B. Rosenholm, Layer buildup on two-layered porous substrate by dip-coating: modeling and effect of additives on growth rate, J. Colloid Interf. Sci. 230 (2000) 186.
[18] B.K. Nandi, R. Uppaluri, M.K. Purkait, Preparation and characterization of low cost ceramic membranes for microfiltration applications, Appl. Clay Sci. 42 (2008) 102.
[19] V. Osada, I. Nakagawa, Membrane Science and Technology, Marcel Dekker Inc., New York, 1992.
[20] K.M. Persson, V. Gekas, G. Trägårdh, Study of membrane compaction and its influence on ultrafiltration water permeability, J. Membr. Sci. 100 (1995) 155.
[21] J. Brinck, A.S. Jönsson, B. Jönsson, J. Lindau, Influence of pH on the adsorptive fouling of ultrafiltration membranes by fatty acid, J. Membr. Sci. 164 (2000) 187.
[22] M. Mulder, Basic Principles of Membrane Technology, Kluwer Academic Publishers, Dordrecht, 1991.
[23] M.C. Almandoza, J. Marchese, P. Prádanos, L. Palacio, A. Hernández, Preparation and characterization of non-supported micro-filtration membranes from aluminosilicates, J. Membr. Sci. 241 (2004) 95.
[24] J. Marchese, C.L. Pagliero, Characterization of asymmetric polysulphone membranes for gas separation, Gas Sep. Purif. 5 (1991) 215.
[25] K. Boussu, C. Vandecasteele, B. Van der Bruggen, Study of the characteristics and the performance of self-made nanoporous polyethersulfone membranes, Polymer 47 (2006) 3464.